ELECTROPHYSIOLOGICAL DIFFERENCES IN ATRIA AND VENTRICLES

By

Syeeda Nashitha Kabir

A thesis submitted to the University of Birmingham for the degree of

DOCTOR OF PHILOSOPHY

Institute of Cardiovascular Sciences

College of Medical and Dental Sciences

The University of Birmingham

September 2023

Abstract

Atrial fibrillation (AF) is the most common arrhythmia, affecting over 1% of the population. Sodium channel blockers are commonly used to treat AF by restoring sinus rhythm. Current anti-arrhythmic drugs such as flecainide, do not specifically target atrial sodium channels, and information on electrophysiological differences between atria and ventricles is limited. Furthermore, flecainide is contraindicated in ischaemic heart disease (IHD) patients due to increased mortality. The mechanisms are unknown, necessitating further study. Understanding electrical differences and drug sensitivities is vital for effective treatment and improved patient outcomes.

The project aimed to characterise electrophysiological properties in left atria (LA) and left ventricles (LV), distinguish the differential effects of flecainide, in LA and LV, and investigate interaction of flecainide and ischaemia. Electrical activity from ex vivo hearts were measured using optical mapping from healthy wildtype (WT) mice aged 10 to 15 weeks. Global ischaemia was triggered using low perfusion pressure method, and regional ischaemia was triggered by ligating left anterior descending artery (LAD) *ex vivo*.

Our data showed a significantly slower conduction and shorter action potential duration (APD) in the LA compared to LV. Flecainide showed inhibition of the sodium current and slowed conduction to a greater degree in the LA compared to LV. CV was further slowed in ischaemic hearts in the presence of flecainide. Ischaemia prolonged the APD when compared to baseline APD. Further investigation of molecular drivers of the atrial and ventricular resting membrane potential (RMP) and the molecular interaction partners of flecainide may help to identify new targets for early rhythm control therapy in patients with AF.

Acknowledgements

An immense thank you to my lead supervisor, Associate Professor Davor Pavlovic for support, encouragement and patience throughout my project. Your guidance and advice have been invaluable and has helped me become a better scientist. Many thanks to my additional supervisor, Associate Professor Steve Thomas who has always been there to provide knowledge and support. I would also like to show my gratitude to Professor Larissa Fabritz and Professor Paulus Kirchhof for allowing me the opportunity to be part of their research team.

Many thanks to the Heart Failure and Arrhythmia cluster for their kindness and support and making my time at University of Birmingham enjoyable. I would like to especially thank Winnie Chua for being a great friend and Jasmeet Reyat Singh for sharing his extensive knowledge.

Finally, I would like to thank my family for their lifetime of sacrifice and support.

Dedication

To Safiyah & Amara

Contents

Figures

Tables

List of abbreviations

AAD	Anti-arrhythmic drug
AF	Atrial fibrillation
AFFIRM	Atrial Fibrillation Follow-up Investigation of Rhythm Management trial
AFNET	Atrial Fibrillation NETwork
ANOVA	Analysis of variance
AP	Action potential
APD	Action potential duration
APD30	Action potential duration at 30% repolarisation
APD50	Action potential duration at 50% repolarisation
APD70	Action potential duration at 70% repolarisation
APD80	Action potential duration at 80% repolarisation
APD90	Action potential duration at 90% repolarisation
A.U.	Arbitrary unit
ATP	Adenosine triphosphate
AVB	Atrioventricular block
AVN	Atrioventricular node
AVNRT	Atrioventricular re-entrant tachycardia
BPM	Beats per minute
Ca^{2+}	Calcium ion
CaCl	Calcium chloride
Casq2	Calsequestrin

CAST	Cardiac arrhythmia suppression trial
CaT	Calcium transient
CaTD	Calcium transient duration
CHD	Coronary heart disease
CO2	Carbon dioxide
CPVT	Catecholaminergic polymorphic ventricular tachycardia
CV	Conduction velocity
CVD	Cardiovascular disease
DMSO	Dimethyl sulfoxide
EAST-AFNET	Early treatment of atrial fibrillation for stroke prevention trial
ECG	Electrocardiogram
ECHO	Echocardiography
EMCCD	Electron multiplied charged coupled device
ERP	Effective refractory period
Flec-SL	Flecainide short long study
H^+	Hydrogen ion
HCN	Hyperpolarisation-activated cyclic nucleotide gated
HEK	Human embryonic kidney
hERG	human Ether-à-go-go-Related Gene
hiPSC-CMs	Human induced pluripotent stem cells derived cardiac myocytes
HR	Heart rate
Hz	Hertz

IC_{50}	Half maximal inhibitory concentration
ICa(L)	L-type calcium current
IHD	Ischaemic heart disease
$I_{K(ATP)}$	ATP sensitive potassium channel
I_{K1}	Inward rectifier current
I_{KACh}	G-protein-gated potassium channel
I_{Kr}	Rapid delayed rectifier K^+ channels
I_{Ks}	Slow delayed rectifier potassium current
I_{Kur}	Ultrarapid outward K^+ current
IL-6	Interleukin-6
I_{Na}	Sodium channel current
IP	Intraperitoneal
I_{to1}	Voltage gated potassium channel
K^+	Potassium ion
KCl	Potassium chloride
KCNH2	Gene encoding potassium voltage gated channel
kDa	Kilodalton
kHz	Kilohertz
[K]i	Intracellular potassium current
$[K]_o$	Elevated extracellular potassium
Kir	Inwardly rectifying potassium channel
Kir3.1	Inward rectifier potassium channel

Kir3.4	Inwardly rectifying potassium channel
LA	Left atria
LAD	Left anterior descending artery
LBBB	Left bundle branch block
L-type	Long lasting calcium channel
LTCC	L-type calcium channel
LV	Left ventricle
MAP	Monophasic action potential
$MgSO_4$	Magnesium sulphate
MI	Myocardial infarction
mV	Millivolts
Na^+	Sodium ion
NaCl	Sodium chloride
NaH_2PO_4	Monosodium phosphate
$NaHCO_3$	Sodium bicarbonate
NCX	Sodium calcium exchanger
NHE	Sodium hydrogen exchanger
NHLBI	National Heart, Lung, and Blood Institute
NKA	Sodium potassium pump
PAC	Premature atrial contractions
PNS	Parasympathetic nervous system
PSVT	Paroxysmal supraventricular tachycardia

PVC	Premature ventricular contraction
RA	Right atria
RATE-AF	Rate Control Therapy Evaluation in Permanent Atrial Fibrillation
RBBB	Right bundle branch block
RMP	Resting membrane potential
RyR	Ryanodine receptor
S.E.M	Standard error of mean
SAN	Sinoatrial node
SERCA	Sarcoendoplasmic reticulum calcium ATPase
SNS	Sympathetic nervous system
SPAF	Stroke prevention in atrial fibrillation study
SR	Sarcoplasmic reticulum
SVT	Supraventricular tachycardia
SWORD	Survival With ORal D-sotalol trial
V	Voltage
VF	Ventricular fibrillation
VGSC	Voltage gated sodium channel
VT	Ventricular tachycardia
WT	Wildtype

1. Introduction

1.1. The heart

1.1.1. Anatomy and function

The heart is a muscular organ made up of four chambers; left atrium and right atrium, left ventricle and right ventricle, with a septum wall separating the left and right ventricles. The atria are separated by a thin wall of tissue known as interatrial septum. The heart lies between the lungs and the sternum, in the thoracic cavity, with the base of the heart located along the body's midline and the apex pointing towards the left side of the body's midline. The four chambers are relaxed during diastole and systole is initiated with an action potential originating in the sinoatrial node (SAN) in the right atrium. The main function of the right atrium is to receive deoxygenated, carbon dioxide (CO_2) enriched blood via inferior and superior vena cava and pump it into right ventricle, through the tricuspid valve. The right ventricle pumps the blood to the lungs via pulmonary artery to be oxygenated. The left atrium receives the oxygenated blood from the lungs and pumps it to the left ventricle via the mitral valve. The left ventricle pumps the oxygenated blood out to the rest of the body via the aorta, the largest artery in the human body. The flow of blood through the circulatory system once makes up a single heartbeat. The number of heart beats per minute varies from species to species. Smaller animals generally have faster heart rates than larger animals [1]. In humans, a normal heart rate typically ranges from 60 and 100 beats per minute (bpm), whereas in mice it ranges between 400 and 800 bpm [2].

The heart is made up of 3 main layers, pericardium, myocardium and endocardium. The pericardium is a thin, double layered sac that surrounds and protects the heart. The pericardium itself is made up of several layers, the outer fibrous pericardium and the inner serous pericardium. The outer fibrous pericardium provides protection to the heart and anchors it to the surrounding structures. The inner serous pericardium is made up of a further two layers, the parietal layer and visceral layer. The parietal layer lines the inside of the outer fibrous pericardium, while the visceral layer is attached to the heart muscle. The parietal and visceral layer is divided by a space known as the pericardial activity and contains lubricating fluid allowing the heart to move within the pericardial sac [3]. The visceral layer is also known as the epicardial layer, and the epicardium is characterised by high cellular plasticity and is critical in heart development and regeneration. It is composed of connective tissue, fat and coronary blood vessels and is involved in the formation of the heart's coronary arteries, Figure 1.1.

The myocardium is the muscular, middle layer of the heart and is responsible for the heart's ability to contract and pump blood throughout the body. The myocardium is made up of striated cells connected by intercalated discs called cardiomyocytes and these have specific structures and properties enabling cell contractility [4]. There are two major types of cardiomyocytes: contractile cells which make up 99% of the cardiac myocytes and conducting cells which make up 1% of the cardiac myocytes. In total, cardiomyocytes account for approximately 30% of all cardiac cells. Cardiac cells consist of fibroblasts, endothelial cells, mesothelial cells, and adipocytes. Contractile cells are responsible for receiving electrical impulses and contraction of the heart with the aid of contractile proteins, actin and myosin. Conducting cells form the conduction system of

the heart which will be discussed later in the chapter. Cardiomyocytes are enveloped by sarcolemma and contain a nucleus and several mitochondria. One main feature of cardiomyocytes is the intercalated discs consisting of junctional components, adherens junction, desmosomes and gap junctions, Figure 1.1. These junctional components enable cells to communicate with one another. Adherens junctions associate with the actin cytoskeleton, joining them with neighbouring cells [5]. Desmosomes create a stronger connection than adherens junction and join intermediate filaments of neighbouring cells [6]. Gap junctions are specialised intercellular channels and connect cytoplasm of adjacent cells through protein channels. Ions and small molecules are diffused between adjacent cells via the gap junctions which are gated by voltage [7]. Voltage of cell membranes are mediated by sodium, calcium and potassium ions.

Finally, the endocardium is the innermost layer of the heart wall which is highly vascularised and lines the chambers of the heart, heart valves, chordae tendinae and papillary muscles [8]. It comprises of a layer of endothelial cells and a layer of connective tissue. The endocardium is involved in the regulation of the heart's contraction and relaxation. It contains specialised cells called Purkinje fibres that help to coordinate electrical impulses and contraction of heart.

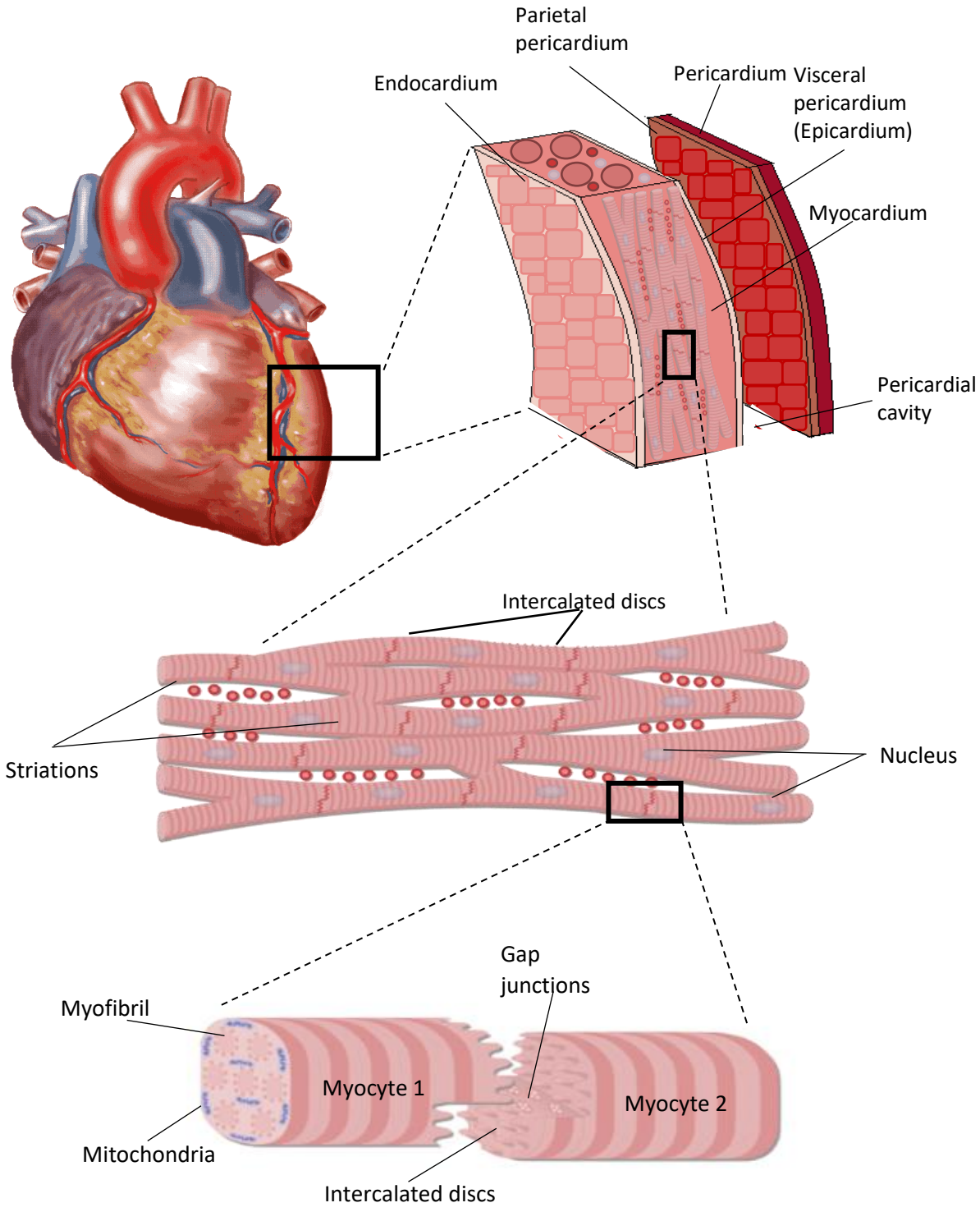

Figure 1.1 Structure and layers of the heart. Top panel shows layers within the heart wall, pericardium, parietal pericardium, visceral pericardium, myocardium and endocardium. Middle panel shows composition of myocardium. Bottom panel shows two cardiomyocytes linked together through gap junctions. Figure adapted from Sheffield 2020.

1.1.2. Cardiac conduction system

The cardiac action potential (AP) is the electrical signal that travels through the heart during each heartbeat, leading to contraction of the heart muscle and pumping of blood throughout the body. The action potential originates in the sinoatrial node (SAN), a crescent-like shaped cluster of myocytes, which is located in the right atria. SAN is made up of pacemaker cells responsible for setting the rate and rhythm of the heart and acts as the primary pacemaker of the heart. The SAN generates spontaneous electrical impulse at a rate determined by the sympathetic nervous system (SNS) and parasympathetic nervous system (PNS) [9]. It can also be affected by other factors such as ion concentrations, hormones, medication and ischaemia. The SNS governs the "fight or flight" response, increasing the heart rate, and the PNS governs the "rest and digest" response, decreasing the heart rate [10]. Through gap junctions, the action potential propagates from the SAN in right atria to left atria at a velocity of ≈ 0.5 m/s, through Bachmann's bundle, initiating atrial muscular contraction and the filling of ventricles. The action potential travels to the atrioventricular node (AVN), a structure found on the interatrial septum that connects the electrical systems of the atria and ventricles [11]. The AVN plays a gatekeeping role in delaying the signal between atria and ventricles. The conduction velocity slows to ≈ 0.05 m/s at the AVN, preventing premature contractions of the ventricles. The 0.1 s pause in depolarisation ensures atrial systole is complete [12]. In the event of SAN failure, the AVN functions as a protective role by becoming the dominant pacemaker of the heart [13]. The electrical impulse is then

transmitted down Bundle of His and Purkinje fibres, finally reaching the ventricles and initiating contraction of the ventricles.

There are several types of conduction disorders that can occur along the conduction system. These include sinus node disease, AV block, SA block, SA pauses and bundle branch block. The SA and AV nodes are also susceptible to re-entry arrhythmia, a self-sustaining propagation of action potential in a circus-like closed loop circuit [14].

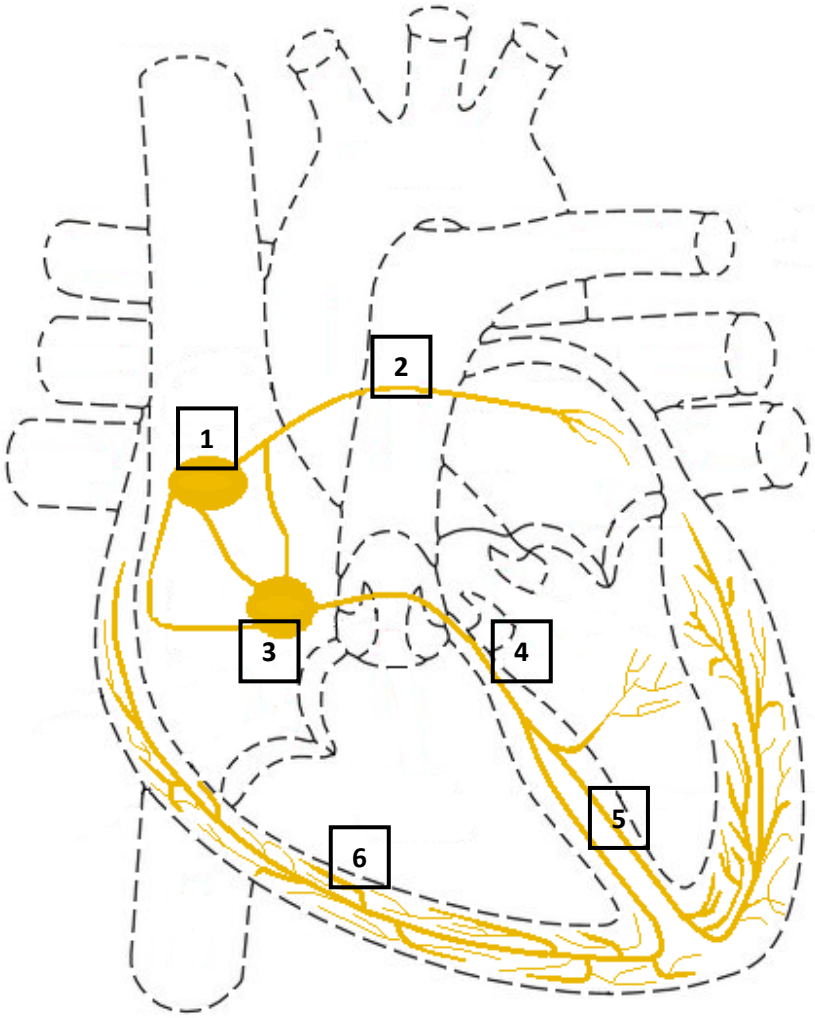

Figure 1.2. Transverse section of human heart showing the cardiac conduction system. A summary of the cardiac conduction system in the human heart with the main components, SA node, AV node, Bachmann's bundle, bundle of His, Purkinje fibres, left posterior bundle and right bundle. AP initiates at sinoatrial node [**1],** before spreading to Bachmann's bundle **[2]** reaching the left atria**.** The AP is transmitted to AV node **[3],** through bundle of His **[4]**, down the bundle branches **[5]** and through Purkinje fibres **[6].** Figure adapted from Sahu 2015 [15].

1.1.3. Cardiac action potential

The cardiac action potential refers to the change in electrical charge of the cell during a single heartbeat. The change in voltage in electrical charge is caused by the flow of ions across cell membranes leading to depolarisation and repolarisation of the cell membrane. The main ions involved include sodium (Na^+), calcium (Ca^{2+}) and potassium (K^+) which travel in and out of cells via specific ion channels, pumps and exchangers, depending on changes in permeability of the ion transporters. The action potential consists of 5 phases, phase 0, 1, 2, 3 and 4. At phase 4, the cell is at rest. The cell membrane is polarised with an intracellular negative charge and extracellular positive charge. At rest, the resting membrane potential (RMP) is ≈ -90 mV. Phase 0 is a rapid depolarisation of the cell, caused by the opening of voltage gated Na^+ channels and influx of Na^+ ions. There is an increase in Na^+ and a decrease in K^+ conductances and the membrane potential rises to a more positive voltage range, ≈ +50 mV. Phase 0 is represented by the initial upstroke of the action potential. Phase 1 is the initial repolarisation of the cell membrane. The voltage gated Na^+ channels become inactive, terminating influx of Na^+ ions, and voltage gated K^+ channels (I_{to1}) and Na^+/Ca^{2+}exchanger (NCX) become active, allowing efflux of K^+ and Ca^{2+} ions and influx of Na^+ ions. This causes the membrane potential to go from ≈ +50 to +30 mV. Phase 2 is the plateau phase, characterised by a sustained membrane potential. This is due to an influx of Ca^{2+} ions through voltage gated Ca^{2+} channels, known as L-type calcium channels (LTCC), and efflux of K^+ ions through delayed rectifier K^+ channels (I_{Ks}) [16]. Phase 3 refers to the rapid repolarisation of the cell membrane. LTCC close, stopping the

influx of Ca^{2+} ions, while I_{Ks} channels remain open allowing continued efflux of K^+ ions from the cell. During this phase, other K^+ channels open, the rapid delayed rectifier K^+ channels (I_{Kr}) and the inwardly rectifying K^+ (Kir) channels. As the membrane potential returns to phase 4 state, I_{Ks} channels close and Kir channels remain open [17].

1.1.3.1. Atrial action potential

As shown in Figure 1.3, the atrial action potential is slightly different from the ventricular action potential. Like the ventricular action potential, atrial action potential is also divided into 5 phases. The key difference is in phase 2, the plateau caused by activation of I_{Ks} is sustained for a shorter time in atrial action potential compared to ventricular action potential. The atrial action potential often has a triangular shape as opposed to the ventricular counterpart's spike-and-dome structure and significant plateau phase. The atrial RMP, which is more depolarised than that of the ventricular RMP, has been reported to range between -65 and -80 mV [18].

1.1.3.2. Pacemaker cell action potential

Unlike the ventricular and atrial action potential, the pacemaker cell action potential consists of 3 phases, phase 0, 3 and 4. The opening of voltage gated Ca^{2+} channels and an influx of Ca^{2+} ions result in an upstroke in membrane potential, phase 0. The membrane potential goes from ≈ -40 mV to +10 mV less rapidly than myocardial action potential upstroke since Ca^{2+} channels are slow channels compared to voltage gated Na^+

channels. This results in a slower depolarisation and slower action potentials. Phases 1 and 2 are absent in pacemaker cells and phase 0 is followed by phase 3. In phase 3, Ca^{2+} channels close, preventing the efflux of Ca^{2+} ions and voltage gated K^+ channels to open, allowing an efflux of K^+ ions. This results in a decrease of membrane potential from +10 mV to -60mV. Phase 4 consists of a gradual depolarisation which occurs through the slow influx of Na^+ ions via hyperpolarisation-activated cyclic nucleotide–gated (HCN) channels. As the name suggests, HCN channels are activated by hyperpolarisation and only open when the cell is at rest or is repolarising. They are important in generation of pacemaker potentials, sinoatrial impulse propagation, cardiac excitability and precision of heartbeat [19]. The slow influx of Na^+ ions through HCN channels cause a slow depolarisation during phase 4 to go from a membrane potential of ≈ -60 mV to the threshold potential, ≈ -40 mV. The SAN pacemaker cells depolarise at a rate of 60 to 100 per minute whereas the AVN pacemaker cells depolarise at a rate of 40 to 60 per minute. The slope of phase 4 from the primary pacemaker, which is the SAN, determines the heart rate [17].

1.1.3.3. Differences in atrial and ventricular action potential

The changes in action potential morphology between atria and ventricles is largely down to handling of ions and their underlying transcripts. Differences in expression of some of the ion channels, pumps and transporters in the atria and ventricles, and also between species have been characterised.

In the mammalian heart muscle, action potential amplitudes and durations are mainly influenced by K^+ channels that are sensitive to voltage changes. Based on differences in time and voltage dependent properties, two classes of voltage gated K^+ currents have been distinguished: rapidly activating and inactivating transient outward K^+ currents, I_{to}, and slowly inactivating outward rectifying K^+ currents, I_K. I_{to} currents contribute towards the early phase of action potential repolarisation while the I_K current contributes towards the late phase of the repolarisation [20].

In the human heart, the I_{Kur} current can be found in the atria, but is absent in the ventricles. I_{Kur}, also known as the ultrarapid rectifier potassium current, is a major contributor towards the repolarisation process of the heart. It is carried by the $K_v1.5$ channels and predominantly expressed in the atria, contributing little towards ventricular repolarisation [21]. The fast I_{to}, current, encoded by $K_v4.3$, and known as fast cardiac transient outward potassium current, is detected in the human atrium whereas both fast and slow I_{to}, current can be detected in the ventricles [22] [23]. The G-protein-gated potassium channel, responsible for I_{KACh}, known as acetylcholine-activated inward rectifier potassium current is encoded by GIRK channels. I_{KACh}, density has also been shown to be greater in the atrium than in the ventricle [24]. A representation of ion currents in atria and ventricles can be seen in Figure 1.4.

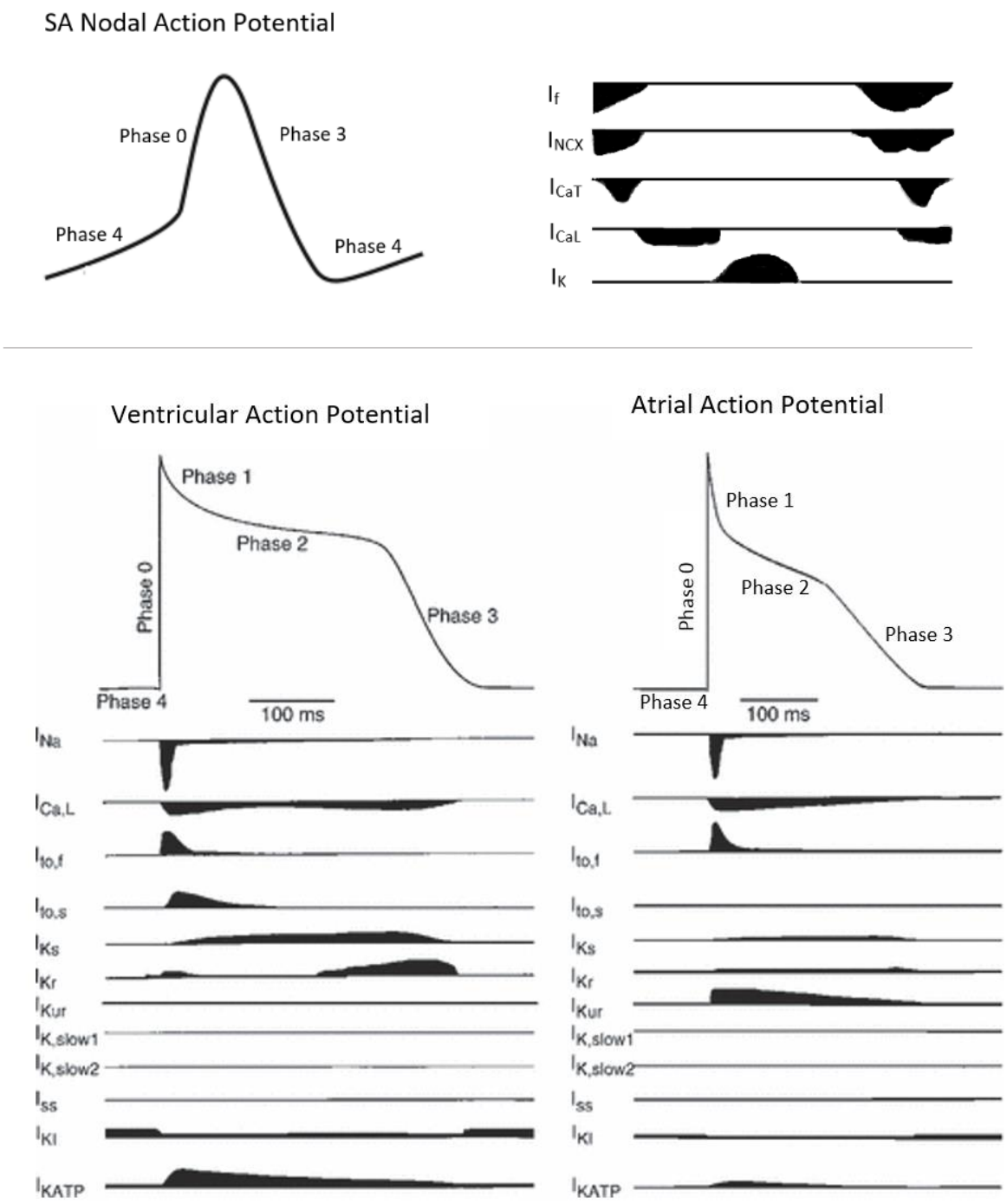

Figure 1.3. Action potential waveform of SA nodal, ventricular and atrial cell, and their underlying currents, in humans. This figure shows different phases of action potentials in the SAN, ventricles and atria and the influx (below the line) and efflux (above the line) of currents. Figure taken from Jost 2009 [25].

1.1.3.4. Mouse action potentials

It is important to note the action potentials and underlying currents vary between cell types, chamber type and species type. In mice, ventricular RMP has been recorded at ≈ - 73 mV, while the human ventricular RMP has been recorded at ≈ 90 mV [26]. This difference in resting membrane potential may come from the differential expression and density of potassium currents [26]. Much like the atrial action potential, mouse action potential is more triangular in morphology. In mice, L-type Ca^{2+} current contribute less to the ventricular action potential compared to humans resulting in a gradual repolarisation rather than a plateau which is observed in humans. Similar to human SAN action potential, mouse SAN action potential is also similar in morphology but depolarises at a faster rate. Heart rates of mice range between 431 and 800 bpm. Action potentials in mouse ventricles is ≈ 50 ms, compared to ≈ 250 ms in humans. According to Figure 1.5, there are differences in density of potassium channels between human and mouse ventricular action potential resulting in a change during the repolarisation phase. For humans, rabbits, and guinea pigs, ventricular repolarisation mostly depends on I_{Kr} and I_{Ks} potassium channels, whereas in rats and mice, transient outward K^+ current (I_{to}) and ultrarapid outward K^+ current (I_{Kur}) have a dominant effect [26]. Despite these differences, there are still many similarities across both species. The basic mechanisms of depolarisation, Na^+ influx, K^+ efflux and repolarisation are similar in humans and mice.

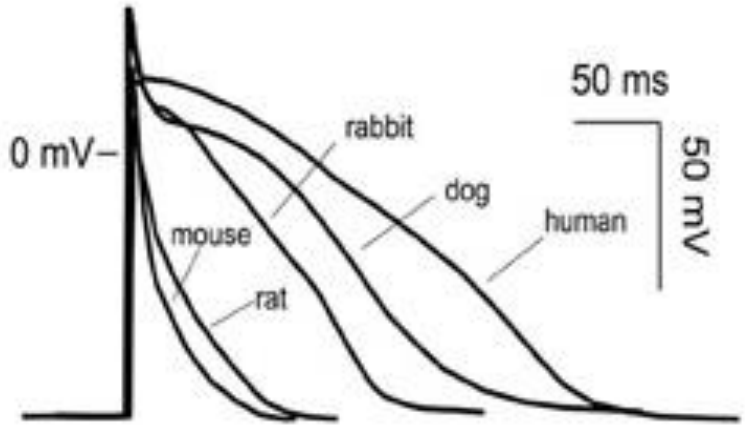

Figure 1.4. Atrial action potentials in different species. Representation of atrial action potential in mouse, rat, rabbit, dog and human [27].

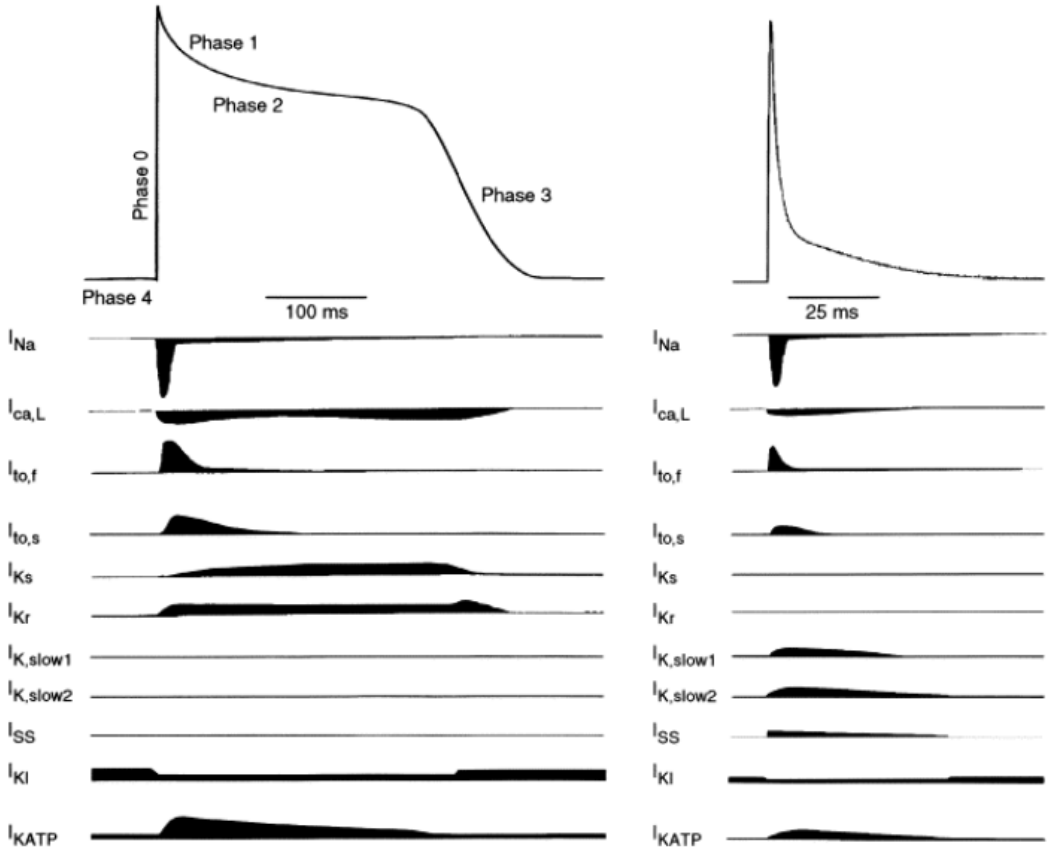

Figure 1.5. Ventricular action potentials of human and mouse. Human action potential with their underlying currents shown on the left. Mouse action potential and underlying currents shown on the right [28].

1.2. Ion homeostasis

The heart is a complex organ that requires precise regulation of ions to maintain normal electrical and mechanical function. Exchange of positive charged ions including Na^+, Ca^{2+} and K^+, play a key role in action potential generation, contractility and maintaining a pH balance in the cells. Ion homeostasis in the heart is maintained through passage of charged ions through a variety of ion channels, pumps and exchangers. These ion transporters are highly selective ion pores that span across the phospholipid bilayer of the cell membrane.

During diastole, the intracellular Ca^{2+} concentration typically ranges from 0.05 to 0.1 µmol/L. Action potentials travel along the sarcolemma and into transverse tubules (T-tubules) initiating depolarisation of the cell membrane. In systole, L-type Ca^{2+} channels open allowing Ca^{2+} entry into cells during phase 2 of the action potential. Intracellular Ca^{2+} concentration rises rapidly to approximately 1 µmol/L. The Ca^{2+} influx triggers the release of large amounts of stored Ca^{2+} from the sarcoplasmic reticulum (SR) through the ryanodine receptors, a phenomenon known as calcium-induced calcium release. Most of the Ca^{2+} required for contraction comes from the SR [29]. At the end of the contraction, the intracellular Ca^{2+} concentration rapidly decreases back to diastolic levels. Breitweiser 2008 reported extracellular fluid Ca^{2+} concentration to be 1.2 mmol/L [30].

98% of the entire pool of K^+ ions are located intracellularly with only 2% located in the extracellular fluid. The typical intracellular K^+ in human cardiomyocytes ranges between

140 and 150 mmol/L. Extracellular concentration of K^+ is usually conserved between 3.5 to 5 mmol/L [31].

Human cardiomyocytes maintain a large electrochemical Na^+ gradient across the plasma membrane. Na^+ concentration in extracellular fluid is approximately 140 mM, while intracellular Na^+ concentration is between 4 and 16 mM [32]. This large electrochemical gradient is maintained by the activity of the sodium-potassium (NKA) pump, which uses energy from ATP hydrolysis to actively transport Na^+ ions out of the cell and K^+ ions into the cell [32].

Maintaining ion homeostasis is critical for maintaining cardiac function and preventing cardiac disorders. Dysregulation of any one of these ionic concentrations can lead to cardiac dysfunction.

1.2.1. Sodium pathways

As mentioned, cardiac function is maintained through ion transporters that tightly regulate delivery of ions in and out of cells. Ion transporters can be divided into channels, pumps and exchangers, and collectively these govern the influx and efflux of Na^+ into and out of cell, thus maintaining intracellular Na^+ levels. There are several transport mechanisms for Na^+ influx and efflux, voltage gated sodium channels, sodium-potassium ATPase pump (NKA), sodium-hydrogen exchangers (NHE) and sodium-calcium exchanger (NCX), Figure 1.6. The main Na^+ entry pathways are the voltage gated

channels, NCX and NHE. NKA pump constitutes the only significant sodium extrusion pathway [30].

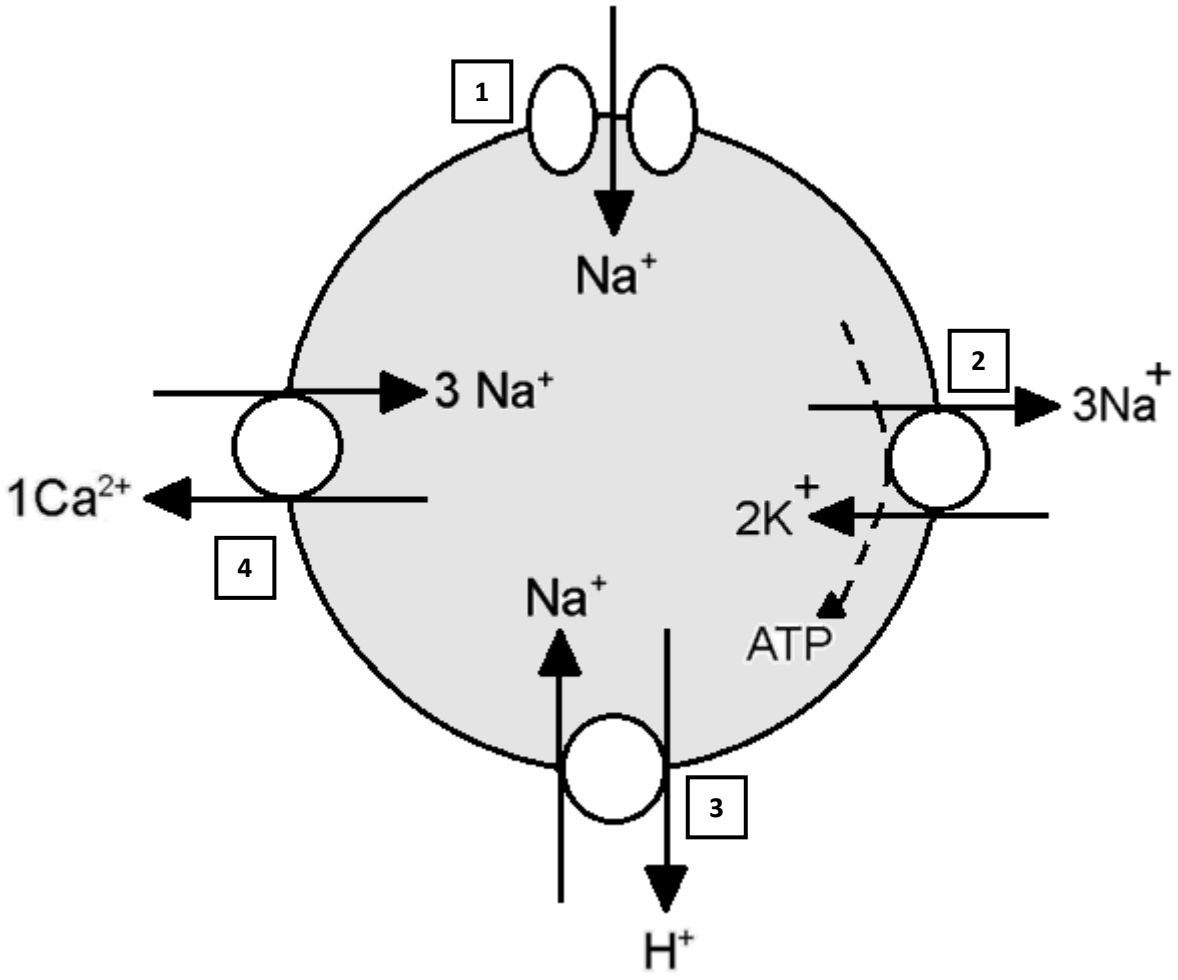

Figure 1.6. Summary of sodium influx and efflux pathways. Sodium is regulated by voltage gated sodium channels, $Na_v1.5$, **[1]**, NKA pumps, **[2]**, NHE **[3]** and NCX **[4]**. Arrows determine movement of ions, either against the concentration gradient with the aid of ATP, or down its concentration gradient. Figure created by author of this thesis.

1.2.1.1 Voltage-gated sodium channels

Voltage-gated sodium channels (VGSCs) are transmembrane proteins which are responsible for the rapid upstroke of the cardiac action potential and rapid conduction through the heart. Nine subtypes of voltage gated sodium channels have been identified, $Na_v1.1$ to $Na_v1.9$. $Na_v1.5$ is the primary cardiac voltage gated sodium. The $Na_v1.5$ consists of a principal ≈220 kDa pore-forming α-subunit and one or more 30 kDa auxiliary β-subunits. α-subunits are composed of four homologous domains, I – IV, C-terminus and an N-terminus. Each domain contains six transmembrane segments, S1 – S6, with the S4 segment acting as a voltage sensor [33]. S5 and S6 segments form the pore with an intermembrane P-loop and conduct and gate ions, Figure 1.7. Movement of the voltage sensing function of S4 in domains I-III activates the $Na_v1.5$ channel. This movement drives phase 0 depolarisation, activating the cardiac action potential and propagating the electrical impulse to neighbouring cells. Movement of the voltage sensing function in domain IV leads to channel inactivation, driving pore occlusion [34]. There are five β-subunits, β-1, β-1B, β2 to β-4, and these also consist of an N-terminus and a C-terminus. The β-subunits modulate the gating, kinetics and facilitate $Na_v1.5$ localisation at the intercalated disc [35]. β-subunits are encoded by SCN1b-4b genes. The primary α-subunit expressed in the heart, $Na_v1.5$, is encoded by the SCN5a gene located on chromosome 3p21. Most mutations in this gene are linked to cardiac arrhythmias and is also a target for many anti-arrhythmic drugs (AAD). These AADs include flecainide, propafenone, lidocaine and quinidine, amongst many others, and are inhibitors of cardiac $Na_v1.5$ Na^+ channels. Sodium channel blockers work by reducing the

channel's affinity for Na^+ ions, resulting in a slower rate and amplitude of initial depolarisation and delayed conduction [36].

$Na_v1.5$ channels are able to configure structurally into three distinct states: open, closed and inactivated. When the cell is at resting membrane potential, $Na_v1.5$ channels are in the closed state. Upon receiving an electrical stimulus $Na_v1.5$ channels activate and open, and then rapidly become inactivated during the state of non-conductivity. In the inactivated state, the channel pore is open but does not conduct ions. Transmembrane potential, time, temperature, and pH level are the primary determinants of transition between these states. Under physiological circumstances, recovery from inactivation takes place during the repolarisation phase of diastole. The number of $Na_v1.5$ channels that are available for opening determines the upstroke speed of the action potential and conduction [37].

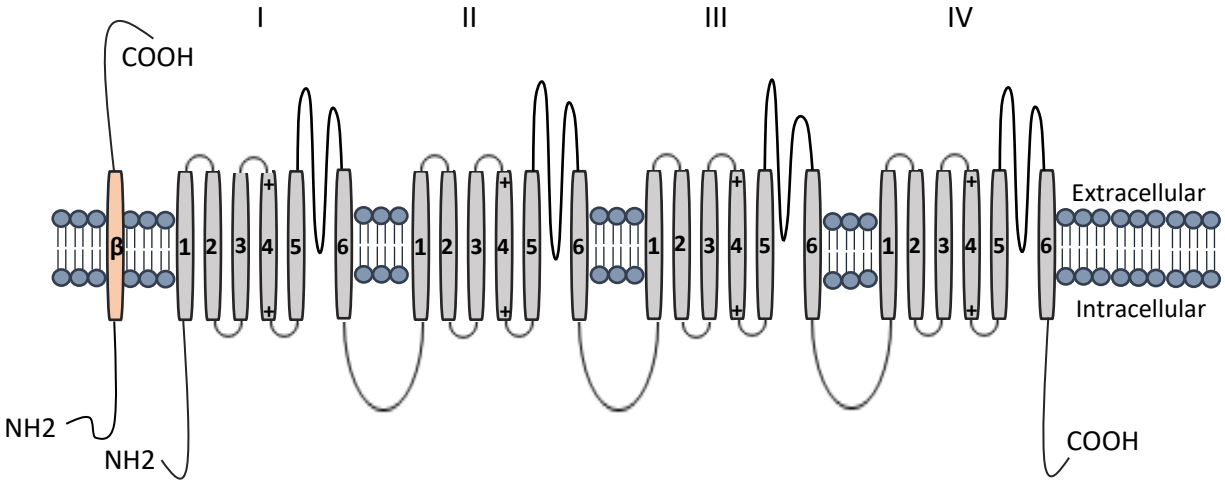

Figure 1.7. Schematic illustration of the structure of $Na_v1.5$. Topology of four domains of α-subunit, I – IV, with associated β-subunit. Each subunit show a C-terminus and N-terminus. Segment 4 acts as voltage sensor and segment 5 and 6 form central pore domain. Figure adapted from DeMarco and Clancy 2017 [38].

1.2.1.2 Sodium-potassium ATPase pumps

The sodium-potassium ATPase pump (NKA) is an electrogenic transmembrane ATPase situated in the outer plasma membrane of the cells. NKA is powered by hydrolysis of ATP to extrude three Na^+ ions out of the cell in exchange for two K^+ ions into the cell, against their concentration gradient [39]. The NKA pump exists in two forms, E1 and E2. The pump is in E1 form when it has high affinity for Na^+ ions and is in E2 form when it has high affinity for K^+ ions [40]. In mammals, the NKA is made up of four catalytic α-subunits and three auxiliary β-subunits and seven tissue specific FXYD subunits [40]. The α-subunit contains a transmembrane region composed of ten helices, MA1-M10. Within these helices, there are three binding sites that bind specifically to Na^+ ions and two binding sites that bind specifically to K^+ ions [39]. There are four α-subunit isoforms, α1-α4. α1- α3 isoforms are expressed in humans, with α1 making up more than half the stoichiometric distribution at 62%, followed by α3 at 23% and α2 at 15% [41]. α1 isoforms have high potassium affinity and is localised in external sarcolemma membranes and T-tubular membranes. It is important in the maintenance of Na^+ and K^+ ions. α2 isoforms have low potassium affinity and preferentially assembles with β2-subunit and is localised in T-tubular membrane. It is important in the role of Ca^{2+} signalling [42]. α3 isoforms have low Na^+ affinity and its relative expression to α1 is several fold higher in men than in women. The β-subunits also have specific roles. β2 reduces K^+ affinity and increases extracellular Na^+ affinity of the pump, compared to β1 and β3. The β1 subunit is the major isoform in the mouse heart. FXYD functions to lower substrate affinities of the NKA pump and also affect functional properties [40].

Mutations in the α and β subunits can result in perturbation of atrial and ventricular action potential which can lead to many types of arrhythmias such as long QT syndrome, short QT syndrome, Brugada syndrome and familial atrial fibrillation (AF) [43]. Mutations in the *ATP1A1* gene which encodes for α1 subunit, has been shown to have a gain-of-function effect and causes the NKA to behave as an ion channel instead of as a pump. Mutations in *ATP1A2* and *ATP1A3*, which code for α2 and α3 respectively, impair pump action. There are currently no confirmed human genetic diseases linked with mutations in FXYD subunits [40]. In patients with dilated cardiomyopathy, there was a 40% decrease of total NKA pump concentration [42]. Commonly used therapeutic drugs that target NKA include cardiac glycosides such as digoxin. Digoxin is frequently used in clinical practice for atrial arrhythmias. Depending on indication, digoxin is administered for its positive ionotropy effects, increasing force of contraction of the heart, or for its vagal effects on the AV node, decreasing heart rate through stimulation of parasympathetic nervous system. Digoxin inhibits ATPase, leading to increased intracellular Na^+ concentrations. This leads to a decreased activity of NCX, increasing levels of intracellular Ca^{2+} [44].

1.2.1.3 Sodium-hydrogen exchanger

Sodium hydrogen exchanger, NHE, is a glycoprotein which electroneutrally exchanges one intracellular hydrogen (H^+) ion for one extracellular Na^+ ion. Nine isoforms of NHE have been identified, NHE-1 to NHE-9. Of all the isoforms, NHE-1 isoform is the most abundant in the heart and is considered to be a cardiac specific isoform. The inward

gradient of Na^+ from NKA provides a constant driving force for H^+ extrusion and Na^+ via NHE-1. NHE-1 plays an important role in the homeostasis of pH. The exchanger releases acid from the cell when there is a reduction in intracellular pH [45]. NHE-1 is involved in several other housekeeping tasks such as regulating intracellular Na^+ and regulating cell volume. NHE-1 is made up of 815 amino acid residues and consists of an N-terminal and C-terminal. There are twelve transmembrane regions with an allosteric H^+ sensor site [45].

Dysfunction of NHE-1 is associated in several pathologies. Hyperactivation of NHE-1 caused ischaemia/reperfusion injury, myocardial infarction, heart failure, cardiac hypertrophy and remodelling. Studies have shown inhibiting NHE-1 provided cardioprotection from diseased states. Examples of NHE-1 inhibitors include cariporide and eniporide, however clinical data showed these inhibitors did not provide cardioprotection and further studies are required [46].

1.2.1.4 Sodium-calcium exchanger

NCX is a reversible transporter membrane protein and exchanges three Na^+ ions coming into the cell for one Ca^{2+} ion leaving the cell, along its concentration gradient [47]. NCX is an antiporter, meaning it transports two molecules simultaneously in the opposite direction. It has a high capacity and low Ca^{2+} affinity [48]. Reversibility of NCX refers to its ability to operate in either forward mode [49]. In forward mode, Na^+ ions enter the cell and Ca^{2+} leave the cell and in reverse mode, Na^+ ions leave the cell and Ca^{2+} ions

enter the cell. The NCX operates in the forward mode when the membrane is hyperpolarised and operates in reverse mode when the membrane is depolarised [50].

The NCX exists in three isoforms, NCX1, NCX2 and NCX3 which all share similar structure, sharing approximately 70% amino acid structure. Each isoform has specific tissue distribution and kinetic properties. All three isoforms are expressed in the brain, with NCX1 being primarily expressed in cardiac muscle. NCX1 is localised in the T-tubule membrane, peripheral sarcolemma and in intercalated discs. It is made up of 970 amino acids with a molecular mass of 110 kDa. NCX1 has been reported to have nine transmembrane segments, separated by an intracellular regulatory loop between transmembrane segment 5 and 6 and two re-entrant loops connecting transmembrane segment two and three, and seven and eight [51]. The NCX1 comprises of α regions and β regions. The α1 and α2 regions are made up of transmembrane segment two and three, and seven and eight respectively, and these are involved in ion binding and transport. The β region is found in the large intracellular loop and aids in binding of Ca^{2+} [42].

Under physiological conditions, NCX ensures the removal of intracellular Ca^{2+} after every heartbeat. NCX dysfunction and alteration in NCX expression has been implicated in a number of diseases including heart failure and post-ischaemic cardiac injury. Accumulation of intracellular Ca^{2+} through common pathologies is also known to trigger arrhythmias [52]. The dysfunction of NCX and Ca^{2+} handling can lead to electrical disturbances such as delayed afterdepolarisations (DADs). DADs are transient depolarisations that occur after an action potential corresponding to the phase 4 of the

action potential and are observed during intracellular Ca^{2+} overload. Increased intracellular Ca^{2+} induce spontaneous Ca^{2+} release from the SR. This activates calcium-sensitive currents, creating a DAD [53]. Hyperactivation of NCX has been observed in failing hearts which leads to Ca^{2+} depletion and contractile dysfunction. Drugs targeting NCX have been developed as potential treatments for conditions such as heart failure and stroke. SAR340835/SAR296968 is a selective NCX inhibitor, inhibiting all NCX isoforms across species [54].

1.3. Contractility

Cardiac contractility refers to the ability of the heart to contract and pump blood around the circulatory system. Initiation of contraction is triggered by the entry of Ca^{2+} ions into the cardiomyocytes and regulated by changes in intracellular Ca^{2+} concentration [29]. The influx of Ca^{2+} triggers Ca^{2+} ions to be released from the sarcoplasmic reticulum (SR) via calcium induced calcium release. Cardiac contractility comprises of structural coupling, and functional coupling. Structural coupling refers to the physical connection and close interaction between Ca^{2+} ions and proteins and structures within the heart responsible for regulating contractions. In cardiomyocytes, SR network including ryanodine receptors (RyR) and t-tubule membranes are closely associated and Ca^{2+} transporters within dyads are organised to allow tight regulation of Ca^{2+} cycling. Functional coupling refers to the balancing of Ca^{2+} ions across all membranes to ensure equilibrium between Ca^{2+} influx and efflux on every heartbeat. Free Ca^{2+} released from the SR binds to troponin on actin filaments in striated muscles, resulting in a

conformational change of tropomyosin. Myosin then binds to actin releasing ADP and inorganic phosphate allowing muscle contraction. After contraction, ATP binds to myosin causing it to detach from actin. This ATP hydrolyses into ADP and inorganic phosphate and the cycle begins again. Relaxation of the heart is initiated through removal of Ca^{2+} ion from the cytoplasm. The RyRs close stopping Ca^{2+} being released from the SR to the cytoplasm and Ca^{2+} is pumped back into the SR via SR Ca-ATPase (SERCA) and pumped out of the cell via NCX [29].

Atria and ventricles perform various haemodynamic roles which are linked to their structural and contractile properties. The chambers exhibit differences in the speed of contraction, volume of blood delivered, and the pressure range generated. The RV wall is significantly thinner than the LV wall as the RV pumps blood into a low-pressure pulmonary vasculature while the LV pumps blood into a high-pressure systemic circulation [55]. The atrial myocardium has highly elastic properties as they primarily serve as a reservoir for blood from the systemic venous network and do not normally have to overcome high pressures during contraction [56]. The contractile properties of atria and ventricles have not been thoroughly studied although limited studies are available with inconclusive findings. In 2020, Nollet *et al*'s study performed a large-scale contractility measurement in WT rat cardiomyocytes from atria, ventricles and interventricular septal (IVS). They measured contractile functions from over 2000 cells and found atrial cells exhibited a lower contraction amplitude and slower kinetics of contraction and relaxation. Compared to LV and IVS cardiomyocytes, RV cardiomyocytes displayed lower velocity of shortening. IVS cardiomyocytes had a higher relaxation velocity compared to LV and RV cardiomyocytes. The ventricles produce a greater

tension of 30 to 50%, and the duration of the contraction and relaxation cycle is almost doubled when compared to the atrium [55]. In humans, the ventricles are noted to predominantly express β-cardiac myosin and the atrium to express mainly α-cardiac myosin. Myosin is fundamental for the generation of cardiac contractions. The two isoforms of myosin have distinct mechanical and biochemical properties. They are made up of two heavy chains and four calmodulin-like light chains. The α myosin is expressed by *MHY6* and the β myosin is expressed by *MHY7.* α isoform is related to higher ATPase activity and faster muscle shortening velocity compared to β isoform. It contributes to the rapid contraction of the atrium allowing efficient filling of the ventricles. Ratio of α and β myosin has been observed to vary greatly between species with smaller mammals having greater amount of α-isoform in the ventricles. In humans, the percentage of α isoform in the ventricle and atrium is 5% and 75% respectively whereas in mice, it is 100% and 100% [57]. The precise number of each isoform and their distribution in the atria and ventricles remains unknown. In patients with atrial fibrillation (AF), there is an increase in the amount of slow β isoform heavy chain in the atrium, possibly accounting for the decrease in contractility. The balance between α and β myosin isoforms ensures efficient cardiac function and the differences in the expression between atria and ventricles partly contribute towards differences in atrial and ventricular contractility [57].

1.4. Cardiac arrhythmias

The complexity and intricacy of the cardiac system gives rise to disturbances in many mechanisms leading to cardiac arrhythmias. Cardiac arrhythmias refer to abnormal heart rhythms, rate or conduction disturbances. Types of arrhythmias can include supraventricular tachycardia (SVT) characterised by a very fast heart rhythm resulting from abnormal transmission of electrical impulses across the heart, atrial flutter characterised by a fast heart rhythm in the atria, sick sinus syndrome, characterised by periods of very fast or slow heart beats, heart blocks characterised by slow heart rates resulting from a delay or blockage in the conduction system, and atrial fibrillation (AF), characterised by an irregular and fast heart rhythm. AF is the most common form of sustained arrhythmia contributing highly to morbidity and mortality of cardiovascular disease (CVD) [58].

1.4.1. Atrial fibrillation

The prevalence of AF has increased 3-fold over the past 50 years and continues to increase globally. As of 2016, prevalence of AF was estimated to be approximately 46.3 million individuals. AF is one of the major causes of stroke, heart failure and sudden death. Major risk factors contributing to AF include advancing age, race or ethnic background, pre-existing heart conditions and lifestyle factors for example smoking, alcohol consumption and obesity [59]. AF is characterised by its occurrence and progression and is divided into paroxysmal AF, persistent AF, permanent AF, lone AF and non-valvular AF. Paroxysmal AF is defined by a brief event of AF usually lasting up 24

hours but can last up to a week, before self-terminating. Persistent AF occurs when AF lasts more than a week. It may terminate on its own or may require treatment to regulate heart rhythm. Permanent AF is defined as such when attempts to maintain sinus rhythm have failed and have been abandoned [60]. Lone AF refers to incidences of AF in individuals under 60 years of age with no other concomitant heart disease. Valvular AF is so called as it is related to valvular disease, replacement or repair [61].

The mechanism for AF arises from a complex interaction between triggers, events responsible for initiating arrhythmia, and substrates, structural or electrical events that maintain the arrhythmia. Atrial extra systoles or a rapid firing focus of atrial tachycardia often present themselves as initial triggers. Cardiac diseases predisposing atria to AF through structural changes such as ischaemic heart disease (IHD), or through electrical changes are known as substrates [62] [63]. AF events are dependent upon rapidly firing focus, multiple re-entrant circuit or rotors. When electrical impulse from extra systoles encounters the myocardium with variable excitability or refractoriness, electrical blocks can occur, giving rise to re-entry. Early and later after depolarisations contribute towards atrial ectopic foci. Reduced refractoriness, slow conduction and conduction barriers contribute towards re-entry [64]. In the event of an electrical block, electrical impulse circulates around an alternative circuit, repetitively exciting a region of the heart [65]. This in turn gives rise to generating additional re-entry circuits, ultimately maintaining arrhythmia. Re-entry occurs in various forms. Re-entrant pathways that affect the AV node, accessory pathways and the ventricular myocardium, often possess a long excitable gap, referring to the head of the re-entrant wavefront and the tail of the previous wavefront. Functional re-entry often occurs in myocardial ischaemia, where

there is little or no excitable gap, and the impulse propagates around a refractory core [66].

AF can be caused by and also causes electrical remodelling, contractile remodelling and structural remodelling in the heart, aiding in further perpetuation of arrhythmia, event otherwise termed as AF begets AF [67]. A study by Wijffels aimed to understand why AF tends to become more persistent over time and provides insights into AF's self-perpetuating cycle. Goats were connected to a fibrillation pacemaker, artificially maintaining AF. Electrophysiological changes observed included shortened atrial effective refractory period, increased inducibility and stability of AF [68]. These changes observed were found to be reversible within a week. Inducibility of AF was tested again goats after conversion to sinus rhythm and the inducibility of AF was still very high. Inducibility of AF decreased after 24 hours and by 1 week, had decreased further. Shortened atrial effective refractory period also became normalised after 1 week of sinus rhythm [68].

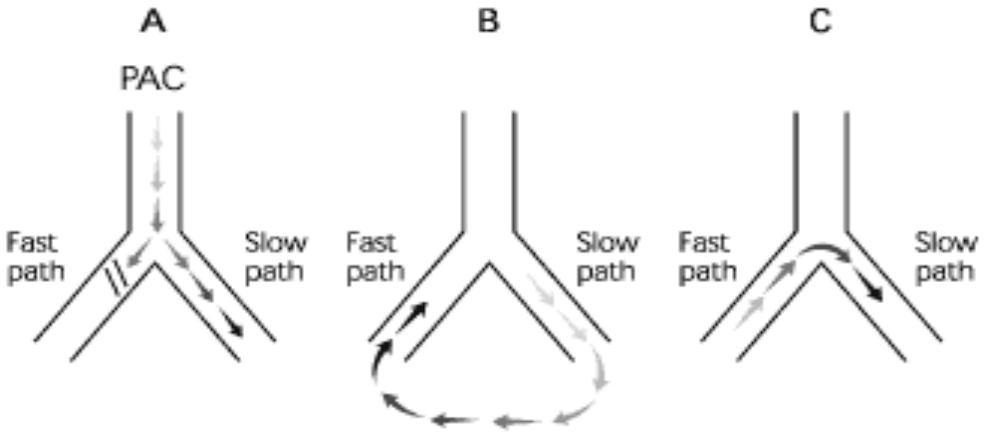

Figure 1.8. Mechanism for re-entry. A. Premature atrial complex arises after a block occurs in a fast pathway. Signals can still propagate down the slower pathway. B. The fast pathway has repolarized by the time the electrical signal reaches the end of the slow pathway, resulting in retrograde conduction of the wave. C. The signal travels back along the slower pathway creating a self-sustaining closed circuit. Figure taken from [69].

When treating patients with AF, their history must be evaluated, along with symptoms and duration of AF. This enables the classification of AF and helps guide the management of AF. Treatment of AF usually involves managing risk factors and concomitant diseases [70]. In patients, if there is presence of hemodynamic instability, they undergo direct current cardioversion and are put on anticoagulation. In the absence of hemodynamic instability, patients are either placed on a rhythm control strategy, where patients are administered drugs which help control heart rate or placed on a rate control strategy, where patients are administered drugs that aim to restore and maintain normal sinus rhythm [71]. Patients with severe asthma would preferentially be administered calcium channel blockers over beta-blockers. Patients with heart failure would not be administered beta-blockers [70]. Chapter 1.4.2 will delve further into classifications and mechanisms of drugs used in the treatment of AF. Patients may also undergo surgery for the treatment of AF. Catheter ablation can be offered as primary treatment or after anti-arrhythmic medication has failed. If catheter ablation is ineffective, surgical ablation may be performed [70].

AF is a multifactorial condition influenced by various factors such as underlying heart disease, genetics and comorbidities and not all patients will respond to treatment. Factors associated with better adherence include older age, history of diabetes or stroke and concomitant cardiovascular medications [72]. Reading's study investigated why some patients with AF struggled to adhere to their prescribed medications. Data were collected from self-reported questionnaires and electronic health records from patients with incident diagnosed AF. Risk factors for higher probability of non-adherence were

ethnicity, physical inactivity, memory decline and younger age, below 65. Patients above the age of 65 and with hypertension had lower probability of non-adherence [73].

1.4.2. Anti-arrhythmic drugs

Anti-arrhythmic drugs (AADs) are a group of medications used to treat abnormal heart rhythms. They work by restoring the heart's normal rhythms by modifying electrical properties within the heart. AADs are categorised according to their main mechanism of action, of which there are four, Class I, II, III and IV.

Class I drugs are sodium channel blockers and are typically used to treat ventricular arrhythmias. Class I drugs are further divided into three groups, Class Ia, Ib and Ic. Class Ia drugs bind to voltage gated Na^+ channels, blocking the Na+ current. Blocking these channels, slows the influx of Na^+ into the cell, decreasing the slope and amplitude of phase 0 of the action potential. The blocking of rapid Na^+ current influx slows the rate of depolarisation, slowing the conduction of signals, suppressing arrhythmias caused by abnormal conduction. In addition to Na^+ channels, class Ia drugs also block the K^+ ions. This leads to a slower rate of repolarisation therefore a longer effective refractory period (ERP). Examples of class Ia anti-arrhythmic drugs include quinidine, disopyramide and procainamide. All three have similar mechanism of action and can be used to treat supraventricular and ventricular arrhythmias. Some differences exist such as quinidine exhibits a longer QTc interval on an ECG compared to procainamide and disopyramide, thus better at restoring QT interval in patients with short QT syndrome [74] [75]. Disopyramide and quinidine exhibit slightly different effects on the $K_v11.1$, the α-subunit

of K^+ ion channel [75]. Class Ib drugs, blocks Na^+ channels and causes a mild degree of blockage and are used for ventricular arrhythmias only. Its weak effect on the Na^+ current means it has little effect on conduction. Class 1b drugs increase the efflux of K^+ ions, shortening the repolarisation and reducing APD. Example of Class Ib drugs include mexiletine, tocainide, aprinide and lidocaine. Class Ib drugs are known to shorten the action potential by shortening the repolarisation duration and reducing the refractory period. They also shorten QTc interval in long QT syndrome [76]. Class Ic drugs causes a more pronounced degree of Na^+ blockage compared to class Ia and Ib and significantly slow the conduction velocity of the heart. Unlike class Ia and Ib, class Ic drugs do not affect the QTc interval. Examples of class Ic drug include flecainide and propafenone and are often prescribed for ongoing management in patients without structural heart disease or ischaemic heart disease. It is generally contraindicated in patients with pre-existing heart disease or structural abnormalities, as they are thought to increase the risk of proarrhythmia [77]. Flecainide is more effective than propafenone for restoring sinus rhythm after acute AF, although propafenone is faster at achieving sinus rhythm [78].

Class II drugs are beta blockers and are used as rate control in patients with AF. Due to their safety profile, class II drugs are the first line of therapy for ventricular rate control in AF [79]. They are also used in management of supraventricular tachycardia. Beta blockers work by binding to beta-adrenergic receptors and blocking effects of epinephrine on the heart. Epinephrine, also known as adrenaline, increases heart rate and blood pressure. When epinephrine is blocked, the inotropic effects on the heart are inhibited, resulting in a potent anti-arrhythmic effect. Corresponding receptors for beta

blockers exist in three subtypes, β1, β2 and β3. Examples of first-generation beta blockers include propranolol and timolol. Examples of second-generation beta blockers include atenolol and bisoprolol [80]. Third-generation beta blockers include nebivolol and carvedilol [81]. This classification is based on their chemical structure and pharmacological properties. First generation beta blockers are non-selective and block both β1 and β2 receptors. Second generation blockers are more selective for β1 receptors and have fewer side effects than first generation beta blockers. Third generation beta blockers are highly selective for β1 receptors and also block β3 receptors and α1-adrenoreceptors.

Class III drugs are K^+ channel blockers and decrease K^+ efflux from the cell. Inhibition of K^+ efflux prolongs the action potential duration (APD) and repolarisation of cells. This results in a decrease in heart rate and stabilisation of electrical activity. Class III antiarrhythmic drugs include amiodarone, dronedarone and sotalol. Amiodarone is often used in the treatment of life-threatening ventricular arrhythmias, atrial fibrillation and ventricular tachyarrhythmias. It blocks the K^+ rectifier currents, prolonging APD and ERP. On an ECG, this presents as prolongation of QRS and QTc interval. Amiodarone also blocks beta-adrenergic receptors, Ca^{2+} channels and Na^+ channels [82]. Dronedarone was developed through modification of the structure of amiodarone. It is a noniodinated amiodarone and reported to be less effective than amiodarone but has less severe side effects. Dronedarone is a multi-channel blocker, blocking K^+, Na^+, Ca^{2+} and exhibits adrenergic properties. It reduces heart rate and blood pressure and has reduced infarct size in ischaemia/reperfusion animal models [83]. Early trials have suggested dronedarone prolongs time to recurrence of AF and reduces cardiovascular death and

hospitalisation [84]. Sotalol is a beta blocker as well as a K^+ channel blocker. Its K^+ channel blocking effect of sotalol is more dominant therefore it is considered a class III drug rather than class II drug. At low doses, sotalol exhibits adrenergic activity and at higher doses, it exhibits class III antiarrhythmic effects. Sotalol is used in treatment for premature ventricular contractions (PVC), hemodynamically stable ventricular tachycardia, maintaining sinus rhythm and supraventricular tachycardia. Like other class III drugs, sotalol prolongs APD and ERP in atria, ventricles, and nodal and extranodal tissues. It exhibits reverse use-dependent effects, meaning the slower the heart rate, the larger the block of K^+ current. [85].

Class IV drugs are known as Ca^+ channel blockers. These drugs block the voltage gated slow Ca^{2+} channels inward current. They decrease the slope of phase 0 and 4 and prolong phase 2 of the cardiac action potential, slowing down electrical conduction in the heart, increasing ERP, increasing AV node repolarisation, increasing PR interval and reducing heart rate. Class IV drugs are used to treat AF, atrial flutter, paroxysmal supraventricular tachycardia, hypertension and atrial tachycardia. Examples of class IV drugs include verapamil and diltiazem [77].

In addition to the four main classes of AADs, there are other drugs that have been developed for the treatment of arrhythmias which do not fit into the class system. These include adenosine and digoxin among many others. Adenosine is used for diagnosing and terminating SVT and also helps diagnose atrial flutter or tachycardia. Digoxin is used for ventricular rate control in patients with AF, in combination with a class II or class IV drug [77].

1.4.2.1. Flecainide pharmacology

Flecainide is a class Ic antiarrhythmic drug that was first synthesised in 1972 and FDA approved for use in 1984. It is used to prevent and treat abnormal heart rates, paroxysmal supraventricular tachycardia (PSVT) atrioventricular nodal re-entrant tachycardia (AVNRT), AV re-entrant tachycardia (AVRT), atrial fibrillation and atrial flutter in patients who do not have structural heart disease. It is administered orally and has been proven to be effective in treating cardiac arrhythmias. Flecainide has been studied in numerous clinical trials in humans and animal models and is now recommended as one of the first line of therapy in patients with AF and SVT to restore sinus rhythm. Studies have shown approximately 90% efficacy without profound adverse effects. It is considered to be highly effective at converting AF to sinus rhythm. The half maximal inhibitory concentration (IC_{50}) of flecainide is 1 – 2 µM at which flecainide blocks the cardiac fast inward Na^+ current, slowing the conduction in the heart and inhibits opening of K^+ channel including rapid component of the delayed K^+ current (I_{Kr}), prolonging the APD. At higher concentrations with IC_{50} of 19 µM, flecainide inhibits the late Na^+ current and other K^+ channels [86]. Scamps *et al* 1989 reported at higher doses, flecainide inhibited L-type Ca^{2+} current, when IC_{50} is at 20 µM. Reports have confirmed even at low doses, flecainide reduced premature ventricular contractions and ventricular tachycardia [87]. It has a high affinity for open-state Na^+ channels and slow unbinding kinetics from these channels, prolonging refractoriness and decreasing excitability [86]. On an ECG, this presents as prolongation of PR interval and the widening of the QRS complex. Interestingly, flecainide shortens the APD in the Purkinje fibres. During the plateau phase of the action potential, flecainide inhibits the slow

inward Na^+ current responsible for maintaining phase plateau, thus leading to a faster repolarisation, hence a shorter APD [86].

The binding mechanism of flecainide to $Na_v1.5$ channel has been studied extensively. It binds to the Na^+ voltage gated channel, $Na_v1.5$, occupying a hydrophobic cavity within the pore lumen of the intracellular side, making contact with S6 within domain IV, Figure 1.7. Under resting conditions, when $Na_v1.5$ channels are closed, flecainide has a low affinity inhibition, binding weakly to the channel. As frequency of stimulation increases, flecainide inhibition also increases, which progressively increases over the range of voltages when the channels are activated. The study revealed that flecainide preferentially interacts with $Na_v1.5$ channel in either its open or inactivated state and displays weak inhibition when the channel was in a closed state [88] [89]. Na^+ ions and flecainide compete for distinct and functionally overlapping binding sites within the pore. Flecainide occupying the binding site within the pore lumen of $Na_v1.5$ channel prevents Na^+ ions accessing the sites, ultimately inhibiting Na^+ current passing through the channel [88].

Flecainide also inhibits the rapid delayer rectifier K^+ current, $I_{Kr,}$ encoded by human Ether-à-go-go-Related Gene (hERG), also known as $K_v11.1$ or KCNH2, at clinically relevant concentrations. Mutations in the hERG can cause long QT syndrome and increased risk of sudden cardiac death. Flecainide binds to the inner cavity of Kv11.1 and interacts with S6 helix F656 residue, a principal binding determinant within the channel.

In voltage-gated K^+ channels $K_v2.1$ and $K_v1.5$, flecainide also interacts with the inner cavity at the subunit interface between S6 and P-helices [90].

Recent studies have reported flecainide use in the treatment of catecholaminergic polymorphic ventricular tachycardia (CPVT) in patients where β-blocker therapy was ineffective in suppressing arrhythmias. CPVT is characterised by hyperactivity of ryanodine receptor (RyR2) channels, caused by mutations in either *RyR2* gene or in its binding partner, calsequestrin (Casq2). Recent studies have reported that flecainide inhibits RyR2 activity [91]. Kryshtal *et al* 2021 also found flecainide significantly reduced RyR2 channel activity, even when Na^+ channels were blocked and exhibited a marked efficacy in prevention of ventricular arrhythmias in patients with CPVT [92]. Salvage's study explored the effects of flecainide on ryanodine receptor channel and demonstrated that at low concentrations, RyR2 channels were activated. However, at higher concentrations, flecainide inhibited the RyR2 channels [87]. This suggests that flecainide can bind to separate activation and inhibition sites on RyR2, with activation dominating in lower activity channels and inhibition dominating in more active channels [87]. The specifics of the binding mechanism of flecainide to RyR2 is unclear, but it has been established there are at least four inhibitory binding sites and one activation site in RyR2 channel. The specific location of the binding sites is unknown but it is thought that due to the voltage-dependence of three of the four inhibitory sites, these binding sites are located in the pore or transmembrane assembly. The activation site and one of the inhibitory sites is thought to be located on the cytoplasmic domains of the RyR2 channel. [87]. Flecainide inhibits RyR2 activity through two modes, via a fast block and

a slow block mechanism. The fast block mode refers to the rapid binding of flecainide to RyR2, stabilising the closed state of the channel. The channel is open for a significantly shorter time with a brief interaction between flecainide and the channel protein before the channel closes. The slow block mode refers to a slower transition between open and closed states of the channel, Figure 1.9. [93].

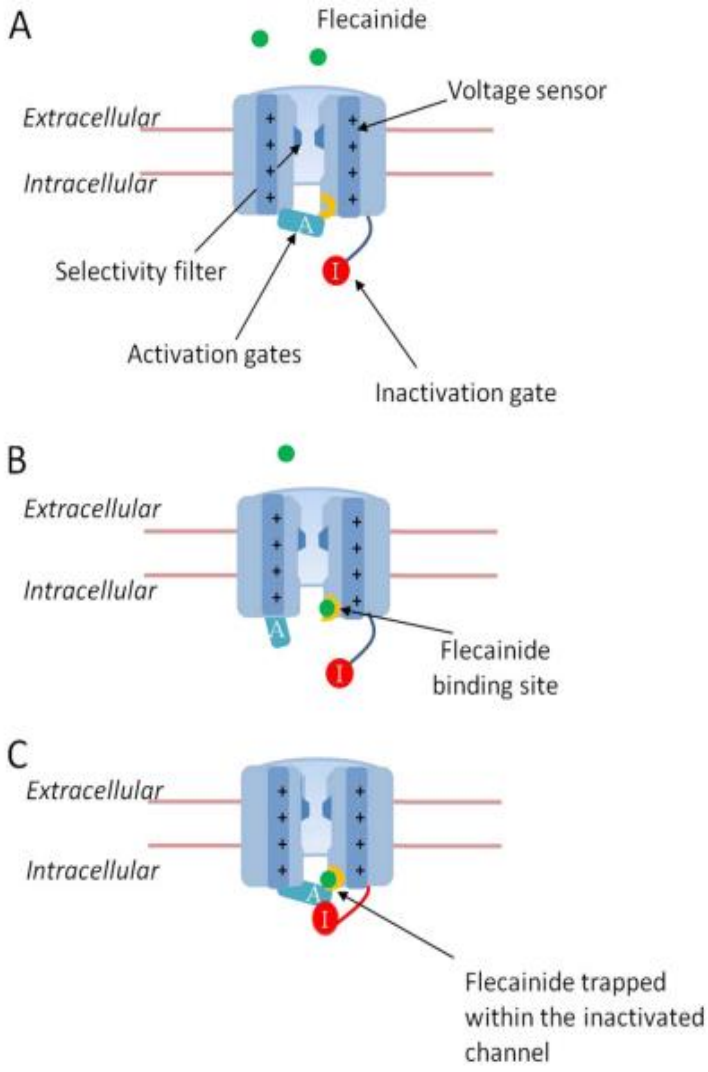

Figure 1.9. Schematic of binding of flecainide to VGSC in open, closed and inactivated state. A. $Na_v1.5$ channel in its closed state with flecainide unable to bind the channel. B. Voltage sensor detects membrane depolarisation driving the opening of activation gates, permitting selective Na^+ ion entry. Flecainide gains access to its binding site within the channel pore. C. Inactivation of the channel, involving the closing of inactivation gate occludes the pore trapping the flecainide in the channel. Figure taken from [94].

1.4.2.2 Flecainide and myocardial ischaemia interaction

Despite the successful antiarrhythmic effects of flecainide, the Cardiac Arrhythmia Supression Trial (CAST) revealed that flecainide and encainide, also a class Ic antiarrhythmic drug, was associated with increased proarrhythmic events in patients with pre-existing structural heart disease and coronary heart disease. CAST was designed to investigate if suppression of ventricular ectopy after a myocardial infarction (MI) reduced the incidence of sudden death. The trial revealed increased mortality in patients surviving MI. Flecainide suppressed arrhythmia in 1727 of 2309 post-MI patients with asymptomatic or mildly symptomatic ventricular arrhythmia and showed a higher incidence of 8.9% of arrhythmic death than placebo with 1.2% [87]. It was concluded that the excess number of deaths was due to arrhythmia and shock after acute recurrent MI in patients treated with flecainide and encainide [95]. The trial was terminated early due to excess mortality. Since the trial, flecainide has been contraindicated in patients with structural heart disease, second- and third-degree AV block, left bundle branch block (LBBB), right bundle branch block (RBBB), non-sustained ventricular tachycardia and patients with reduced ejection fraction below 35% [86]. The mechanisms underlying excess mortality associated with flecainide and encainide remain unknown. It is thought the interaction between active ischaemia and flecainide treatment may be responsible for the increased mortality observed in the CAST trial. Animal studies have shown ventricular proarrhythmia attributed to using flecainide and is suggested to be caused by rate-dependant conduction slowing in ischaemia and infarcted myocardium. This promotes heterogeneous conduction, facilitating initiation of re-entry. Echt *et al* 1991 also suggested that the negative inotropic properties of

flecainide and encainide contribute to the mortality of MIs and ventricular tachyarrhythmias [95]. Additionally, ischaemia significantly impacts action potentials and calcium handling. When there is reduced oxygen availability, ATP is depleted within cells causing K_{ATP} channels to open and allow K^+ to leave he cell. As extracellular K^+ concentration increases, and intracellular K^+ decreases, the cells end up becoming depolarised. This results in a shorter action potential due to earlier phase 3 repolarisation [96]. The loss of ATP also impacts the NKA pump leading to a further accumulation of extracellular K^+ ions. An ischaemia induced slow depolarisation leads to inactivation of Na^+ channels causing a reduction in the number of fast Na^+ channels available for action potential generation. Slope of the phase 0 of an action potential is slowed, slowing the rate of depolarisation [96]. The loss of ATP also inactivates the NCX, reducing Ca^{2+} efflux thus limiting the reuptake of Ca^{2+} into the endoplasmic reticulum resulting in calcium overload [97]. Since publication of CAST, there have been many flecainide safety analyses performed in patients with SVT which reported a 99% survival in control as well as drug groups including AADs such as flecainide [91].

Further studies are required to dissect the interaction between flecainide and ischaemia and understand the mechanism which leads to increased mortality.

1.4.2.3. Digoxin pharmacology

Digoxin is a cardiotonic steroid that comes from the foxgloves plant of *Digitalis lanata*. It is administered either intravenously or orally for management and treatment of mild to moderate heart failure and arrhythmias and was approved for clinical use in 1954. Digoxin has a bioavailability of approximately 75%, this can vary depending on diet of the patient [98]. Digoxin is usually used as a backup, when first line of therapy is ineffective. Ideally digoxin is used in patients with systolic heart failure with a reduced ejection fraction below 40%.

Digoxin has two mechanism of action, positive ionotropic and AV node inhibition. Through positive ionotropy, digoxin inhibits pumping of ions through NKA pump [99]. This partial NKA pump inhibition which induces an increase in intracellular Na^+ is sufficient to drive an influx of Ca^{2+} into the cells and reduce Ca^{2+} efflux via NCX. The resulting increase in intracellular Ca^{2+} in cytoplasm and SR enhances the force of contraction. Digoxin's second mechanism of action is through stimulation of the parasympathetic nervous system, slowing the electrical conduction of the AV node, decreasing the heart rate. Digoxin has the ability to mimic the action of the vagus nerve on the AV node.

Isoforms of NKA have various sensitivity to cardiac glycosides. α1 has low sensitivity to digoxin and α2 has high sensitivity to digoxin. The binding site of digoxin is located on the extracellular side on the NKA pump's α subunit. Specifically, it binds to the site on the fourth transmembrane helix of the α subunit, in close proximity to where ATP is hydrolysed [100].

Digoxin has a narrow therapeutic index. The recommended serum levels for digoxin is 0.8 to 1.2 ng/ml. Patients of digoxin therapy must be monitored to prevent digoxin toxicity. Digoxin toxicity causes a further inhibition of NKA that may lead to hyperkalaemia, a condition defined as excess levels of plasma potassium levels, causing arrhythmias and intracellular Ca^{2+} overload causing acidosis [99]. Like flecainide treatment, digoxin is also contraindicated in patients with acute myocardial infarction, ventricular fibrillation and myocarditis. Despite this, digoxin showed a neutral effect on mortality in clinical trials. The Rate Control Therapy Evaluation in Permanent Atrial Fibrillation (RATE-AF) aimed to compare the efficacy and safety of digoxin to bisoprolol in patients with permanent AF. Patients enrolled were over 60 years of age with AF and symptoms of heart failure and randomised to digoxin and bisoprolol treatment. The study found no significant difference in patient-reported quality of life at 6 months but digoxin was associated with symptom improvement at 12 months with fewer adverse effects compared to bisoprolol [101].

The aims of this thesis were to: -

- investigate atrial and ventricular differences in healthy wildtype mouse hearts.
- investigate the differential effects of flecainide in atria and ventricles from healthy wildtype mice.
- investigate the effects of flecainide in ischaemic conditions.
- Investigate the pro-arrhythmia effects of flecainide.

2. Methods

2.1. Ethics

All animal procedures were conducted in compliance with the rules and regulations of The Animals (Scientific Procedures) Act 1986, and approved by UK Home Office, PPL PFDAAF77F, and the institutional review board at the University of Birmingham. Mice were housed in ventilated cages with sex matched littermates, with a 12 hour light/dark cycle at 22°C and 55% humidity. Food and water were available *ad libitum.* Health of all mice were monitored daily, and pre and post procedures. The reporting of animal use conformed to the ARRIVE guidelines (Animal Research: Reporting of In Vivo Experiments).

2.2. Animal Models

Experiments were conducted on male and female wildtype (WT) mouse models, aged between 10 and 15 weeks. Animals were bred on the CD1 background. WT mice were purchased from Charles River Laboratories.

2.3. Optical Mapping Methods

2.3.1. Heart extraction

Using refined mouse handling technique, a technique using a tunnel or cupped hands to handle mice to avoid excess stress, mice were placed into an anaesthesia induction chamber [102]. Oxygen was switched on to 2 L/min and isoflurane to 5%. Once respiration rate had lowered and there was an absence of righting reflex, scavenger system was turned on and mice were transferred to mask to maintain anaesthesia. An intraperitoneal (IP) injection of 100 µl of heparin was administered as soon as anaesthesia was induced to prevent thrombus formation and allowed to distribute through the bloodstream for 1 minute. A pedal reflex was performed to ensure depth of anaesthesia. Mice were placed in supine position and limbs were taped down, leaving one limb free to allow retesting of pedal reflex. After loss of pedal reflex, ethanol was wiped across the chest and fur was removed from thoracic area. Thoracotomy was performed by making an incision below the diaphragm, and cutting ribcage on both sides and deflecting back, exposing the heart. Excess tissue was cut until the thoracic tissue pulled away from the torso. The dorsal ribcage and heart were removed and immediately placed into a beaker with filtered Krebs-Henseleit buffer with 50 µL of heparin, to remove excess blood. Krebs buffer contained (in mmol/L): sodium chloride (NaCl) 114.0, potassium chloride (KCl) 4.0, calcium chloride (CaCl) 1.6, sodium bicarbonate ($NaHCO_3$) 24.0, magnesium sulphate ($MgSO_4$) 1.0, monosodium phosphate (NaH_2PO_4) 1.1, glucose ($C_6H_{12}O_6$) 11.0 and sodium pyruvate (C3H3NaO3)1.0. Calcium chloride and glucose were added on the day of the experiment. As shown in Figure 2.1,

the heart preparation was placed onto a silicon dish and pinned down. Lung tissue and adipose tissue were removed. Using a surgical silk suture, the descending aorta was cannulated, and heart was retrogradely perfused with 2 ml of Krebs-Henseleit buffer and 100 µl of heparin with a strength of 1000 I.U./ml, to flush out blood from the heart. After cannulation, the preparation was transferred to the optical mapping rig.

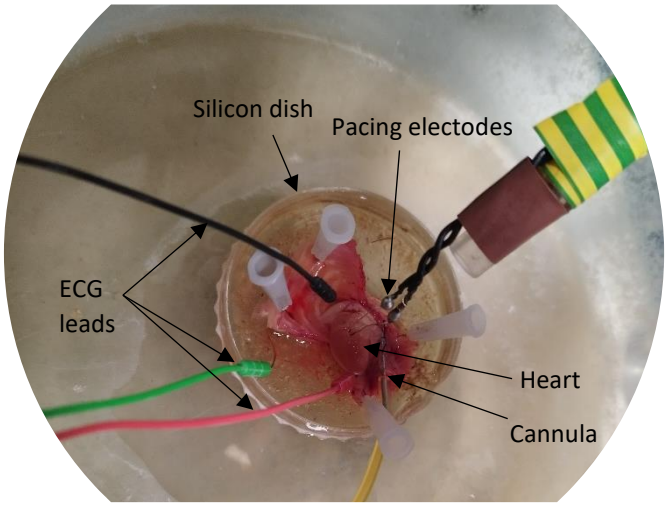

Figure 2.1. Experimental heart preparation for optical mapping. An image of a heart preparation for optical mapping. Heart preparation is pinned onto the silicon dish and descending aorta is cannulated allowing perfusion of the heart with Krebs-Henseleit solution. ECG leads are attached accordingly to record a pseudo ECG signal.

2.3.2. Optical mapping setup

Figure 2.3 shows a schematic representation of a typical optical mapping system. Hearts were placed in a double water jacketed chamber to maintain an environmental temperature of 37°C for the heart. The perfusate was oxygenated with 95% O2 - 5% CO2 and kept at 37°C in a water-bath. Blebbistatin was added to the perfusate at a final

concentration of 12 µM. Blebbistatin (100 mg; Axon Medchem, The Netherlands) was reconstituted in 1 ml dimethyl sulfoxide (DMSO) and stored in 70 µl aliquots of 50 mg/ml at -20°C. Blebbistatin was added to the experiments to remove motion artefacts. The oxygenated perfusate was pumped through the system at 4 ml/min, 80 mmHg in accordance with other studies, using an Ismatec pump [103] [104]. Electrocardiogram (ECG) leads were attached, and a pseudo bipolar ECG was recorded on LabChart, a signal generated from propagation of electrical signals undergoing inhibition of contraction, Figure 2.2. After 10 minutes of recovery, and spontaneous ECG recording, voltage membrane dye, Di-4-ANEPPS (5 mg/ml) was injected at a rate of 1 ml over 5 minutes, into the heart via a perfusion port. Di-4-ANEPPS (50 µM; Biotium, California, USA) was reconstituted in 1 ml DMSO and stored in 25 µl aliquots of 5 mg/ml at 4°C. For each experiment, each aliquot was mixed with 1 ml Krebs solution and injected. Hearts were illuminated with three LED lights (530 ± 25 nm) and emitted light collected at >630 nm. The LED lights were controlled by Dual Optoled Power supply (Cairn, UK), and was adjusted accordingly to minimise phototoxicity and photobleaching. The LED lights illuminate the heart or tissue sample, exciting the photons which are detected by Evolve Delta, electron multiplied charged coupled device (EMCCD) cameras. Two EMCCD cameras (Photometrics, USA), with a 500 Hz sampling rate, 64 x 64 pixels and a spatial resolution of 320 µm/pixel, were used to each capture action potentials and calcium transients separately. The EMCCD cameras enable high resolution recording therefore ideal for recording rapid fluorescent changes on the epicardial surface. The cameras were run by MetaMorph software (California, USA) which control binning, exposure time and number of frames. Either Winfluor software or Spike software were used to

run pacing protocols. Pulse height and pulse width were fixed at 5 V and 0.001 s respectively and pacing protocol was designed according to experiments. The voltage for driving the pacing stimulus was controlled by a constant voltage isolated simulator (Digitimer, UK).

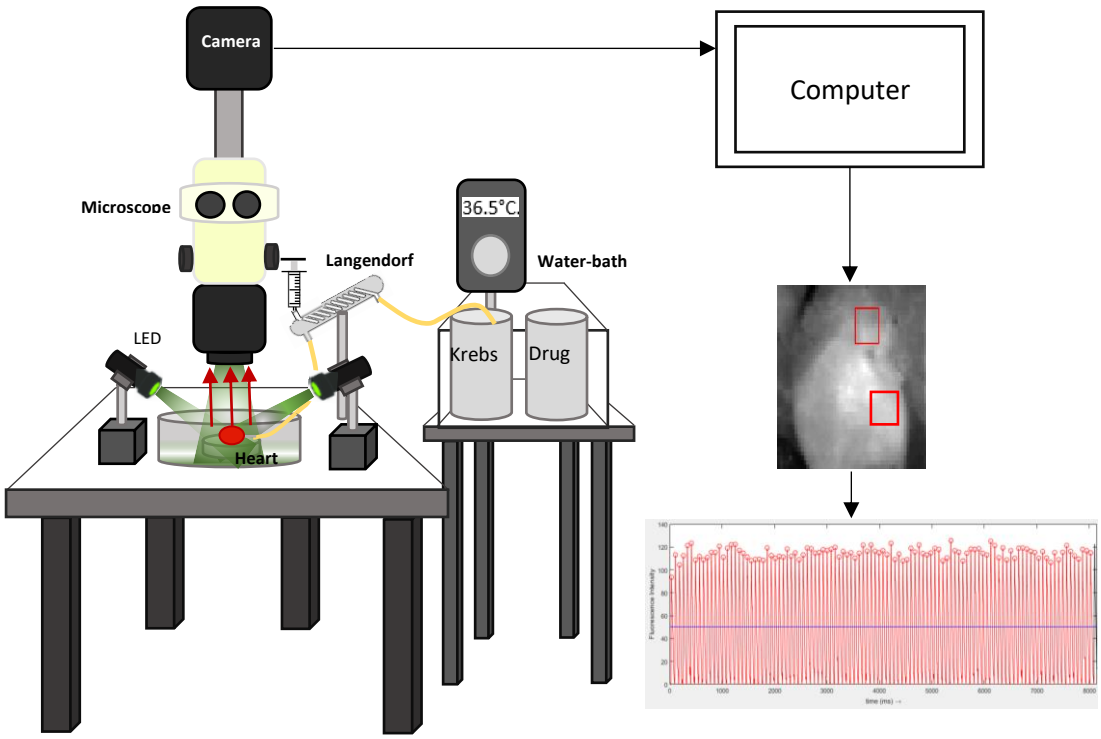

Figure 2.2 Typical optical mapping setup. Heart is continuously perfused with oxygenated buffer. A voltage sensitive dye, Di-4-ANEPPS, is injected into heart. LEDs illuminate the sample, and the dye is excited and emits fluorescent photons, indicated by red arrows. Photons are filtered and directed to an imaging detector to produce a time series dataset. Dataset was processed using ElectroMap (developed by O'Shea). Figure created by author of this thesis.

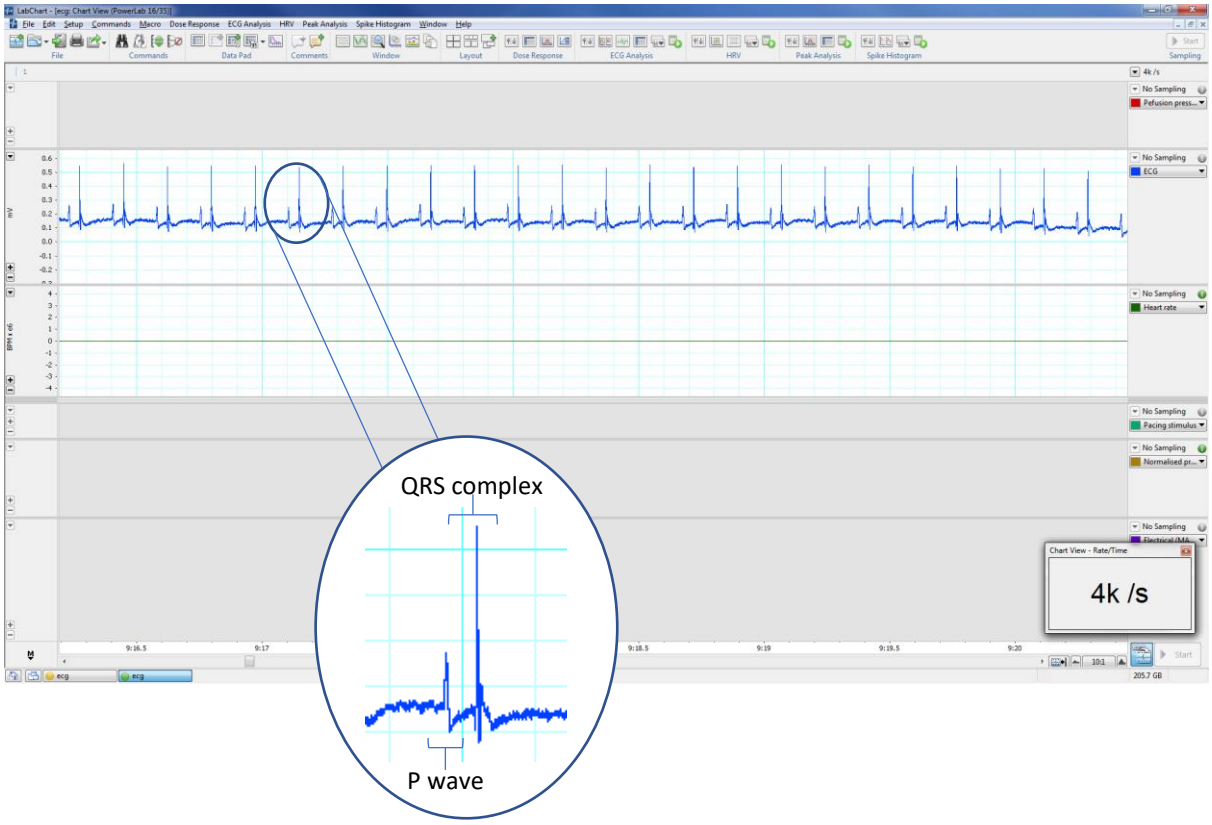

Figure 2.3. Pseudo ECG recording from mouse heart. *In-vitro* recorded pseudo-ECG recorded from electrodes surrounding the heart, on LabChart, and a magnification of a single ECG trace with P wave and QRS complex labelled.

2.3.3. Ventricular recordings

Whole hearts were mounted onto the optical mapping rig and perfused with filtered, oxygenated Krebs-Henseleit buffer. ECG electrodes were attached around the heart within close proximity. Heart was allowed to recover for 10 minutes and di-4-ANEPPS was added. Using live imaging in MetaMorph, we observed ventricles loading with fluorescent dye first. Success of dye loading and quality of action potential signals were checked before continuing with the experiment. Silver bipolar electrodes were placed at the base of the ventricles for pacing. Pacing threshold was established and doubled.

The ventricles were paced from 160 ms/CL, decreasing in 10 ms/CL decrements to 50 ms/CL, as shown in Table 1, using LabChart or Spike. The pacing protocol was created to enable us to observe electrophysiological changes at a physiological heart rate ranging between 500 and 700 bpm and observe rate-dependent differences (Ho et al 2011). Ventricles were paced for 60 seconds to achieve a steady state, before being captured at a framerate of 0.454 kHz with a pixel size of 196 μM. MetaMorph was used to image and record electrical activity detected by the camera. All ventricular recordings in this study were taken from a 9 x 9 pixel area in the left ventricle (LV) region. Ventricular recordings were initially taken from the whole ventricles, but in order for the data to be comparable to atrial recordings, we decided to keep the region of interest the same in ventricles and atria. A summary of the experimental protocol is shown in Figure 2.6.

2.3.4. Regional recordings in ventricles

In order to measure regional differences in ventricles, the ventricles were divided into six 9 x 9 pixel sections, LA-apical, LA-middle, LA-basal, RA-apical, RA-middle and RA-basal, as shown in Figure 2.5. APD, CV, amplitude, activation measurements were taken from each section and compared to one another.

2.3.4.1. Data analysis

Optical mapping recordings were processed using ElectroMap. Data comparing the regional differences in the ventricles at a range of pacing frequency, were analysed using

a two-way Analysis of Variance (ANOVA) with Tukey's post hoc analysis. Data comparing regional differences at 10 Hz were analysed using paired t-tests. Statistical analysis was performed using GraphPad Prism 8.0. Data were expressed as mean ± standard error and significance was taken as $P<0.05$, with * denoting $P<0.05$, ** denoting $P<0.01$, *** denoting $P<0.001$, and **** denoting $P<0.0001$.

2.3.5. Atrial recordings

Ventricular and atrial recordings were taken from the same heart. Ventricles were paced first, then the heart was loaded further with Di-4-ANEPPS until atria was loaded and pacing protocol, Table 1, was repeated. Loading the atria resulted in overloading of ventricles, therefore recordings would no longer be able to be collected from the ventricles. To prevent dye loading of the atria, quality of action potential signals were checked during the loading of the dye. Pacing electrodes were placed on the right atria (RA) and recordings were taken from left atria (LA). Atria was paced for 60 seconds to achieve a steady state, before being captured at a framerate of 0.454 kHz with a pixel size of 196 μM. A summary of the experimental protocol is shown in Figure 2.6.

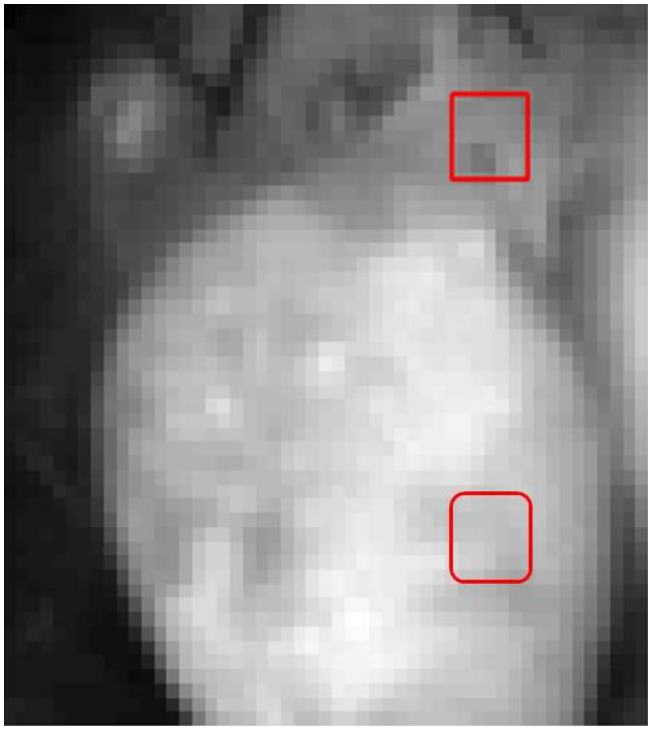

Figure 2.4. Region of interest selected in the atria and ventricles. A 9 x 9 pixel region of interest selected in atria and ventricles for direct comparison.

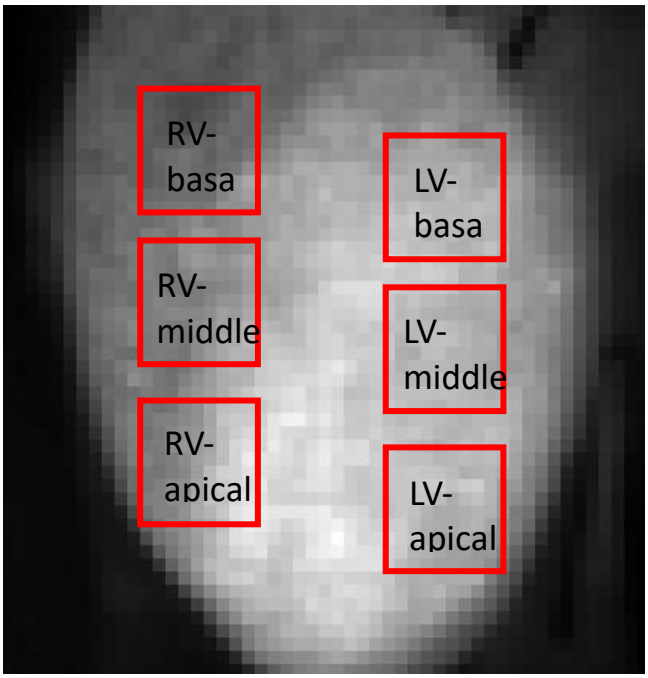

Figure 2.5. Ventricular regional sections. Ventricles were divided into six sections, RV-basal, RV-middle, RV-apical, LV-basal, LV-middle and LV-apical.

Frequency	Cycle length	Beats per minute	Duration
6.25 Hz	160 ms/CL	375 bpm	1 minute
6.67 Hz	150 ms/CL	400 bpm	1 minute
7.14 Hz	140 ms/CL	428 bpm	1 minute
7.69 Hz	130 ms/CL	460 bpm	1 minute
8.33 Hz	120 ms/CL	500 bpm	1 minute
9.09 Hz	110 ms/CL	545 bpm	1 minute
10.00 Hz	100 ms/CL	600 bpm	1 minute
11.11 Hz	90 ms/CL	667 bpm	1 minute
12.50 Hz	80 ms/CL	750 bpm	1 minute
14.29 Hz	70 ms/CL	857 bpm	1 minute
16.67 Hz	60 ms/CL	1000 bpm	1 minute
20.00 Hz	50 ms/CL	1200 bpm	1 minute

Table 1. Pacing frequencies, in Hz, ms/CL and bpm, used to pace atria and ventricles. Atria and ventricles were paced via bipolar silver pacing wires for 1 minute at each pacing frequency.

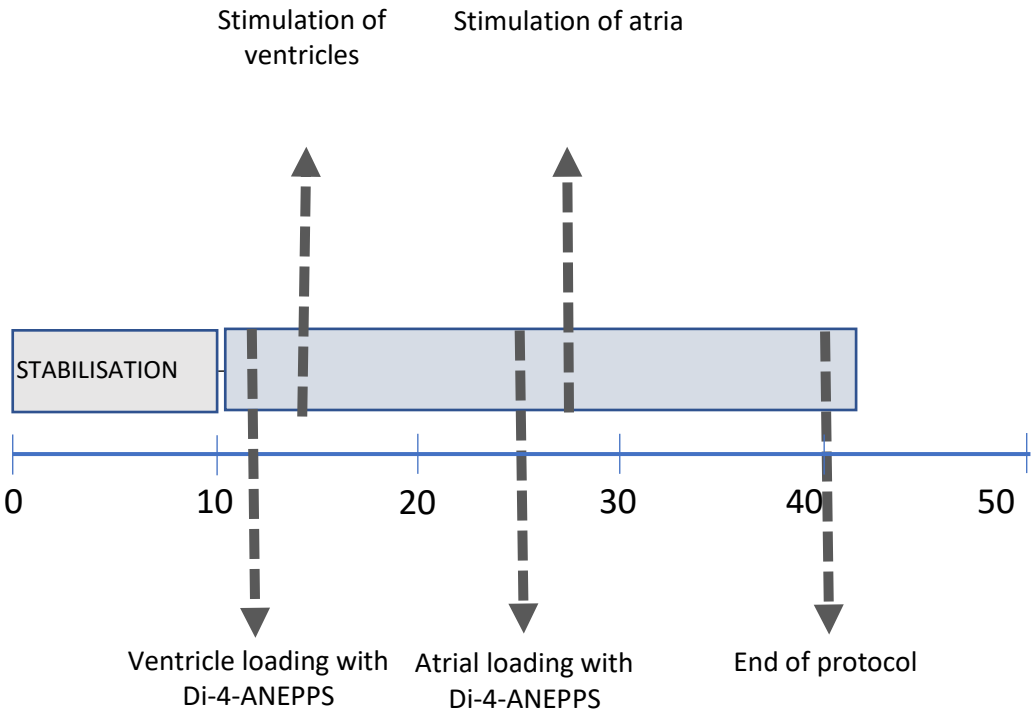

Figure 2.6. Summary of ventricular and atrial pacing protocol. Hearts were stabilised for 10 minutes. Ventricles were loaded and pacing protocol performed. Atria were loaded in the same hearts and pacing protocol repeated.

2.3.5.1. Data Analysis

Optical mapping recordings taken from the atria and ventricles were processed using ElectroMap. Measurements comparing baseline atria and ventricles at a range of pacing frequencies were analysed using two-way ANOVA with Tukey's post hoc analysis. Student's t-test was performed when comparing atrial and ventricular recordings at 10 Hz. Statistical analysis was performed using GraphPad Prism 8.0. Data were expressed as mean ± standard error and significance was taken as $P<0.05$, with * denoting $P<0.05$, ** denoting $P<0.01$, *** denoting $P<0.001$, and **** denoting $P<0.0001$.

2.3.6. Drug treatment

Hearts were isolated and loaded onto optical mapping rig as described in section 2.3.1. Recordings from atria and ventricles were taken from different hearts. This was because ventricles and atria loaded at different rates. Ventricles loaded before the atria, therefore it was not possible to measure baseline recordings in both atria and ventricles together before adding the relevant drug. Ventricles and atria were loaded with Di-4-ANEPPS and paced according to Table 1. At the end of baseline pacing, flecainide was washed in for 15 minutes. This accounted for the time it took for the drug solution to reach the heart and the onset of action. After 15 minutes of flecainide perfusion, pacing threshold was established and pacing protocol was repeated. A summary of the experimental protocol is shown in Figure 2.7.

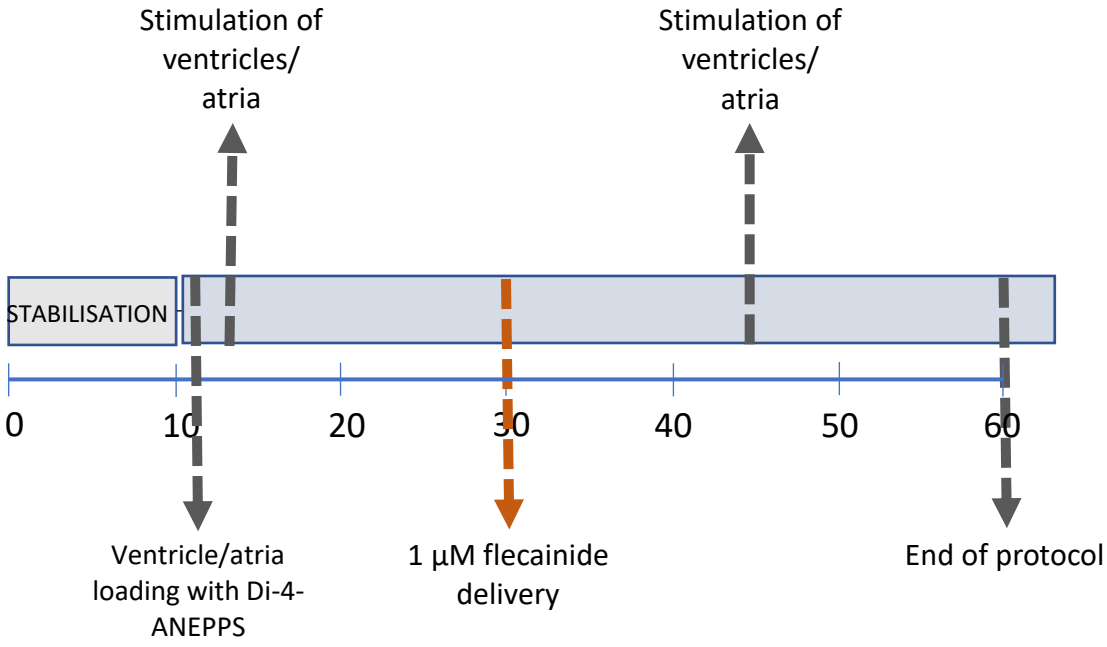

Figure 2.7. Summary of ventricular and atrial pacing protocol with drug treatment. Hearts were stabilised for 10 minutes. Atrial and ventricular recordings were taken from different hearts. Ventricles or atria were loaded and pacing protocol performed. Flecainide was added and perfused through the heart for 15 minutes. Pacing protocol was repeated for the stimulation of either ventricles or atria.

2.3.3.1 Data analysis

Recordings taken from the atria and ventricles at baseline and after flecainide treatment were processed using ElectroMap. Measurements comparing atria and ventricles at baseline and after flecainide treatment at a range of pacing frequencies were analysed using two-way ANOVA with Tukey's post hoc analysis. Unpaired t-test was performed when comparing baseline and flecainide, atrial and ventricular recordings at 10 Hz. Statistical analysis was performed using GraphPad Prism 8.0. Data were expressed as mean ± standard error and significance was taken as $P<0.05$, with * denoting $P<0.05$, ** denoting $P<0.01$, *** denoting $P<0.001$, and **** denoting $P<0.0001$.

2.4. Ischaemia protocols

2.4.1. Low flow rate perfusion

Hearts were prepared and loaded as specified in section 2.3.1. Once di-4-ANEPPS had been loaded and diastolic threshold had been established, a baseline recording was taken. Ventricles were paced from 7.14 Hz to 14.29 Hz in a 10 ms/cL increment. A pacing protocol was created using Spike software. Hearts were stimulated at each cycle length for 10 beats and paced at 120 ms/CL between pacing ramps. For the pilot study, two flow rates were tested. After baseline, ischaemia was induced by lowering the flow rate by 40%, from 4 ml/min to 2.4 ml/min and lowering the flow rate by 60%, from 4 ml/min to 1.6 ml/min. Pacing protocol was repeated every 10 minutes. A summary of the experimental protocol is shown in Figure 2.9.

2.4.2. Low perfusion pressure perfusion

Hearts were prepared and loaded as specified in section 2.3.1. Di-4-ANEPPS was loaded and diastolic threshold was established. Ventricles were paced from 7.14 Hz to 14.29 Hz in a 10 ms/cL increment. A baseline recording was taken and ischaemia was induced by lowering the perfusion pressure by 40%, from 80 – 90 mmHg to 50 mmHg. After 10 minutes of stabilisation period, di-4-ANEPPS was added and threshold was established. Ventricles were paced and a baseline recording was taken. As shown in Figure 2.9, ischaemia was induced for 30 minutes and 1 µM flecainide was added 15 minutes after

ischaemia was induced. Flecainide was allowed to wash in for 15 minutes. Pacing protocol was done every 10 minutes.

2.3.4.3 Data analysis

Optical mapping recordings taken from the ventricles were processed using ElectroMap. Hearts with a heart rate that fell below 300 bpm, or did not load with dye evenly were excluded from the study. Measurements comparing different treatment groups at a range of pacing frequencies were analysed using multiple t-test. One-way ANOVA was performed when comparing treatment groups at 10 Hz. Statistical analysis was performed using GraphPad Prism 8.0. Data were expressed as mean ± standard error and significance was taken as $P<0.05$, with * denoting $P<0.05$, ** denoting $P<0.01$, *** denoting $P<0.001$, and **** denoting $P<0.0001$.

2.4.3. Regional ischaemia via LAD ligation

After isolation and cannulation, the heart was immediately loaded with voltage membrane dye, RH-237 and calcium dye Rhod 2 AM. Unlike previous datasets, dyes were added before loading onto optical mapping rig. This was to ensure even loading of dyes across the heart before ligation. For each experiment, a needle was inserted around the left anterior descending artery (LAD), above the Diagonal 1 and Diagonal 2 coronary arteries, Figure 2.8. This was to eliminate the effects of the needle damaging the tissue and determine the effects of the LAD ligation itself. The heart was loaded onto

the optical mapping rig. ECG leads were attached and heart was given time to stabilise. A baseline recording was taken and then the suture tightened in the relevant experiments, ligating the LAD. Excess suture was snipped off, and pacing protocol was repeated. The ventricles were paced every 10 minutes and 1 µM flecainide was added 15 minutes after LAD ligation. At the end each experiment, Evans blue dye was flushed through the heart via the cannula to visualise the area of blockage and ensure accuracy and success of LAD ligation.

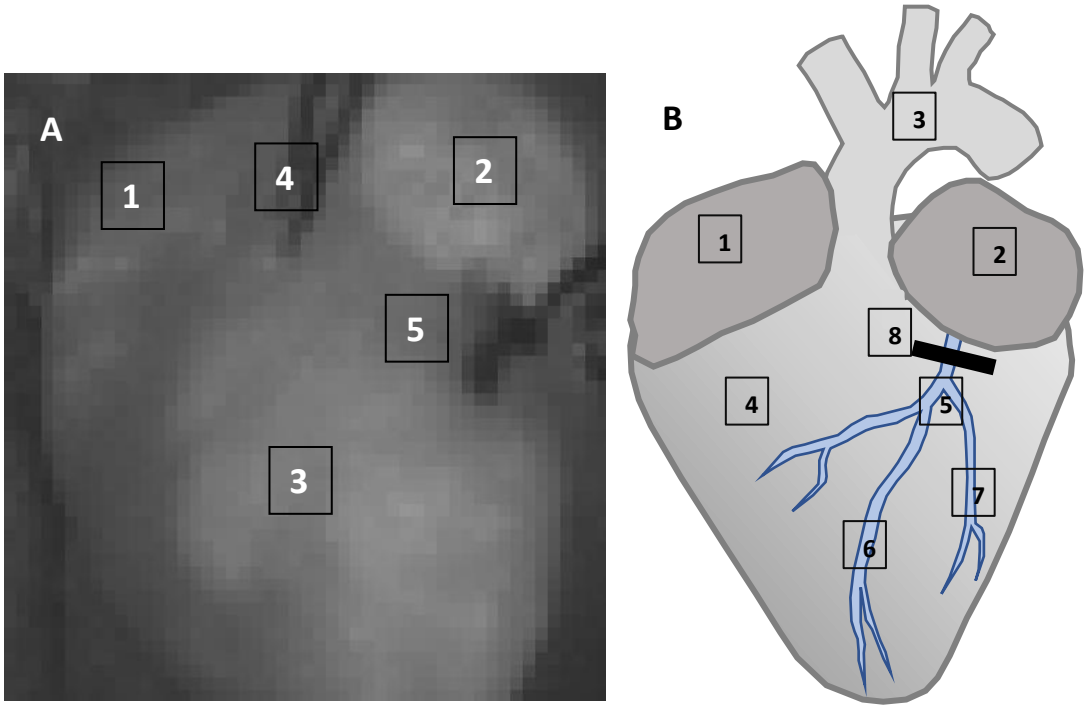

Figure 2.8. Image and schematic of a LAD ligation. A. Ligated heart imaged under EMCCD camera during optical mapping showing, 1. RA, 2. LA, 3. Ventricles, 4. Pacing electrodes, 5. Ligation. B. Representation of a LAD ligation in *ex vivo* mouse heart showing 1. RA, 2. LA, 3. aortic arch, 4. ventricles, 5. left anterior descending artery, 6. Diagonal 1, 7. Diagonal 2, 8. location of the ligation. Figure created by author of this thesis.

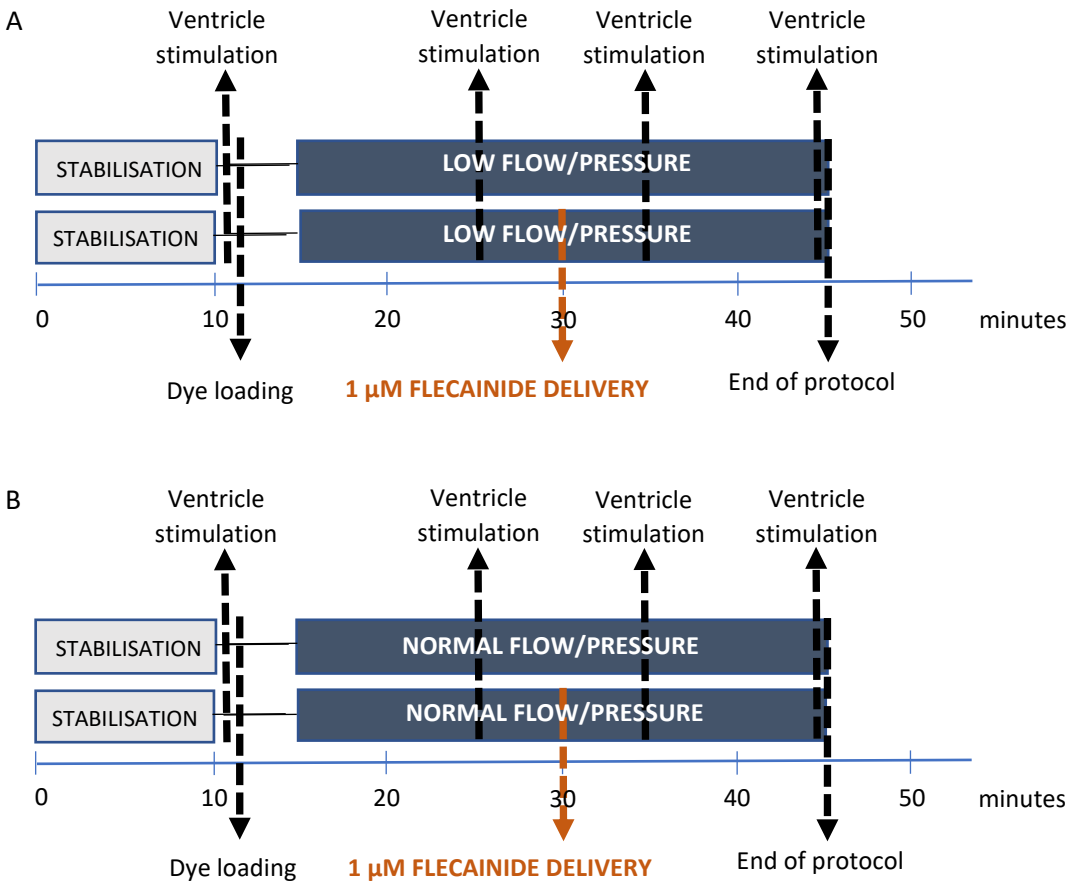

Figure 2.9A-B. Summary of ischaemia experimental protocol. Hearts were allowed to stabilise for 10 minutes. Pacing protocol was performed and ischaemia was induced in relevant experiments, either by reducing flow rate or reducing perfusion pressure. Pacing protocol was repeated every 10 minutes. 1 µM flecainide was added at 30 minutes. Flecainide was washed in for 15 minutes and pacing protocol repeated.

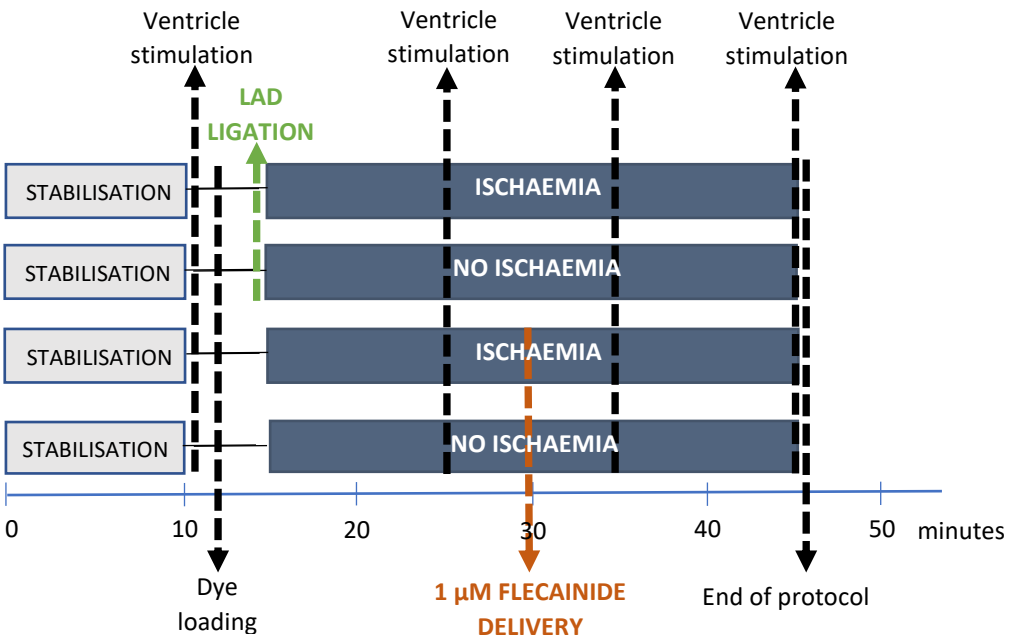

Figure 2.10A-B. Summary of ischaemia experimental protocol. Hearts were allowed to stabilise for 10 minutes. Pacing protocol was performed and ischaemia was induced in relevant experiments, through LAD ligation. Pacing protocol was repeated every 10 minutes. 1 µM of flecainide was added at 30 minutes in relevant experiments. Flecainide was washed in for 15 minutes and pacing protocol repeated.

2.5. Calcium transient recordings

Calcium transients were recorded simultaneously to voltage membrane potential with two separate EMCCD cameras. To record calcium transients and action potentials simultaneously, fluorescent dyes, fast-responding potentiometric probe, RH-237, and high affinity calcium indicator, Rhod-2 AM, was used to prevent overlapping of wavelength emission. RH-237 used for visualising action potentials, has an excitation peak at 550 nm and an emission peak at 786 nm. Rhod-2 AM, used for visualising calcium transients, has an excitation peak at 553 nm and an emission peak at 577 nm. The dyes should have distinct excitation and emission wavelengths to avoid overlap and allow for clear differentiation of the signals. Wavelength excitation and emission of Di-4-ANEPPS, which was used for initial optical mapping experiments, is 482 nm and 686 nm respectively and signals would not have been clearly defined from the calcium transient. Calcium transient duration (CaTD) was measured from the upstroke to 50% repolarisation or calcium decay.

2.6. Data Analysis

Optical mapping recordings taken from the ventricles were processed using ElectroMap. Measurements comparing different treatment groups at a range of pacing frequencies were analysed using mixed factor ANOVA. Statistical analysis was performed using GraphPad Prism 8.0. Data were expressed as mean ± standard error and significance was taken as $P<0.05$, with * denoting $P<0.05$, ** denoting $P<0.01$, *** denoting $P<0.001$, and **** denoting $P<0.0001$.

2.7. ElectroMap processing

All optical mapping data were analysed using ElectroMap which ran on MATLAB. ElectroMap is an adaptable, high-throughput, open source software that allows processing of complex electrophysiology datasets that require high spatio-temporal resolution. It provides analysis of important electrophysiological properties such as action potential morphology, conduction velocity (CV), activation time, calcium transient morphology, amplitude, diastolic interval and time to peak [105]. A region of interest i.e. left atria or ventricle, was selected and image processed using Gaussian spatial filtering of 3 x 3. Action potential duration (APD) was taken at 50% and 80% repolarisation with the APD start time being defined as the maximum upstroke of the action potential [105]. CV was measured using a multi vector method, and single vector method was also used to compare both methods. The CV was quantified using the Bayly method with a 5 x 5 window size. Activation time was defined as the midpoint of depolarisation [105].

3. Investigating differences in electrical properties in atria and ventricles

3.1 Chapter Introduction

Atria and ventricles are distinct in their physical characteristics as well as their functions. They also exhibit significant differences in their electrical properties. They differ in size, thickness, mass, contractile properties, refractory periods, calcium handling, and there are also differences between atria and ventricles in structure and organisation of ionic channels [106]. It has been firmly established that action potentials differ in atria and ventricles. The ventricles have a longer repolarisation phase compared to atria. This is due to differences in ionic channel composition and presence of certain ion channels, such as $K_v1.5$ channels. This difference in action potential waveform has been observed among many species including humans and mice [107].

Our study investigated the biophysical properties of sodium channels. We quantitively compared Na^+ current in cardiomyocytes isolated from mouse left atria and left ventricles and found significantly lower Na^+ current in the atria compared to ventricles at physiological resting membrane potential [108]. This is a fundamental finding since previous studies have investigated Na^+ currents at non physiological resting membrane potential. Differences in peak sodium channel currents in atria and ventricles would indicate a difference in the conduction velocity (CV). CV is defined as the speed at which APs are propagated across the heart. It plays a pivotal role in ensuring synchronicity and time of excitation and contractions. Lower expression of Na^+ channels result in slower

CV, as observed in the AV node [109]. Other factors that affect CV include efficiency and density of gap junctions and cellular architecture [110]. Thomas *et al*, 1998, investigated effects of connexin43 deficiency on the conduction velocity of atria and ventricle in isolated mouse hearts. They found in wildtypes (WTs), atrial (CV) was slower than ventricular conduction velocity [111]. Draper and Mya-Tu, 1959, studied conduction velocities across different tissue types and species. They found little differences between chambers in cat and dog hearts, and slower ventricular conduction velocity in goat ventricles compared to atria [112]. These studies demonstrate a need for further study into looking at conduction in atria and ventricles. The differences observed between papers in conduction velocities between atria and ventricles is possibly down to differences in ion channel expression and density of gap junctions between species. Many of these studies have not investigated mouse models and our data could add to why there are differences among species. Although there are studies available that have investigated ion channel expression between atria and ventricles in different species, studies investigating the differences in the density of gap junctions is very limited. Gap junctions are mediated by connexins and the major cardiac connexin proteins are Cx40, Cx43 and Cx45 [113]. These proteins have distinct expression patterns. Atrial connexin expression has been shown to have a larger variation between species compared to ventricular expression [114]. It could be that differences in conduction observed may be down to connexin expression and future studies can potentially investigate expression of connexin isoforms in atria and ventricles.

The susceptibility to arrhythmias differs markedly between atria and ventricles due to anatomical, physiological and electrophysiological differences. The shorter refractory

period and higher automaticity possessed by atria increases vulnerability to re-entry mechanisms and ectopic activity, and the differences in ion channel expression and resting membrane potential affect the responsiveness to triggers for arrhythmias such as atrial fibrillation (AF). Atria are also more susceptible to stretch and oxidative stress which are also triggers for arrhythmias as well as other heart diseases [115]. In contrast to atria, ventricles are less prone to automaticity and have longer refractory periods, reducing the risk of re-entry-based arrhythmias. However, ventricles can still develop life-threatening arrhythmias such as ventricular tachycardia (VT) and ventricular fibrillation (VF). Ventricles have a large impact on cardiac output, meaning ventricular arrhythmias are usually immediately life threatening. Although atrial arrhythmias are not as immediately life threatening, they can still lead to increased morbidity and increase risk of stroke and other cardiovascular diseases further down the line [115].

Through comprehensively studying electrical differences in the atria and ventricles, we strengthen our understanding of cardiac physiology and mechanisms behind arrhythmias and other cardiovascular diseases, leading to targeted interventions for cardiac diseases.

In this chapter, we aim to answer some of these questions. Using optical mapping technique, we will measure electrical activity in the atria and ventricles and discuss the importance of our findings. The patch clamp and western blot data presented in Chapter 3, Figures 3.1 and 3.2, were performed and analysed by Dr O'Brien. The data has been added as it provides a strong rationale for measuring conduction velocity differences

between atria and ventricles and has been published in article for which I am a co-author on.

The aims of this investigation were to: -

- determine electrophysiological characteristics in atrial and ventricular tissue using optical mapping and understand chamber specific differences.

- determine electrophysiological heterogeneities across ventricular tissue, using optical mapping.

3.2 Chapter Results

3.2.1. $Na_v1.5$ and β subunit expression in mouse LA and LV

Firstly, we examined the differences in protein expression of Na^+ channel subunits in atria and ventricles. In mouse hearts, $Na_V1.5$ expression was higher in the left atria when compared to left ventricles, $Na_V\beta2$ and $Na_V\beta4$ expression was lower in left atria when compared to left ventricles, Figure 3.1. This indicates that the β-subunits may be responsible for the sodium ion channels opening at a more negative membrane potential. A negative shift in activation usually leads to earlier activation of the sodium ion channel, altering the excitability of the cell. This also correlates with our data which found that expression of $Na_V\beta4$ is significantly lower in healthy human LA compared to the LV, which can potentially be pro-arrhythmic [108].

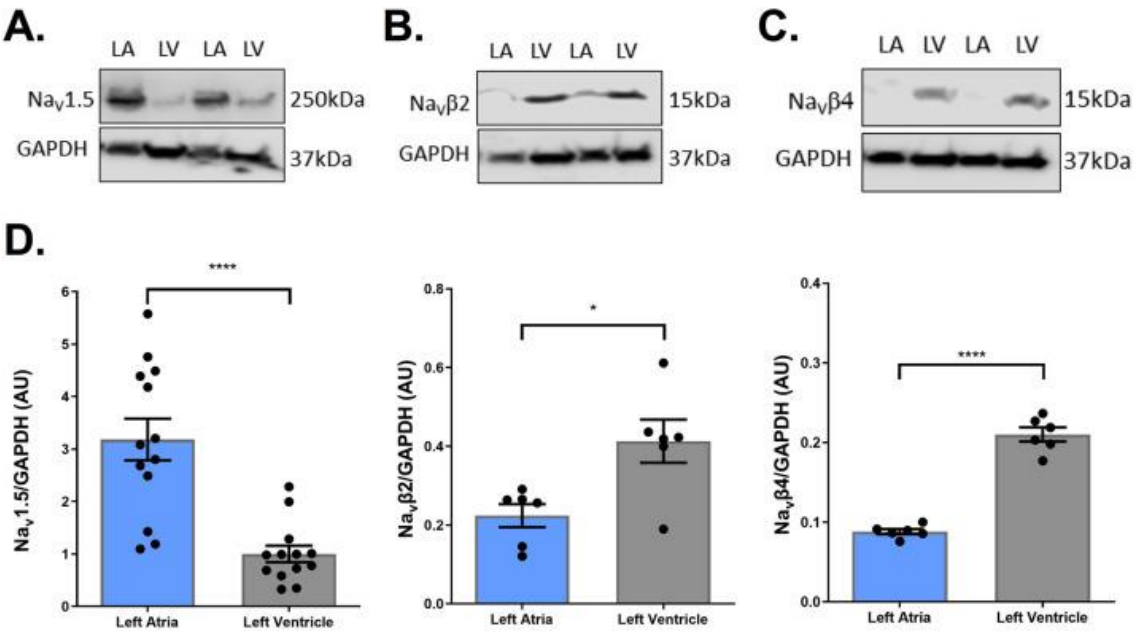

Figure 3.1 Protein expression of sodium channel proteins in mouse tissue. A. Western blots showing the protein expression of $Na_V1.5$ from mouse left atrial (LA) and left ventricular (LV) samples. B. Western blots showing the protein expression of $Na_V\beta2$ from mouse LA and LV

samples. C. Western blots showing protein expression of $Na_V\beta4$ from mouse LA and LV samples. D. Blots were normalized to GAPDH. $Na_V1.5$ showed a higher relative expression in the LA, when compared to the LV (LA = 3.18 ± 0.40 AU; LV = 1.00 ± 0.16 AU; *n* = 13) ****$p < 0.0001$. Both $Na_V\beta2$ (LA = 0.22 ± 0.03 AU; LV = 0.41 ± 0.05 AU; *n* = 6, *$p < 0.05$) and $Na_V\beta4$ (LA = 0.09 ± 0.003 AU; LV = 0.21 ± 0.01 AU; n = 6, *****$p < 0.0001$) are expressed at higher levels in the ventricle when compared to the atria. Each dot represents an individual heart, **$p < 0.01$, ***$p < 0.001$, ****$p < 0.0001$ (Two tailed Student's t-test). [**Experiments performed by Sian O'Brien**].

3.2.2. Sodium current density in LA and LV cardiomyocytes

In subsequent experiments sodium channel current (I_{Na}) was measured in isolated mouse cardiomyocytes using whole cell patch clamp technique. At physiological holding potential, (-75 mV), I_{Na} was lower in atria compared to ventricles. In addition to this, voltage at which 50% of the sodium channels were available for activation is more negative in the LA compared to the LV, Figure 3.2. Although we have seen that the LA expressed more $Na_V1.5$ protein than the LV, at physiological membrane potentials, the peak sodium current density is reduced in the LA compared to LV. This data suggests that sodium handling differs between atria and ventricles and may cause a difference in conduction. The study of conduction in the heart is particularly interesting as it helps us understand the determinants of re-entrant arrhythmias. In a healthy heart, with normal electrical function, a long wavelength and fast excitation ensures the heart is activated once each heartbeat. Each wavelength refers to the distance travelled by the depolarisation wave during the functional refractory period. The wavelength is the product of the CV and the effective refractory period (ERP) [116]. As the wavelength becomes shorter through slower CV, multiple excitation waves can occur as it allows

more waves to fit within the same period of cardiac cycle [117]. This re-excites tissue several times without initiation of a new sinus excitation, increasing the likelihood of a self-sustained arrhythmia [118].

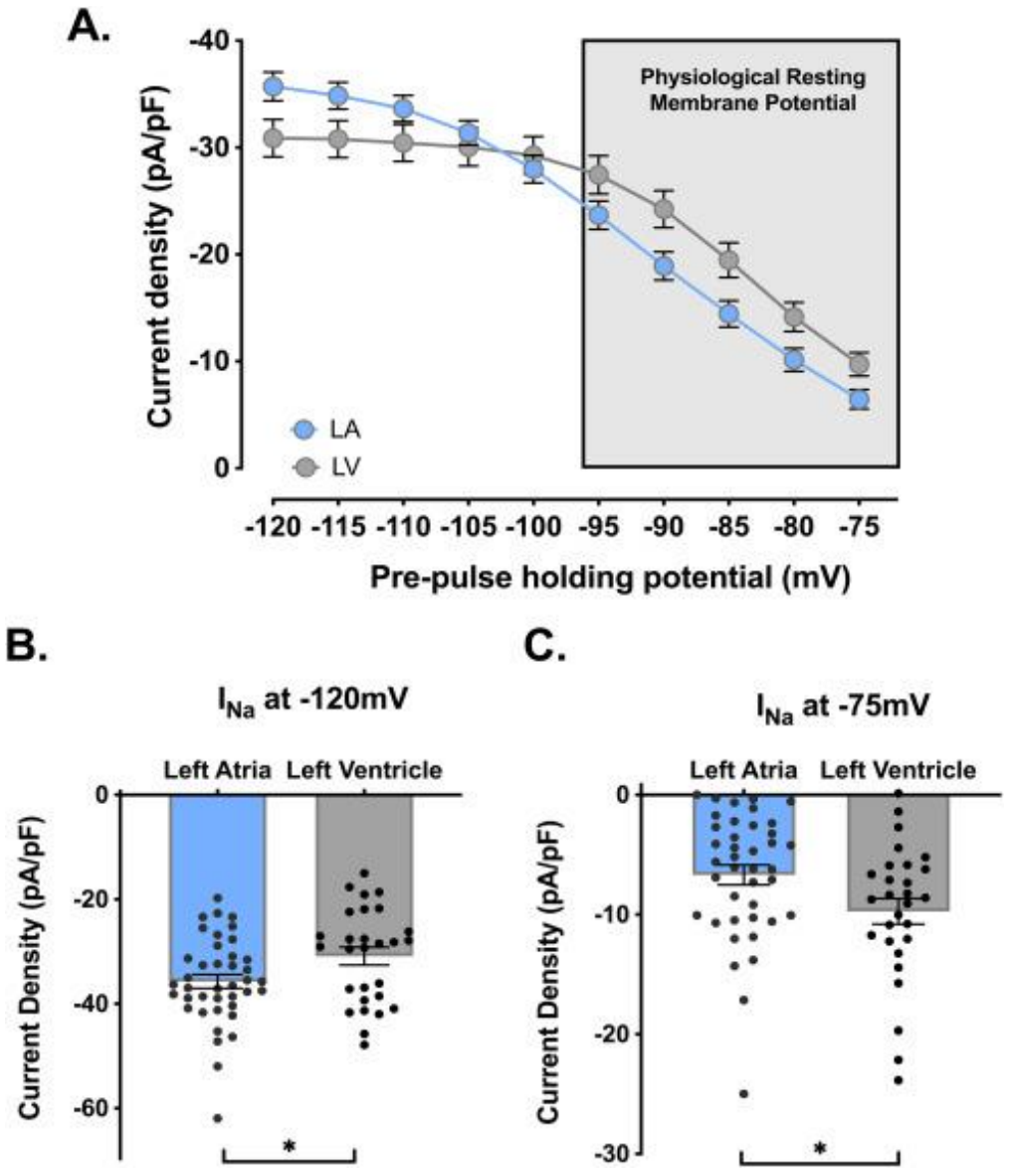

Figure 3.2. ***I*Na density in LA and LV cardiomyocytes at varying holding potentials.** A. I_{Na} mean density/holding potential relationship, LA (n=24/7 cells/mice) and LV (n=38/10 cells/mice). B. I_{Na} density at -120 mV holding potential in LA (-35.72 ± 1.718 pA/pF; n=40/13 cells/mice), LV (-30.89 ± 1.322 pA/pF; n=28/13 cells/mice). C. I_{Na} density at -85 mV holding potential in LA (-6.569 ± 0.8474 pA/pF; n=40/13 cells/mice), LV (-9.735 ± 1.075pA/pF; n=28/13 cells/mice). Statistical significance determined by two-way nested ANOVA, **P*<0.05, ***p*<0.01. [**Experiments performed by Sian O'Brien**].

The differential expression of Na^+ channels along with the difference in the Na^+ current at physiological resting membrane potential, led us to hypothesise that conduction in the atria would be slower. We used optical mapping to measure electrical activity in the heart. Cardiac optical mapping is a method used to study cardiac electrophysiology in health and disease. It allows the study of transmembrane voltage and intracellular calcium using fluorescent dyes. Here, optical mapping was used to determine electrophysiological differences between atria and ventricles, using voltage membrane dye, Di-4-ANEPPS. Atrial and ventricular recordings were taken from the same heart, ventricular measurements were taken first followed by atrial measurements. Due to differences in the atria and ventricle's vasculature, the ventricles loaded first. We stimulated the ventricles and at the end of the ventricular protocol, we loaded the heart further until the atria were sufficiently loaded. Atria were then stimulated with the same pacing protocol. A more detailed experimental and pacing protocol can be found in Chapter 2. This study was performed on CD1 wildtype (WT) mice aged 10 to 15 weeks. Figure 3.3 demonstrates the regions that were selected for the atrial and ventricular analysis. A 9 x 9 pixel region was selected in the atria and ventricles for direct comparison. Data were analysed using two-way ANOVA with a Tukey post hoc test and are presented as average values with mean ± S.E.M. Additionally we also looked at values from 10 Hz, which would represent the physiological heart rate of mice. Data were analysed using a paired t-test with a Gaussian distribution.

3.2.3. Conduction velocity is slower in mouse LA tissue than mouse LV tissue

Figure 3.4 shows measurements of electrical parameters in left atria and left ventricles, across a range of pacing frequencies, from 6.25 Hz up to 16.67 Hz. Conduction velocity (CV) was acquired from activation maps using the multi-vector method with 5 x 5 window size. Our previous finding of difference in sodium channel protein levels suggested that conduction velocity would also be different in atria and ventricles. A slower conduction was observed in the LA compared to LV at each pacing frequency, however this was not significantly different, Figure 3.4B. Average atrial CV ranged between 17.5 and 48.3 cm/s and average ventricular CV ranged between 42.1 and 64.2 cm/s. Average values were calculated by taking average of each data point at each frequency rates. A line of best fit showed a gradual slowing in CV with increasing pacing frequency, but this was not significant. N numbers varied between 5 and 7 and was analysed using two-way ANOVA. In Figure 3.4B, we used values from 10 Hz, Figure 3.5B. At 10 Hz, we see a significant difference in CV between left atria and left ventricle, 30.4 ± 6.9 cm/s vs. 40.5 ± 9.3 cm/s, $p = 0.03$. CV was significantly faster in ventricles compared to atria. Average atrial CV was 30.4 ± 7.7 cm/s and average ventricular CV was 40.5 ± 10.4 cm/s. Data was analysed using student's t-test.

3.2.4. Action potential duration is shorter in mouse LA tissue than mouse LV tissue

APDs were calculated as the time from maximum upstroke velocity to 50% repolarisation. It has been observed from previous studies that action potential duration is shorter in the atria compared to ventricles. This correlates with our observation, and we found a significant difference in action potential duration at 50% repolarisation at every pacing frequency, $p<0.0001$, Figure 3.4.A. Average atrial APD 50 ranged between 12.9 and 15.2 ms and average ventricular APD50 ranged between 27.8 and 32.8 ms. There was no apparent effect of the pacing frequency on APD50. N numbers varied between 6 and 7 and was analysed using two-way ANOVA. At 10 Hz, Figure 3.4A, APD50 was still significantly different between atria and ventricles. APD50 was significantly shorter in atria compared to ventricles, 13.1 ± 1.7 ms vs. 31.5 ± 7.1 ms, $p = 0.006$.

3.2.5. No difference in diastolic interval between mouse LA and mouse LV

Diastolic interval was measured at different pacing frequencies, Figure 3.4C. The diastolic interval refers to the period during which the heart is relaxed, and the ventricles are filling with blood. Diastolic interval measurements were similar within atria and ventricles, although it was slightly shorter in ventricles, and showed an overall shortening as pacing frequency got faster. Average diastolic intervals ranged between 75.1 ± 6.0 ms and 139.9 ± 18.0 ms in LV and between 81.3 ± 7.3 cm and 142.9 ± 18.4 ms in LA. N numbers varied between 6 and 7 and was analysed using two-way ANOVA. At

10 Hz, we observed no differences in diastolic interval, average atrial diastolic interval was 100.4 ± 23.2 and 100.6 ± 18.2 in ventricular diastolic interval, Figure 3.4C.

3.2.6. Amplitude is greater in mouse LV compared to mouse LA

Amplitude refers to the intensity of fluorescence emitted by Di-4-ANEPPS and is dependent on tissue thickness, concentration of dye, dye loading, position of recording electrode and tissue conductivity. Amplitude was significantly greater in the LV when compared to LA, at each pacing frequency, Figure 3.4D. N numbers varied between 6 and 7 and was analysed using two-way ANOVA. Overall, amplitude also became shorter over increased pacing frequency. At 10 Hz, amplitude in LV was significantly greater than in LA, 1840 ± 384.7 a.u. vs. 564.7 ± 244.8 a.u., p = 0.005, Figure 3.5D. Data was analysed using a student's t-test.

3.2.7. Time to peak in mouse LV compared to mouse LA

Average time to peak ranged from 4.6 ± 0.3 ms to 5.4 ± 1.0 ms in the LV, and 6.0 ± 1.0 ms to 8.4 ± 1.7 ms in the LA. Mean time to peak was faster in ventricles compared to atria at every pacing frequency, but this was not significant, Figure 3.4E. At 10 Hz, time to peak was slightly faster in the ventricles than in the atria, Figure 3.5E. Average atrial time to peak was 6.2 ± 0.8 ms and average ventricular time to peak was 5.4 ± 1.0 ms, but the difference was not significant, p=0.1.

3.2.8. Activation time is faster in mouse LV compared to mouse LA

Activation time, which is the time it takes for an area of tissue to be activated, was established as the midpoint of depolarisation. Activation time was measured as the time it took from 10% of the tissue being activated to 90% of the tissue becoming activated. Activation time between atria and ventricles was not significant at 10 Hz, but Figure 3.6.D shows when the data is plotted as an activation curve, LA activation curve is shifted to the right, indicating that LA has a slower activation time compared to LV. 100% of LA tissue was activated in approximately 4.3 ms while 100% of LV tissue was activated in 3.3 ms. This correlates with the CV data since the shorter the activation time, the faster the CV.

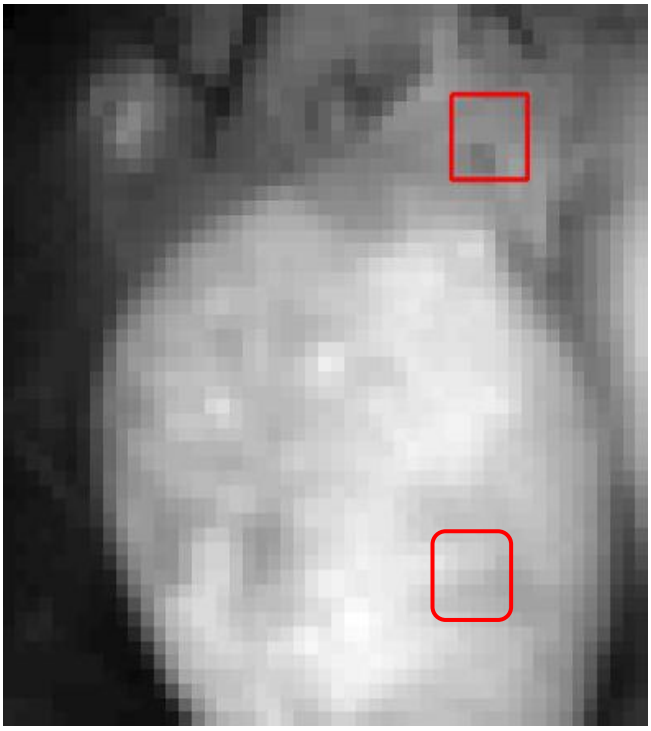

Figure 3.3. Regions of interest in mouse heart. Camera image depicting a 9 x 9 pixel region of interest in LA and LV.

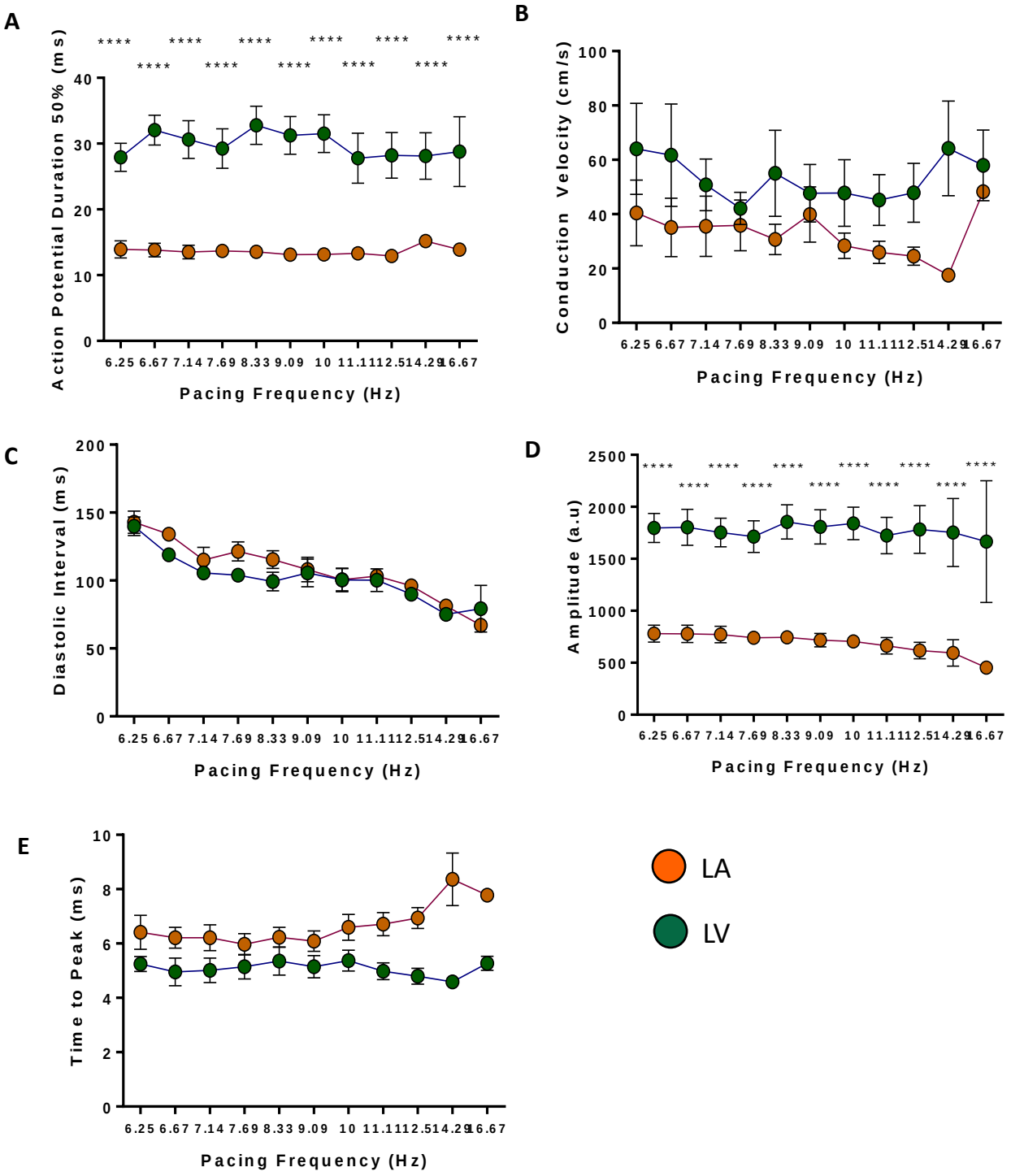

Figure 3.4A-E. APD50, CV, Amplitude, Diastolic Interval, activation time and time to peak in mouse LA and LV. Measurements were taken in left atria and ventricles of CD1 mice over a range of pacing frequency. Baseline measurements were taken from same heart. A. Action potential duration at 50% repolarisation in LA (n = 5-7) and LV (n = 6-7) from CD1 WT mouse hearts. Significant differences observed at each pacing frequency, P<0.0001. B. Conduction velocity in LA (n = 5-7) and LV (n = 6-7) from CD1 WT mouse hearts. No significant differences observed. C. Diastolic interval in LA (n = 5-7) and LV (n=6-7) in mouse hearts. D. Amplitude in LA and LV from

CD1 WT mouse hearts. Significant differences observed at each pacing frequency, P<0.0001. E. Time to peak in mouse hearts in LA and LV. Statistical difference was determined using two-way ANOVA with Sidak's post hoc test and significance quantified as P<0.05. Error bars indicate ± S.E.M. * represents significance between atrial and ventricular tissue. * denotes *P*<0.05, ** denotes *P*<0.01, *** denotes *P*<0.001, **** denotes *P*<0.0001, N=5.

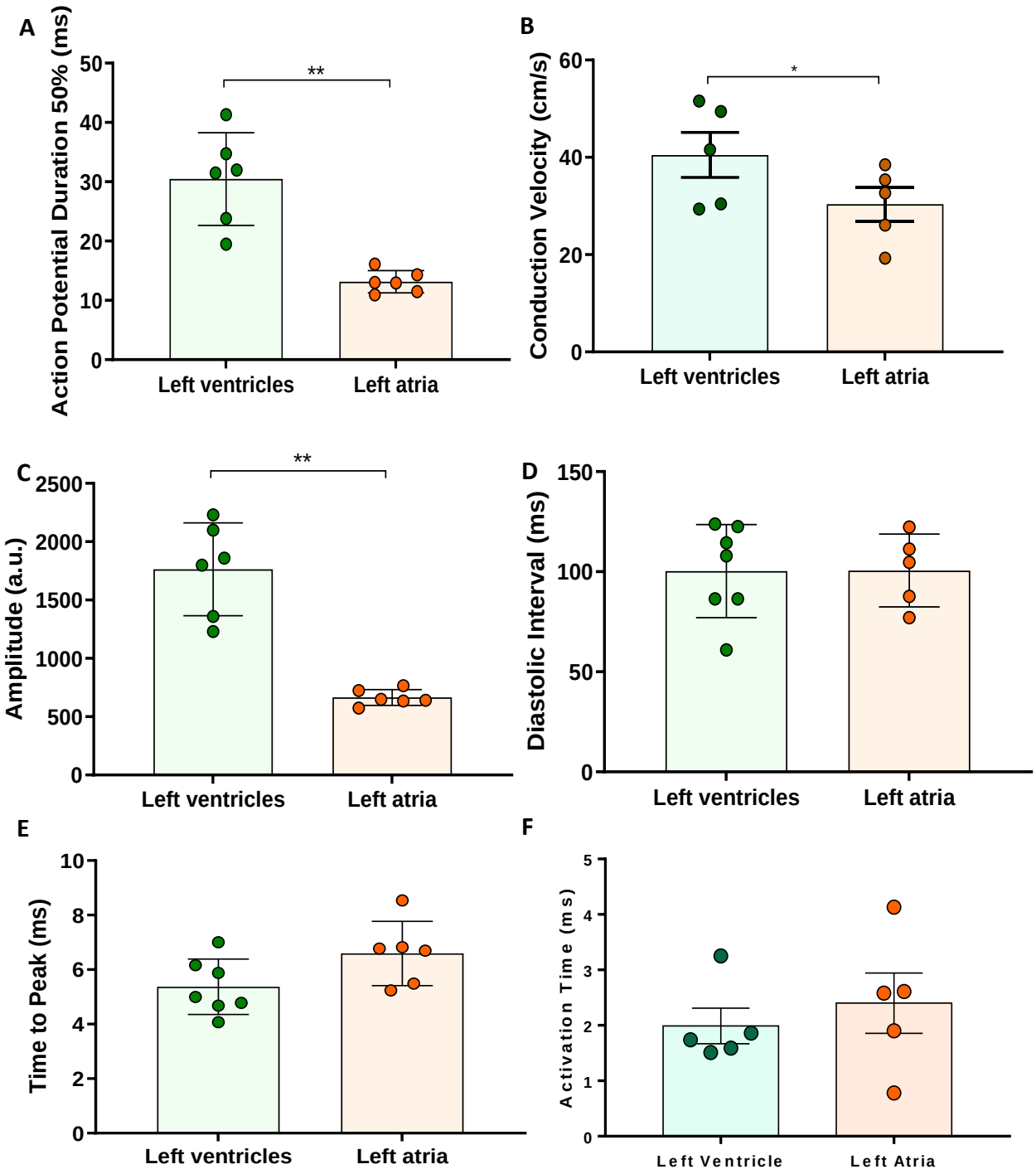

Figure 3.5A-F. APD50, CV, amplitude, diastolic interval, activation time and time to peak at 10 Hz. Measurements were taken in left atria and ventricles of CD1 mice. Baseline measurements were taken from same heart. A. Significant difference was observed in APD50 between LV and LA, 31.5 ± 7.1 ms vs. 13.1 ± 1.7 ms respectively, n=6, $p = 0.006$. B. CV between LV and LA at 10 Hz, 40.5 ± 9.3 cm/s vs. 30.4 ± 6.9 cm/s, n=6, $p = 0.03$. C. Amplitude in LV and LA at 10 Hz, 1840 ± 384.7 a.u. vs. 564.7 ± 244.8 a.u., $p = 0.005$. Statistical difference was determined using student's paired t-test and significance quantified as P<0.05. * represents significance between atrial and ventricular tissue. * denotes $P<0.05$, ** denotes $P<0.01$, *** denotes $P<0.001$, **** denotes $P<0.0001$, N=5.

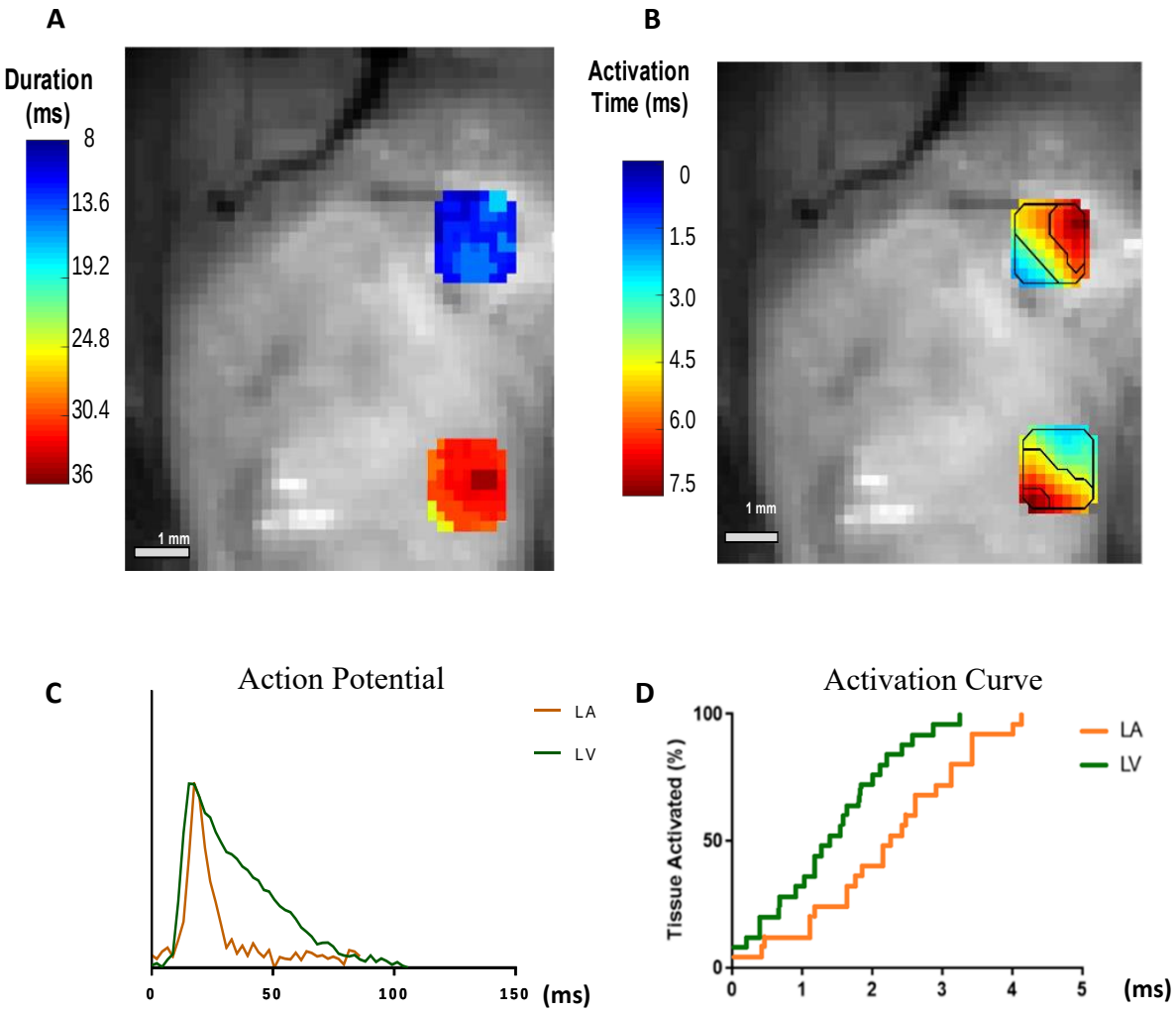

Figure 3.6A-D. Action potential duration and conduction velocity in left atria and left ventricles taken from 9x9 pixel region of interest. A. Representative APD50 maps recorded from mouse LA and LV tissue paced at 10 Hz. B. Representative CV maps recorded from mouse LA and LV tissue paced at 10 Hz. Contour lines are spaced by 2 ms. C. Representative example of AP recorded from LA (orange) and LV tissue (green) at 10 Hz. D. Representative example of activation curve recorded from LA and LV tissue at 10 Hz.

3.2.9. Direct comparison of atria and ventricles

To enable direct comparison of atria and ventricles, a 9 x 9 pixel region was analysed from the left atria and the left ventricles, as shown in Figure 3.7A. The purpose of this was to select a same sized region in both chambers. To ensure there was no skewing of dataset by selecting a 9 x 9 pixel region from the left ventricle, we also analysed the whole ventricles and compared this to 9 x 9 pixel region, Figure 3.6B.

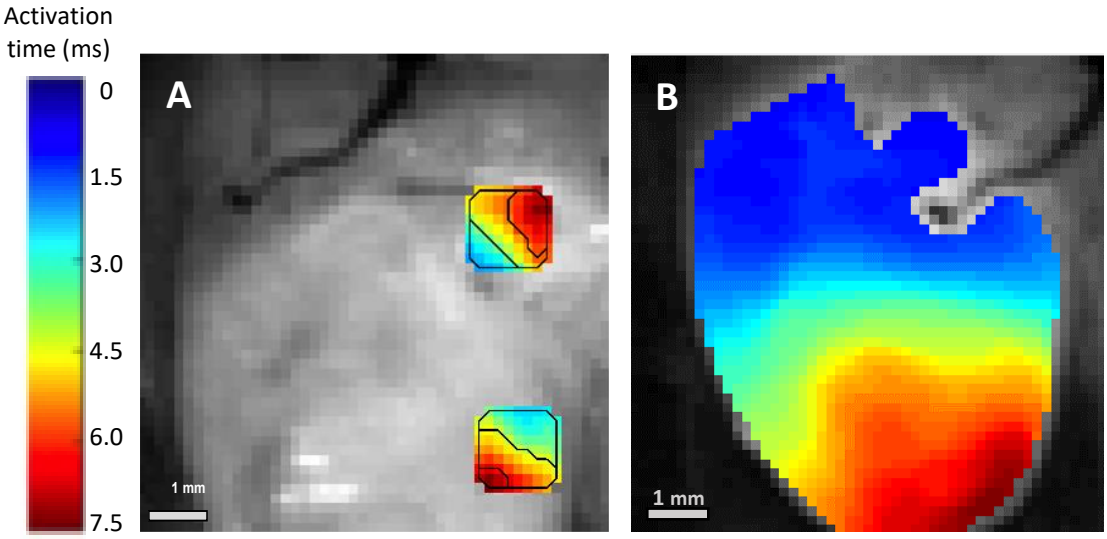

Figure 3.7. Representative example of how regions of interest were selected and compared. A) Hearts were analysed through selecting a 9x9 pixel region in the left atria and left ventricle. B) Hearts were analysed through selecting the whole region of atrial tissue and whole region of ventricular tissue.

Figure 3.8 shows the different electrophysiological parameters measured and compared between whole region of ventricles and 9 x 9 pixel region in the left ventricles, at baseline. The parameters measured, Figures 3.7.A to 3.8.E include APD50, CV, amplitude, diastolic interval, and time to peak. No significant differences were observed between the two regions. Significant differences were determined using a mixed factor

ANOVA, a statistical method which compares mean differences between groups with two variables [119]. APD50, CV, amplitude and time to peak stayed constant across the pacing protocol. Diastolic interval became shorter with a faster frequency rate in both regions. This is to be expected as an increase in heart rate would decrease the duration of diastole [120].

At 10 Hz, there were no differences in APD50, CV, diastolic interval and time to peak. Amplitude was slightly increased in the 9 x 9 pixel region compared to the whole ventricles, but this was not significant.

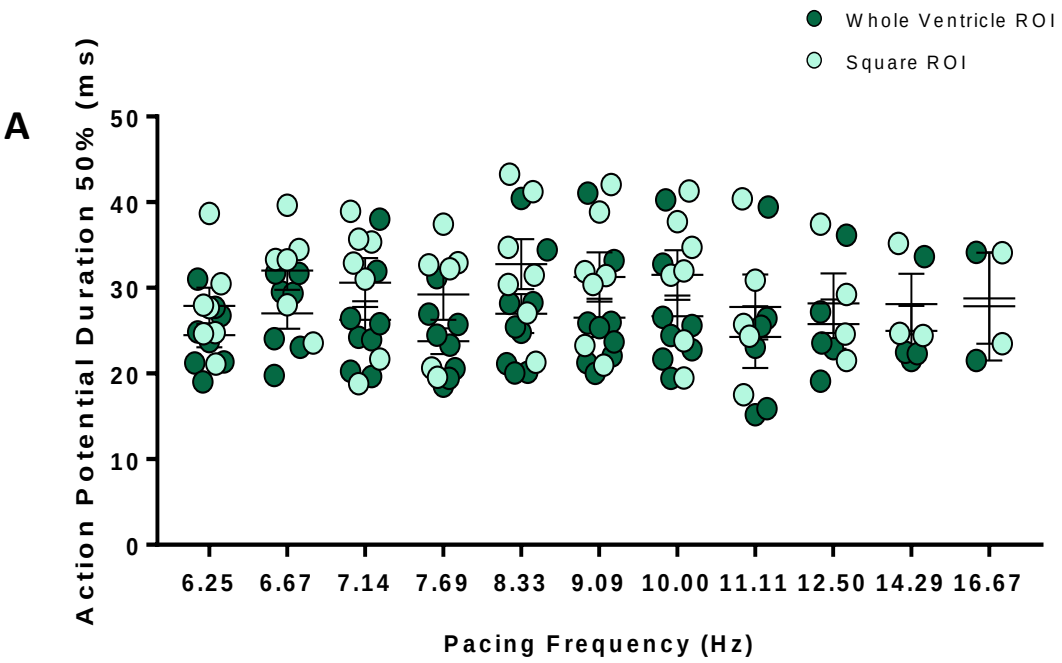
A
Whole Ventricle ROI
Square ROI
Action Potential Duration 50% (ms)
0
10
20
30
40
50
6.25
6.67
7.14
7.69
8.33
9.09
10.00
11.11
12.50
14.29
16.67
Pacing Frequency (Hz)

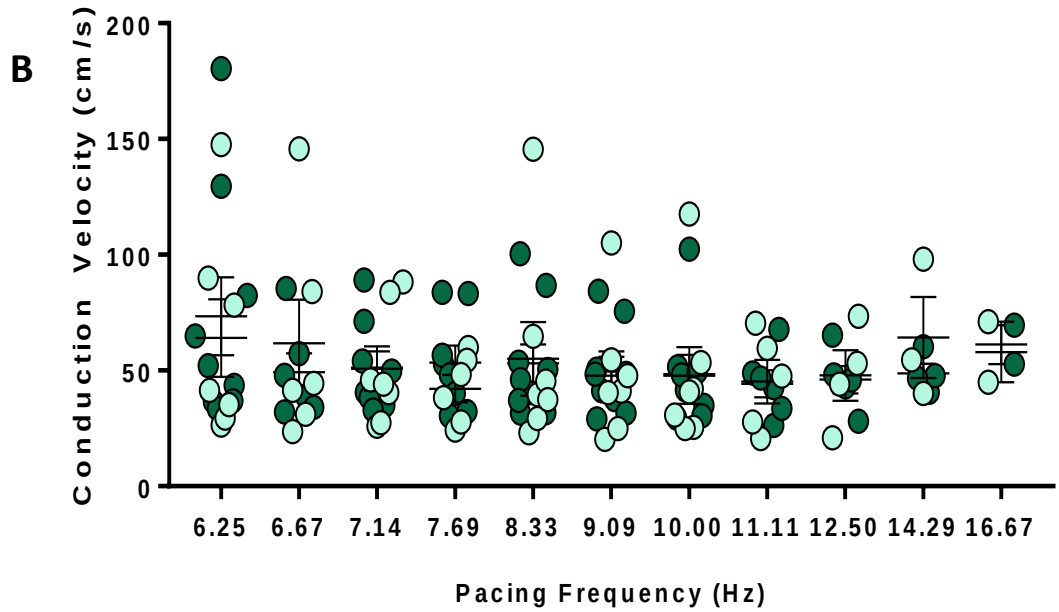
B
Conduction Velocity (cm/s)
0
50
100
150
200
6.25
6.67
7.14
7.69
8.33
9.09
10.00
11.11
12.50
14.29
16.67
Pacing Frequency (Hz)

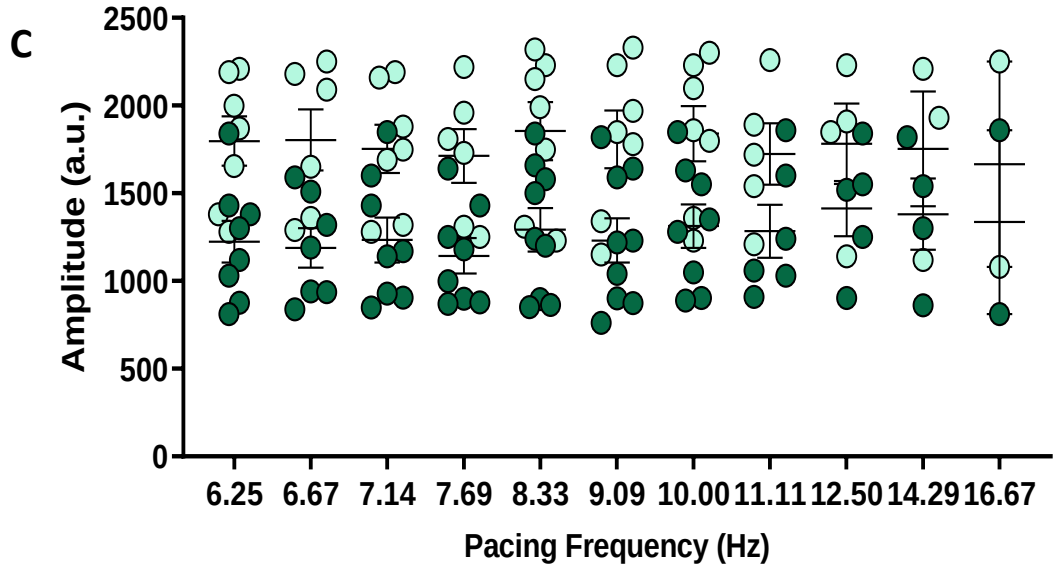
C
Amplitude (a.u.)
0
500
1000
1500
2000
2500
6.25
6.67
7.14
7.69
8.33
9.09
10.00
11.11
12.50
14.29
16.67
Pacing Frequency (Hz)

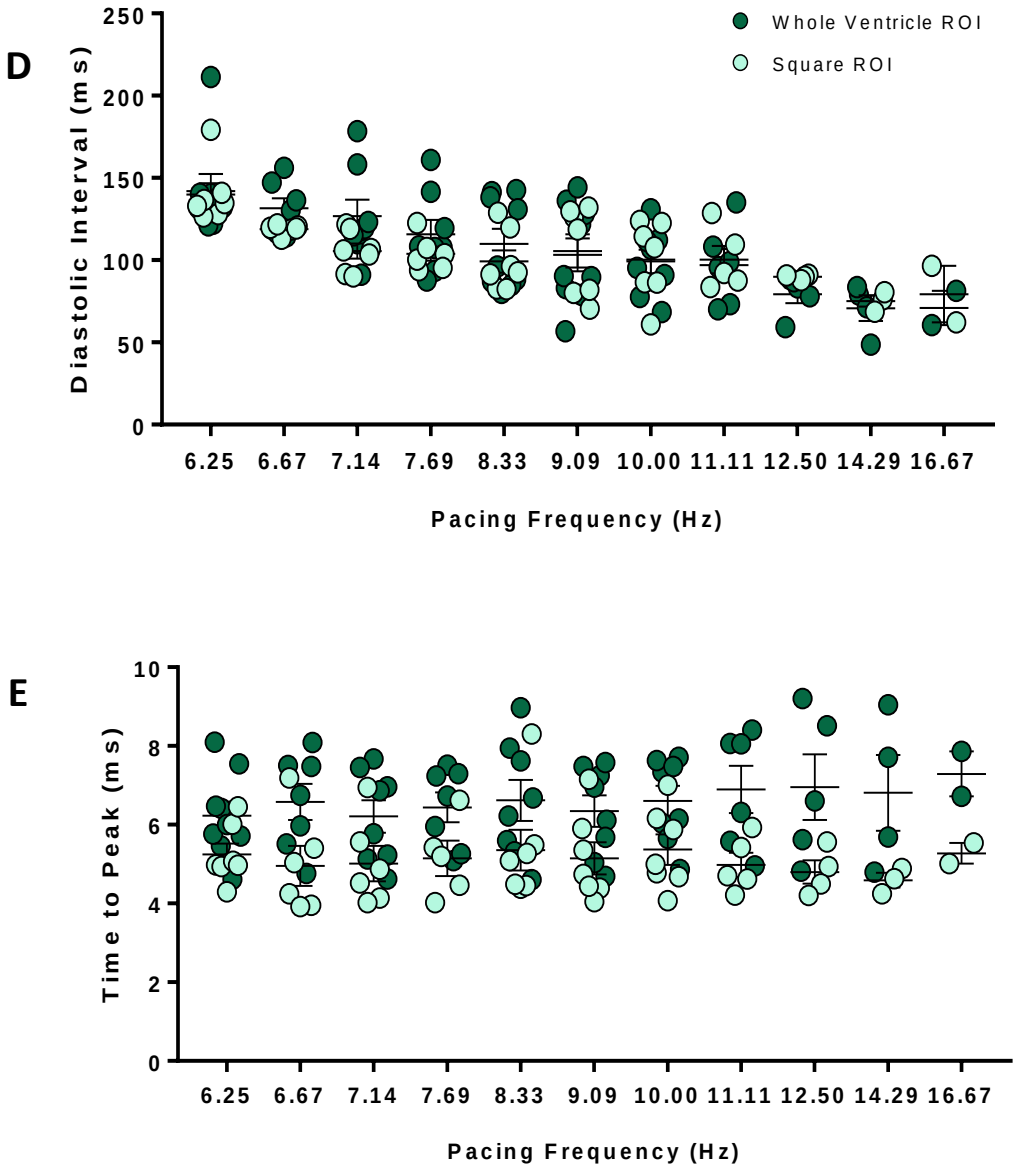

Figure 3.8A-E. Comparison of electrophysiological parameters in the ventricles between 9x9 pixel region in the LV and whole ventricles. A) Individual data points of APD50 from 9x9 pixel region (light green) and whole region (dark green) paced between 6.25 Hz and 16.67 Hz. B) Individual data points of CV from 9x9 pixel region and whole region. C) Individual data points of amplitude from 9x9 pixel region and whole region. D) Individual data points of diastolic interval from 9x9 pixel region and whole region. E) Individual data points of time to peak from 9x9 pixel region and whole region. Each point represents an individual heart. Statistical difference determined by mixed factor ANOVA, n = 7 for each group.

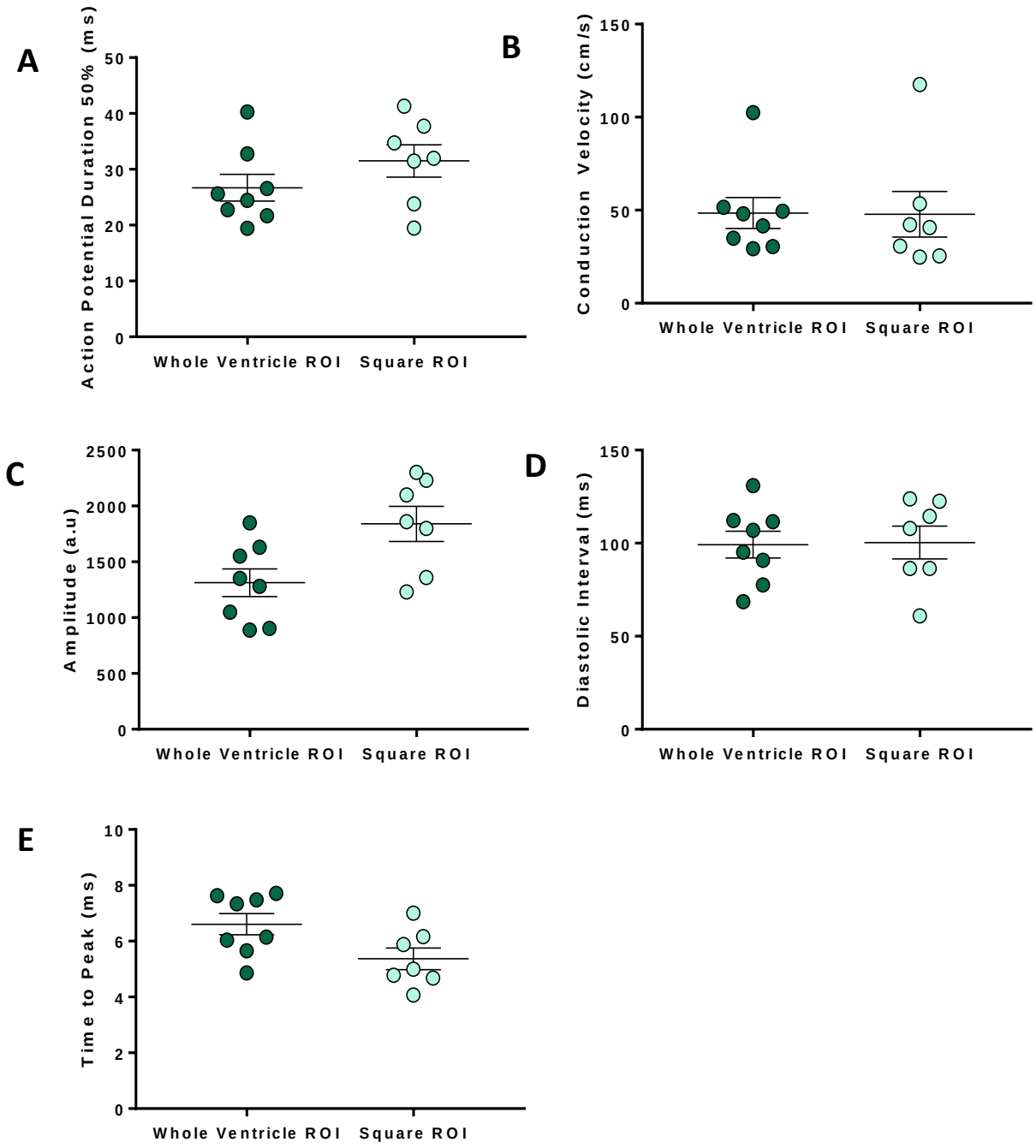

Figure 3.9. Comparison of electrophysiological parameters in the ventricles between 9x9 pixel region in the LV and whole ventricles, at 10 Hz. A) Individual data points of APD50 from 9x9 pixel region (light green) and whole region (dark green) paced at 10 Hz. B) Individual data points of CV from 9 x 9 pixel region and whole region. C) Individual data points of amplitude from 9x9 pixel region and whole region. D) Individual data points of diastolic interval from 9x9 pixel region and whole region. E) Individual data points of time to peak from 9x9 pixel region and whole region. Each point represents an individual heart. Statistical difference determined using paired t-test, n = 7.

3.2.10. Conduction velocity: Single vector and multi vector analyses methods

For this study, we used the multi vector method to obtain CV measurements. This method calculates the CV across the whole tissue Figure 3.10.C, a method which was developed by Bayly et al 1998, opposed to single vector method which measures conduction speed along a vector connecting two points, Figure 3.10.A [121]. The calculation of CV across the entire tissue offers an overall view of the heart's electrical activity. Ideally, the vector would run along the apparent longitudinal axis. We also measured the CV using single vector method as a comparison which consisted of measuring CV between two manually selected points perpendicular to the wavefront. Using the single vector method, a minor deviation in the vector can alter the CV value. For instance, Figure 3.11 illustrates an area from a single ventricle at 10 Hz with a vector drawn from point A to B. In both images, point B is chosen at two different locations, with a single pixel difference between them, resulting in a change in CV. Over a span of 5.31 seconds, the CV was measured at 38.54 cm/s across 0.20 cm, and 42.09 cm/s across 0.22 cm, Figure 3.13A. Despite this, both multi vector and single vector methods revealed a significant difference in CV in atria and ventricles at 10 Hz, although CV recordings taken from single vector method were more variable than CV recordings taken from multi vector method, Figure 3.10.

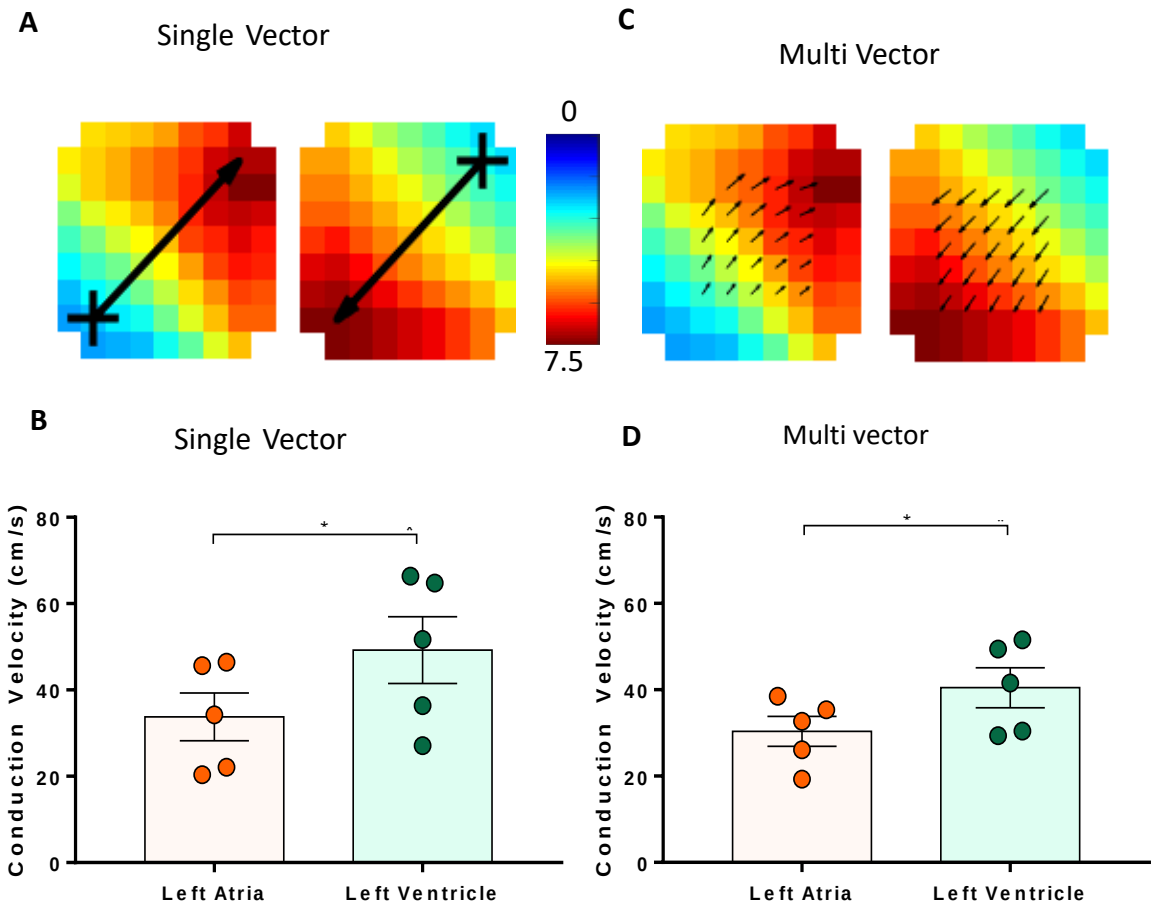

Figure 3.10. Single vector and multi vector conduction velocities are reduced in LA compared to LV. A. Representative single vector CV from mouse LA and LV tissue paced at 10 Hz. B. Grouped data of single vector CV in LA 33.8 ± 5.5 cm/s and LV, 49.3 ± 7.7 cm/s, p=0.03, N=5, two tailed student's t-test. C. Representative multi vector CV from mouse LA and LV paced at 10 Hz. D. Grouped data of multi vector CV in LA, 30.4 ± 3.4 cm/s, and LV, 40.5 ± 4.6 cm/s, p=0.03, N=5, two tailed student's t-test.

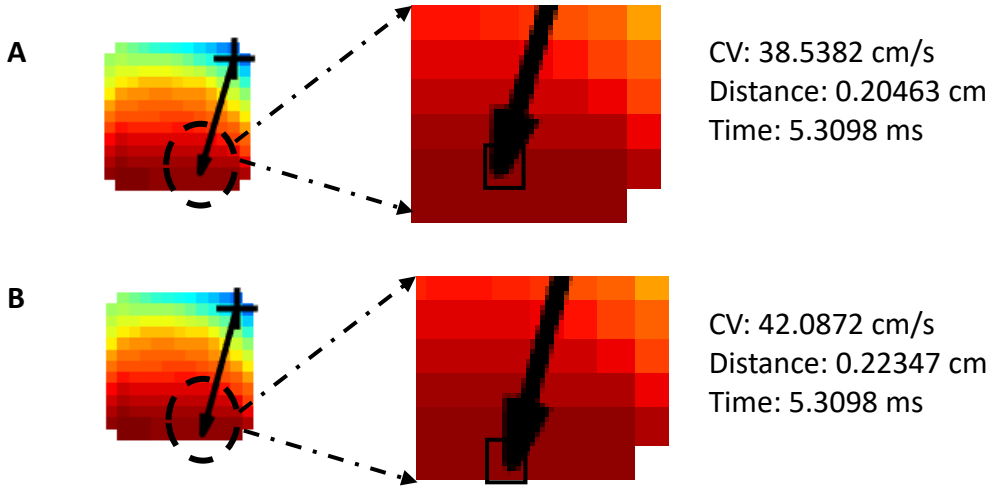

Figure 3.11A-B. Conduction velocity measurement using single vector methodology. A and B show differences in CV values when points selected differ by a pixel. A. CV is 38.5 cm/s over a distance of 0.205 cm. B. CV is 42.1 cm/s over a distance of 0.223 cm.

3.2.11. Heterogeneity of electrical activity across ventricular epicardium

In order to assess variance in electrical activity across the ventricular epicardium of the heart, sections of the heart were measured independently of one another from WT CD1 mice. A square region of 9 x 9 pixel was selected from 6 regions of the heart; LV basal, LV middle, LV apical, RV basal, RV middle and RV apical, as shown in Figure 3.11. From these sections, action potential duration at 50% and 80% repolarisation, conduction velocity, amplitude, time to peak, diastolic interval and activation time was measured at 10 Hz.

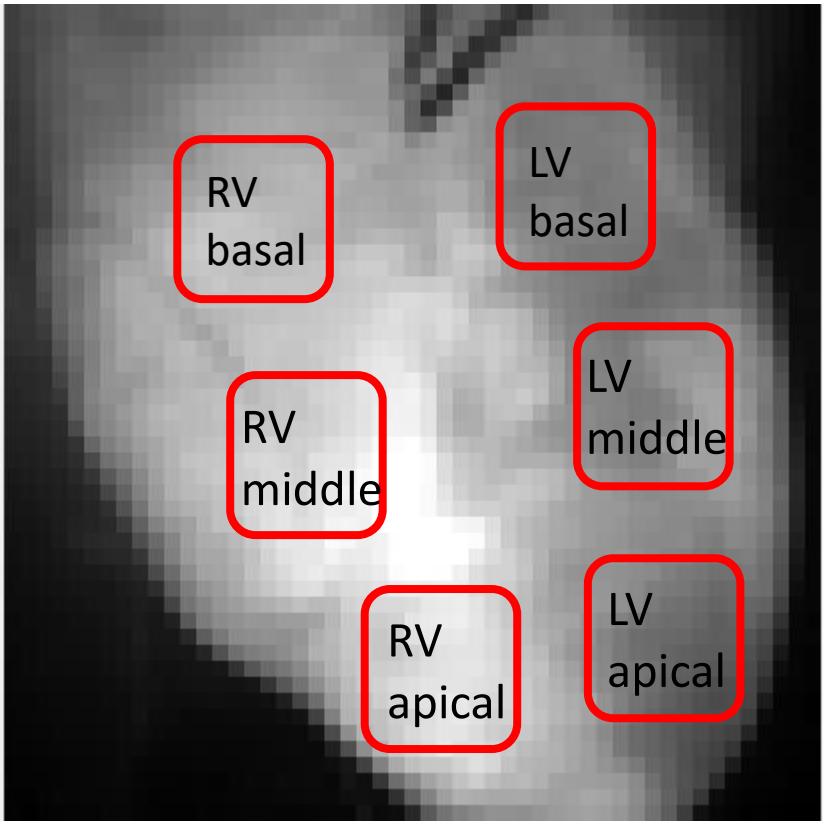

Figure 3.12. Regions of interest in mouse heart. A 9 x 9 pixel selected across 6 regions; LV basal, LV middle, LV apical, RV basal, RV middle and RV apical to measure heterogeneity of electrical activity across the epicardium.

We observed significant differences in APD50 and APD80 within different sections of the heart. APD50 was the longest in middle of LV while it was the shortest in the apex of the RV. APD80 was the longest in the basal area of LV and shortest in the apical area of the RV. CV was analysed using the multi vector method. CV was the fastest in the LV apex and shortest in the middle area of LV. CV was significantly different between the following regions, LV base and LV apex, LV base and RV apex, LV middle and RV base, LV middle and RV middle, and LV middle and RV apex. Amplitude also showed difference between several regions. Amplitude was the longest in the middle region of LV and shortest in the basal region of RV. Time to peak was significantly different between LV

base and RV apex, and RV base and RV apex. Time to peak was the fastest in the basal region of RV and slowest in the apical region of RV. There was no difference in diastolic interval across any regions. Activation times showed some differences across some of the regions. Activation time was significantly different between LV middle and RV base, LV middle and RV middle, and LV middle and RV apex, with the fastest activation time being observed in the apex of RV and slowest being in middle of LV.

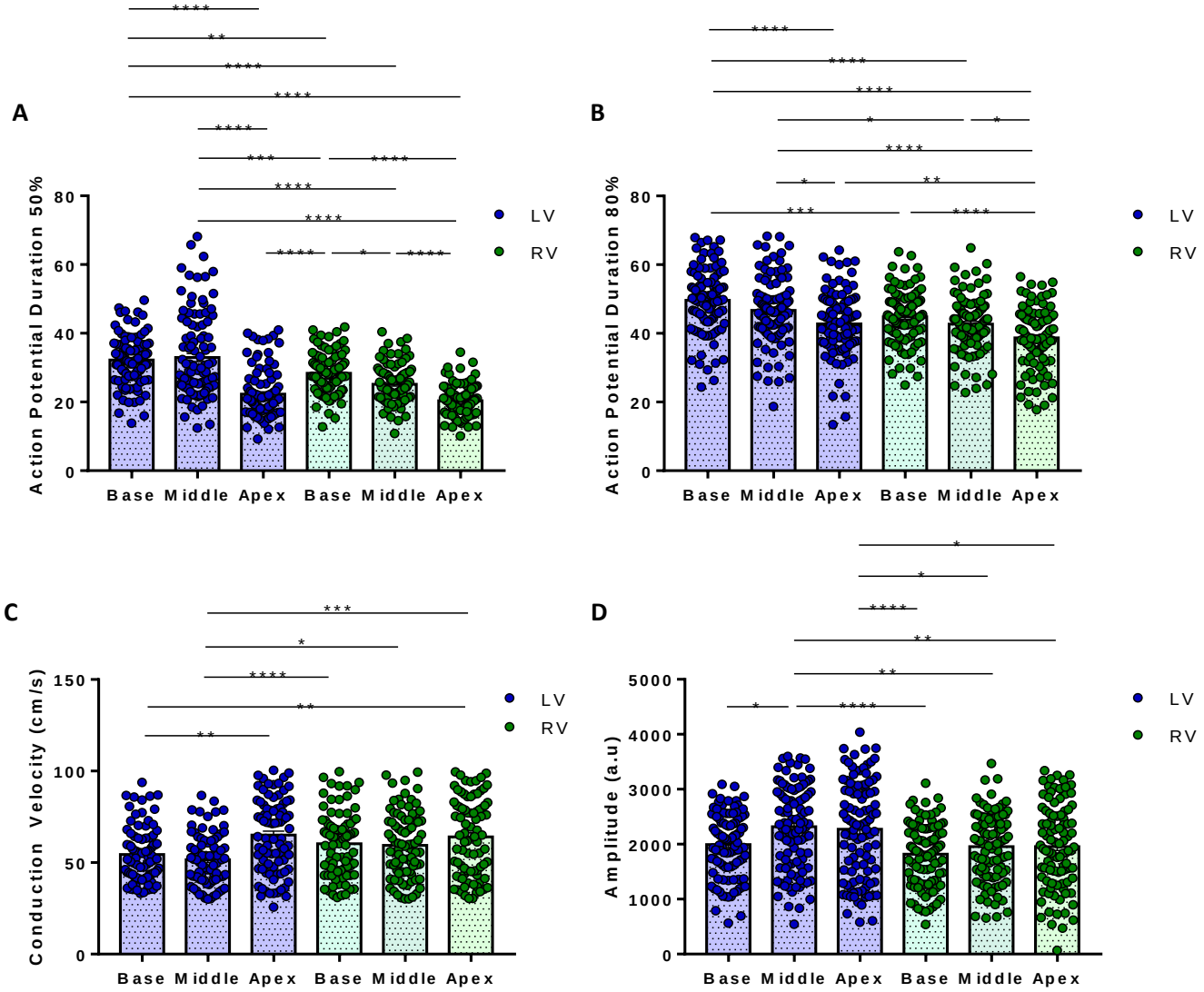
A
Action Potential Duration 50%
0
20
40
60
80
Base Middle Apex Base Middle Apex
LV
RV
B
Action Potential Duration 80%
0
20
40
60
80
Base Middle Apex Base Middle Apex
LV
RV
C
Conduction Velocity (cm/s)
0
50
100
150
Base Middle Apex Base Middle Apex
LV
RV
D
Amplitude (a.u)
0
1000
2000
3000
4000
5000
Base Middle Apex Base Middle Apex
LV
RV

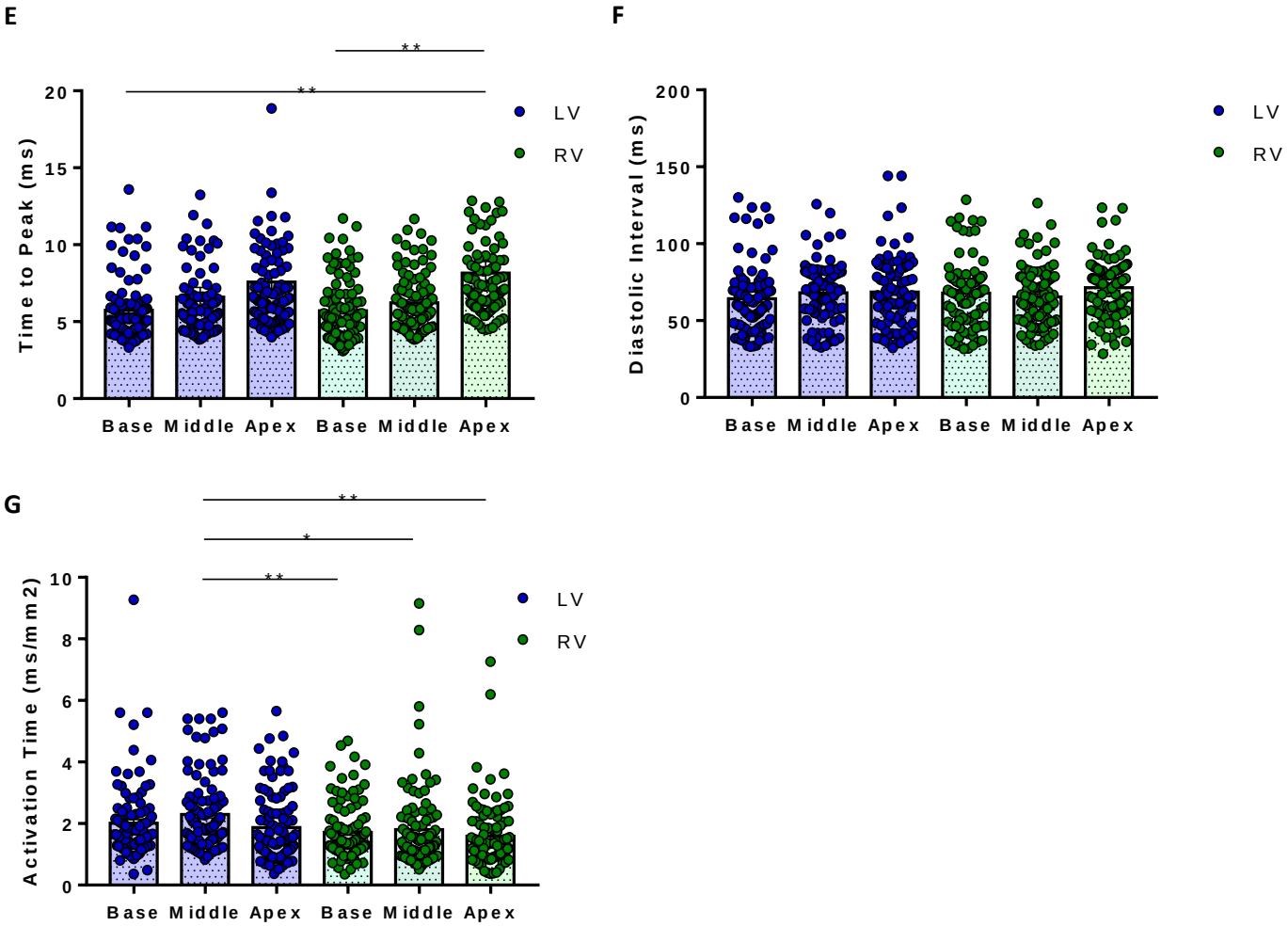

Figure 3.12. Electrical activity across epicardium at 10 Hz. Ventricles were separated into six 9x9 pixel regions, LV-Base, LV-Middle, LV-Apex, RV-Base, RV-Middle, RV-Apex. APD50, APD80, CV, amplitude, time to peak and activation time was measured in each region. Significant differences were observed and is denoted by asterisks in A. APD50, B. APD80, C. CV, D. Amplitude, E. Time to peak, F. Diastolic interval, and, G. Activation time. Statistical difference was determined by mixed factor ANOVA with Tukey post-hoc. Significance quantified as $P<0.05$. * denotes $P<0.05$, ** denotes $P<0.01$, *** denotes $P<0.001$, **** denotes $P<0.0001$, n=75.

3.3. Chapter Discussion

3.3.1. Overview of main findings

The main findings from this chapter are summarised as follows:

- Action potential duration is longer in ventricles compared to atria.
- Conduction velocity is slower in the atria compared to ventricles.
- Activation time is slower in the atria compared to ventricles.
- Significant differences in action potential duration and conduction velocity exist across regions of the ventricles.

3.3.2. Electrical differences between LA and LV

3.3.2.1. Action potential duration comparison between LA and LV

There have been a few recent studies investigating electrical differences between atria and ventricles. It has long been determined that there are significant differences in the action potential (AP) configuration and conduction, in atria and ventricles. In most mammalian species, atrial AP is characterised by a shorter repolarisation phase, compared to the ventricular AP, which has a more prolonged repolarisation phase [122]. Clercq *et al*, 2018, observed shorter action potential duration in right atria compared to right ventricle, in healthy, non-sedated horses. They reported an overall mean of APD90 from RA and RV at rest, 1000 ms/CL and 600 ms/CL as 263 ± 39 ms and 467 ± 23 ms, 262 ± 41 ms and 412 ± 38 ms, 236 ± 47 ms and 322 ± 29 ms [123]. Haverinen and Vornanen

2006 also demonstrated larger action potentials in ventricles compared to atria, in rainbow trout [124]. Knollmann *et al*, 2007, characterised the cardiac action potential in a mouse heart. They took monophasic action potential (MAP) recordings from mouse LA and LV epicardium from the same heart and observed significantly shorter atrial MAPs than ventricular MAPs. This difference was due to a shorter final repolarisation phase at APD70 and APD90. However APD30 was significantly longer in the LA compared to ventricle, and it is likely this is due to lower Kv4.2/4.3 current density in atrial myocytes compared to ventricular myocytes [122].

The difference in atrial and ventricular repolarisation is due to expression of a number of ion channels and channel subunits in atrial myocytes which are almost absent in ventricular myocytes. These include the ultrarapid delayed rectifier current (I_{Kur}) which initiates atrial repolarisation faster than the ventricular myocyte channel equivalent, rapid delayed rectifier current, (I_{Kr}). The outward transient K^+ current (I_{TO}) also facilitates a shorter atrial APD as it is expressed more in atrial myocytes than ventricular myocytes. This current greatly influences the early rapid phase 1 repolarisation [125]. Workman *et al* 2012 also concluded that contribution of I_{TO} potentially shortened APD in atrial myocytes [126].

Our results correlate with published data. The WT hearts were put through a dynamic pacing protocol, and as shown in Figure 3.3.A, showed a significant difference in APD50 at every single pacing frequency. Published data have reported, in mice, in the atrial tissue, APD50 ranging between 10 ± 0.5 and 16 ± 1.7, at 10 Hz [127]. This is on par with our findings in this study, where APD50 was 13.13 ms. In ventricles, it was reported that

APD50 is approximately 50 ms [27], we reported an average of 32 ms. LA APD50 decreased from 13.9 ± 2.9 ms at 6.25 Hz, to 12.9 ± 1.2 ms at 11.11 Hz. Although this was not significant, it is usual for APDs to shorten with faster pacing frequencies to enable a sufficient diastolic interval [128]. Shorter APD, which is commonly observed in atria compared to ventricles, is also associated with shortening of refractoriness, potentially creating re-entrant arrhythmias. When APD is reduced, the threshold for re-entry decreases, thus requiring a shorter path length for re-entry [129].

3.3.2.2. Conduction differences between LA and LV

Conduction velocity (CV) depends on several factors including expression and distribution of specific ionic proteins, tissue excitability and cell size [130]. There are opposing data published with some reporting that there is no difference in mouse atrial and ventricular CV, some reporting atrial CV was slower than ventricular CV and some reporting atrial CV is faster than ventricular CV. Several studies have reported an atrial CV ranging between 30 – 60 cm/s and a ventricular CV of also ranging between 30 – 60 cm/s in mice [131] [132]. Draper and Mya-Tu, 1959, studied CV across different tissue types and species and found little differences between chambers in cat and dog hearts, and slower ventricular conduction velocity in goat hearts compared to atrial conduction velocity [112]. One of the more recent study published in 2003 by Alcolea *et al,* show in their WT mouse models, the CVs in different chambers. They reported a CV of 31.5 ± 1.6 and 30.8 ± 1.8 cm/s in LA and RA respectively. In the LV and RV, they reported 46.3 ± 4.2 and 37.5 ± 2.7 respectively [133]. The findings from this study correlates with our

findings. Another study published in 1998 by Thomas *et al,* also demonstrated a slower CV in atria compared to ventricles. CV in the atria was approximately 0.35 m/s and 0.4 m/s in the ventricles [111].

A change in CV is primarily caused by a change in sodium channel availability. As mentioned previously, it has been shown there is a difference in sodium channel function in the atria and ventricles. Using Western Blot technique, we showed that $Na_v1.5$ expression in the LA was greater than in LV in mouse tissue. The study also showed that Na+ current density is reduced in the atria compared to ventricles at a physiological resting membrane potential, meaning that more of the channels in the LA are inactivated at physiological resting membrane potential.

Although our CV data showed no significant difference when analysed as a two-way ANOVA, at 10 Hz, a paired t-test revealed a significant difference. The atrial tissue displayed approximately a 30% reduced CV compared to ventricles, regardless of methodology. This result is in agreement with the patch clamping dataset which showed a greater negative shift in the voltage dependence of sodium channel inactivation in left atrial cardiomyocytes [108]. With faster pacing frequency, CV became slower, this is caused by a reduced availability of sodium channels which are still inactive from the previous excitation. A decrease in CV is usually associated with an increased risk of re-entrant excitation, predisposing to arrhythmia by reducing length scale over which re-entry can occur [77]. Along with their unique electrical properties, the shortened APD and slowed conduction are likely part of the reason why atria are more susceptible to arrhythmia compared to the ventricles.

Previous reports have shown inconsistency in whether CV is different among atria and ventricles and recent studies are limited. Many of these studies were also performed in animal models other than mice. We have demonstrated that CV is modulated by Na+ channel activation and inactivation. Atrial Na^+ channels were inactivated at more negative RMPs compared to ventricular Na^+ channels meaning the number of available $Na_v1.5$ channels is expected to be reduced and the peak I_{Na} lowered in the atria compared to ventricles [108]. The importance of precise measurement of CV is crucial for the study of arrhythmias and electrical remodelling. Understanding how conduction is modulated would be beneficial in understanding the mechanisms of conduction disorders. Changes in CV provides a critical foundation for the development of arrhythmias. A slowing of CV increases the likelihood of re-entrant arrhythmias [118].

3.3.2.3. Preference of using multi vector method over single vector method

We investigated differential CVs in the LA and LV in the same heart using multi vector and single vector methodologies. Multi vector method and single vector method are two different approaches to assess electrical activity. The multi vector method calculated CV across whole tissue, implementing the method from Bayly *et al* [121]. This provides a more comprehensive view of the heart's electrical activity [134]. The single vector method required manually selecting two points perpendicular to the wavefront and measuring the CV using the distance between the two points, providing a limited view of the heart's electrical activity. Selecting two points perpendicular to the wavefront often proved to be difficult due to complex activation patterns across the tissue. A slight

deviation from the perpendicular direction could skew the CV value significantly. Figure 3.11 shows an example of an area from a single ventricle at 10 Hz with a vector drawn from A to B. In both images, point B is selected at two different points, with a single pixel difference from one another. This resulted in a change in CV. Over 5.31 seconds, CV was measured at 38.54 cm/s across 0.20 cm, Figure 3.13A and 42.09 cm/s across 0.22 cm, Figure 3.11B. The 0.02 cm increase in distance, yielded a slower CV. Both multi and single vector methods demonstrated CV was slower in the LA compared to LV.

3.3.2.4. Amplitude differences in LA and LV

Amplitude generally refers to the magnitude of electrical signal generated by the heart. However, in the context of this study, the amplitude is considered arbitrary and is modulated by several factors. Amplitude can be affected by dye loading, tissue thickness, tissue conductivity, location of recording electrode, light illumination and health of the tissue. Taking these factors into account, amplitude can be compared in a single chamber at different timepoints, i.e. at baseline and after drug treatment or between different pacing frequencies but will come with limitations when compared between chambers and between different experiments due to differential dye loading of atria and ventricles. In this study, we consistently found the amplitude to be larger in the ventricles compared to the atria. Thicker tissues tend to generate signals with larger amplitudes compared to thinner tissues. Since ventricles have larger tissue size and mass, it is unsurprising that ventricles would generate a significantly stronger amplitude at all pacing frequencies compared to atria. Knollmann *et al* 2007, measured action

potential amplitude in mouse hearts at 130 ms/CL (8.33 Hz) and observed a shorter amplitude in the LA compared to the LV [122]. Regardless, in our study, atria were loaded with more dye compared to ventricles which can affect signal amplitude greatly. In all our experiments, atria and ventricles remained intact during imaging – chambers were not separated. When loading the heart with di-4-ANEPPS, ventricles loaded first. Once ventricle signals were optimal, ventricles were paced and imaged, and then heart was loaded further with di-4-ANEPPS until atrial signals were visible. Without knowing accurately the amount of dye perfused into atria and ventricles separately, it is difficult to determine accurate amplitude changes between atria and ventricles. Signal amplitude could be normalised to the change in fluorescence, $\Delta F/F$, where F represents baseline level of fluorescence and ΔF represents change in fluorescence from the baseline.

3.3.2.5. Time to peak differences in LA and LV

Time to peak, which refers to the time it takes for the cardiac tissue to reach its maximum contraction during the cardiac cycle, is measured by the rise time between 10% and 90% of the depolarisation phase of the action potential. It is known that ventricles usually display a slower time to peak compared to atria, due to differences in the intrinsic heart rate. Here, we found that LV time to peak was slightly slower in ventricles compared to atria but did not show a significant difference. Studies have also shown an increase in time to peak with faster pacing frequency, this was not observed in our study.

Time to peak represents an average time to peak value from several action potentials from several cells in a single pixel. Since each cell is activated at different times due to electrical propagation, this skews the time to peak average. Therefore, data obtained for time to peak must be accepted with reservations.

3.3.2.6. Diastolic differences in LA and LV

Diastolic interval was measured from APD90 to the activation time of the following action potential and is dependent upon heart rate and action potential duration. Diastolic interval is often shorter in the ventricles compared to the atria, due to the fact that atria have shorter APDs. We observed a shortening of the diastolic interval with faster pacing frequency in both LA and LV. This is to be expected, as with a faster heart rate, there is less time for the heart to relax, hence a shorter diastolic interval [120].

3.3.2.7. Activation differences in LA and LV

Activation time is measured as the time it takes for the whole tissue to be activated. Excitation is initiated from the sinoatrial node (SAN) and propagates across the RA and the LA from the lower right through to the upper left of the tissue [135]. In previous studies, activation times in atria and ventricles have not been directly compared in the mouse model. In this study, we didn't see a significant difference in activation times between LA and LV at 10 Hz, however when the values were plotted as a curve, there is a clear shift of LA activation time to the right compared to the LV, indicating LA activation

time was slower. Since CV is slower in the LA compared to LV, it stands to reason that the same would be observed that activation times would be slower in the LA. Su *et al* 2022, reported an activation time of approximately 2.5 ms in the LA. This is on par with our data with average activation time also being 2.5 ms [136]. Boukens *et al* 2012 reported an activation time of 3.8 ms in ventricles, slower than our findings which was 2 ms [137].

3.3.3. Heterogeneity within ventricles

There have been a few studies investigating heterogeneity within the ventricular wall and within the ventricular layers, endocardium, myocardium and epicardium. It has been established that the three layers of the heart exhibit different characteristics in regard to anatomy, topography and electrophysiology [138]. Lou *et al* 2011, measured intrinsic heterogeneities of excitation-contraction coupling and calcium handling in human hearts and found differences in APD and calcium transient (CaT) durations at sub-endocardium level [139]. Antzelvitch *et al* 1991 summarised findings of heterogeneity within epicardial, endocardial and myocardial cells [140]. Using a 3D simulation study, Franzone *et al* 2008 investigated effects of apex to base heterogeneities in APDs [141]. Most studies studying apex to base heterogeneities are simulation model studies, therefore not comparable to our study. Understanding heterogeneity in the heart is important as it helps to understand sequence of repolarisation and whether abnormalities in ventricular heterogeneity can lead to arrhythmias and other cardiac disorders.

Our study showed a significant difference in APD50, APD80, CV and amplitude between almost all regions. It is important to note that the positioning of pacing electrodes can affect the CV measurement. This may explain why CV was slightly slower in the LV base and LV middle, but further examination is required. A study from 1983 by Sekiya *et al*, investigated APDs in the apex and base in the endocardium and epicardium canine left ventricle and found APD60 and APD90 was longer in the apex compared to the base [142]. This was opposite to what we found, which was that APD50 and APD80 was shorter in the apex compared to the base. This could be due to differences in potassium ion concentration across the heart between species, i.e. dogs vs. mice. Kanai and Salama, 1995 showed APDs are shorter at the apex than the base of the LV in guinea pigs which correlated with our findings, however this study was carried out in dissociated myocytes [143].

Following on from these studies, it will be crucial to investigate differences in expression and function of ion channels in these regional areas in the ventricles. It will be especially useful to look at sodium and potassium ion channel expression levels due to differences in APD and CV. Further experiments can be done to study heterogeneity within sections of the myocardium. The myocardium can be isolated from mouse hearts and CV and APD can be measured in the different regions, also allowing comparison between the epicardium and myocardium. This would be considered more physiological since the cardiac conduction system is located in the myocardium where APs are also propagated. Furthermore, it will be interesting to see how these basal heterogeneities change under cardiac stress such as ischaemia. An elevated risk of ventricular arrhythmias is correlated with increased heterogeneity in myocardial activation and APD [144].

4. Investigating differential effects of flecainide in atria and ventricles

4.1. Chapter Introduction

Anti-arrhythmic drugs (AADs) are used to treat cardiac arrhythmias. These medications work by modulating the electrical conduction system to restore sinus rhythm or to prevent occurrence of arrhythmias [145]. AADs are grouped into four classes based on their mechanism of action, Class I – sodium channel blockers, Class II – beta blockers, Class III – potassium channel blockers, and Class IV – calcium channel blockers. These are further divided into subclasses and are detailed in Chapter 1.1. The classification of the AADs is traditionally based on the Vaughan Williams classification, which was introduced by Miles Vaughan Williams. Lei *et al* 2018 have developed a modernised classification incorporating a wider range of pharmacological targets and including principal action of current and potential AADs [146].

Sodium channel blockers belong to Class I drugs and work by inhibiting the flow of sodium ions through sodium channels. They can be used to treat hyperexcitability-related diseases including cardiac arrhythmias [147]. It is used for rhythm control therapy of patients with atrial fibrillation (AF) with normal ventricular function and without ischaemic heart disease. AADs were initially developed to suppress ventricular arrhythmias [108]. Flecainide is a class Ic AAD, signifying its primary action on sodium channels within cardiac cells. Flecainide blocks the sodium channels, with $Na_v1.5$ being the predominant pore-forming alpha subunit, inhibiting the fast inward sodium current. This decreases the rate of depolarisation during phase 0 of the action potential and

delays conduction across the heart tissue [36]. It also has prolonged refractoriness due to flecainide's slow release from the binding site [86].

We have discussed significant differences in sodium channel expression and conduction observed between atria and ventricles in Chapter 3. Protein expression of $Na_v1.5$ was larger in the left atria compared to left ventricles, and sodium current density was smaller in the left atria compared to left ventricles [108]. We also showed that conduction was slower in the atria compared to ventricles due to the lower sodium current density at -85 mV, and action potential duration was shorter in the left atria compared to the left ventricle. These fundamental differences observed between atria and ventricles potentially indicate a differential effect of flecainide in the atria and ventricles. Holmes *et al* investigated whether changes in atrial resting membrane potential altered the effectiveness of clinically used AADs such as dronedarone, propafenone and flecainide. The study demonstrated in isolated mouse cells and HEK293 cells and human induced pluripotent stem cells derived cardiac myocytes (hiPSC-CMs), that a more positive RMP increased the effectiveness of propafenone, flecainide and dronedarone. Sodium current inhibition was greater with the AADs at more positive RMP [148].

As current AADs do not specifically target atrial sodium channels and no studies have directly compared the effectiveness of flecainide in atrial and ventricular chambers, there is a need for atrial selective sodium channel blockade. Different arrhythmias originate in different areas of the heart, for instance, AF often originates in the pulmonary veins and is propagated in the atria, and VF originates in the ventricles [149]

[150]. Pulmonary vein isolation has become a widely used technique to supress AF. In a study of patients with 1 to 4 points of origin for AF, 65 out of 69 total ectopic foci originated in the pulmonary veins, 3 in the right atria and 1 in the posterior left atrium [151] [152]. Chamber specific drugs can allow for targeted therapy which could improve the efficacy of the treatment. The specificity of AADs can be critical for effectively managing arrhythmias while minimising potential adverse effects. Although flecainide has a reasonable safety profile and is recommended as one of the first line of treatment in patients who do not have ventricular disease or coronary heart disease, large studies have shown flecainide to cause proarrhythmia in some patients. The Cardiac Arrhythmia Suppression Trial (CAST) showed increased mortality in patients surviving myocardial infarction after treatment with either flecainide or encainide [86]. Determining the effects of flecainide in atria and ventricles will help with development of chamber specific drugs with improved efficacy and safety profiles.

The aims of this investigation were to:

- Using patch clamping, assess differential effects of flecainide on sodium channels in isolated mouse atrial and ventricular cells.

- Using optical mapping, assess the differential effects of flecainide on conduction velocity in the mouse atrial and ventricular tissue.

The patch clamp data presented in Chapter 4, Figures 4.1 and 4.2, were performed and analysed by Dr O'Brien and Dr O'Reilly. The data has been published in article for which I am a co-author on and has been added here as it provides a strong rationale for measuring differential responses to flecainide between atria and ventricles using optical mapping.

4.2 Chapter Results

4.2.1 Flecainide displays greater inhibition of maximal upstroke velocity

Experiments were performed on cells isolated from wildtype (WT) mouse LA and LV. The cells were patch clamped to compare RMP and measure maximal upstroke velocity of the AP and sodium channel activation.

We were able to confirm differences in RMP between atrial and ventricular myocytes. When cells were paced at 1 Hz, left atrial myocytes had an RMP of 70.8 ± 1.4 mV and left ventricular myocytes had an RMP of −74.4 ± 1.0 mV, indicating that atrial myocytes were significantly more depolarised, Figure 3B. This significance was also present at 3 Hz. According to Figure 3C, the maximal upstroke velocity of the AP was significantly greater in ventricular myocytes compared to atrial myocytes at 1 Hz and 3 Hz. When flecainide was added to the myocytes, we found that more ventricular myocytes were able to still generate an AP compared to atrial myocytes. Out of 23 atrial cells, 14 were excitable (61%), and out of 19 ventricular cells, 17 were excitable (89%), Figure 3D. Flecainide also significantly decreased the maximal upstroke velocity to a larger degree in atrial cells compared to ventricular cells, at 1 Hz and 3 Hz. This shows a preference for flecainide to inhibit sodium current in atrial cells.

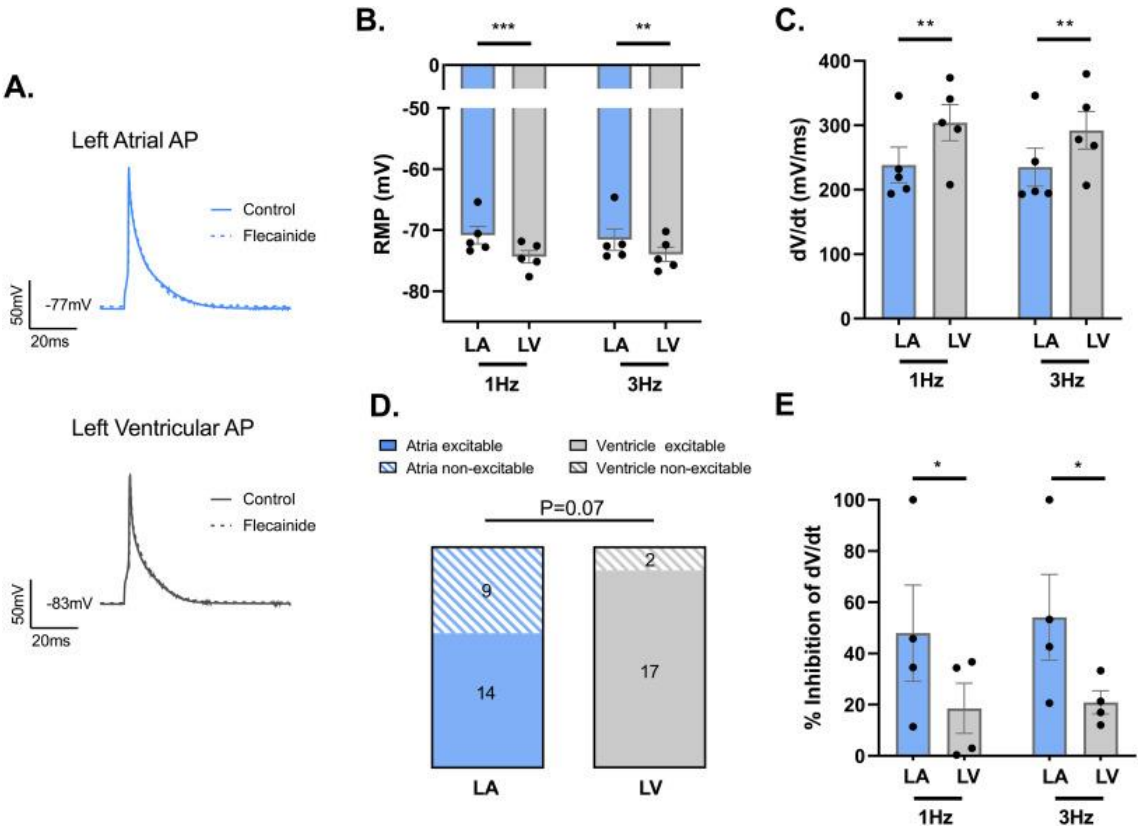

Figure 4.1. Resting membrane potential and maximal upstroke velocity in left atrial and left ventricular cells. A. Raw action potential traces. B. Resting membrane potential in LA and LV cells. RMP is significantly less negative in LA cells compared to LV cells; at 1 Hz, LA −70.8 ± 1.4 mV; LV -74.4 ± 1.0 mV p = 0.0002, n = 23–40/5 cells/mice. Each dot represents average per mouse from at least 3 cells, **p < 0.01, ***p < 0.001. Statistical significance determined by two-way ANOVA. C. Maximal upstroke velocity in LA and LV cells. dV/dt is significantly larger in ventricular cells compared to atrial cells; at 1 Hz, LA 238.6 ± 27.7 mV/ms; LV 304.2 ± 27.9 mV/ms, *p = 0.0018, n = 23–40/5 cells/mice. Each dot represents average per mouse from at least 3 cells, **p < 0.01, ***p < 0.001. Statistical significance determined by two-way nested ANOVA. D. After flecainide treatment, 14 of 23 atrial cells remained excitable, and 17 of 19 ventricular cells remained excitable, p = 0.07, Fisher's Exact Test, n = 4 mice. E. Flecainide significantly decreased dV/dT to a greater extent in atrial cells, at 1 Hz 47.9 ± 18.8% when compared to ventricle cells (At 1 Hz, 18.6 ± 9.8%, p = 0.04, Each dot represents average of at least 3 cell per mouse. Statistical analysis determined by two way nested ANOVA, n = 4. **[Experiments performed by Molly O'Reilly].**

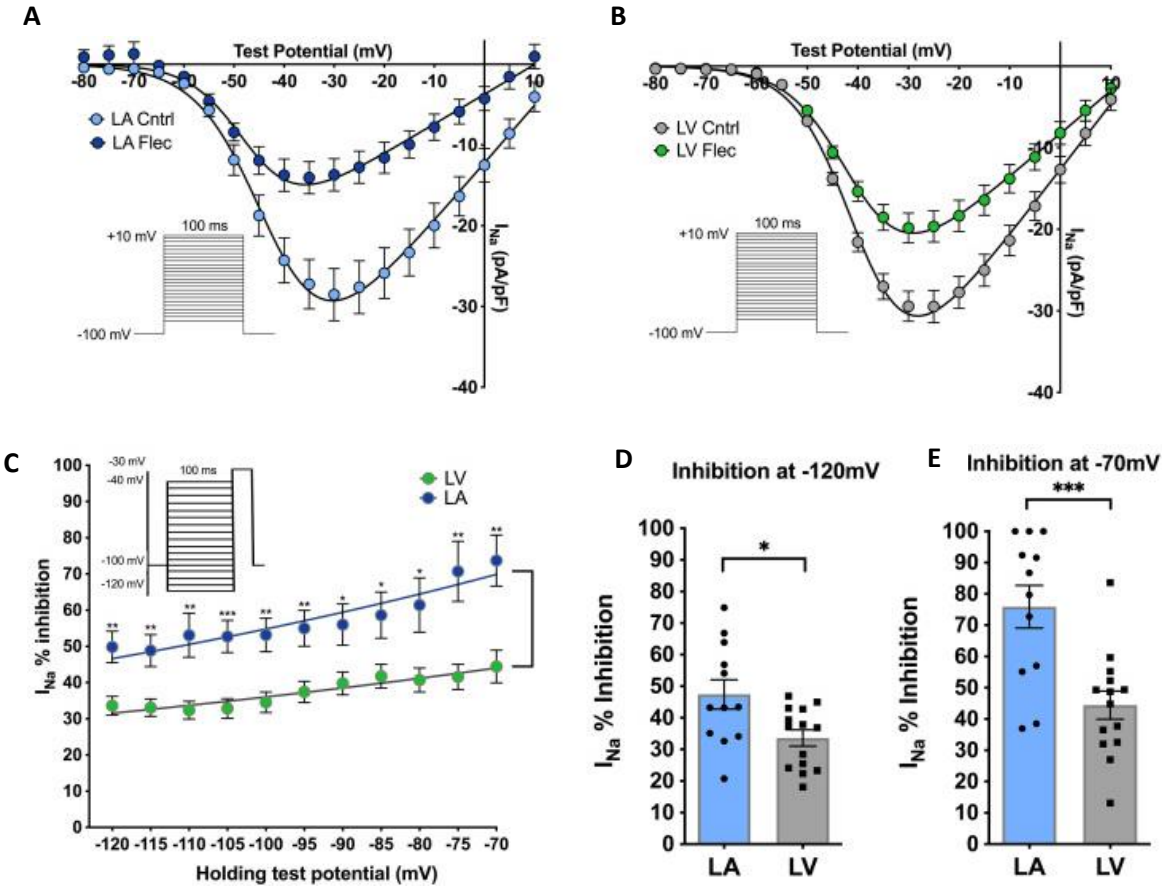

Figure 4.2. LA and LV representative raw I_{Na} traces from cardiomyocytes from WT mouse hearts, +/- 1 µm flecainide, with patch clamp protocol. A. Current-voltage relationship of I_{Na} density in LA (n=11/6 cells/mice). B. Current-voltage relationship of I_{Na} density in LV (n=14/4 cells/mice). C. I_{Na} current inhibition at different holding test potentials in LA and LV, with protocol inset. D. Inhibition of I_{Na} in LA and LV at -120 mV, LA = 75.9% ± 6.8; LV = 44.4% ± 4.5; ***p < 0.001. E. Inhibition of I_{Na} in LA and LV at -70 mV, LA = 47.4% ± 4.6; LV = 33.6% ± 2.6. *n* = 12/6 cells/mice for LA and 14/4 for LV. Each dot represents an individual cell, **p < 0.01, ***p < 0.001, ****p < 0.0001, unpaired *t*-test. **[Experiments performed by Sian O'Brien].**

To assess current-voltage relationships, we measured sodium current in atrial and ventricular cells at baseline and with 1 µM flecainide addition. I_{Na} density was measured at different test potentials in both atrial and ventricular cells. I_{Na} was generated at 1 Hz and the test potentials were increased from -80 mV to +10 mV, in 10 mV increments from a holding potential of -100 mV. The addition of flecainide reduced the I_{Na} density in both atrial and ventricular cells and was more apparent at more positive potentials with the difference being maintained across the range of test potentials. Furthermore,

I_{Na} in the LA cells was inhibited to a greater degree in compared to LV cells. From Figure 4.2D and E, we can see that at -120 mV, when all the sodium channels are activated, and -70 mV, at physiological resting membrane potential, flecainide significantly inhibited I_{Na} in both LA and LV cells but to a larger degree in the LA cells.

4.2.2. Flecainide prolongs action potential duration in LA mouse tissue

Optical mapping experiments were performed in CD1 WT mouse hearts to compare effects of flecainide on the conduction in LA and LV. Recordings were taken from the LA and LV from different hearts. This is because the atria and ventricles cannot be optically imaged at the same time. Ventricles were loaded first with Di-4-ANEPPS, and baseline and flecainide recordings were taken. Atria requires more loading of Di-4-ANEPPS which results in the ventricles becoming overloaded. Hence why, after recording ventricles with flecainide, we are unable to measure atrial baseline. The experimental and pacing protocol for this study is described in Chapter 2. Data were statistically analysed using either two-way ANOVA or a t-test, depending on dataset. Data measured across a pacing frequency was analysed using two-way ANOVA, and data measured at 10 Hz, was analysed using a paired t-test.

Addition of flecainide showed a prolongation of APD50 in the LA, Figure 4.3A. A two-way ANOVA statistical test showed this was significant across all pacing frequencies. Flecainide slightly prolonged APD50 in the LV, but this was not significant, Figure 4.3B. APD80 was also prolonged after flecainide introduction in the LA across all pacing frequencies, but not in the LV, Figure 4.3C and 4.3D. Figure 4.10 shows representative

action potentials in LA and LV at baseline and after flecainide perfusion. In the LA, there is a slight increase in the APD during late repolarisation, whereas in the LV action potential, there is no change after flecainide perfusion. The change in APD50 and APD80 with flecainide was increased at higher pacing frequencies. This correlates with the use dependence characteristic of flecainide, where the effect of flecainide is enhanced with faster stimulation rates [153]. As pacing frequency increased, the APD50 in the LA also became prolonged. As we observed in Chapter 3, baseline APD50 in the LA was shorter than baseline APD50 in the LV. At 10 Hz, flecainide significantly prolonged APD 50 and APD80 in the LA. Flecainide did not significantly affect the APD in the LV, Figure 4.4A and 4.4B.

4.2.3. Flecainide slows conduction in LA mouse tissue

CV measurements were recorded at baseline and after flecainide introduction. A two-way ANOVA demonstrated that flecainide significantly slowed conduction across all pacing frequencies in the LA. Conduction slowing was not observed in the LV however, and CV data was more variable with larger standard error means (S.E.M.s). With increased pacing frequency the CV appeared to slow in the LA at baseline and after flecainide addition, Figure 4.3E. At 10 Hz, CV was still significantly slower in the LA after flecainide addition. In the LV, it is more apparent that CV is slower after flecainide addition, but not significantly slower, Figure 4.4C. When compared to time matched controls, the significance remained. The time control experiments were performed with the flecainide experiments and served as a negative control. This demonstrates that the

slowing of conduction and the increase in APD in the LA is due to flecainide, Figure 4.5. This was reflected in the activation time in the LA and LV. We observed a slower activation time in the LA after flecainide treatment, compared to baseline. Since the CV is slower, the time it takes for the tissue to be activated will also be longer, increasing the activation time. In the ventricles, the activation time did become longer, but not to the same extent as in the atria. This is evident in the representative activation maps and activation curves, Figures 4.6 to 4.9. At baseline, the time it takes for 90% of the LA tissue to be activated was just under 3.5 ms, Figure 4.7A. After flecainide perfusion, it took approximately 5.5 ms for 90% of the LA tissue to be activated, Figure 4.7B. In the LV, 90% of the LV tissue was activated in 2.25 ms and after flecainide perfusion, activation time increased to 2.75, Figure 4.9A and B.

4.2.4. Flecainide reduces amplitude in LA mouse tissue

Amplitude was decreased in the LA after the addition of flecainide. The decrease in amplitude was maintained at all pacing frequencies. With faster pacing frequencies, the difference in amplitude between baseline and flecainide became larger, Figure 4.3G. Despite the significance, the data was highly variable, as evidenced by the high S.E.M.s. In the LV, amplitude did not significantly change before and after flecainide, Figure 4.3H. At 10 Hz, amplitude was significantly reduced after flecainide addition in the LA. No differences were observed between baseline and flecainide in the LV, Figure 4.4D.

4.2.5. Flecainide does not affect diastolic interval and time to peak in the LA and the LV

The addition of flecainide did not significantly affect the diastolic interval, but there was a trend of mean diastolic interval being shortened after flecainide was added, in the LA and LV. The diastolic interval also shortened with faster pacing frequency, Figure 4.3I and 4.3J. At 10 Hz, no significant differences were observed between LA baseline and flecainide, or LV baseline and flecainide, Figure 4.4E.

Flecainide did not significantly affect time to peak in the LA or LV. In the LV, the average time to peak was slower with flecainide at each of the pacing frequency, but was not significant, Figure 4.3K and 4.3L. In both LA and LV, there was a trend of time to peak becoming longer with faster pacing frequency. At 10 Hz, flecainide appeared to prolong the time to peak in both LA and LV, but was not significant, Figure 4.4F.

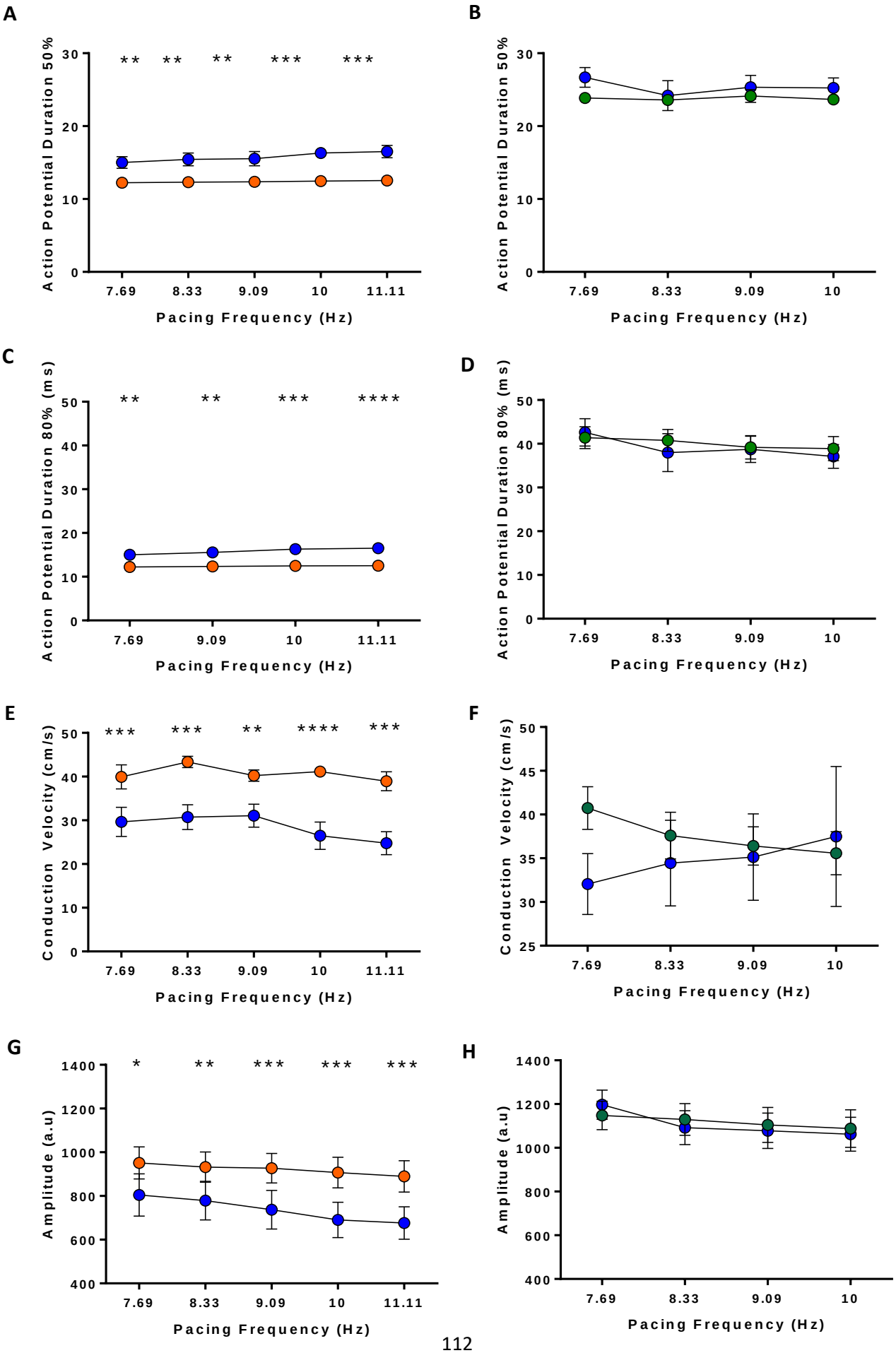
A
B
C
D
E
F
G
H
Action Potential Duration 50%
Action Potential Duration 80% (ms)
Conduction Velocity (cm/s)
Amplitude (a.u)
Pacing Frequency (Hz)
7.69
8.33
9.09
10
11.11

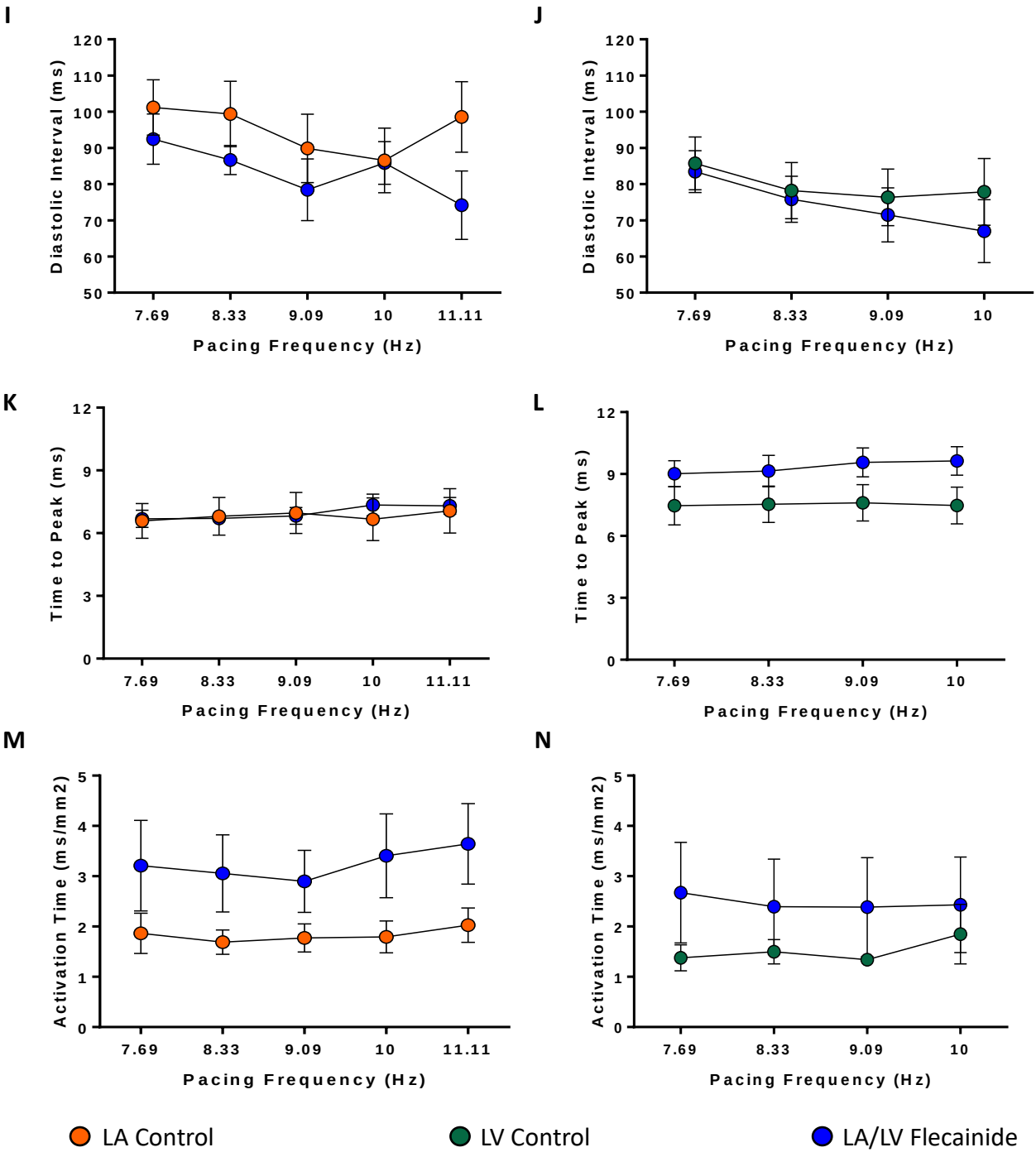

Figure 4.3A-N. APD50, conduction velocity, amplitude, diastolic interval, time to peak and activation time at different pacing frequencies. Measurements were taken in left atria (left panel) and ventricles (right panel) of CD1 mice. Measurements were taken at baseline and with flecainide. A. LA APD50 baseline v flecainide at 7.69 Hz, 12.2 ± 1.1 ms v 15.01 ± 2.1, p=0.0078, at 8.33 Hz, 12.3 ± 0.9 ms v 15.4 ± 2.4 ms, p=0.0025, at 9.09 Hz, 12.4 ± 1.2 ms v 15.5 ± 2.6 ms, p=0.002, at 10.00 Hz, 12.5 ± 1.2 ms v 16.3 ± 1.8 ms, p=0.0002 and at 11.11 Hz, 12.5 ± 1.1 ms v 16.5 ± 2.7 ms, p=0.0001. Statistical difference was determined using 2-way ANOVA with Tukey's post hoc test and was quantified as P<0.05. * represents significance between baseline and flecainide treated tissue. * denotes P<0.05, ** denotes P<0.01, *** denotes P<0.001, **** denotes P<0.0001. N=7 for each group.

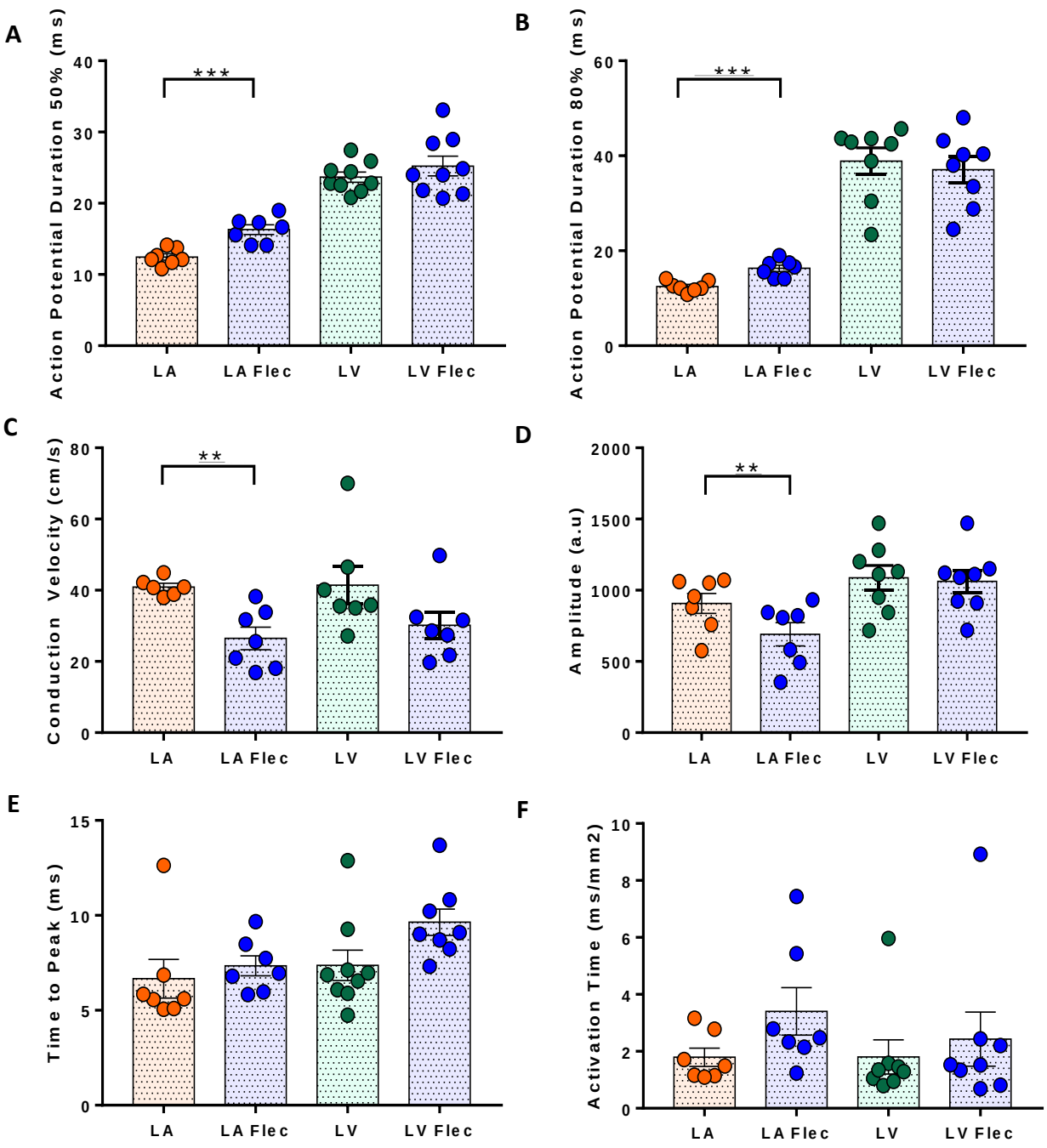

Figure 4.4A-f. APD50, APD80, conduction velocity, amplitude, time to peak and activation time between LA and LV and flecainide treatment at 10 Hz. Measurements were taken in left atria and left ventricles of WT CD1 mice. Measurements were taken at baseline and +/- flecainide. Statistical difference was determined using paired t-test and quantified as P<0.05. * represents significance between baseline and flecainide treated tissue. * denotes *P*<0.05, ** denotes *P*<0.01, *** denotes *P*<0.001, n=7.

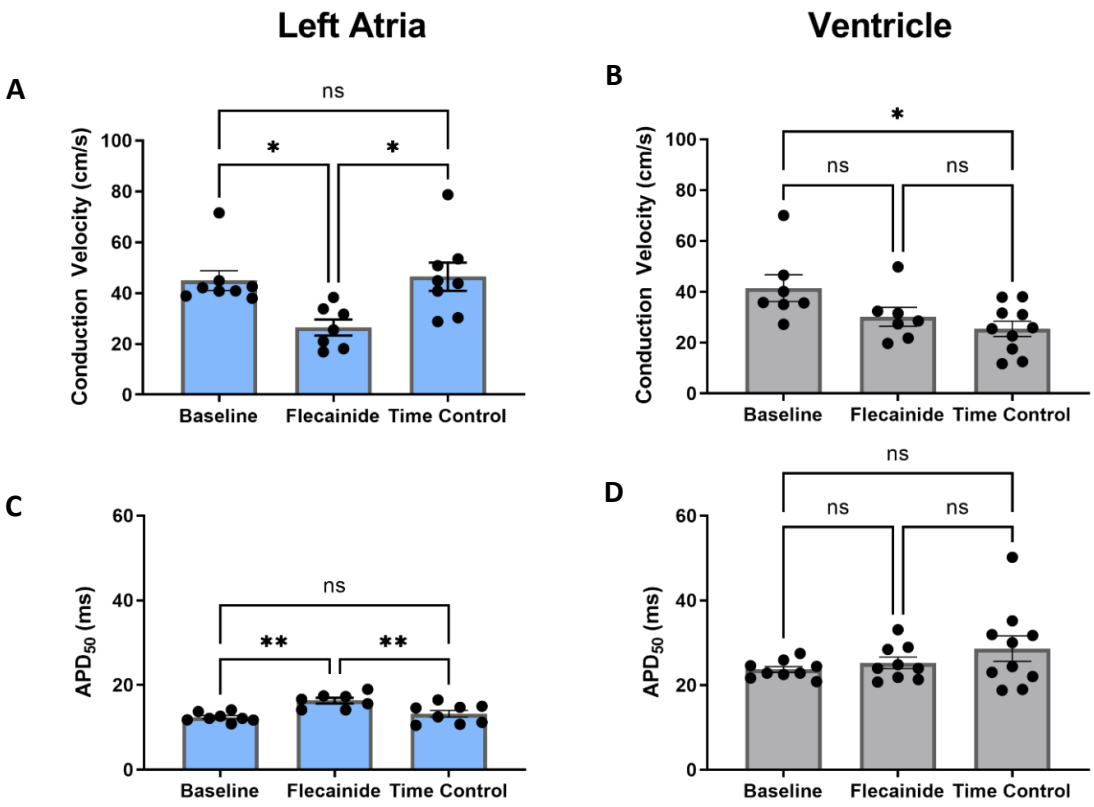

Figure 4.5. APD50 and conduction velocity in LA and LV, before and after flecainide compared to time matched controls, at 10 Hz. A. Conduction velocities (CV) are reduced in left atria (LA) when compared to the baseline and time control. B. Flecainide does not significantly affect CV in the left ventricles (LV). C. APD50 is significantly prolonged by flecainide compared to baseline and time control. D. Flecainide does not significantly affect APD50 in the LV. Each dot represents an individual heart. *$p < 0.05$, two tailed student's t-test, n = 5-7.

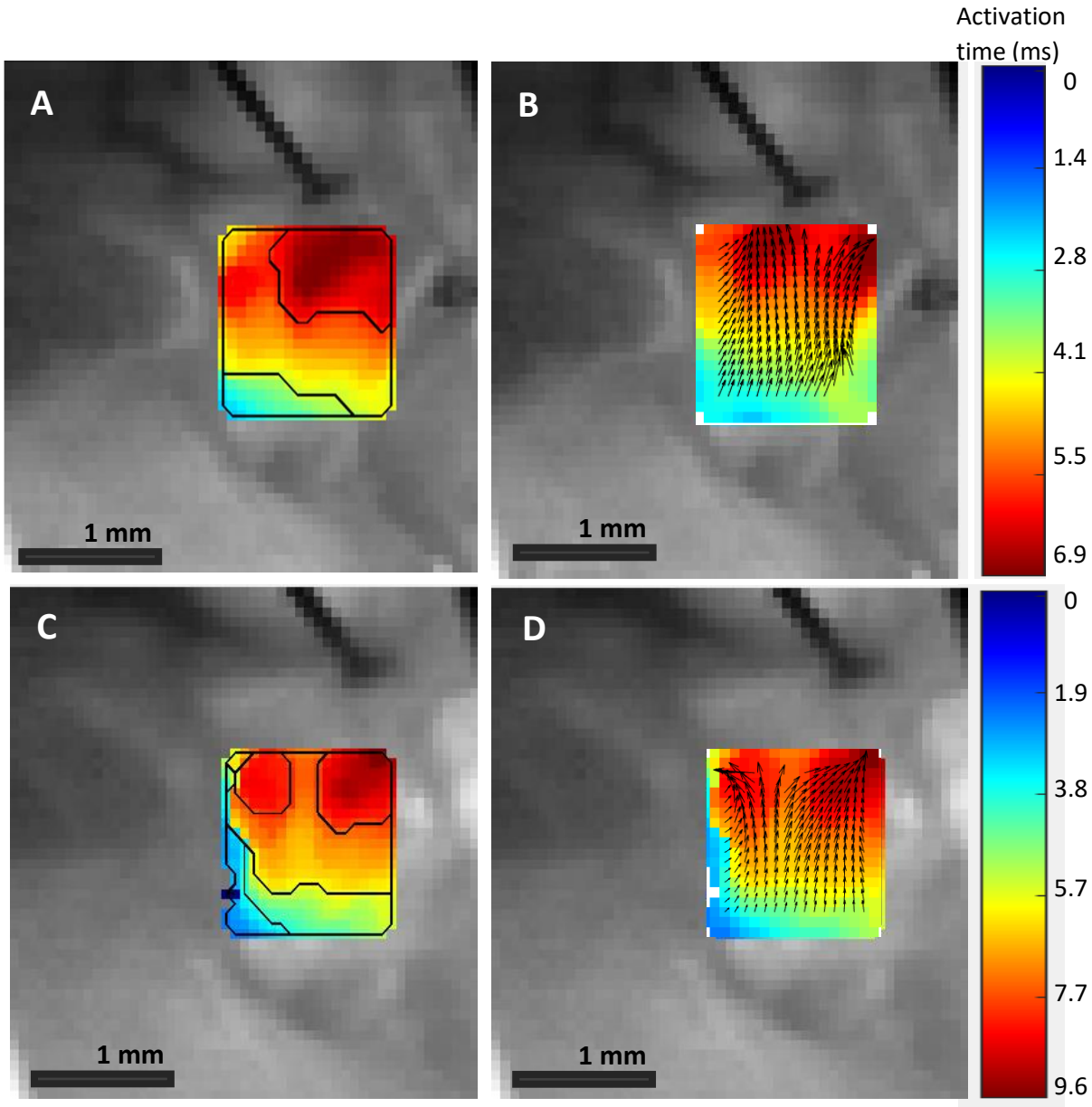

Figure 4.6A-D. Activation maps in LA at baseline and with flecainide at 10 Hz. A. Representative activation map in the LA at baseline at 10 Hz. Contour lines are spaced by 2 ms. B. Representative isomap with vectors in the LA at 10 Hz. C. Representative activation map in the LA after perfusion of 1 µM of flecainide, at 10 Hz. Contour lines are spaced at 2 ms. D. Representative isomap with vectors in the LA after flecainide was added, at 10 Hz.

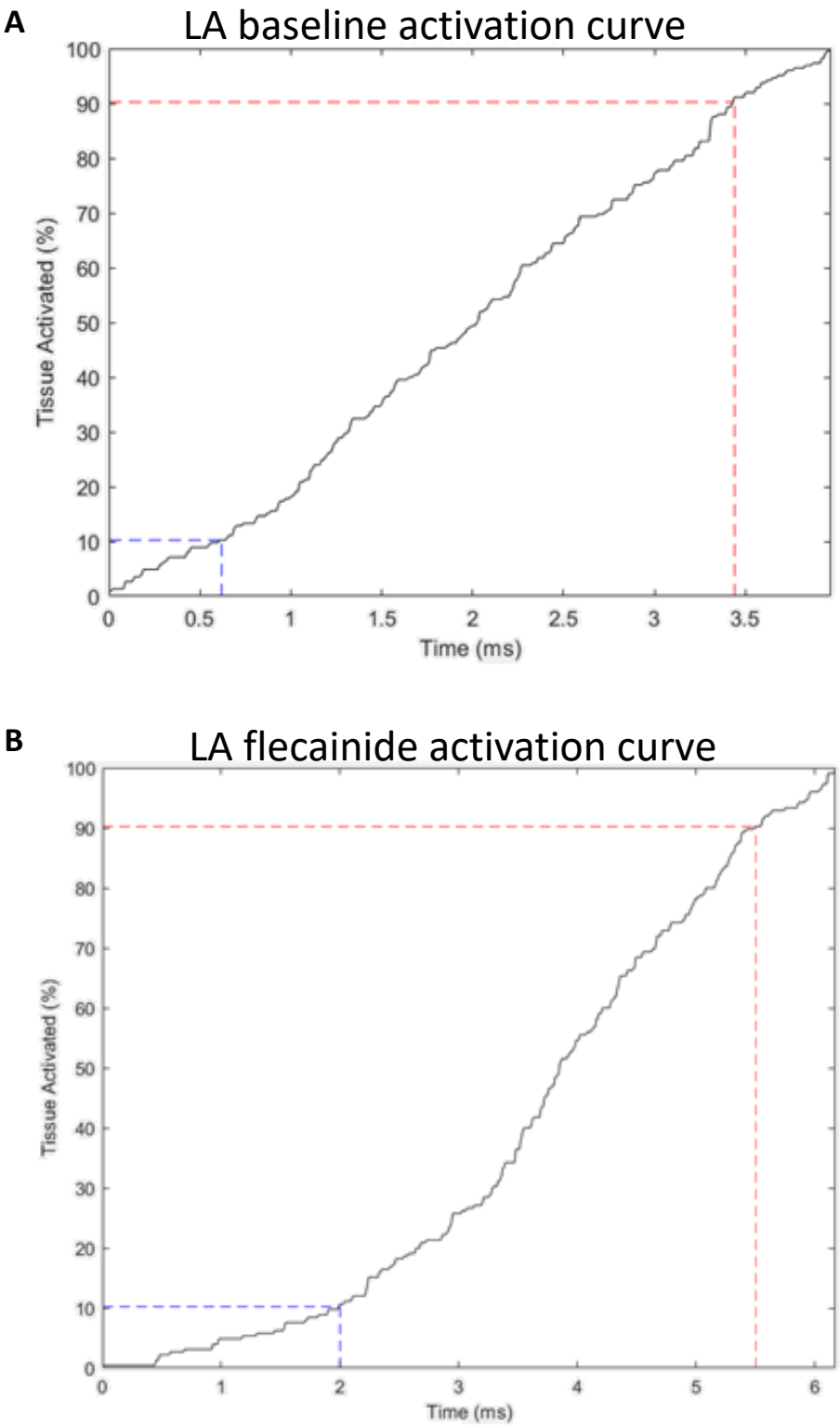

Figure 4.7A-B. Activation curve in LA baseline and LA flecainide at 10 Hz. A. Representative activation curve in the LA at baseline at 10 Hz. B. Representative activation curve in the LA after perfusion of 1 µM of flecainide at 10 Hz. Blue dashed line indicates time it takes for 10% of tissue to be activated. Red dashed lines indicate time it takes for 90% of tissue to be activated.

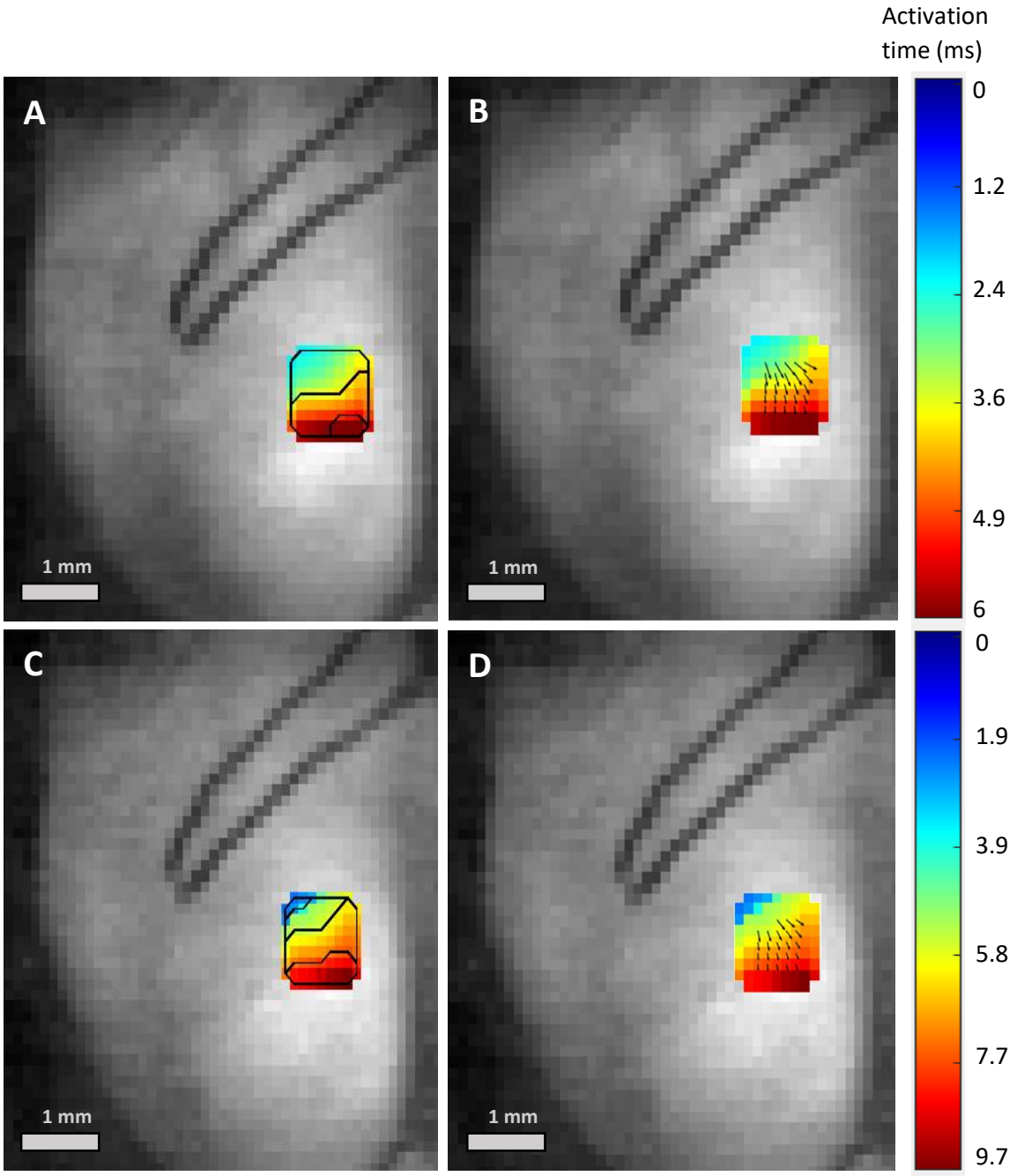

Figure 4.8A-D. Activation maps from ventricles at baseline and with flecainide at 10 Hz. A. Representative activation map in the LV at baseline at 10 Hz. Contour lines are spaced by 2 ms. B. Representative isomap with vectors in the LV at 10 Hz. C. Representative CV map in the LV after perfusion of 1 µM flecainide, at 10 Hz. Contour lines are spaced at 2 ms. D. Representative isomap with vectors in the LV after flecainide was added, at 10 Hz.

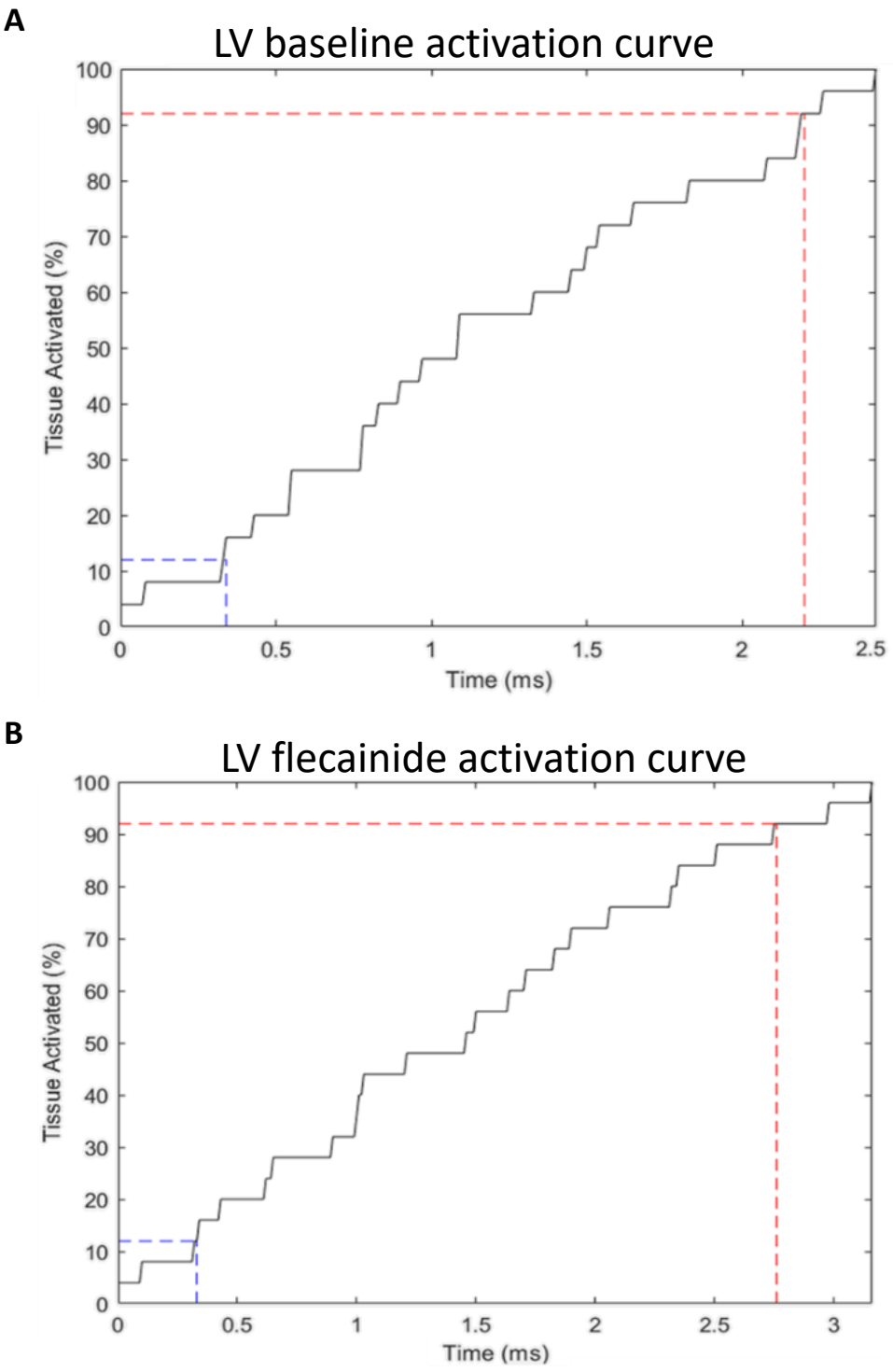

Figure 4.9A-B. Activation curve in LV baseline and LV flecainide at 10 Hz. A. Representative activation curve in the LA at baseline at 10 Hz. B. Representative activation curve in the LA after perfusion of 1 µM of flecainide at 10 Hz. Blue dashed line indicates time it takes for 10% of tissue to be activated. Red dashed lines indicate time it takes for 90% of tissue to be activated.

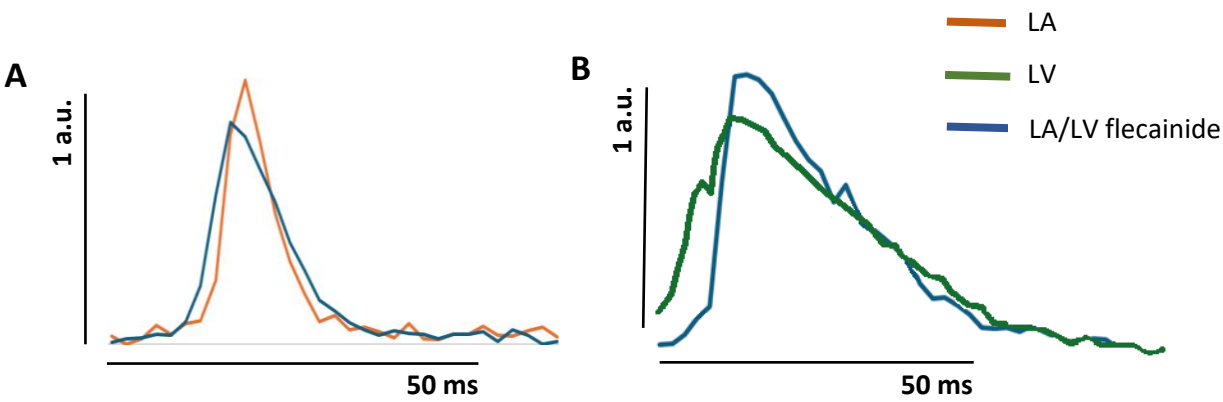

Figure 4.10A-B. Representative action potentials in LA and LV at baseline and after flecainide perfusion at 10 Hz. A. Representative example of action potential recorded from the LA at baseline (orange) and after flecainide perfusion (blue), at 10 Hz. B. Representative example of action potential recorded from the LV at baseline (green) and after flecainide perfusion (blue), at 10 Hz.

4.3 Chapter Discussion

4.3.1. Overview of main findings

The main findings from this chapter are summarised as follows:

- Flecainide slows conduction velocity to a larger degree in the atria compared to ventricles.
- Flecainide prolongs action potential duration to a larger degree in the atria compared to the ventricles.
- Flecainide slows tissue activation in atria and ventricles.

4.3.2. Flecainide and sodium channel inhibition

These results provide insight into the electrophysiological differences between atria and ventricles and how they respond to flecainide. At baseline, we have shown clear distinctions between atrial and ventricular characteristics. The difference in sodium channel expression, peak sodium current density, RMP, have the potential to alter effectiveness of sodium channel blockers. Our study demonstrates that flecainide exhibits atrial specific inhibition of sodium current in a healthy normal heart. We observe a difference in the RMP between atrial cells and ventricular cells, with atrial cells displaying a more positive RMP. This is relevant because our previous study showed that a more positive RMP increased the effectiveness of AADs [148]. The RMP is regulated by the inward rectifier channel current I_{k1} and unsurprisingly, studies have found I_{k1} channel expression to be higher in the ventricles compared to the atria [154].

In addition to this, ventricular cells displayed significantly greater maximal upstroke velocity of the AP compared to the atrial cells. This is critical for rapid signal conduction through the heart [155]. The effect of flecainide was more pronounced in atrial cells, with a larger reduction in the maximal upstroke velocity and a higher proportion of unexcitable cells after flecainide treatment. The differential sensitivity of flecainide is more apparent at more positive RMPs, demonstrating that small fluctuations in RMP can have significant effects on AAD efficacy [148].

4.3.3. Differential effects of flecainide in LA and LV in WT mouse

From our optical mapping data, we observe the effects of flecainide clearly in the atria and ventricles. We find that flecainide prolongs the APD significantly in the LA yet did not have a significant effect in the ventricles. Andrikopoulos 2015 notes that flecainide inhibits the opening of potassium channels, especially the rapid component of the delayed rectifier K^+ current (I_{Kr}), which is responsible for repolarisation of the cardiac cells. This prolongs the action potential duration in atrial and ventricular tissue [156]. Interestingly, in the Purkinje fibres, flecainide caused a shortening of the APD. This is supported by a study by Ikeda 1985, where they investigated effects of flecainide on electrophysiological properties of isolated canine and rabbit myocardial fibres. They measured changes in APD50, APD90 and effective refractory period (ERP), after flecainide, in canine Purkinje fibres and ventricular muscle fibres. With increasing flecainide concentration (0.1, 1 and 10 μg/ml), APD50, APD90 and ERP were prolonged

in the ventricular muscle fibres. In Purkinje fibres, APD50 and APD90 was truncated, and the ERP was shorter at 1 μg/ml and returned to baseline values at 10 μg/ml [157].

Flecainide interacts with Kir2.1 channels, a major determinant for I_{K1}. The I_{K1} plays a critical role in the final phase of repolarisation. In the ventricles, increasing the I_{K1} current through flecainide helps the ventricles reset faster, i.e. reach RMP faster. Although flecainide blocking other Kv channels result in prolonging the APD, the increase in I_{K1} may be balancing the prolongation out, therefore overall ventricular APD is not affected. In the atria, flecainide does not increase the I_{K1} making the atrial APD prolongation more apparent [158].

We also observed conduction slowing in the LA after flecainide treatment at each pacing frequency. The effect of flecainide slowing CV in the LA is to be expected. The primary mechanism of flecainide's action is the blockade of sodium channels, which are essential for the initiation and propagation of electrical signals in the heart. By blocking these channels, flecainide prevents sodium ions from entering the cardiac cells, which is a crucial step for the generation and propagation of the action potential, slowing the conduction. Flecainide did not cause the conduction to slow in the LV. This may be due to flecainide’s preference for sodium channel blocking in the atria. We do see some slowing of the conduction in the LV but not enough to show significance. Therefore, this further demonstrates the preferential effects of flecainide in the atria and ventricles. The activation time, which has an inverse correlation with CV, did not show significant difference between baseline and flecainide, but we do see an increase in activation time in both LA and LV.

To validate the drug induced effects of flecainide, we concurrently performed time control experiments. This was essential as action potential morphology and conduction can change over time without intervention. APDs tend to become prolonged and CV becomes slower with increased time due to effects of run down. This refers to loss of ion channel activity and can be caused by changes in the intracellular environment, loss of essential cofactors, or even phototoxicity [159]. The time control experiments were identical to the flecainide experiments except the time control experiments did not include addition of flecainide. Figure 4.5A showed flecainide significantly slowed down conduction in the LA, but there was no difference with the time control. Figure 4.5 showed a significant difference in CV between baseline and flecainide measurements, and between flecainide and time control measurements. In the ventricles, flecainide had no effect on the APD or the CV. Firstly, this demonstrates that the effects we are seeing are the effects of flecainide and not due to time. Secondly, flecainide has a preferential effect on the atria compared to ventricles and this can be attributed to the more positive resting membrane potential of the atria and the availability of sodium channels in the atria. The greater effect of flecainide in the atria could result in a more pronounced increase in refractoriness.

The distinct responses to flecainide between atria and ventricles highlight a potential avenue for the development of chamber specific AADs. Development of atrial specific AAD which does not alter the electrophysiology of normal function ventricles may be possible. Patients diagnosed with early stages of AF, with normal ventricular function can be administered flecainide with minimal modulation of ventricular electrophysiological characteristics. This selective targeting could also minimise adverse

effects associated with AADs and improve patient outcomes. Future work could investigate combining clinically relevant AADs with drugs that modulate the RMP to enhance their effectiveness.

5. Investigating effectiveness of flecainide in global ischaemia

5.1. Chapter Introduction

Cardiac ischaemia is the inadequate blood supply to an area of the heart which is caused by blockage of the blood vessels. Inadequate blood supply results in lack of oxygen and nutrients being delivered to the ischaemic region. Ischaemic heart disease (IHD) also known as coronary heart disease (CHD), is defined as heart problems resultant of narrowing of coronary arteries via blood clot clot or constriction of blood vessel, or more commonly by buildup of plaque. Ischaemia is a major cause of mortality in the developed world. It is the leading cause of death in men and women. Each tissue or organ has a unique mechanism in which ischaemia occurs and responds to it differently [160].

Ischaemia in the heart can result in biochemical and metabolic disturbances causing arrhythmias. During ischaemia, reduced oxygen delivery to tissue causes intracellular ATP levels to fall as there is no oxygen for the mitochondria to use to produce ATP. 60 – 70% of ATP is used to drive the contraction of the heart muscle while the remaining 30 – 40% is used in the function of ion pumps. Fatty acids account for most of the cardiac ATP, with the remainder ATP coming from glucose, lactate, ketone bodies and amino acid. Under ischaemic conditions, the heart shifts from aerobic metabolism to anaerobic metabolism. Under normal conditions, the heart produces energy in the form of ATP using oxygen, glucose and lipids. When oxygen transport and tissue oxygenation are compromised, like in the case of ischaemia, anaerobic metabolism occurs. In anaerobic metabolism the heart produces energy from fatty acid utilisation and upregulation of glucose oxidation. As a result, during ischaemia, there is a further decrease in the

production of ATP, the main energy source of the heart muscle. Since sodium pumps require ATP to function, the unavailability of ATP means that the movement of ions into and out of cell is altered, achieving elevated extracellular K^+ ions and elevated intracellular Ca^{2+} and Na^+ ions. This causes significant changes in resting membrane, action potential characteristics and conduction of cells. Resting membrane potential becomes less negative, action potential becomes shorter and conduction becomes slower [161]. Furthermore, ischaemia triggers an inflammatory response leading to accumulation of excessive collagen and other extracellular matrix proteins in the affected tissue, replacing the damaged myocardial tissue with collagen-based scar, known as fibrosis, further contributing to the arrhythmogenic milieu [162]. The presence of fibrosis in the heart also causes slowing of conduction, re-entry and ventricular desynchronization, exacerbating effects of ischaemia [163].

Treatment for ischaemic heart disease depends on the underlying cause and the severity of the condition. The primary goal of treatment is to improve blood flow to the heart muscle, control their symptoms and prevent further damage. Some of the treatments available include medications, lifestyle changes or surgical procedures. Drugs that are used to manage symptoms and during acute phase of ischaemic heart disease include β-blockers, Ca^{2+} antagonists and nitrates. Ranolazine and ivabradine have recently been added to ischaemia treatment for reducing angina. Patients also receive aspirin, an antiplatelet drug, and statins, a lipid lowering compound [164]. If medication is insufficient, examples of surgery treatment include angioplasty, a minimally invasive form of surgery.

The Cardiac Arrhythmia Suppression Trial (CAST) I was instituted by the National Heart, Lung, and Blood Institute (NHLBI), to test the hypothesis that suppression of premature ventricular contractions (PVCs) with antiarrhythmic agents such as flecainide and encainide reduced mortality. Encainide and flecainide are both class IC antiarrhythmic agents that are reported to be effective in suppressing ventricular arrhythmias [165]. Saini *et al* study established whether response to one agent predicted the response to the other agent. They concluded that despite the similarity in electrophysiological profile, the antiarrhythmic effect of the two agents was different [165]. The CAST I was conducted between 1986 and 1989 and was prompted by the fact that patients that suffered from myocardial infarctions had a higher risk of mortality due to arrhythmia. 1498 patients were recruited and randomized to different treatments, 857 to encainide or placebo and 641 to flecainide or placebo. In CAST I, antiarrhythmic drugs effectively suppressed asymptomatic ventricular arrhythmias but increased arrhythmic death [166]. The trial was terminated early due to lethal arrhythmias. Encainide and flecainide treated patients had a 3.6-fold excessive risk of arrhythmic death compared to placebo treated patients. Within two years after enrollment, encainide and flecainide were discontinued due to increased mortality and sudden cardiac death. Studies pertaining to the trial hypothesised that an interaction between flecainide and ischaemia could account for the observed increase in cardiac and sudden deaths in the study group in the CAST I.

According to Andrikopoulos *et al* 2015, the main precaution for flecainide administration is to rule out structural heart disease and/or ischaemic cardiomyopathy for the purpose of preventing increased risk of proarrhythmia [156]. This was based on the CAST I trial.

We have seen recent trials such as EAST-AFNET 4 and Flec-SL (flecainide short - long) demonstrate a low rate of ventricular arrhythmia when flecainide is used after cardioversion and during rhythm control therapy. However there is a lack of evidence of the effects of flecainide treatment in patients with ischaemia, without structural heart disease. Flec-SL study only enrolled 600 patients. They were randomised into different treatment groups and treated with flecainide for either four weeks or six months. Patients enrolled either had early AF, over 75 years old, and had had a transient ischaemic attack, or fulfilled two of the following requirements, female sex, over 65 years of age, diagnosed with diabetes mellitus, heart failure, hypertension, coronary artery disease, chronic renal disease, or left ventricular hypertrophy [167]. The study found that while long-term treatment with flecainide was superior, short-term flecainide treatment was almost as effective in preventing recurrences of AF. The study suggested that short-term treatment with flecainide can be considered for AF patients who are at increased risk for adverse drug effects, potentially making therapy safer and applicable for more patients. A larger cohort is required to properly determine the effects of flecainide in ischaemic hearts [167].

The primary aim of this study was to

- determine the ideal flow rate required to induce ischaemia; this will be determined by changes in conduction velocity (CV)
- assess the interaction between flecainide and ischaemia in healthy wildtype (WT) hearts, using optical mapping.

- investigate the interaction of ischaemia and flecainide on CV and action potential in the ventricles.

5.2. Chapter Results

5.2.1. Pilot study

A pilot study was designed to determine the ideal flow rate to achieve ischaemia. Baseline flow rate was set as 4 ml/min. Flow rate was reduced by 60% and 30% to induce ischaemia, achieving flow rates 2.4 ml/min and 1.2 ml/min, respectively. Data was recorded from WT CD1 hearts from ventricles and di-4-ANEPPS was used to image the heart. Normal flow rate (4 ml/min) and correct temperature (37^{o}C) was established before each experiment. Hearts were prepared as described in Chapter 2.3.4.1. Once the heart was loaded onto the optical mapping rig, the heart was allowed to stabilise for 10 minutes. Every 10 minutes, the heart underwent a dynamic pacing protocol ranging from 7.14 Hz to 14.29 Hz. This was to determine how long it took for the ischaemia to take effect.

Figure 5.1 shows how reduced flow rates of 2.4 ml/min and 1.2 ml/min compared with normal flow rate at 10 Hz. With low flow rates, APD50 became shorter whereas with normal flow rates, APD increased over time. APD50 was the shortest at 30 minutes in both of the lower flow rates (Figure 5.1A). At 30 minutes, average control APD50 was 19.4 ± 5.8 ms with a 38.9% increase from baseline. At 30 minutes with 2.4 ml/min flow rate, average APD50 was 14.4 ± 1.9 ms with a 33.9% decrease from baseline and with 1.2 ml/min flow rate, average APD50 was 10.5 ± 1.5 ms with a 44.6% decrease from baseline. As expected, experiments that had the lowest flow rate, 1.2 ml/min, had the shortest APD, indicating a more severe ischaemia.

Figure 5.1B shows the change in conduction velocity (CV) over 60 minutes, at 10 Hz. CV became slower at the lowest flow rate, at 1.2 ml/min. At 2.4ml/min and in the control group, the CV stayed consistent, or became slightly faster over time.

We summarised from the pilot data that the ideal flow rate to achieve ischaemia was 2.4 ml/min, a 40% decrease of normal flow rate at 4 ml/min. The effect of ischaemia was observed by the decrease in APD50 and slowing of conduction after 10 to 20 minutes of low flow perfusion. Although ischaemia was observed with a flow rate of 1.2ml/min, collecting data with such a low flow rate proved difficult. Measurements were more variable and often difficult to analyse with several missing datapoints.

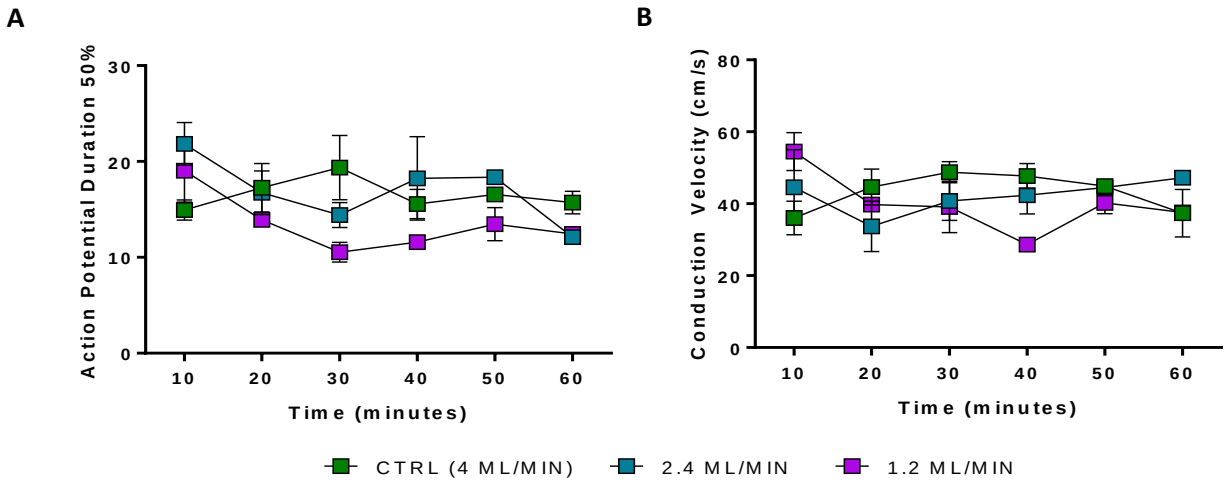

Figure 5.1A-B APD50 and CV in ventricles with low flow rate at 10 Hz over 60 minutes. APD50 and CV were measured in WT ventricles in mice every 10 minutes, for 60 minutes. The 3 groups consisted of control (green points), 2.4 ml/min (blue points) and 1.2 ml/min (purple points), n=3.

Figures 5.2, 5.3 and 5.4 show isomaps and APD50 maps in the ventricles at different timepoints during ischaemia. Maps were generated at 10 Hz every 10 minutes. Figure 5.2 has been taken from the control group. Figure 5.3 represents low flow group with 2.4 ml/min and Figure 5.4 represents low flow group with 1.2 ml/min. Figures 5.3A and 5.3G and Figures 5.4A and 5.4G represents baseline, before ischaemia has been induced.

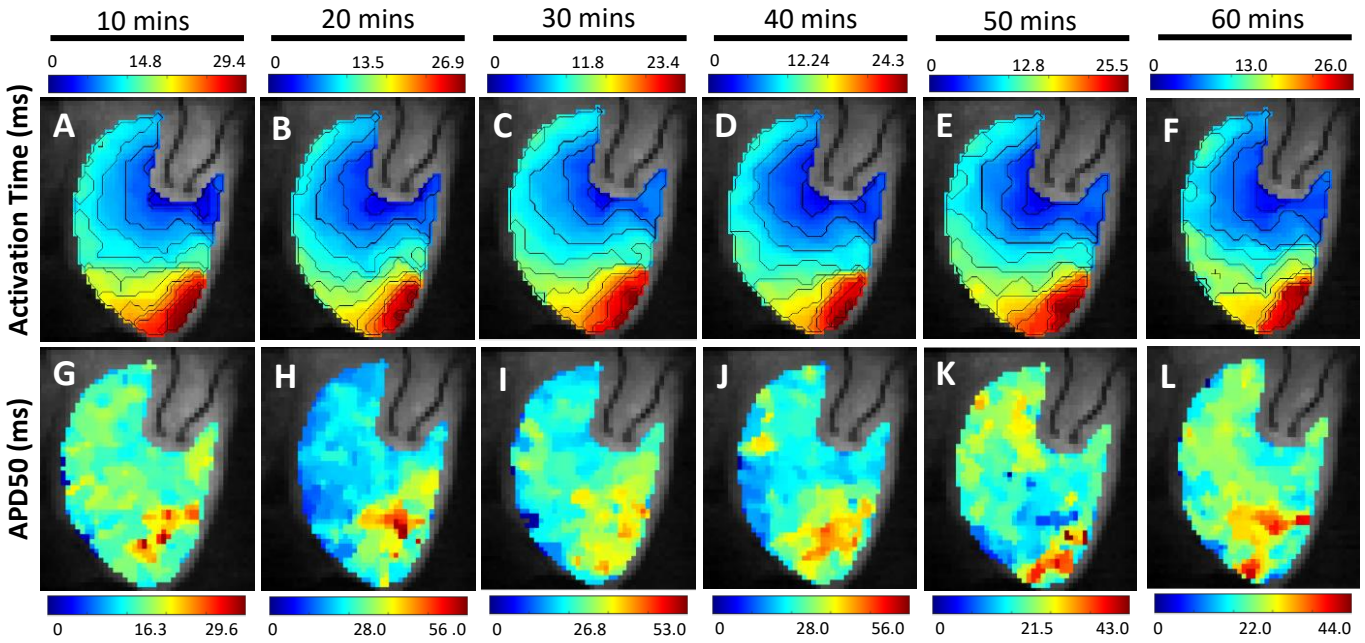

Figure 5.2A-L APD50 and CV in control hearts at 10 Hz over 60 minutes. APD50 and CV were measured in WT ventricles in mice every 10 minutes, for 60 minutes. The 3 groups consisted of control (green points), 30% reduced flow rate (blue points) and 60% reduced flow rate (purple points), n=3.

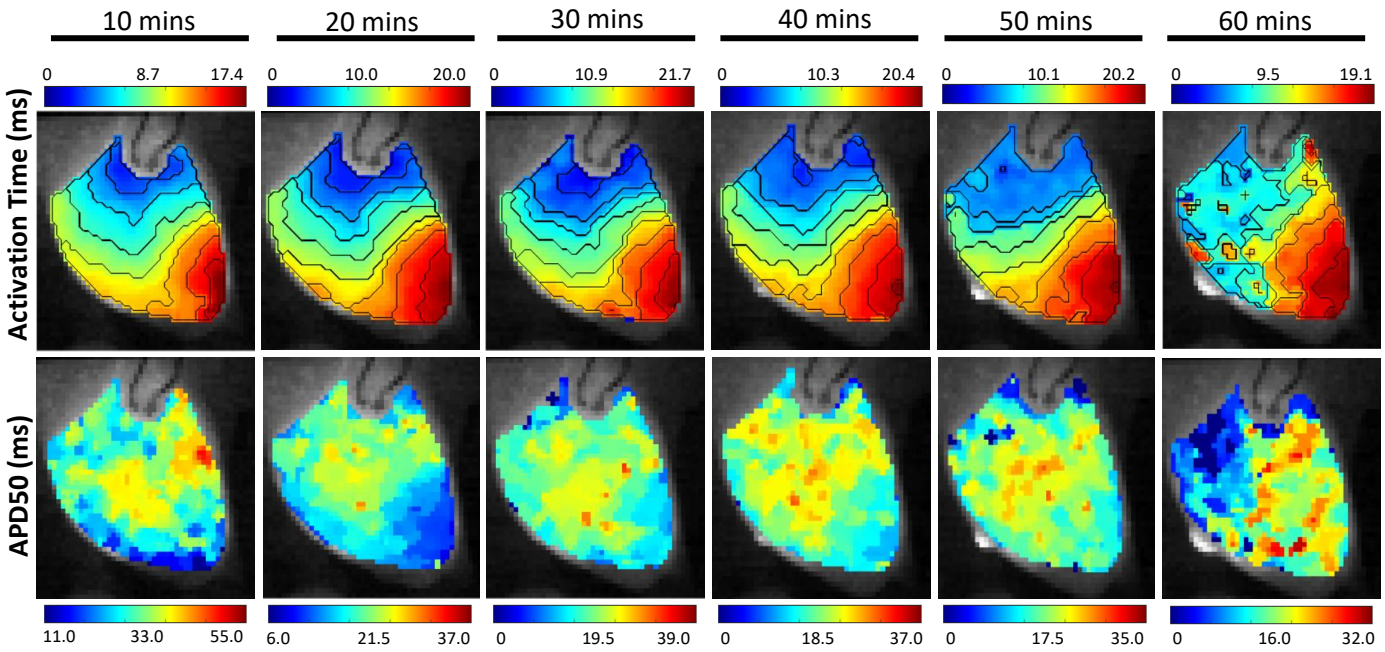

Figure 5.3A-B APD50 and CV in ventricles with 2.4 ml/min flow rate at 10 Hz over 60 minutes. APD50 and CV were measured in WT ventricles in mice every 10 minutes, for 60 minutes. The 3 groups consisted of control (green points), 30% reduced flow rate (blue points) and 60% reduced flow rate (purple points), n=3.

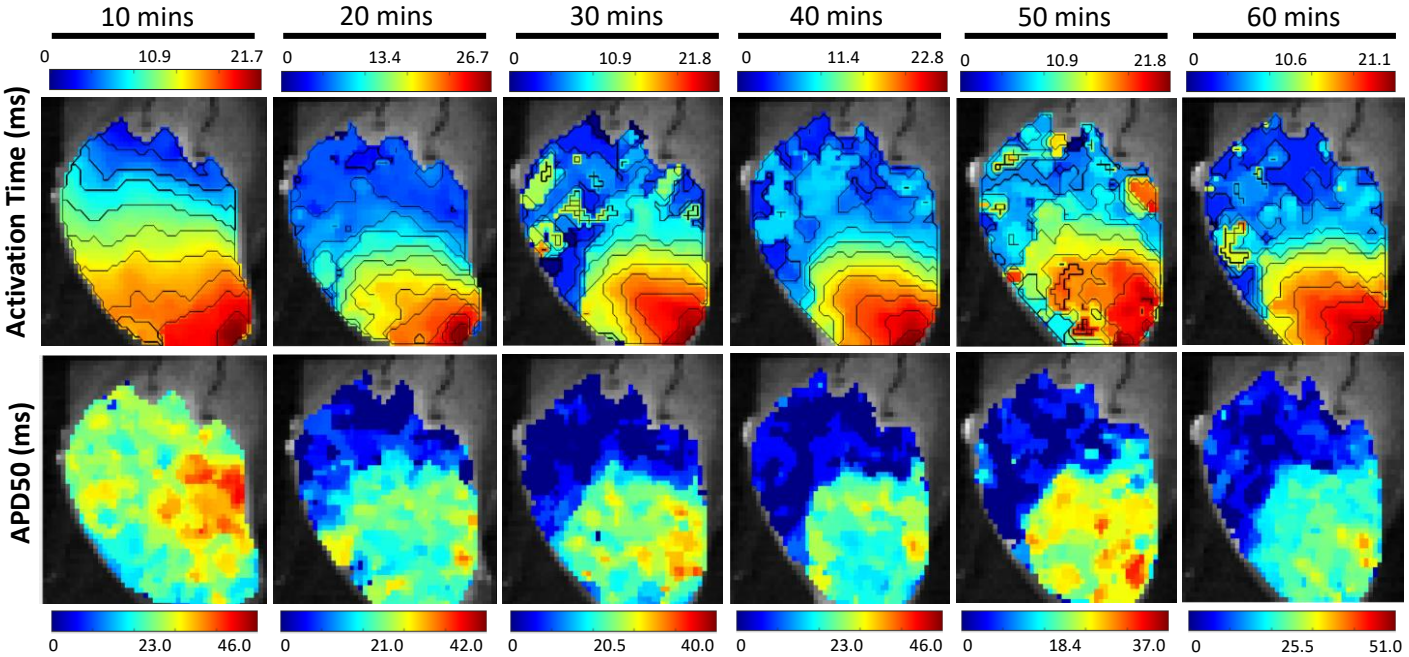

Figure 5.4A-B APD50 and CV in ventricles with 1.2 ml/min flow rate at 10 Hz over 60 minutes. APD50 and CV were measured in WT ventricles in mice every 10 minutes, for 60 minutes. The 3 groups consisted of control (green points), 30% reduced flow rate (blue points) and 60% reduced flow rate (purple points), n=3.

5.2.2. Effect of flecainide with global ischaemia via low flow rate

Our dataset was divided into four groups to address our research question. These groups were: normal flow without flecainide, normal flow with flecainide, low flow without flecainide, and low flow with flecainide. We used a concentration of 1 μM flecainide, which is commonly used in clinical settings, with a typical target range between 0.2 and 4 μM [86].

We measured three parameters, APD50, APD80 and CV, at various timepoints: baseline, during ischaemia, and after the addition of flecainide. Once hearts were loaded onto the rig, hearts were given 10 minutes to recover from the stress of the isolation process and to allow stabilisation of the heart rate. This ensured that cardiac function was optimal before the experiment began. Baseline recordings were taken after the recovery period. Ischaemia was induced immediately after the baseline recording, and a recording was taken after 15 minutes of low flow rate perfusion. Flecainide was then introduced and allowed to wash in for 15 minutes before another recording was taken. The protocol used for the low flow ischaemia can be found in Chapter 2.3.4.1.

5.2.2.1. Effect of ischaemia on APD and CV compared to baseline

Figure 5.2 shows the APD50 in each of the 4 groups. Figure 5.2A represents hearts that underwent ischaemia and flecainide. Figure 5.2B represents hearts that did not undergo ischaemia but were treated with flecainide. Figure 5.2B represents hearts that

underwent ischaemia but were not treated with flecainide. Figure 5.2C represents hearts that did not udergo ischaemia or flecainide treatment and was used as a control.

Causing ischaemia via low flow perfusion prolonged the APD50 and APD80 in some of the hearts, but not all. Figure 5.2A and 5.3A showed no difference between baseline and ischaemia, however, in Figure 5.2C and 5.3C, ischaemia caused APD shortening compared to baseline. Ischaemia is expected to shorten APDs as ischaemia causes a large outward flow of K^+ from cells affecting the repolarisation [161]. We observe a slowing of CV caused by ischaemia but this is not significant, Figures 5.4A and 5.4C.

5.2.2.2. Effect of flecainide on APD and CV compared to baseline

Figures 5.5C and 5.6C looks at the effects of flecainide only on the APD50 and APD80. Interestingly, flecainide caused a shortening of the APDs and this was shown to be significant at APD80. Flecainide is commonly known to increase APD It caused CV to slow significantly at all pacing frequencies tested. This is to be expected as when flecainide blocks Na^+ channels, it slows the upstroke of the action potential, reducing the conduction velocity.

5.2.2.3. Effect of flecainide in presence of low flow ischaemia

The interaction between ischaemia and flecainide appears to be inconclusive from this dataset. Figures 5.5A, 5.6A and 5.7A shows effects of flecainide in the presence of ischaemia. There was no difference from the baseline when ischaemia is induced and

flecainide is added. For example, at 10 Hz, the average APD50 value at baseline was 26.0 ± 4.2 ms. During ischaemia, this was 24.8 ± 8.3 ms and after flecainide was added, average APD50 value was 24.0 ± 10.7 ms.

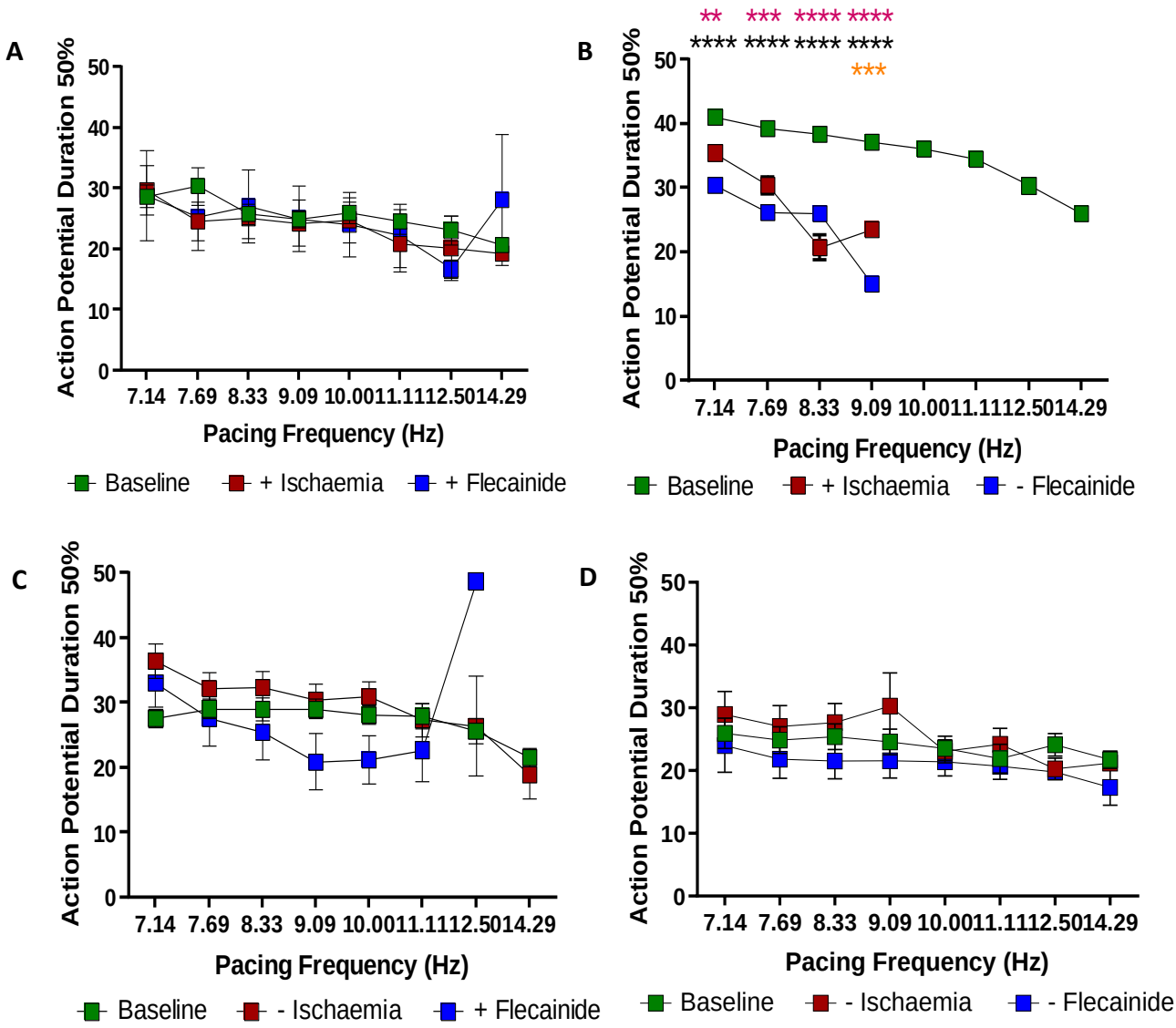

Figure 5.5A-D. APD50 in ventricles at baseline and with ischaemia and flecainide. APD50 was measured in ventricles of WT mouse hearts. Green points represent baseline, red points represent ± ischaemia and blue points represent ± flecainide. Each panel represents the 4 groups. A. Group + ischaemia and + flecainide, no significant differences observed, n=7. B. Group + ischaemia and – flecainide. Significant difference at slower pacing frequencies, between baseline and + ischaemia and baseline and - flecainide (ischaemia), n=7. C. Group – ischaemia and + flecainide. Significant difference observed at 10 Hz, between – ischaemia (control) and +

flecainide, n=7. D. Group – ischaemia and – flecainide. No significant differences observed between control groups, n=7. Statistical significance determined by multiple t test. Significance quantified as P<0.05. * denotes P<0.05, ** denotes *P<0.01*, *** denotes *P<0.001*, **** denotes *P<0.0001*. * = baseline vs. ± ischaemia, * = baseline vs. ± flecainide, * = ± ischaemia vs. ± flecainide.

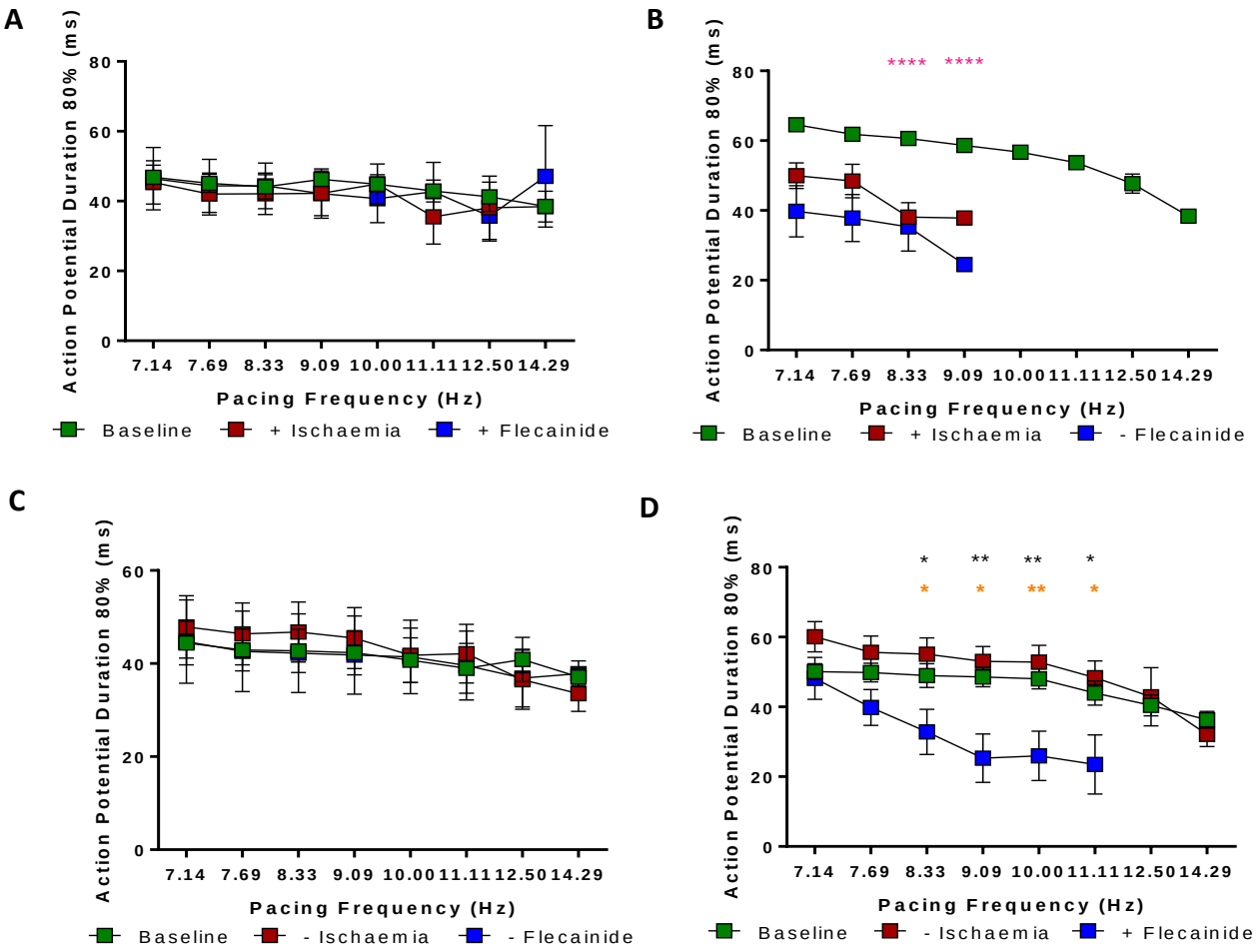

Figure 5.6A-D. APD80 in ventricles at baseline and with ischaemia and flecainide. APD80 was measured in ventricles of WT mouse hearts. Green points represent baseline, red points represent ± ischaemia and blue points represent ± flecainide. A. Group + ischaemia and + flecainide. No significant difference observed between groups, n=7. B. Group + ischaemia and – flecainide. Significant difference observed at 8.33 Hz and at 9.09 Hz between baseline and ischaemia, n=7. C. Group -ischaemia and _ flecainide. Significant difference observed between 8.33 Hz and 11.11 Hz between baseline and +flecainide, and between – ischaemia and + flecainide, n=7. D. Group – ischaemia and – flecainide. No significant difference observed, n=7. Statistical significance determined by multiple t test. Significance quantified as P<0.05. * denotes *P<0.05*, ** denotes *P<0.01*, *** denotes *P<0.001*, **** denotes *P<0.0001*. * = baseline vs. ± ischaemia, * = baseline vs. ± flecainide, * = ± ischaemia vs. ± flecainide.

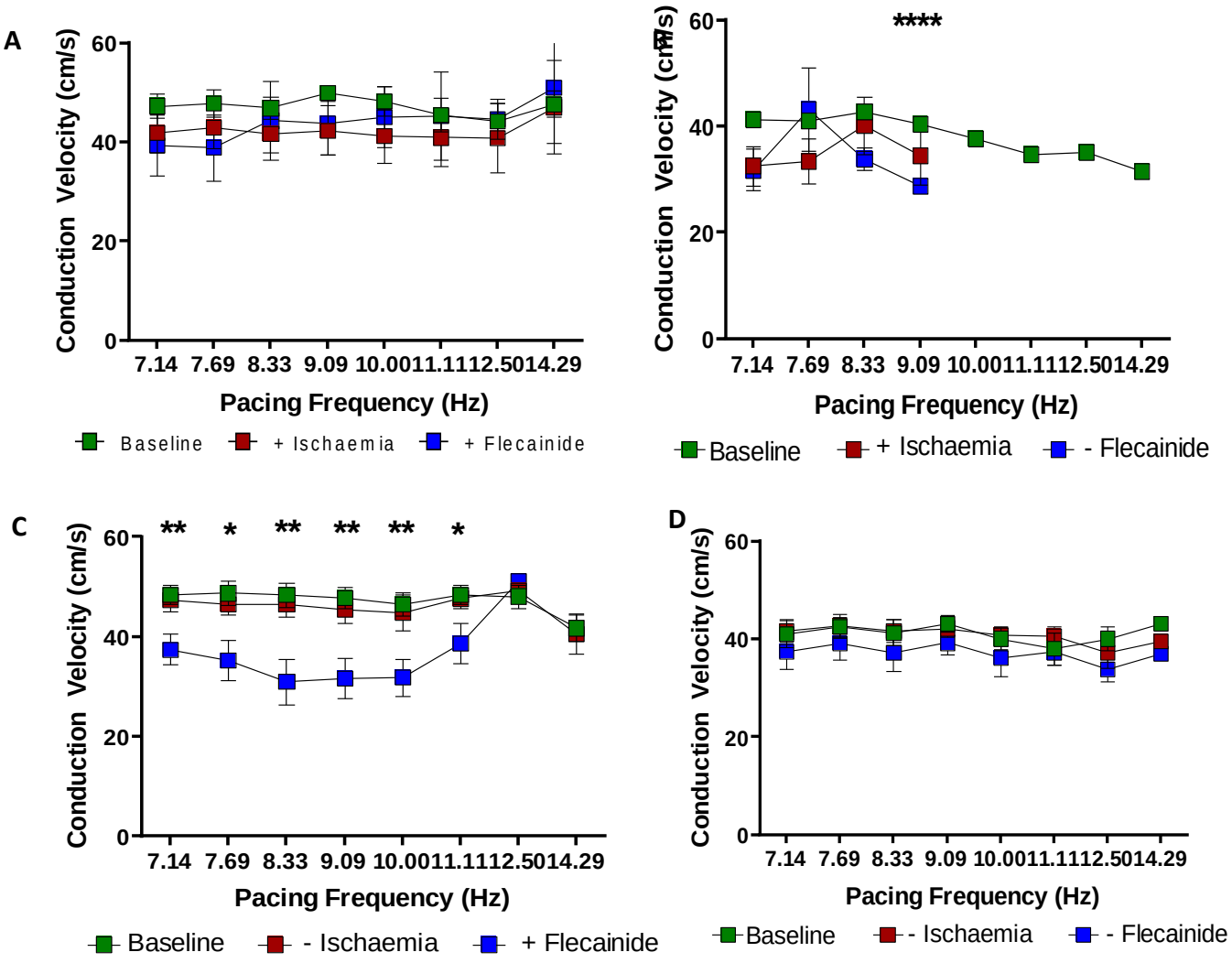

Figure 5.7A-D. Conduction velocity (CV) in ventricles at baseline ± ischaemia and ± flecainide. CV measured in WT mouse hearts across pacing frequencies. A. CV in group +ischaemia and +flecainide. No significant difference observed between groups, n=7. B. CV in group + ischaemia and – flecainide. Significant difference at 9.09 Hz between baseline and – flecainide, n=7. C. CV in group –ischaemia and +flecainide. Significant difference observed between baseline and flecainide between 7.14 Hz and 11.11 Hz, n=7. D. CV in group –ischaemia and –flecainide. No significant difference observed within the groups, n=7. Statistical significance determined by multiple t test. Significance quantified as P<0.05. * denotes P<0.05, ** denotes *P<0.01*, *** denotes *P<0.001*, **** denotes *P<0.0001*. * = baseline vs. ± flecainide.

5.2.3. Global ischaemia via low perfusion pressure

5.2.3.1. Constant flow rate vs. constant perfusion pressure

When experimental conditions were maintained by flow rate, hearts showed severe atrioventricular block (AVB) and slower heart rates (below 200 bpm), even in the control experiments. We plotted a graph to observe the heart rate over the duration of the experiment, measuring the heart rate every 10 minutes, Figure 5.8, over the course of 50 minutes. We found that the heart rates dropped very quickly from the first timepoint, in the constant flow rate experiments, Figure 5.8A. In the group with normal flow rate (4 ml/min) and + flecainide, indicated by green points, initial heart rate at timepoint 1 was 373.3 ± 60.6 bpm, dropping to 146.7 ± 98.7 bpm at 50 minutes, a decrease of 60.7%. In group 2.4 ml/min +flecainide, indicated by orange points, initial heart rate (pre-ischaemia) was 240 ± 58.9 bpm, dropping to 40 ± 20 bpm at 50 minutes, an 83.3% decrease. In group 4 ml/min –flecainide (control group), indicated by pink points, initial heart rate started at 140 bpm, increasing to 160 bpm, 14.2% increase after 50 minutes.

We followed up with constant perfusion pressure experiments to see how this compared with constant flow rate experiments and see how it would affect heart rates and heart viability in comparison. We used low pressure to induce ischaemia in the hearts. Using the same percentage decrease, the perfusion pressure was reduced from 80 mmHg to 50 mmHg, a 40% decrease. In the control group, at baseline, timepoint 1, heart rate was 315 ± 75.5 bpm. After 50 minutes, in experiments with normal pressure, heart rate went down to 300 ± 60 bpm, a 4.5% decrease than baseline. In experiments with low pressure, heart rate at baseline was 346.7 ± 140.5 bpm and came down to 220

± 91.7 bpm at the final timepoint, a 36.5% decrease, Figure 5.8B. From this it can be observed that the heart rate was more stable when controlled by perfusion pressure rather than flow rate. The number of experiments that were successful was also higher when the experiments were controlled by perfusion pressure compared to flow rate. Heart rates that fell below 300 bpm were excluded from the study.

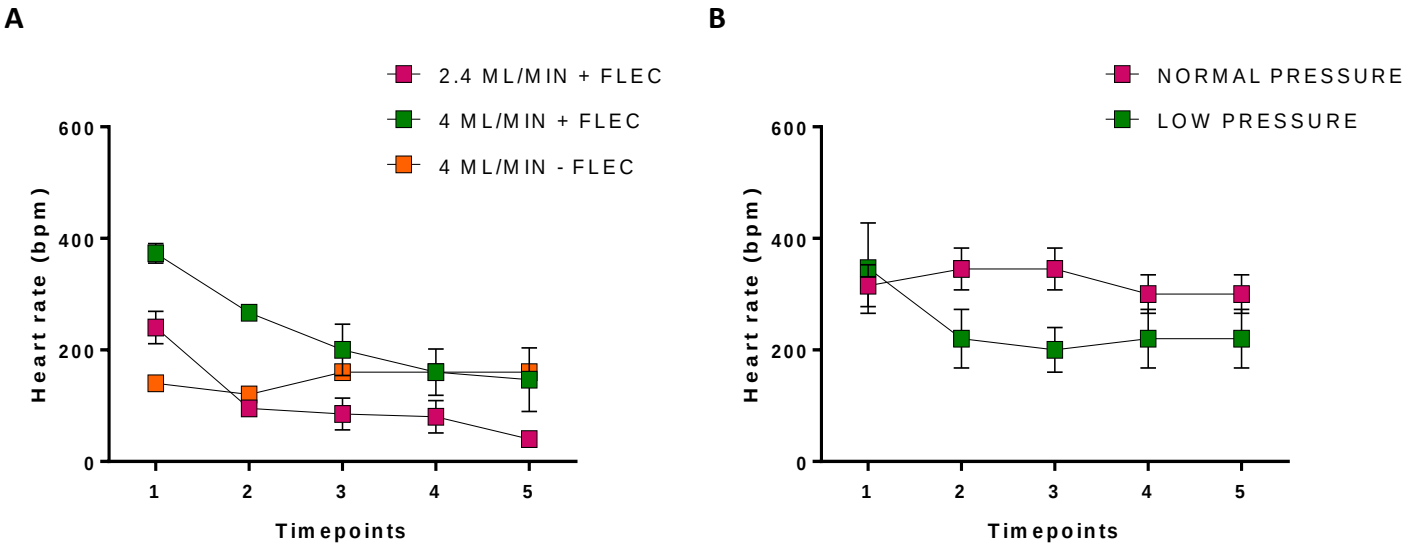

Figure 5.8A-B Heart rates in mouse ventricles in experiments with constant flow rate compared to experiments with constant perfusion pressure over 50 minutes. Heart rates were measured in WT ventricles in mice every 10 minutes, for 50 minutes. Figure 5.4.A, in 4 ml/min +flecainide group (n=3), at baseline, timepoint 1, the heart rate decreased from 373.3 ± 60.6 bpm to 146.7 ± 98.7 bpm, a decrease 60.9%. In 2.4 ml/min +flecainide (n=4), heart rate went from 240 ± 58.9 bpm to 40 ± 20 bpm, an 83.3% decrease. In control group, 4 ml/min –flecainide (n=1), heart rate went from 140 bpm to 160 bpm, a 14.3% increase. ■ indicates group low-flow +flecainide, ■ indicates group normal flow +flecainide, ■ indicates group normal flow –flecainide. Figure 5.4.B, in normal pressure group (n=3), heart rate with from 315 ± 75.5 bpm to 300 ± 60 bpm, a 4.5% increase. In low pressure group (n=4), heart rate went from 346.7 ± 140.5 bpm to 220 ± 91.7 bpm, a 36.5% decrease from baseline.

5.2.3.2. Effect of ischaemia and flecainide on APD50

Following on from the heart rate comparison between the experimental setups, we repeated the ischaemia and flecainide experiments, triggering ischaemia through 40% reduction of perfusion pressure. As before, experiments were divided into four groups, ischaemia without flecainide, ischaemia with flecainide, no ischaemia without flecainide, and no ischaemia with flecainide. Baseline measurements were taken immediately after stabilisation of the heart. In the relevant groups, ischaemia was induced immediately after baseline recording and flecainide was added 30 minutes after baseline recording.

Figure 5.9 shows the APD50 in the four groups across several pacing frequencies. Ischaemia appeared to prolong the APD50, Figure 5.6A and 5.6B. APD50 prolongation was not statistically significant in Figure 5.9A but showed significance in Figure 5.9B, specifically at 7.14 Hz and 7.69 Hz. We did not observe the effects of flecainide on baseline. In Figure 5.9, there were no differences on the APD50 between baseline and flecainide. In the presence of ischaemia, flecainide did not alter the APD50. Overall, the APD50 was longer after ischaemia compared to baseline and became more prolonged when ischaemia was extended, represented by –flecainide. With increased pacing frequency, APD50 became shorter, however this was not significant. We isolated values at 10 Hz only and this showed no significant differences in any of the groups between baseline, ± ischaemia and ± flecainide.

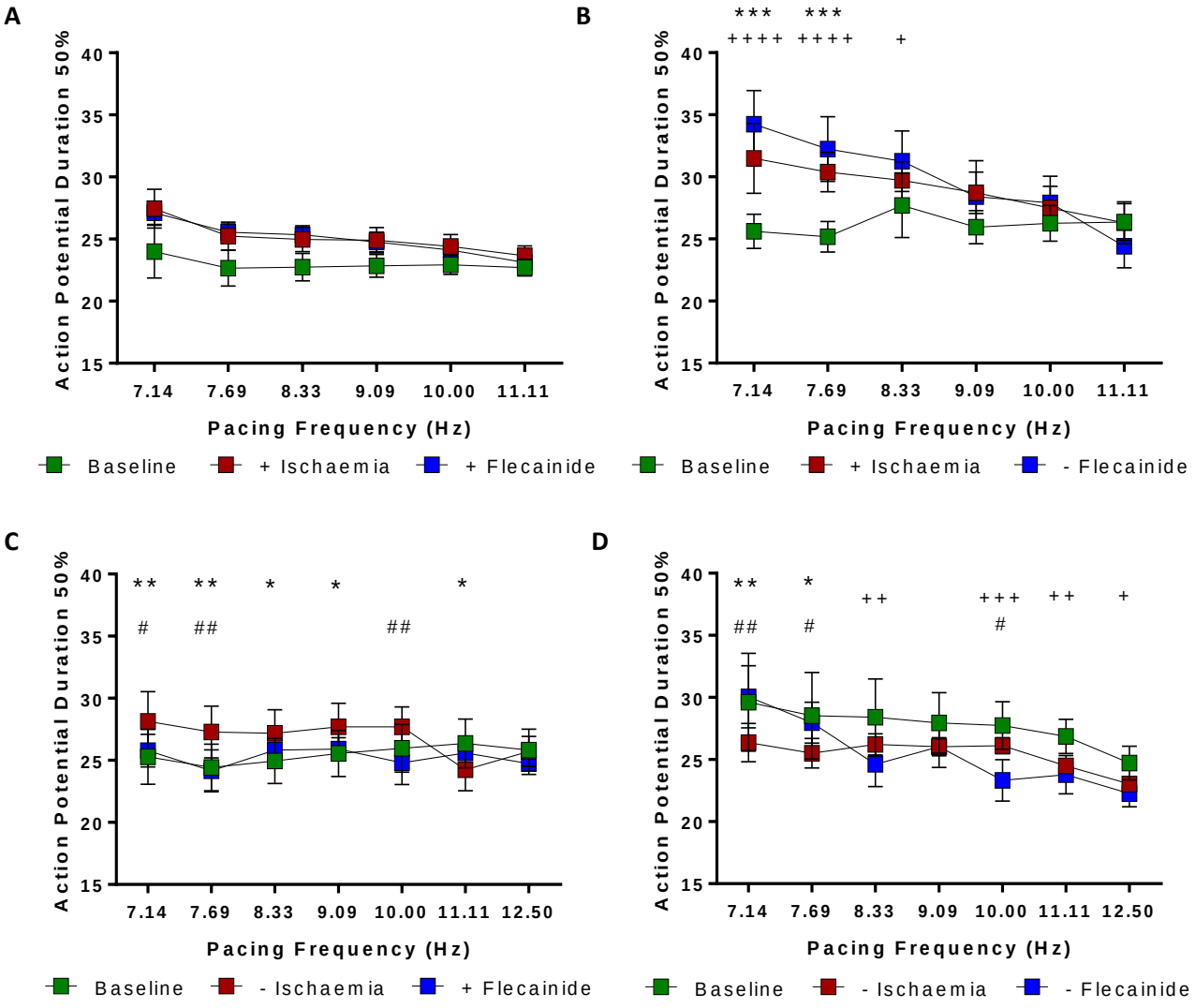

Figure 5.9A-D APD50 in ventricles at baseline and with ischaemia and flecainide. A) APD50 at baseline with ischaemia and with flecainide. B. APD50 at baseline with ischaemia and without flecainide. No significant differences between baseline and ischaemia, baseline and flecainide, and ischaemia and flecainide. C) APD50 at baseline with no ischaemia and with flecainide. D. APD50 at baseline without ischaemia and without flecainide. Each dot represents average number of hearts, n=5. Experiments were analysed using two-way ANOVA with Tukey post hoc test, *$p < 0.05$, **$p < 0.01$, ***$p < 0.001$, ****$p < 0.0001$. * represents difference between baseline and ± ischaemia, + represents difference between baseline and ± flecainide, and # represents difference between ± ischaemia and ± flecainide.

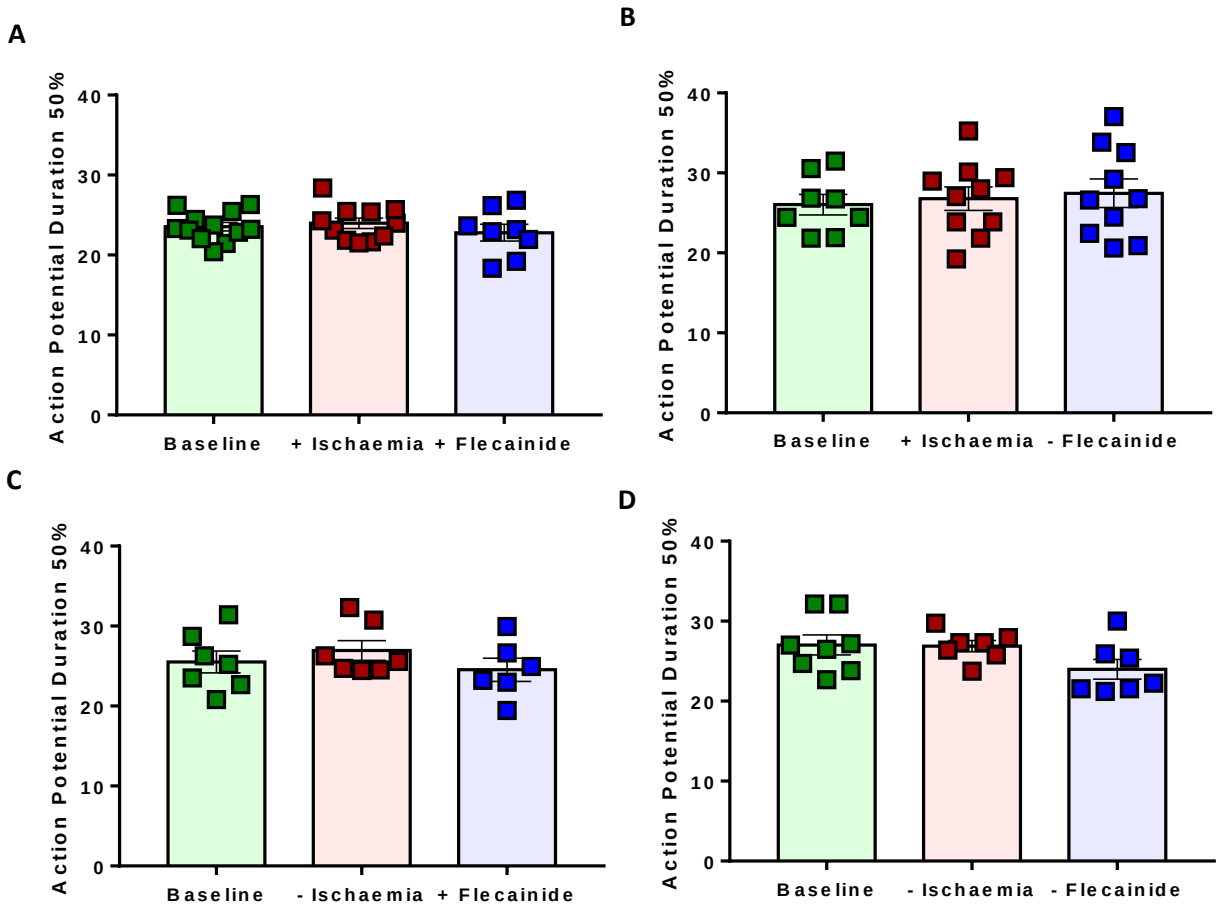

Figure 5.10A-D APD50 in ventricles at baseline and with ischaemia and flecainide, at 10 Hz. A. APD50 in group + ischaemia and + flecainide. No significant differences between treatments, n=8-10. B. APD50 in group + ischaemia and - flecainide. No significant differences between treatments, n=8-12. C. APD50 in group – ischaemia and + flecainide. No significant differences between treatments, n = 7-8. D) APD50 in group – ischaemia and - flecainide. No significant differences between treatments; 25.5 ± 3.6 ms vs. 27.0 ± 3.2 ms vs. 24.5 ± 3.6 ms, n = 6-7. Experiments were analysed using one-way ANOVA with Tukey post hoc test.

5.2.3.3. Effect of low-pressure ischaemia and flecainide on conduction velocity

Conduction velocity (CV) was measured in WT hearts at baseline and with ± ischaemia and ± flecainide, at several pacing frequencies. Using a two-way ANOVA we showed statistical differences CV in the four groups across several pacing frequencies, Figure 5.11.

Under ischaemic conditions, CV became slower when compared to baseline. This was shown to be significant in Figure 5.11A but wasn't significant in Figure 5.11B although the shortening of CV is present at all pacing frequencies. In hearts without ischaemia, the same slowing of CV is not observed, indicating that the effect we see is down to ischaemia.

The effect of flecainide was also apparent. Figure 5.11C shows that flecainide significantly slowed the CV at all pacing frequencies. When flecainide was not added, CV remained at values closer to baseline or ischaemia levels, indicating that the slowing of CV was down to flecainide. In the presence of ischaemia, flecainide reduced CV from 69.9 ± 7.2 cm/s at baseline to 42.4 ± 2.5 cm/s, a 39.9% decrease. In the absence of ischaemia, flecainide reduced the CV from 69.8 ± 4.0 cm/s at baseline down to 49.9 ± 5.9 cm/s, a 28.5% decrease. This indicates that flecainide could potentially cause a further slowing of the CV when ischaemia is present which could be proarrhythmic and may have been one of the contributing factors for increased mortality in clinical trials. The significant difference between CV during ischaemia and after flecainide at all pacing frequencies further solidifies that flecainide slows the CV to a greater extent in the presence of ischaemia, Figure 5.11A. The significant differences observed between

baseline, ± ischaemia and ± flecainide was maintained when the data was isolated at 10 Hz, Figure 5.12.

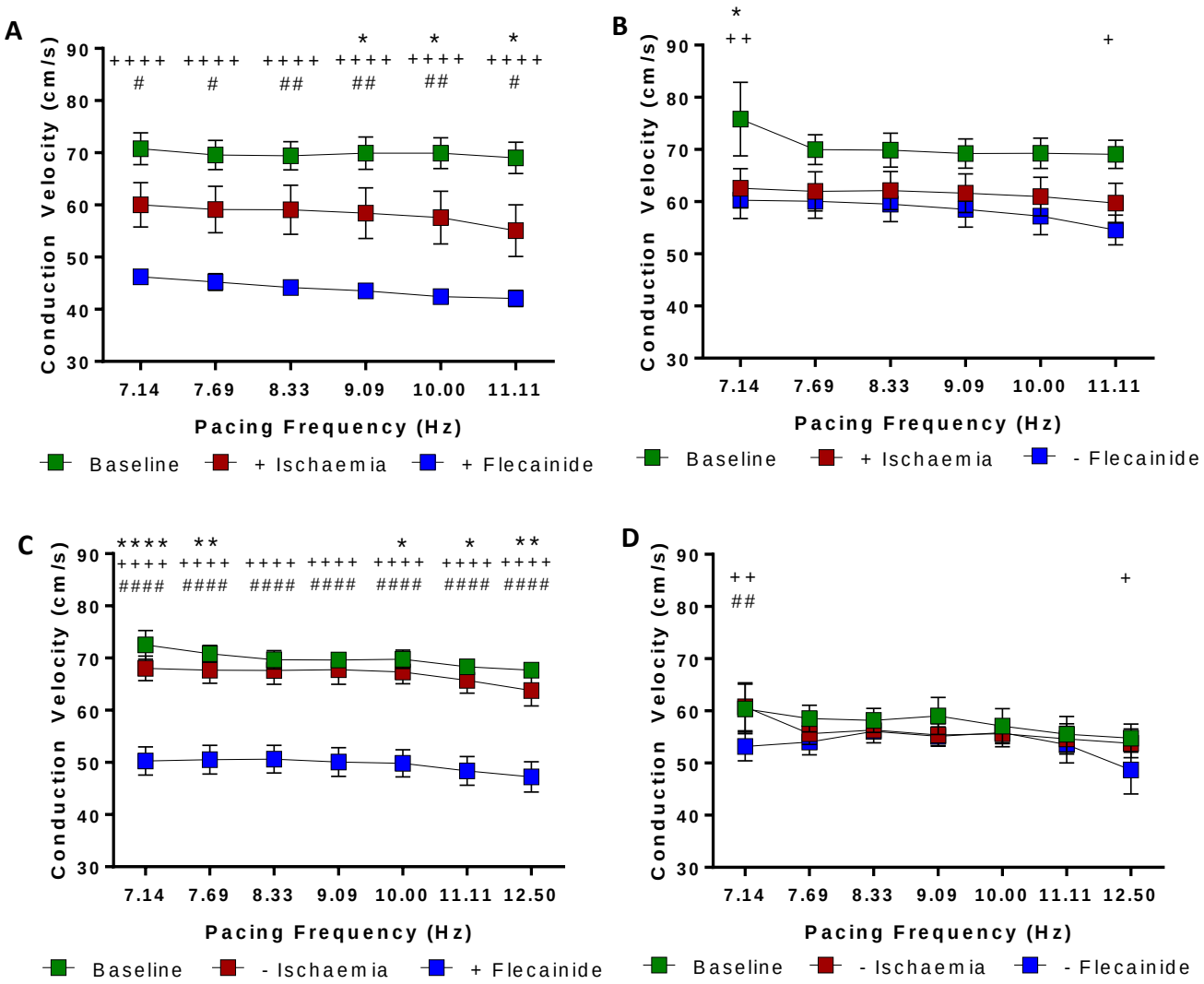

Figure 5.11A-D. CV in ventricles at baseline and with ischaemia and flecainide. A. CV in group + ischaemia and – flecainide. Significant differences between baseline vs. ischaemia and baseline vs. -flecainide at 7.14 Hz only. N = 7. B. CV in group + ischaemia and + flecainide. Significant differences between baseline and ischaemia at faster pacing frequencies. Significant differences between baseline and + flecainide at all pacing frequencies. Significant differences between + ischaemia and + flecainide at all pacing frequencies. N = 6. C. CV in group – ischaemia and – flecainide. Significant difference between baseline and – flecainide, and between – ischaemia and – flecainide at 7.14 Hz. Significant difference between baseline and – flecainide at 12.5 Hz. N = 5. D. CV in group – ischaemia and + flecainide. Significant difference between baseline and + flecainide, and between -ischaemia and + flecainide at all pacing frequency. N = 5. Each dot represents average number of hearts. Experiments were analysed using two-way ANOVA with Tukey post hoc test, *$p < 0.05$, **$p < 0.01$, ***$p < 0.001$, ****$p < 0.0001$. * represents difference between baseline and ± ischaemia, + represents difference between baseline and ± flecainide, and # represents difference between ± ischaemia and ± flecainide.

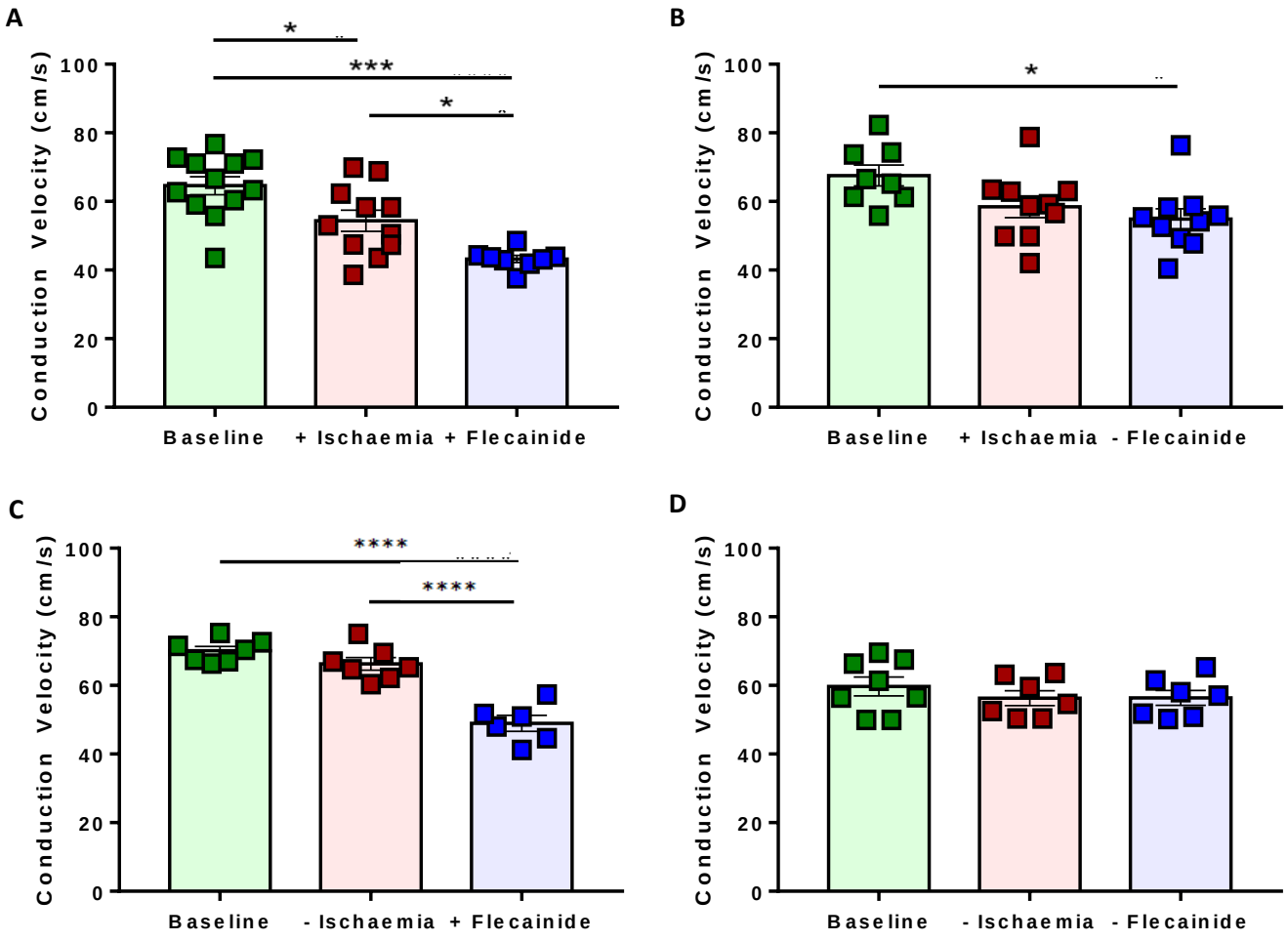

Figure 5.12A-D. CV in mouse ventricles at baseline, ± ischaemia and ± flecainide, at 10 Hz. A. CV at baseline with ischaemia and with flecainide. Significant difference observed between baseline and –flecainide, 67.6 ± 3.5 cm/s vs. 54.9 ± 3.0 cm/s, *p=0.02.* B. CV at baseline with ischaemia and without flecainide. Significant difference observed between baseline and ischaemia, 64.6 ± 2.7 cm/s vs. 54.4 ± 3.0 cm/s, *p=0.02,* between baseline and flecainide, 64.6 ± 2.7 cm/s vs. 43.2 ± 1.1 cm/s, *p<0.0001,* and between ischaemia and flecainide, 54.4 ± 3.0 cm/s vs. 43.2 ± 1.1 cm/s, *p=0.02*. C. CV at baseline with no ischaemia and with flecainide. No significant difference observed between groups. D. CV at baseline without ischaemia and without flecainide. Significant difference observed between baseline and flecainide, 70.1 ± 1.3 cm/s vs. 49.0 ± 2.3 cm/s, *p<0.0001,* and between –ischaemia and flecainide, 66.3 ± 1.8 cm/s vs. 49.0 ± 2.3 cm/s, *p<0.0001.* Statistical significance determined by one-way ANOVA. Significance quantified as P<0.05. * denotes *P<0.05*, ** denotes *P<0.01*, *** denotes *P<0.001*, **** denotes *P<0.0001*.

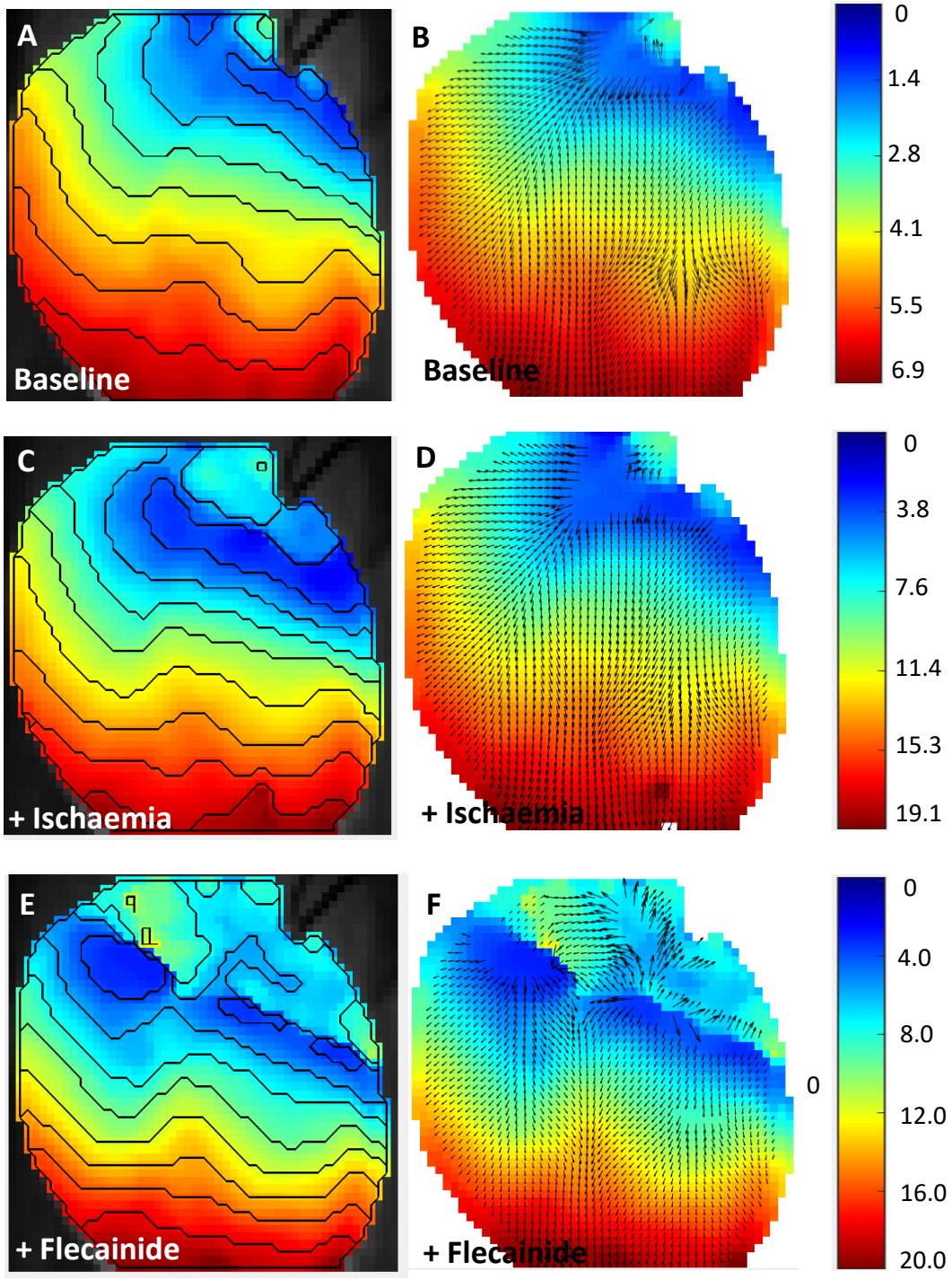

Figure 5.13A-F. Activation maps in ventricles at baseline, ischaemia and flecainide at 10 Hz. A. Representative activation map in the ventricles at baseline at 10 Hz. B. Representative isomap with vectors in the ventricles at 10 Hz. C. Representative activation map in the presence of ischaemia, at 10 Hz. D. Representative isomap with vectors in the presence of ischaemia, at 10 Hz. E. Representative activation map in the presence of ischaemia and flecainide, at 10 Hz. F. Representative isomap with vectors in the presence of ischaemia and flecainide at 10 Hz. Contour lines are spaced at 2 ms.

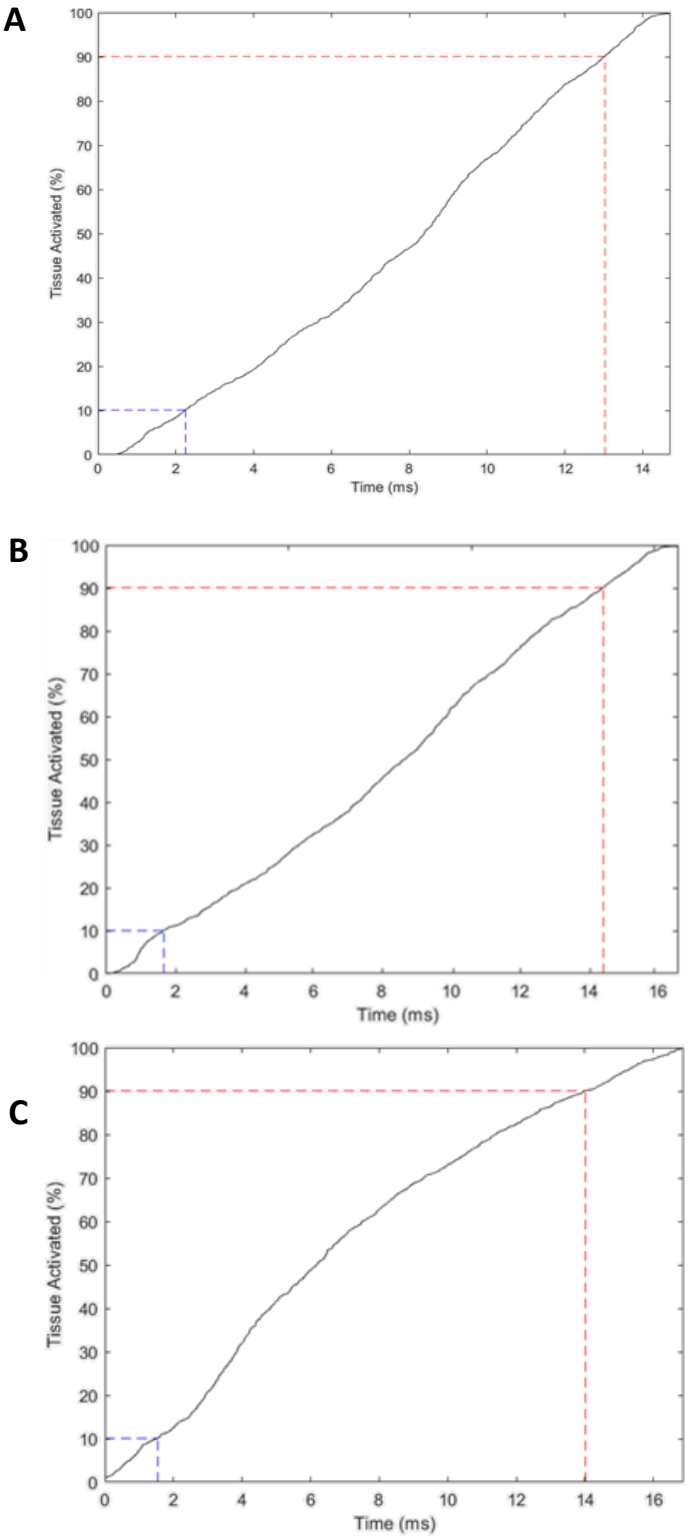

Figure 5.14A-C. Activation curve in ventricles at baseline, ischaemia and flecainide at 10 Hz. A. Representative activation curve in the ventricles at baseline at 10 Hz. B. Representative activation curve in the ventricles in the presence of ischaemia, 10 Hz. C. Representative activation curve in the presence of ischaemia and flecainide at 10 Hz. Blue dashed line indicates time it takes for 10% of tissue to be activated. Red dashed lines indicate time it takes for 90% of tissue to be activated.

5.3. Chapter Discussion

5.3.1. Overview of main findings

The main findings from this chapter are summarised as follows:

- Low flow and low perfusion ischaemia caused a prolongation of action potential duration from baseline.
- Low flow and low perfusion ischaemia caused a slowing of conduction velocity from baseline.
- Presence of both ischaemia and flecainide caused a higher degree of conduction slowing compared ischaemia alone.
- Low perfusion ischaemia provided a more stable heart rate, with more hearts surviving the duration of the experiment, compared to low flow ischaemia.

5.3.2. Constant flow rate vs. constant perfusion pressure

The cardiac ischaemia model is commonly used in isolated mouse hearts to investigate ischaemia reperfusion injury, myocardial infarction and other ischaemic syndromes. Global ischaemia can be triggered through low-flow perfusion or low perfusion pressure. In a global ischaemia model, ischaemia is induced in the whole heart, opposed to regional ischaemia, where ischaemia is induced in a smaller region of the heart. The two modes of perfusate delivery, constant perfusion flow mode and constant perfusion pressure mode have their advantages and disadvantages and are used depending on experimental requirements. In a constant perfusion flow mode, the perfusate being

circulated into the heart is maintained at a constant rate, via a peristaltic pump. This enables the monitoring of changes in pressure, however one downside is that this mechanism can override autoregulatory mechanism of the heart. In a constant perfusion pressure mode, the perfusion pressure is maintained at a constant rate and is monitored by measuring the pressure and adjusting the flow rate to account for changes in pressure. This allows the heart to auto-regulate coronary vascular tone and alter perfusion flow to accommodate the demands of the heart [168].

5.3.3. Effect of low-flow ischaemia and flecainide on action potential duration at 50% repolarisation

We firstly established the conditions of global low-flow ischaemia in the pilot study. We determined a suitable flow rate of 2.4 ml/min and the duration of ischaemia to be 20 minutes. In literature, studies using the low-flow method had a flow rate ranging from 10% of baseline to 75% of baseline. Duration of ischaemia also varied amongst studies. Assayag *et al* 1998 achieved ischaemia in mouse hearts by reducing flow rate by 15% and 30% of coronary flow for 180 minutes whereas House *et al* 2003 used a low-flow rate of 1 ml/min for a minimum of 30 minutes to achieve a global ischaemia insult [169] [170]. Ebel *et al* 2001 reduced flow rate in rats from 14 ml/min to 0.5 ml/min, a reduction of 186%, for 45 minutes [171]. Many studies also subject hearts to no-flow ischaemia. Ultimately, ideal flow rate or perfusion pressure and duration of ischaemia is dependent on the research question. For the purpose of our study, we selected flow rate and ischaemia duration on the lower end of severity, where we were able to see effects of

ischaemia, such as slowing of conduction and heart rate, without compromising the quality of the data.

Following on from the pilot study, we designed an experimental setup to look at interaction of ischaemia and flecainide, with ischaemia being achieved through low-flow perfusion. As shown in Figure 5.5A and 5.5C, we observed a significant increase in APD after ischaemia in one group but no effect caused by ischaemia in another group. We know from literature, ischaemia causes a decrease in APD, through mechanisms mentioned in Chapter 1, which contradicts our data. Bethell *et al* 1998 demonstrated significant APD90 shortening in a ferret heart model during 7.5% low-flow ischaemia. Interestingly, this study also highlighted an initial increase in APD90 before a marked shortening of APD [172]. This is corroborated by other studies which observe an initial prolongation of the action potential accompanied by a subsequent shortening of the action potential. It is thought the initial prolongation is down to changes in I_{CaL}, I_{to}, and I_{K1}, a phenomenon observed in sub-epicardial and sub-endocardium cells [173] [174]. However, the interchange from a prolonged APD to a truncated APD has been reported to be rapid, within 5 minutes of inducing ischaemia, therefore unlikely to be the reason for our observations. Time is also an important factor which must be considered in these experiments. It is established in literature that APD becomes longer with increased time which has also been observed in our previous work. To factor effect of time, we implemented control groups in the study. Figure 5.5C and 5.5D represent control for ischaemia as ischaemia was not induced in those hearts. In both groups, APD remained insignificantly different between baseline and –ischaemia (control) timepoint. From this we can conclude it is unlikely that the prolongation of APD we are observing

is caused by a time lapse. The combination of differential effects of ischaemia in Figures 5.5A and 5.5B, missing data points due to inability of the heart to keep up with the pacing protocol, and low heart rates, point to low data quality.

Flecainide is typically used to treat arrhythmias in patients without ischaemic heart disease or structural heart disease. The effect of flecainide in hearts with ischaemic heart disease without structural modelling has not been thoroughly investigated. In normal, healthy hearts, with normal cardiac function, flecainide slows the upstroke of the action potential. We can see the effects of flecainide in Figure 5.5A and 5.5c in the presence and absence of ischaemia. Figure 5.5A demonstrates that neither ischaemia nor flecainide affected APD50. In the absence of ischaemia, Figure 5.5C, flecainide caused a shortening of APD50. Plenty of studies have shown that flecainide prolongs the APD in the ventricular cells but shortens APD in the Purkinje fibres [86] [175]. Lavalle *et al* 2021 showed a minimal prolongation of the action potential after flecainide treatment. It is important to note the differences in flecainide concentrations used in different studies [176]. We know that different doses of flecainide block different currents. With a half maximal inhibitory concentration [IC_{50}] between 1 – 2 μM, flecainide blocks the fast inward Na^+ current (I_{Na}) and the rapid component of the delayed rectifier K^+ current (I_{Kr}), and at higher doses, with an IC_{50} of 19 μM, flecainide inhibits the late Na^+ current and other cardiac K^+ channels [86]. Inhibition of I_{Na} and I_{Kr} causes prolongation of the APD and ERP. Inhibition of the late Na^+ current also prolongs the APD and ERP [177]. Our previous work measuring differential effects of flecainide in atria and ventricles showed flecainide increased APD in the atria while it had no effect in the ventricles [108]. Interestingly, there was a single study that showed a shortening

of APD after treatment with flecainide in WT hearts at the epicardial and endocardial level [178]. While investigating arrhythmogenesis in long QT type 3 syndrome, they demonstrated with 10 μM of flecainide treatment, APD was shorter compared to the baseline in mouse hearts. Wang *et al* 1990 used a concentration of 4.5 μM of flecainide and observed shortening of APDs [175]. In our studies, a concentration of 1 μM of flecainide was used. In clinical settings, the usual target range is between 0.4 – 2 μM. To be able to delve further into the mechanism or reason behind APD shortening after flecainide treatment, more experiments will need to be done to enable a robust overview of the data. The therapeutic dose of flecainide ranges between 0.2 – 1 μg/ml which translates to 0.5 μM to 2.4 μM [179]. O'Shea demonstrated significant differences in CV in the ventricles using 1 μM, 2 μM and 3 μM of flecainide. 2 μM of flecainide caused a greater significance in slowing of the CV compared to 1 μM [134]. This suggests that differences in flecainide concentration within the therapeutic range can be significant.

5.3.4. Effect of low flow ischaemia and flecainide on conduction velocity

From our study we found that low flow ischaemia did not affect the CV. In the group with ischaemia and flecainide, Figure 5.7A, no differences were observed between treatments. This is unexpected as both ischaemia and flecainide are known to slow the CV separately. This could suggest that a low-flow model of ischaemia is not ideal, or flow rate used to achieve ischaemia was not ideal. Preferably, more time would be required to robustly determine what an ideal flow rate would be.

We know from literature that ischaemia affects CV in the heart through depressed action potentials initiated by inactivated Na^+ current, and flecainide slows the conduction velocity in the heart [180] [134]. O'Shea *et al* 2019 investigated the effects of conduction slowing in action potentials in mouse hearts. They achieved low-flow global ischaemia by using 25% of original flow rate for a duration of three minutes and observed a time-dependent slowing of CV during low-flow ischaemia [105]. In Figure 5.3, we show the effect of ischaemia and flecainide on the CV. Figure 5.2A shows ischaemia did not cause a significant effect on the CV, however it was apparent that CV was slightly slower after ischaemia at most pacing frequencies. Figure 5.2C similarly showed CV was shortened after ischaemia but only showed statistical significance at 9.09 Hz.

Ferrero *et al* 2007, studied effects of flecainide on longitudinal CV and transverse CV in the ventricular myocardium of rabbits. Flecainide significantly slowed the CVs at each coupling interval [181]. O'Shea *et al* 2019 administered 1–3 µmol/L of flecainide into mouse hearts and showed flecainide association with a concentration dependent slowing of CV in the ventricles [105]. Our previous study also showed that CV was significantly reduced in WT mouse hearts in the atria but did not show a significant shortening in the ventricles [108]. Figure 5.3A and Figure 5.3B show the effect of flecainide on the CV in the presence and absence of ischaemia.

Considering the possibility of low data quality, the average APD and CV values fall in the normal range for a healthy heart, according to previous literature. A normal APD is approximately 50 ms and a normal CV varies between 50 – 60 cm/s [108]. However, despite the normal APD and CV values in control experiments and pre-ischaemic

conditions, we found that using a low-flow method to trigger ischaemia, severely affected the heart rate and caused several experiments, including the control experiments, to fail. We hypothesised that the flow rate was not maintained after blebbistatin was added. The presence of blebbistatin, a myosin inhibitor used commonly in optical mapping experiments to prevent motion artefacts, inhibited the physical contraction of the heart, resulting in the pressure within the heart and vessels not being maintained, thus causing experiments to fail. The flow rate used as normal flow rate was 4 ml/min which falls within the range published in literature [182/]. Flow rate was measured before the start of each experiment and adjusted to 4 ml/min. The flow rate of 4 ml/min could have decreased once the blebbistatin started to take effect. It would have been useful to measure the flow rate again after blebbistatin had stopped the heart physically contracting to ensure the flow rate was maintained.

5.3.5. Effect of low perfusion pressure and flecainide on APD50

Following on from the results of the low flow ischaemia experiments, we set up another study using low perfusion pressure to trigger ischaemia. Perfusion pressure was reduced by 40% from 80 mmHg to 32 mmHg and duration of ischaemia remained the same. We found that the control and treated hearts survived the ischaemia and fared better than when experiments were controlled by flow rate, as indicated by Figure 5.8. Heart rates also remained more stable during the course of the perfusion pressure-controlled experiments compared to flow rate-controlled experiments. N numbers varied between 2 and 3 in each group in the pilot study therefore statistical analysis was not performed.

Still, it was apparent with a 40% decrease of flow rate from baseline that APD and CV were affected.

Figure 5.9 shows effects of ischaemia and flecainide on the APD50. In Figure 5.9A, at slower pacing frequencies, we see a significant difference between baseline and ischaemia, and between baseline and –flecainide. –Flecainide represents absence of flecainide at this point and has been exposed to ischaemia for longer. Therefore it stands to reason that significance observed between baseline and ischaemia would be stronger between baseline and –flecainide, after longer exposure to ischaemia. Like the low-flow ischaemia data, ischaemia caused a significant increase in APD, which is contradicted in literature. Under ischaemic conditions, production of ATP falls, directly affecting activity of ion pumps and repolarisation of the action potential, shortening the duration [161]. At –flecainide, the APD50 is further prolonged at slower pacing frequencies. In Figure 5.9B, ischaemia and flecainide did not affect the APD50. APD50 was prolonged after ischaemia but was not significant. Flecainide did not cause a further prolongation of APD50. In the control group, without ischaemia and flecainide, we see significant differences between baseline and –ischaemia, between baseline and –flecainide, and between –ischaemia and –flecainide. Figure 5.9D showed significant difference between baseline and –ischaemia, and between –ischaemia and flecainide treatment. The significant differences within control group and within control treatments suggest the experimental hearts were not healthy at baseline and were prone to time-dependent alterations of action potential waveform.

5.3.5. Effect of low perfusion pressure and flecainide on CV

Overall, flecainide caused CV to slow whether or not ischaemia was present. The extent of CV slowing was greater when ischaemia was present. Figure 5.11 focuses on the CV measurements in presence and absence of ischaemia and flecainide. In groups which ischaemia was present, Figure 5.11A and 5.11B, CV was significantly slower after ischaemia was induced, at most pacing frequencies. This correlates with many studies that have already shown ischaemia to slow the CV [183]. In ischaemic conditions, ionic disturbances causes the depolarisation phase to become slower, causing a delay in electrical propagation across the heart. This results in slowing of the conduction. The absence of ischaemia in Figure 5.11C and 5.11D shows that the CV at –ischaemia remains constant with the baseline, further proving that the effect we are observing of ischaemia slowing the CV is caused by ischaemia and not by time. With prolonged exposure to ischaemia (-flecainide), Figure 5.11A, the CV further slowed down at all pacing frequencies showing statistical significance between baseline and –flecainide (prolonged ischaemia). This is to be expected as the longer the heart remains in ischaemic conditions, the more the heart will deteriorate in function.

The effect of flecainide on the CV can be observed in Figures 5.11B and 5.11D. In both groups, flecainide slowed the CV, in the presence and absence of ischaemia. As mentioned previously, flecainide is known to reduce CV and is administered to patients to terminate AF by slowing conduction [184]. For the purpose of this study, we analysed the extent of CV slowing in hearts with and without ischaemia. In ischaemic hearts, flecainide slowed the CV to a higher degree, with a 42 to 49% change from the baseline.

In non-ischaemic hearts, flecainide slowed the CV to a lesser degree with a 31 to 36% change from baseline.

Overall, we see a strong and clear effect of ischaemia and flecainide on the CV but not on the APD. The time controls show that the effects we are observing are down to ischaemia and flecainide and not time. It could be that the ischaemia is not severe enough to significantly affect the APD or that changes in CV are more sensitive to ischaemic burden. This would indicate that in the sequence of events after ischaemia occurs, that CV is impacted before the action potential duration is. The relationship between APD and CV is complex and is generally associated with one another. In some conditions, slowing of CV can cause a prolongation in action potential waveform, and in some conditions, alteration of action potential waveform can cause a slowing of CV. Most studies have suggested that the initial conduction slowing is caused by a change in APD [185] [186]. Han *et al* 2021 also report changes in CV in ischaemia occurs from the initial ischaemic event and subsequent electrical and structural remodeling of the heart [118]. It will be useful and important to conduct further studies looking at more varying degrees of ischaemia and to investigate APD prolongation in the presence of ischaemia.

Global ischaemia is usually seen in clinical settings accompanied by ventricular fibrillation (VF). It develops from regional ischaemia, increasing risks of VF and if left undiagnosed can become global ischaemia, thus its clinical relevance [187]. Regional ischaemia is discussed further in the next chapter.

5.3.6. Study limitations

Creating a reliable ischaemic model presents several challenges. One of the major limitations is the difficulty in achieving reproducibility. Variations in the severity of ischaemia can lead to significant differences in outcomes making it challenging to compare results. A lot of time is required to robustly determine ideal ischaemic conditions. Although a pilot study was conducted to determine ideal flow rate, the absence of flow rate measurements during the experiment presents a significant limitation in accurately assessing the method of low flow ischaemia. Changes in flow rate can influence the severity and extent of ischaemia and becomes difficult to correlate observed effects of ischaemia with the degree of ischaemia. Future experiments should consider incorporating flow rate measurements during the course of the experiment, especially when blebbistatin is used, to enhance the accuracy and reproducibility of low flow ischaemia method. Also, blebbistatin may exert secondary effects on electrical activity and metabolism. It can influence how quickly a heart becomes ischaemic [188]. Achieving ischaemia through low perfusion resulted in a more stable ischaemic condition and improved heart viability. Determining the ideal perfusion pressure was still required. Additionally, ischaemia may result in fluctuating temperature and should be checked during the course of the experiment.

6. Investigating effectiveness of flecainide in regional ischaemia

6.1. Chapter Introduction

Ventricular fibrillation (VF) usually develops from acute regional ischaemia. Resultant of VF and regional ischaemia, there is an abrupt fall in cardiac output and compromised myocardial perfusion. An episode of VF causes a progressively ischaemic heart ultimately leading to development of global cardiac ischaemia [187].

Importantly, global ischaemia occurs from regional ischaemia, where a part of the heart does not receive flow of blood. In ischaemic heart disease, patients are often diagnosed with regional or local ischaemia. Regional ischaemia is the most common factor triggering lethal arrhythmias [189]. When one to two vessels are less than 30% blocked, it is considered mild ischaemic heart disease. Moderate ischaemic heart disease is defined as 30 to 49% blockage in one to two vessels or mild blockage in three vessels. More than 50% blockage of one to two coronary arteries is considered severe ischaemia heart disease. More than 50% blockage in three or more vessels is considered very severe ischaemic heart disease. There are two forms of ischaemic heart disease, stable ischaemic heart disease which is chronic and develops gradually over many years and presents as stable angina, and acute coronary syndrome which occurs suddenly when pre-existing plaque deposit in the coronary artery suddenly ruptures forming a blood clot that blocks blood flow to the heart [190]. Acute coronary syndrome can be further divided into three groups, ST-elevation myocardial infarction (STEMI), Non-ST elevation MI (NSTEMI) and unstable angina. As indicated by the name, STEMI and NSTEMI are

distinguished through the presence of ST elevation on an ECG, although other conditions can mimic ECG traits of a STEMI [191].

The occlusion of the left anterior descending artery (LAD) is a common cause of ischaemic heart disease. Of the coronary arteries, the LAD is most commonly occluded in patients diagnosed with ischaemic heart disease. The LAD is the largest coronary artery, accounting for the largest cardiac blood supply to the myocardium, almost 50%. The artery extends from the base of the heart to the apex and branches into two smaller arteries, diagonal 1 and 2 (D1 & D2), over the anterior side of left ventricle [3]. The anatomy of the LAD and its branches varies in 78% of healthy individuals. As the LAD supplies blood to a large part of the heart, LAD occlusion puts the patient at greater risk of heart failure and cardiac death [192].

Performing ligation of the LAD is a commonly used method in cardiovascular research to achieve regional ischaemia and can be used to study acute and chronic MI. Blocking the LAD mimics ischaemic heart disease seen in humans, providing a useful tool for research [193]. Here, we performed a LAD ligation *ex vivo* in WT mouse hearts to achieve regional ischaemia and looked at the interaction of ischaemia and flecainide, and its effects on electrical activity and calcium handling.

In addition to conduction dysfunction, ischaemia also causes calcium homeostasis disorder. Calcium homeostasis is essential for normal cardiac function and is especially important in excitation contraction coupling, mechanism by which an electrical signal triggers cardiac contraction. Excitation contraction coupling is achieved through regulation of calcium extrusion, calcium storage and release. Like Na^+ ions, Ca^{2+} ions have

several influx and efflux pathways. The pathways are made up of voltage gated channels, exchangers, pumps, receptor-mediated channels and store operated channels. The main regulatory proteins directly responsible for calcium homeostasis in the heart are T and L type calcium channels (LTCC), ryanodine receptors (RyR2), sarco-endoplasmic reticulum calcium ATPase (SERCA), sodium calcium exchanger (NCX) [194]. The influx and efflux of calcium contributes towards the electrochemical potential. When a cardiac action potential takes place, Ca^{2+} ions enter the cell via the LTCC activating the RyR2 to release Ca^{2+} ions from sarcoplasmic reticulum (SR). Intracellular Ca^{2+} ions bind to troponin C, a myofilament protein, enabling cardiac contraction. At the of contraction, Ca^{2+} is taken up by SERCA as well as extruded out of cell through the NCX, thus dissociating Ca^{2+} ions from troponin C and initiating relaxation of the heart [194].

Calcium is considered to be one of the triggers involved in ischaemic cell death [195]. Metabolic abnormalities occur in cardiomyocytes following an ischaemia event affecting ion channels. Intracellular calcium rises in myocardial ischaemia as a response to an increase in calcium influx. This is triggered by the activity of sodium hydrogen exchanger (NHE), enabling more Na^{+} ions to enter the cells which in turn promotes the sodium calcium exchanger (NCX) to bring in Ca^{2+} ions into the cells leading to calcium overload. Calcium overload within cells causes a surplus of calcium to enter mitochondria inhibiting ATP production, further compounding metabolic abnormalities which can ultimately lead to cell apoptosis. Calcium overload is also responsible for causing structural and functional changes of coronary vessels and release of inflammatory factors exacerbating tissue damage.

The purpose of this study was to accurately and thoroughly investigate the interaction between ischaemia and flecainide in mouse hearts. The Cardiac Arrhythmia Suppression Trial (CAST I) concluded that flecainide and encainide led to poorer outcomes and increased mortality risk, primarily due to arrhythmia and acute myocardial ischaemia. It was speculated that these drugs could exacerbate ischaemia, leading to fatal arrhythmias. Consequently, their use was discontinued within two years due to increased mortality and sudden cardiac death. The study speculates that an ischaemic event was more likely to be fatal in the group receiving flecainide or encainide. It is thought that ischaemia could have facilitated the fatal arrhythmias, or that flecainide or encainide may have increased demand of oxygen during acute myocardial ischaemia, accelerating development of lethal arrhythmias. The increased number of deaths attributed to proarrhythmia and ischaemia may indicate that these two mechanisms are connected [95]. Following on from the CAST I, there have been more recent trials such as EAST-AFNET 4 and Flec-SL that demonstrate a low rate of ventricular arrhythmia when flecainide is used after cardioversion and during rhythm control therapy. EAST-AFNET was designed to investigate whether an early rhythm-control therapy approach would result in better outcomes for patients with early atrial fibrillation than the current standard of care. The trial consisted of a total of 2789 patients, with 1395 patients assigned to early rhythm control and 1394 patients assigned to usual care. Patients assigned to early rhythm control were administered antiarrhythmic drug, either flecainide (36%), dronedarone (36%) or amiodarone (20%), or underwent AF ablation (8%) [196]. Patients assigned to usual care were administered rate control therapy. Patients with newly diagnosed AF treated with early rhythm control therapy showed

fewer adverse effects than patients assigned to usual care with rate control therapy. A large number of patients in the cohort were administered flecainide without safety concerns. The EAST-AFNET 4 trial showed that early rhythm control using antiarrhythmic drugs such as flecainide, reduced cardiovascular events in patients with heart failure [196]. Early rhythm control was considered to be superior to usual care, usually rate control, in improving cardiovascular outcomes. However, the trial was terminated early due to efficacy.

The aims of this study were:

- assess the interaction between flecainide and ischaemia in healthy wildtype (WT) hearts, using optical mapping.
- investigate the interaction of ischaemia and flecainide on CV and action potential in the ventricles.
- assess how calcium is modulated in ischaemia.

6.2 Chapter Results

6.2.1. Effect of regional ischaemia and flecainide on APD

In order to thoroughly investigate the interaction between ischaemia and flecainide, we designed four groups for the study; +ischaemia and +flecainide, +ischaemia and –flecainide, -ischaemia and +flecainide, and –ischaemia and –flecainide. This ensures each variable factor has a time control. Experiments were performed on isolated WT mouse hearts. LAD ligation was performed in relevant hearts. In control hearts without ischaemia, the needle for ligation was inserted around the LAD but not ligated. This was to account for changes in the data, dependent on the puncturing of the LV for the ligation.

Hearts were paced across a range of pacing frequency. Measurements were taken from two regions of the heart, from the ischaemic region, below the ligation, and from the remote region, away from the ligation, Figure 6.1. Regions were composed of a 9x9 pixel. The regions were selected based on proximity to the ligation as well as action potential waveform. For each heart, action potentials were observed pixel to pixel to determine the ischaemic boundary. This ensured the ischaemic regions were ischaemic and the non-ischaemic regions were non-ischaemic. Overall APD and CV measurements were also taken from the whole ventricles. APD30, APD50 and APD80 were calculated along with the CV. Additionally, calcium transients were measured to investigate how calcium handling is modulated during ischaemia and flecainide perfusion. Membrane potential dye, RH-237 and Ca^{2+} indicator, Rhod2-AM, were loaded simultaneously and hearts imaged using two EMCCD cameras.

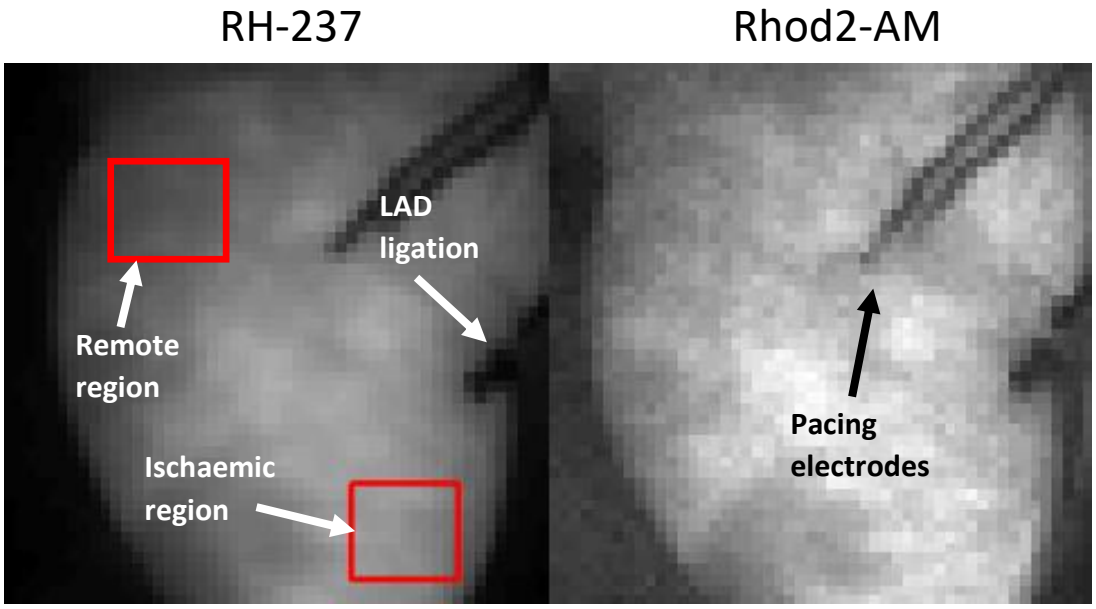

Figure 6.1 Regions of interest in ventricles for measurement of ischaemic regions. A 9x9 pixel square was used to select areas in the ventricles to measure ischaemic and non-ischaemic regions. Image on the left show ventricles loaded with membrane potential dye, RH-237, and image on the right show ventricles loaded with calcium indicator, Rhod2-AM. Hearts were loaded and imaged simultaneously for voltage membrane potential and calcium transients.

Data collected at baseline is represented by green points, presence or absence of iscahemia is represented by purple points and presence or absence of flecainide is represented by blue points. In each group, presence or absence of treatment is indicated by + sign or – sign, respectively.

Ischaemia prolonged APD30 from baseline in the ischaemic region, Figures 6.4A and B, but the prolongation was not maintained at APD50 or APD80, 6.7A and B, 6.10A and B. The prolongation of APD30 however was not significant. In the remote region, ischaemia did not cause a change in the APDs, Figures 6.3A and B, 6.6A and B, 6.9A and B. The

overall APD, which measured APD using the whole ventricles as region of interest, reflected these changes, showing action potential prolongation at APD30 in ischaemic regions only, Figures 6.2A and B, 6.5A and B, 6.8A and B. In ischaemia control hearts, i.e. hearts without LAD ligation, some hearts did show APD prolongation and in some hearts APD did not alter. Figures 6.4C, 6.7C and 6.10C, APD is non-significantly prolonged in the absence of ischaemia, yet in Figures 6.4D, 6.7D and 6.10D, APD did not prolong. This could suggest variations in the ligation technique may be causing ischaemia in hearts to varying degrees.

In the absence of ischaemia, flecainide prolonged APD30 and APD50 compared to baseline in the remote region, Figure 6.3C and 6.6C, and ischaemic region of the heart, Figure 6.4C and 6.7C, but was not significant. At APD80, Figures 6.9C and 6.10C, the prolongation was no longer visible. In the control groups, without ischaemia and without flecainide, there was no change in APD from baseline, Figures 6.2 to 6.10, panel D. However, since we observe APD prolongation in ischaemia controls, it is hard to conclude whether APD prolongation caused by flecainide is the true effect of flecainide or time. In the presence of ischaemia, in the ischaemic region, flecainide prolonged the APD30 from 14.5 ± 3.0 ms at baseline to 18.0 ± 1.7 ms, a 24.6% increase in prolongation. In the absence of ischaemia, flecainide prolonged the APD from 15.9 ± 4.1 ms at baseline to 19.9 ± 2.3 ms, a 25.5% increase in prolongation. Flecainide shortened the APD50 in the ischaemic region in the presence of ischaemia from 28.2 ± 4.9 ms at baseline to 26.3 ± 2.3 ms, a 6.7% decrease in prolongation. In the absence of ischaemia, APD50 was prolonged by flecainide from 27.5 ± 4.4 ms at baseline to 32.5 ± 6.4 ms, an 18% increase in prolongation. Average APD80 was shortened by flecainide from 51.7 ± 6.2 ms to 48.8

± 8.6 ms, when ischaemia was present, a 5.4% decrease in prolongation. When ischaemia was absent, APD80 was prolonged from 51.5 ± 7.2 ms at baseline to 54.7 ± 10.1 ms, a 6.2% increase in prolongation. From the APD data, there does not seem to be an interaction between ischaemia and flecainide.

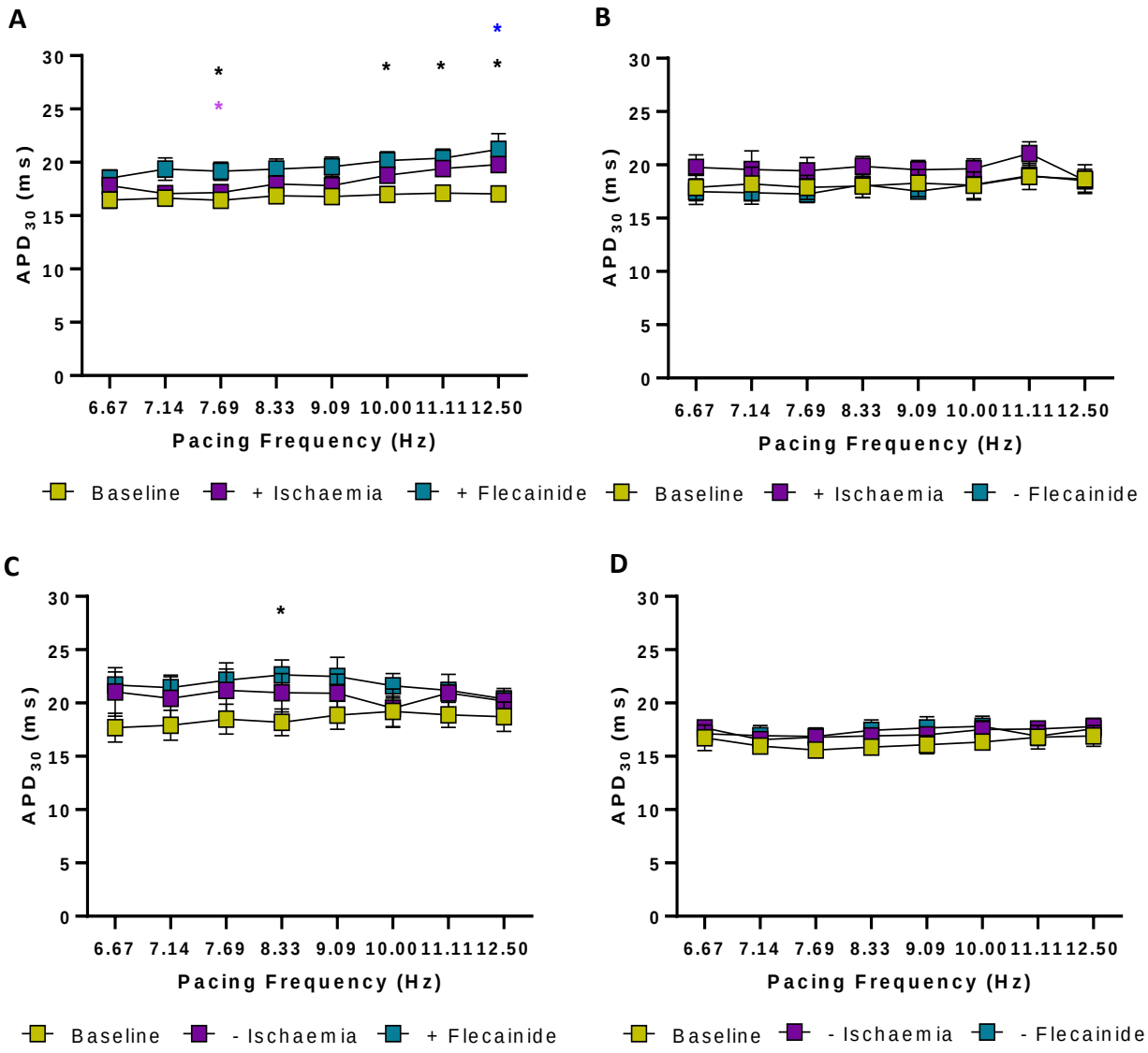

Figure 6.2. Overall APD30 in mouse hearts in presence and absence of ischaemia and flecainide. APD30 measurements taken from whole ventricles as an average in each group. A. Significant difference observed between baseline and +ischaemia at 12.50 Hz, 16.5 ± 2.5 ms vs. 17.8 ± 1.5 ms, *p=0.02.* Significant difference observed between baseline and +flecainide at 7.69 Hz; 17.0 ± 1.9 ms vs. 20.2 ± 2.5 ms, *p=0.05*, at 10.00 Hz; 16.4 ± 1.8 ms vs. 19.2 ± 2.6 ms, *p=0.05,* at 11.11 Hz; 16.6 ± 2.2 ms vs. 19.4 ± 3.2 ms, *p=0.03*, at 12.50 Hz, 16.5 ± 2.5 ms vs. 18.5 ± 2.4 ms, *p*=0.04. Significant difference observed between +ischaemia and +flecainide at 7.69 Hz; 18.8 ± 2.1 ms vs. 20.2 ± 2.5 ms, *p=0.02.* B. No significant differences observed within groups. C. Significant difference observed between baseline and +flecainide at 8.33 Hz, 18.9 ± 3.5 ms vs. 22.5 ± 4.4 ms, *p=0.03.* D. No significant differences observed within groups. Statistical significance determined by two-way ANOVA, significance quantified as P<0.05. * denotes P<0.05, ** denotes P<0.01, *** denotes P<0.001, **** denotes P<0.0001. * indicates significant difference between baseline and ± ischaemia, * indicates significant difference between baseline and ± flecainide, * indicates significant difference between ± ischaemia and ± flecainide.

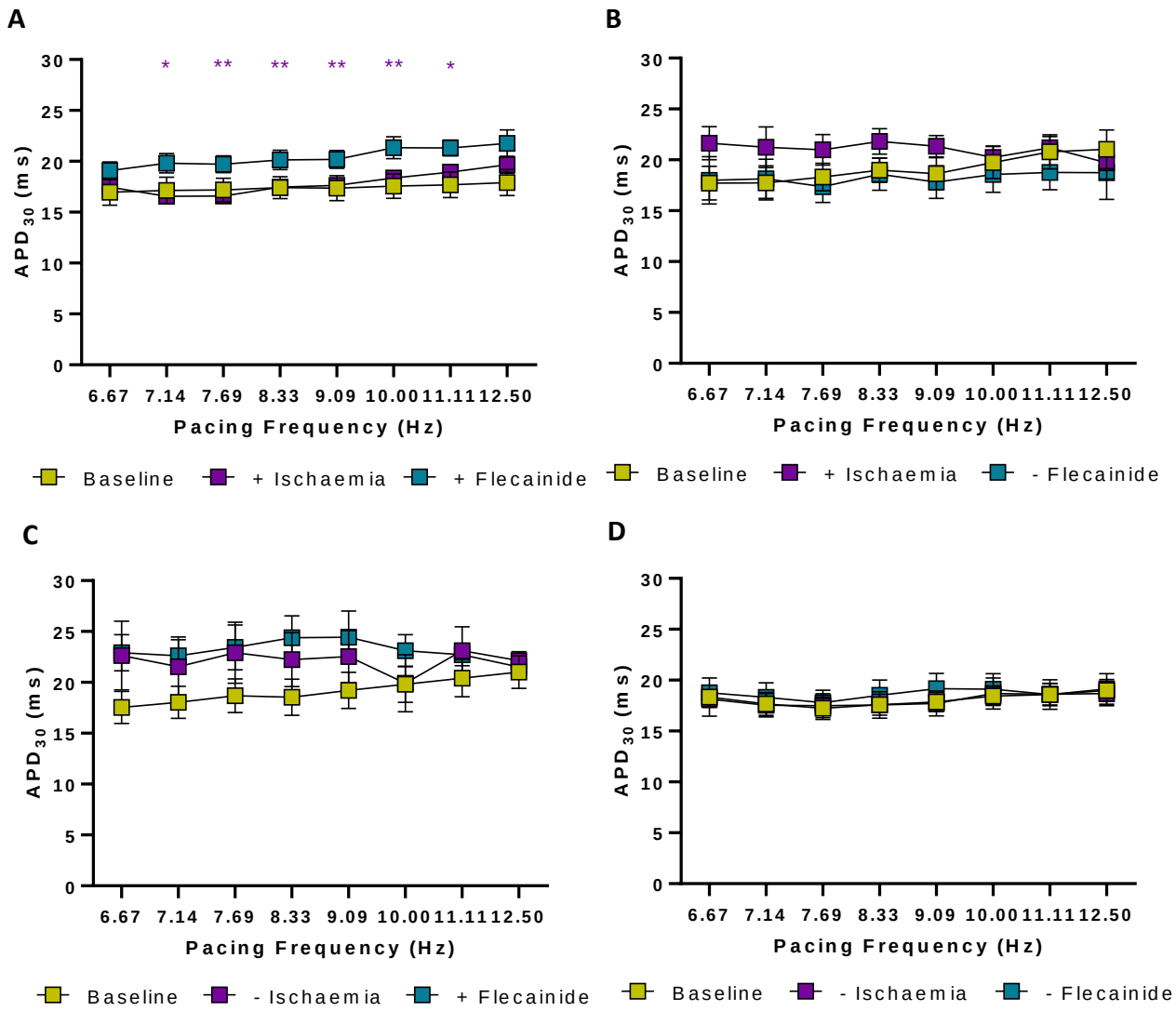

Figure 6.3. APD30 in remote region of mouse hearts in presence and absence of ischaemia and flecainide. APD30 measurements taken from a non ischaemic region of the heart in each group. A. Significant differences observed between +ischaemia and +flecainide at 7.14 Hz; 16.6 ± 2.1 ms vs. 19.8 ± 2.9 ms, *p=0.02,* at 7.69 Hz, 16.6 ± 2.2 ms vs. 19.8 ± 2.9 ms, *p=0.002,* at 8.33 Hz; 17.5 ± 2.1 ms vs. 20.1 ±2.9 ms, *p=0.005,* at 9.09 Hz; 17.6 ± 2.0 ms vs. 20.2 ± 2.6 ms, *p=0.0026,* at 10.00 Hz; 18.4 ± 2.2 ms vs. 21.3 ± 3.2 ms, *p=0.0023,* at 11.11 Hz; 18.9 ± 2.2 ms vs. 21.3 ± 2.2 ms, *p=0.05.* B. Significant difference not observed with +ischaemia and –flecainide. C. Significant difference not observed with -ischaemia and +flecainide. D. Significant difference not observed with -ischaemia and –flecainide. Statistical significance determined by two-way ANOVA, significance quantified as P<0.05. * denotes P<0.05, ** denotes P<0.01, *** denotes P<0.001, **** denotes P<0.0001. * indicates significant difference between baseline and ± ischaemia, * indicates significant difference between baseline and ± flecainide, * indicates significant difference between ± ischaemia and ± flecainide.

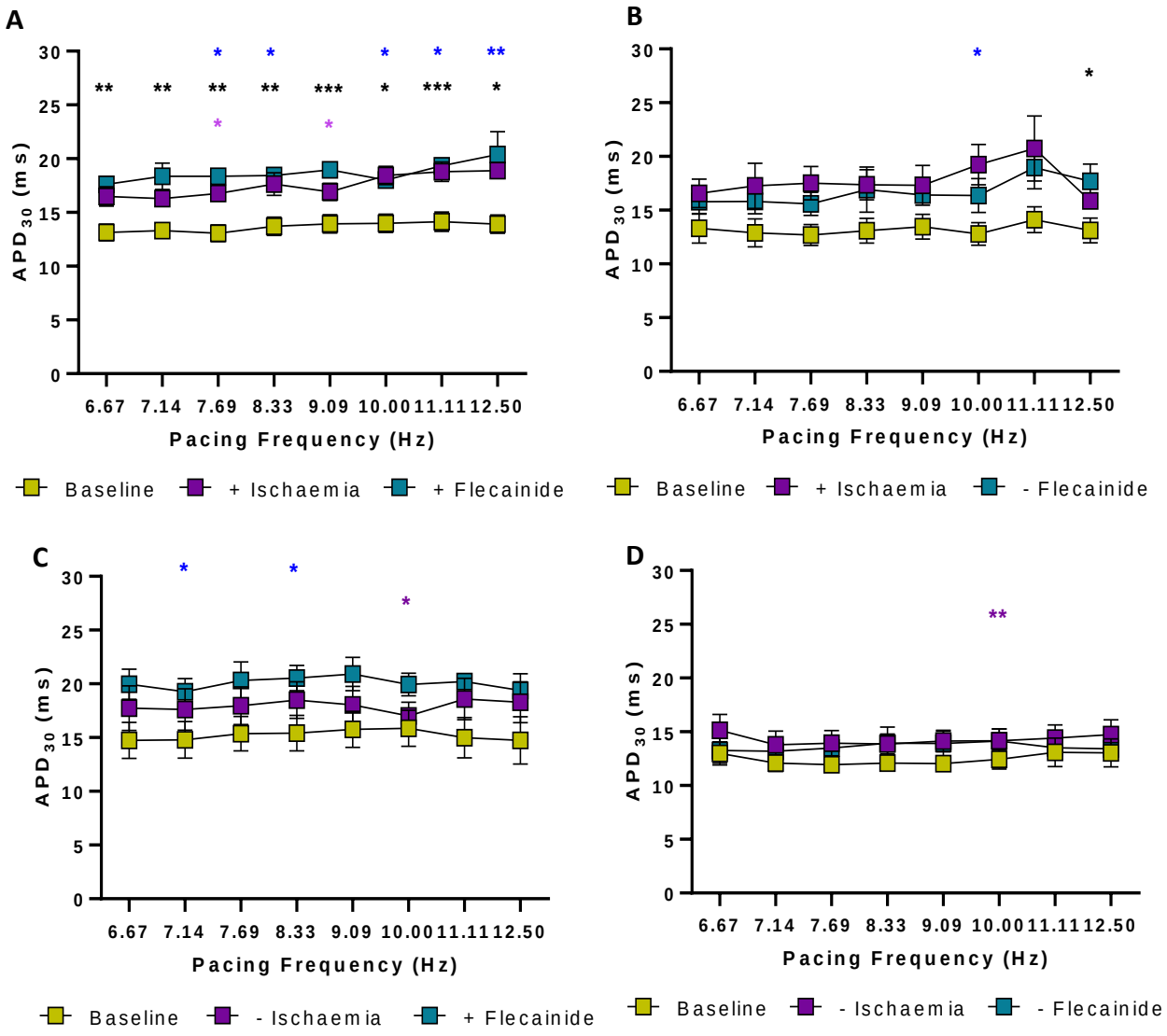

Figure 6.4A-D. APD30 in ischaemic region of mouse hearts in presence and absence of ischaemia and flecainide. APD30 measurements taken from the ischaemic region, close to the ligated region of the heart. A. Group +ischaemia and +flecainide. Significant difference observed between baseline and +ischaemia at 7.69 Hz. Significant difference observed between baseline and +flecainide at 6.67 Hz;. Significant differences observed between +ischaemia and +flecainide at 7.69 Hz. B. Group +ischaemia and –flecainide. Significant difference observed between baseline and +ischaemia at 7.69 Hz; 12.7 ± 2.2 ms vs. 17.5 ± 3.5 ms, *p=0.05,* at 8.33 Hz; 13.1 ± 2.6 ms vs. 17.4 ± 3.2 ms, *p=0.05,* 10 Hz; 12.8 ± 2.4 ms vs. 19.2 ± 4.2 ms, *p=0.03.* Significant difference was observed between baseline and –flecainide at 12.5 Hz; 13.1 ± 2.6 ms vs. 17.7 ± 3.2 ms, *p=0.0135.* C. Group –ischaemia and +flecainide. Significant difference observed between baseline and –ischaemia at 8.33 Hz; 15.8 ± 4.1 ms vs. 18.5 ± 4.2, *p=0.05.* Significant difference between –ischaemia and +flecainide at 6.67 Hz; 17.7 ± 5.1 ms vs. 20.0 ± 3.5 ms, *p=0.0115,* at 10 Hz; 17.0 ± 3.1 ms vs. 19.9 ± 2.3 ms, *p=0.02*. D. Group –ischaemia and –flecainide. Significant difference observed between –ischaemia and –flecainide at 10 Hz; 14.2 ± 2.9 ms vs. 14.1 ± 2.7 ms, *p=0.0036.* Statistical significance determined by two-way ANOVA, significance quantified as P<0.05. * denotes P<0.05, ** denotes P<0.01, *** denotes P<0.001, **** denotes P<0.0001. * indicates significant difference between baseline and ± ischaemia, * indicates significant difference between baseline and ± flecainide, * indicates significant difference between ± ischaemia and ± flecainide.

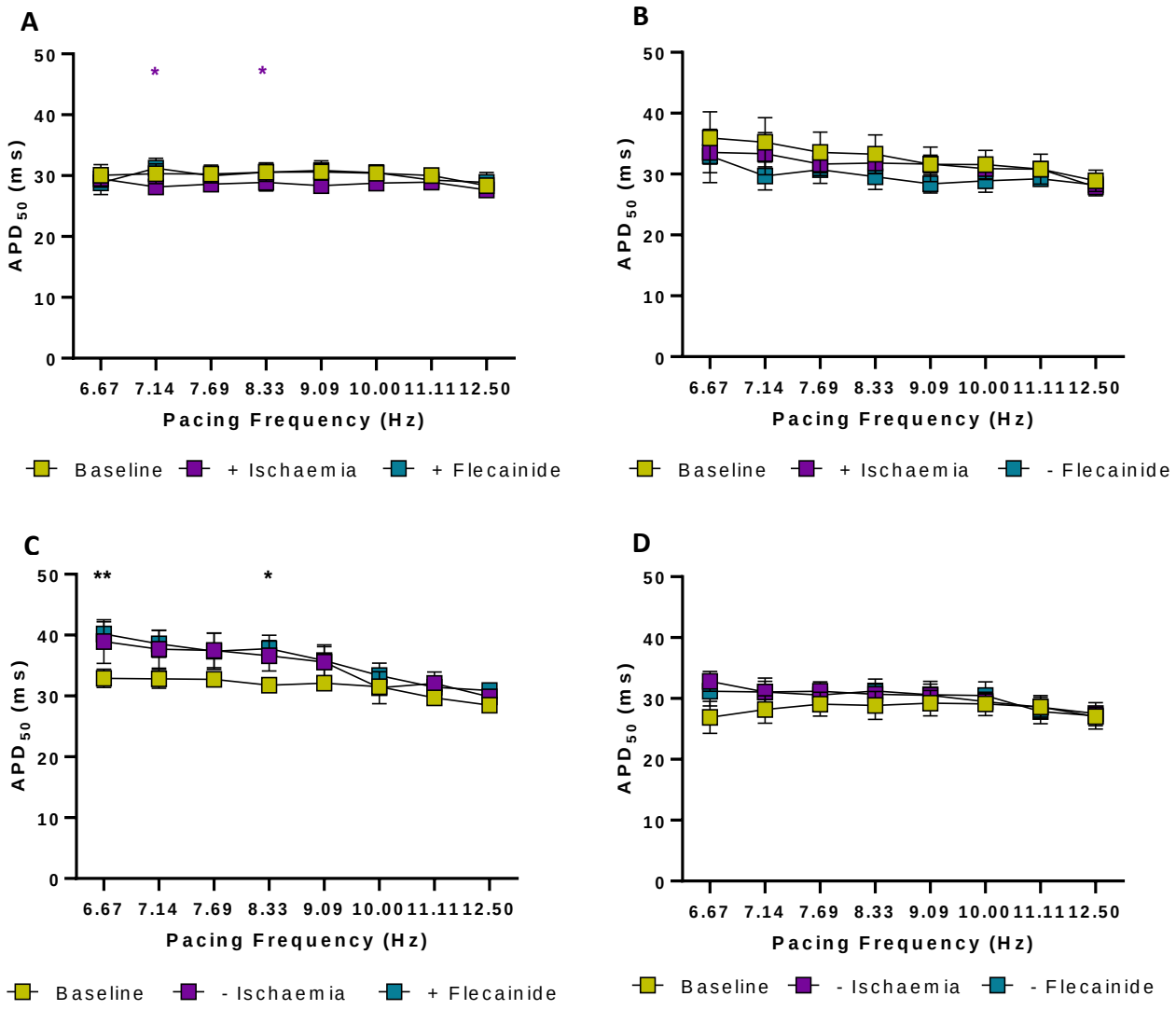

Figure 6.5A-D Overall APD50 in mouse hearts in presence and absence of ischaemia and flecainide. APD50 measurements taken from whole ventricles as an average in each group**.** A. Significant difference observed between +ischaemia and +flecainide at 7.14 Hz; 28.1 ± 3.6 ms vs. 31.2 ± 4.8 ms, *p=0.04,* at 8.33 Hz; 28.9 ± 4.3 ms vs. 30.6 ± 4.7 ms, *p=0.0386.* B. Group +ischaemia and –flecainide. No significant differences observed between +ischaemia and –flecainide. C. Group –ischaemia and +flecainide. Significant difference observed between baseline and +flecainide at 6.67 Hz; 31.6 ± 4.3 ms vs. 34.5 ± 7.3 ms, *p=0.006,* at 8.33 Hz; 29.9 ± 4.0 ms vs. 34.0 ± 6.3 ms, *p=0.02.* D. Group –ischaemia and –flecainide. No significant differences observed between –ischaemia and –flecainide. Statistical significance determined by two-way ANOVA, significance quantified as P<0.05. * denotes P<0.05, ** denotes P<0.01, *** denotes P<0.001, **** denotes P<0.0001. * indicates significant difference between baseline and ± ischaemia, * indicates significant difference between baseline and ± flecainide, * indicates significant difference between ± ischaemia and ± flecainide.

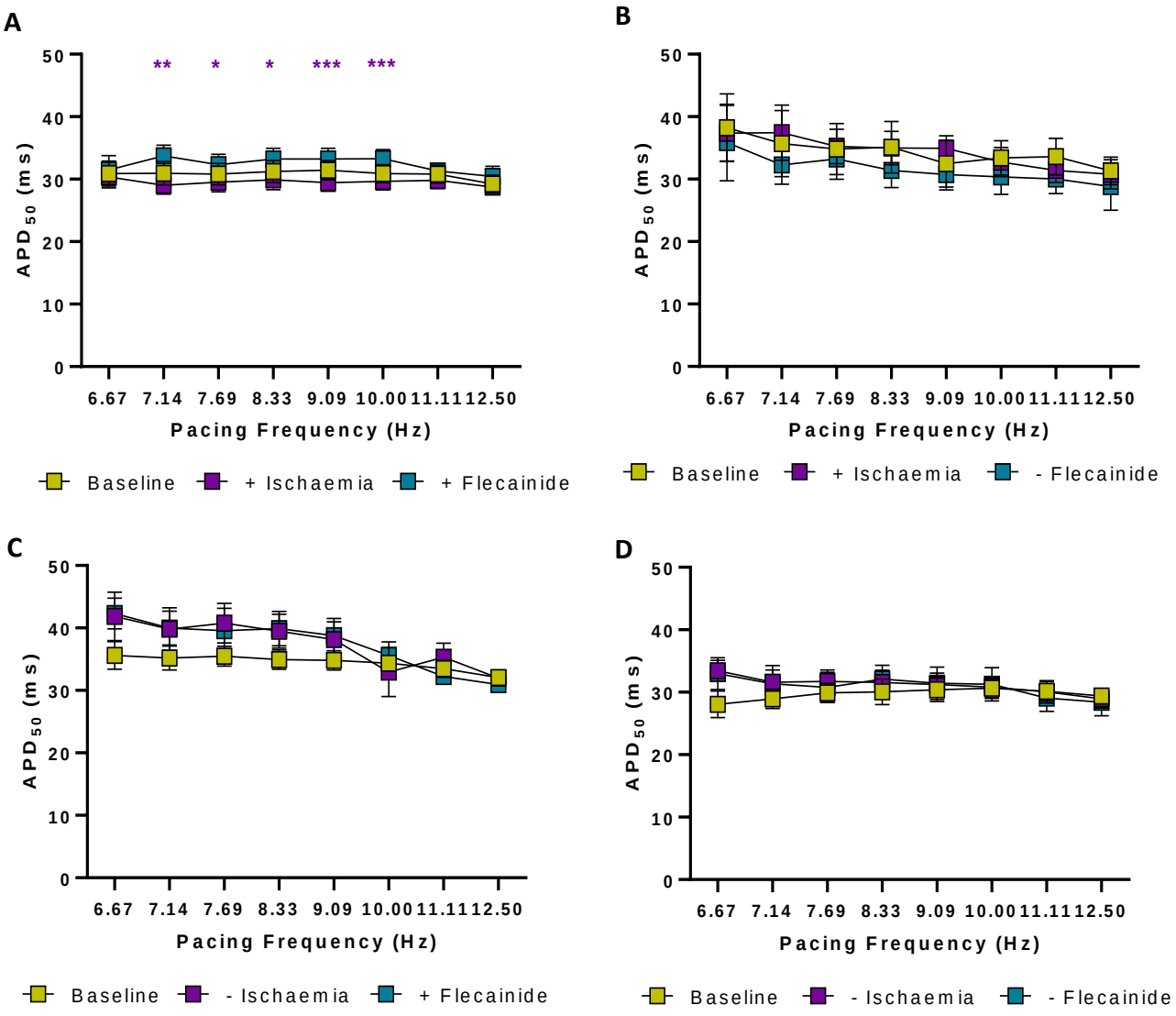

Figure 6.6A-D. APD50 in remote region of mouse hearts in presence and absence of ischaemia and flecainide. APD50 measurements taken from remote regions of the heart at different pacing frequencies. A. Group +ischaemia and +flecainide. Significant differences observed between +ischaemia and +flecainide at 7.14 Hz; 29.0 ± 4.3 ms vs. 33.7 ± 5.2 ms, *p=0.006,* at 7.69 Hz; 29.5 ± 4.7 ms vs. 32.3 ± 5.1 ms, *p=0.034,* at 8.33 Hz; 29.9 ± 4.7 ms vs. 33.2 ± 5.2 ms, *p=0.0113,* at 9.09 Hz; 29.4 ± 4.1 ms vs. 33.2 ± 5.1 ms, *p=0.0004,* at 10 Hz; 29.6 ± 4.1 ms vs. 33.3 ± 4.4 ms, *p<0.0001.* B. Group +ischaemia and –flecainide. No significant difference observed between +ischaemia and –flecainide. C. Group –ischaemia and +flecainide. No significant difference observed between -ischaemia and +flecainide. D. Group –ischaemia and –flecainide. No significant difference observed between -ischaemia and –flecainide. Statistical significance determined by two-way ANOVA, significance quantified as P<0.05. * denotes P<0.05, ** denotes P<0.01, *** denotes P<0.001, **** denotes P<0.0001. * indicates significant difference between baseline and ± ischaemia, * indicates significant difference between baseline and ± flecainide, * indicates significant difference between ± ischaemia and ± flecainide.

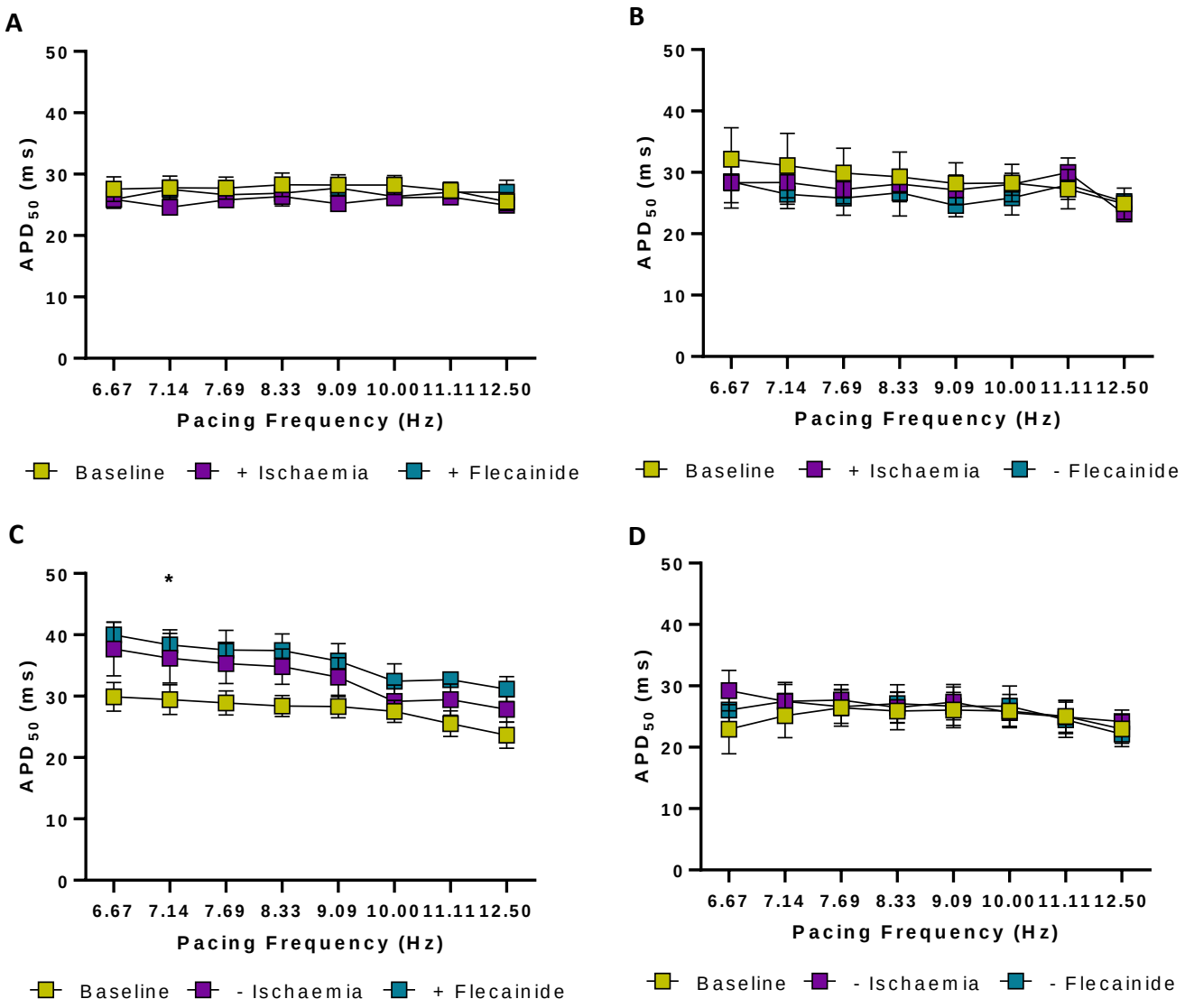

Figure 6.7A-D. APD50 in ischaemic region of mouse hearts in presence and absence of ischaemia and flecainide. APD50 measurements taken from ischaemic region of the heart at different pacing frequencies. A. Group +ischaemia and +flecainide. No significant differences observed between +ischaemia and +flecainide. B. Group +ischaemia and –flecainide. No significant differences observed between +ischaemia and –flecainide. C. Group –ischaemia and +flecainide. Significant difference observed between baseline and +flecainide at 7.14 Hz; 29.5 ± 5.4 ms vs. 38.4 ± 5.5 ms, *p=0.0157.* D. Group –ischaemia and –flecainide. No significant differences observed between –ischaemia and –flecainide. Statistical significance determined by two-way ANOVA, significance quantified as P<0.05. * denotes P<0.05, ** denotes P<0.01, *** denotes P<0.001, **** denotes P<0.0001. * indicates significant difference between baseline and ± ischaemia, * indicates significant difference between baseline and ± flecainide, * indicates significant difference between ± ischaemia and ± flecainide.

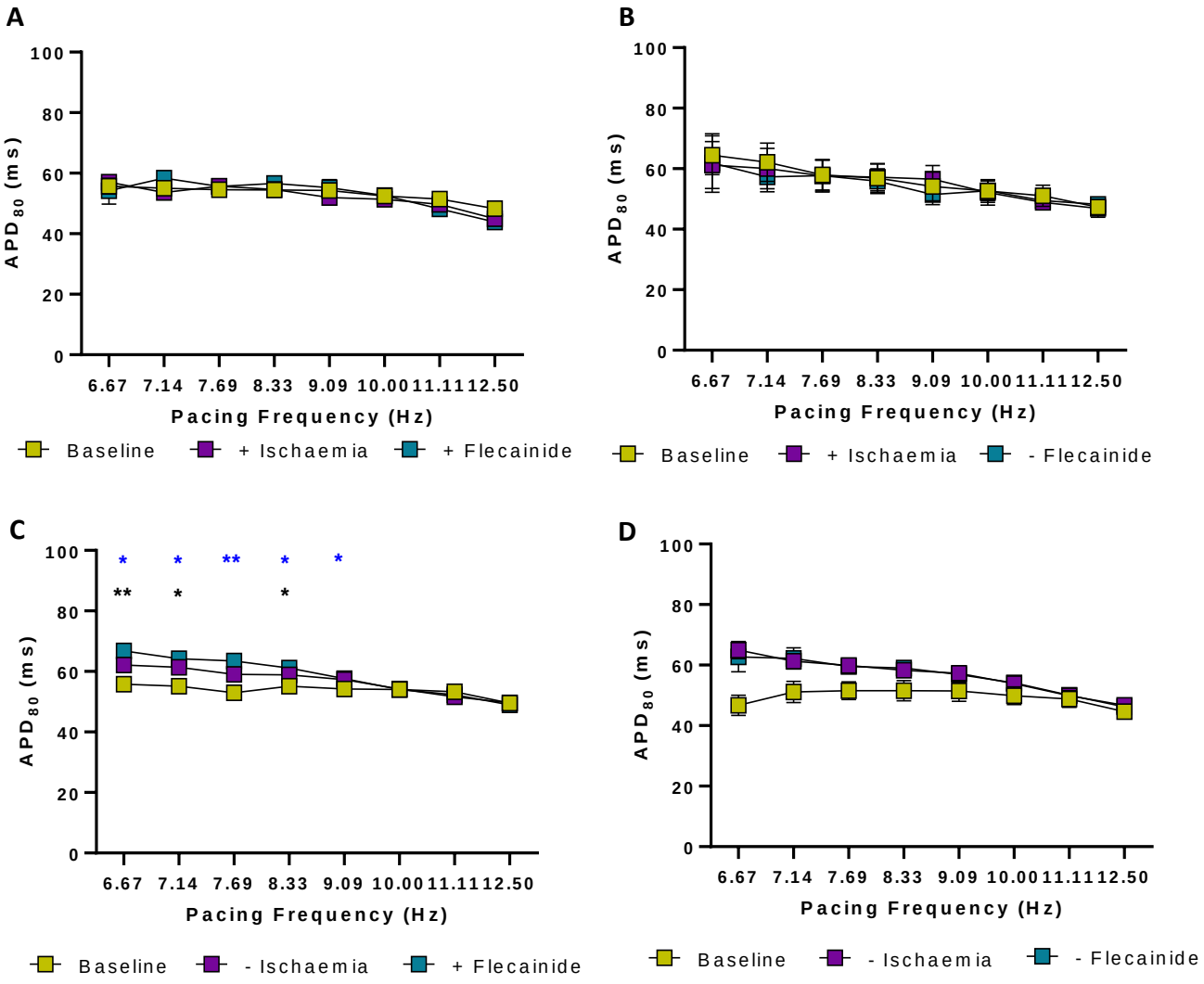

Figure 6.8A-D. Overall APD80 in mouse hearts in presence and absence of ischaemia and flecainide. APD80 measurements taken from whole ventricles at different pacing frequencies. A. Group +ischaemia and +flecainide. No significant differences observed between +ischaemia and +flecainide. B. Group +ischaemia and –flecainide. No significant differences observed between +ischaemia and –flecainide. C. Group –ischaemia and +flecainide. Significant difference observed between baseline and –ischaemia at 6.67 Hz; 30.9 ± 6.4 ms vs. 55.7 ± 8.2 ms, *p=0.0197,* at 7.14 Hz; 30.9 ± 5.9 ms vs. 55.0 ± 7.5 ms, *p=0.0147,* at 7.69 Hz; 30.8 ± 5.4 ms vs. 54.5 ± 6.8 ms, *p=0.0051,* at 8.33 Hz; 31.2 ± 5.6 ms vs. 54.4 ± 7.3, *p=0.0196,* at 9.09 Hz; 31.4 ± 4.9 ms vs. 54.3 ± 6.5 ms, *p=0.0291.* Significant difference observed between baseline and +flecainide at 6.67 Hz; 30.9 ± 6.4 ms vs. 57.1 ± 7.0 m s, *p=0.0052,* at 7.14 Hz; 30.9 ± 5.9 ms vs. 53.6 ± 4.4 ms, *p=0.0108,* at 8.33 Hz; 31.2 ± 5.6 ms vs. 54.7 ± 4.6 ms, *p=0.00203.* D. Group –ischaemia and –flecainide. No significant differences observed between –ischaemia and –flecainide. Statistical significance determined by two-way ANOVA, significance quantified as P<0.05. * denotes P<0.05, ** denotes P<0.01, *** denotes P<0.001, **** denotes P<0.0001. * indicates significant difference between baseline and ± ischaemia, * indicates significant difference between baseline and ± flecainide, * indicates significant difference between ± ischaemia and ± flecainide.

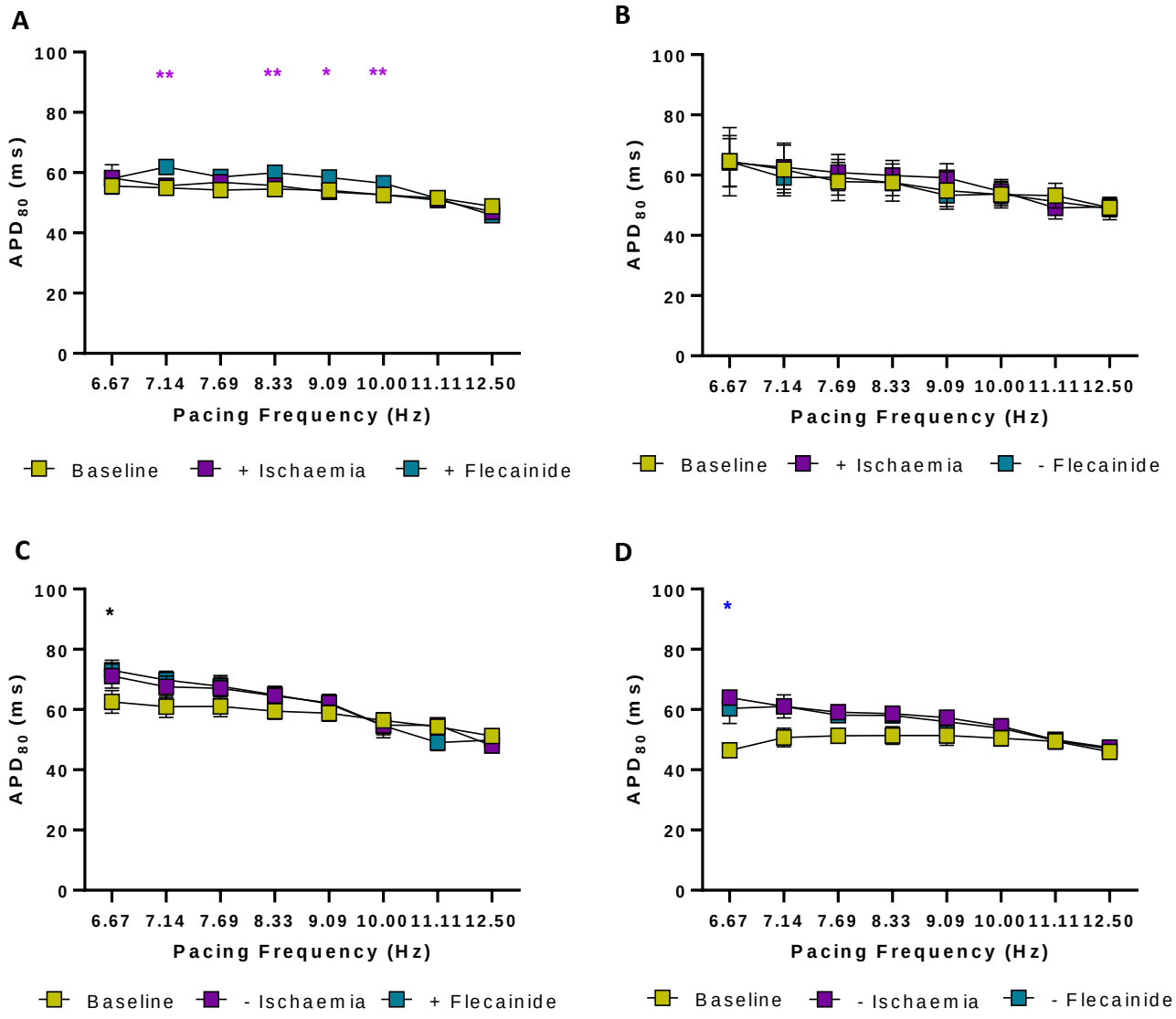

Figure 6.9A-D. APD80 in in remote region of mouse hearts in presence and absence of ischaemia and flecainide. APD80 measurements taken from non-ischaemic region of ventricles at different pacing frequencies. A. Group +ischaemia and +flecainide. Significant difference observed between +ischaemia and +flecainide at 7.14 Hz; 55.6 ± 4.5 ms vs. 61.9 ± 5.5 ms, *p=0.004,* at 8.33 Hz; 55.7 ± 4.3 ms vs. 59.9 ± 5.5 ms, *p=0.009,* at 9.09 Hz; 53.6 ± 4.1 ms vs. 58.3 ± 6.2 ms, *p=0.015,* at 10 Hz; 52.7 ± 5.0 ms vs. 56.5 ± 5.4 ms, *p=0.0088.* B. Group +ischaemia and –flecainide. No significant differences observed between +ischaemia and –flecainide. C. Group –ischaemia and +flecainide. Significant difference between baseline and +flecainide at 6.67 Hz; 62.5 ± 9.3 ms vs. 73.0 ± 8.1 ms, *p=0.0326.* D. Group –ischaemia and –flecainide. Significant difference between baseline and –ischaemia at 6.67 Hz; 46.4 ± 4.6 ms vs. 64.0 ± 4.4 ms, *p=0.043.* Statistical significance determined by two-way ANOVA, significance quantified as P<0.05. * denotes P<0.05, ** denotes P<0.01, *** denotes P<0.001, **** denotes P<0.0001. * indicates significant difference between baseline and ± ischaemia, * indicates significant difference between baseline and ± flecainide, * indicates significant difference between ± ischaemia and ± flecainide.

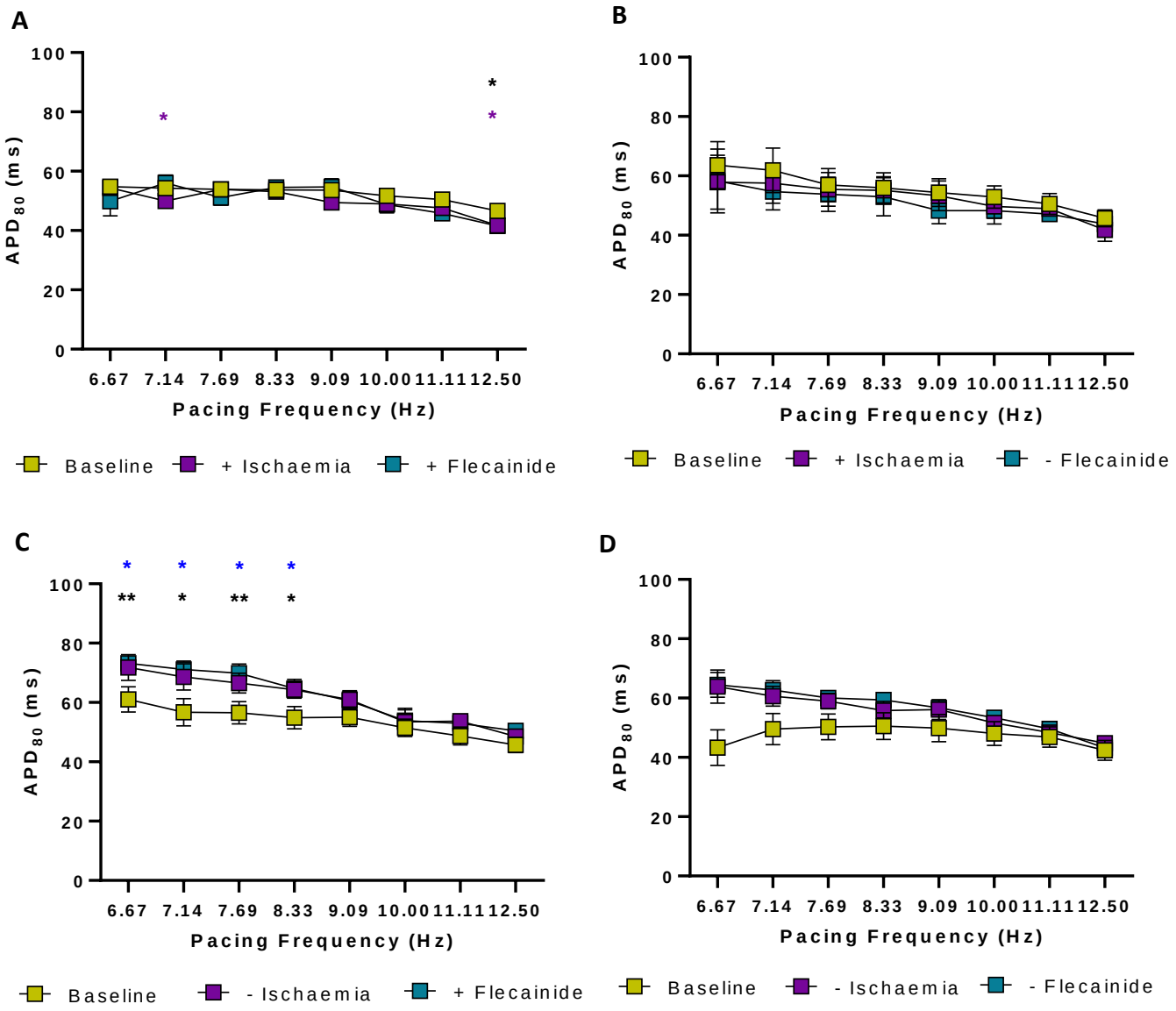

Figure 6.10A-D. APD80 in in ischaemic region of mouse hearts in presence and absence of ischaemia and flecainide. APD80 measurements taken from ischaemic region of ventricles at different pacing frequencies. A. Group +ischaemia and +flecainide. Significant difference observed between baseline and +flecainide at 12.5 Hz;. Significant difference observed between +ischaemia and +flecainide at 7.14 Hz;, at 12.5 Hz; 41.7 ± 4.4 ms vs. 41.5 ± 5.1 ms, *p=0.042.* B. Group +ischaemia and –flecainide. No significant differences observed between +ischaemia and –flecainide. C. Group –ischaemia and +flecainide. Significant differences observed between baseline and –ischaemia at 6.67 Hz; 61.0 ± 10.4 ms vs. 71.8 ± 10.6. Significant differences observed between baseline and +flecainide at 6.67 Hz;, at 8.33 Hz; 54.9 ± 9.3 ms vs. 64.7 ± 6.9 ms, *p=0.012,* at 9.09 Hz; 55.0 ± 7.6 ms vs. 60.6 ± 7.2 ms, *p=0.0104.* D. Group –ischaemia and –flecainide. No significant differences between –ischaemia and –flecainide. Statistical significance determined by two-way ANOVA, significance quantified as P<0.05. * denotes P<0.05, ** denotes P<0.01, *** denotes P<0.001, **** denotes P<0.0001. * indicates significant difference between baseline and ± ischaemia, * indicates significant difference between baseline and ± flecainide, * indicates significant difference between ± ischaemia and ± flecainide.

In addition to APD30, 50 and 80, using these measurements, we also calculated overall AP triangulation, and AP triangulation in the remote and ligated region. AP triangulation was calculated by deducting APD30 from APD80. AP triangulation was significantly smaller after ischaemia compared to baseline at 11.11 Hz only. Overall, ischaemia did not affect the APD triangulation, Figure 6.10A and 6.10B. Flecainide significantly prolonged AP triangulation from the baseline at some pacing frequencies, in the presence and absence of ischaemia, Figure 6.10A and 6.10C. As with the overall AP triangulation, the AP triangulation from the remote region of the heart showed little differences between baseline, ischaemia and flecainide. AP triangulation from the ligated region of the heart showed ischaemia caused a significantly smaller AP triangulation from the baseline between 9.09 Hz and 12.5 Hz, Figure 6.11A. Flecainide also showed a significantly smaller AP triangulation from baseline at faster pacing frequencies, Figure 6.11A. In the absence of ischaemia, flecainide showed a significantly smaller AP triangulation at slower pacing frequencies, Figure 6.11C. In Figure 6.11B, ischaemia did not show a significant difference from the baseline.

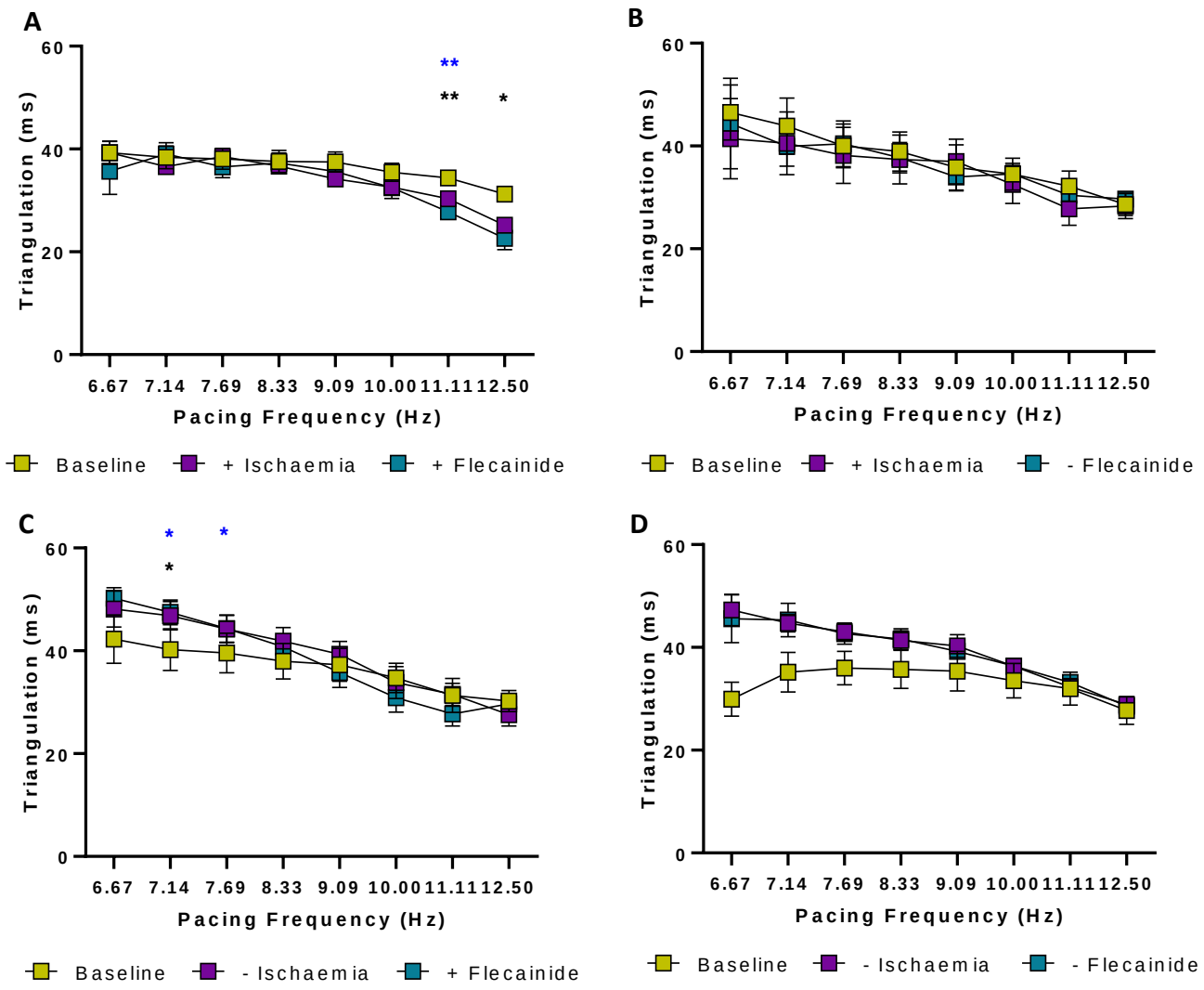

Figure 6.11A-D. Overall APD triangulation in mouse hearts in presence and absence of ischaemia and flecainide. APD triangulation taken from whole ventricles at different pacing frequencies. A. Group +ischaemia and +flecainide. Significant difference between baseline and +ischaemia at 12.5 Hz. Significant difference observed between baseline and +flecainide at 11.11 Hz; at 12.5 Hz. D. Group –ischaemia and –flecainide. No significant differences observed between –ischaemia and –flecainide. Statistical significance determined by two-way ANOVA, significance quantified as P<0.05. * denotes P<0.05, ** denotes P<0.01, *** denotes P<0.001, **** denotes P<0.0001. * indicates significant difference between baseline and ± ischaemia, * indicates significant difference between baseline and ± flecainide, * indicates significant difference between ± ischaemia and ± flecainide.

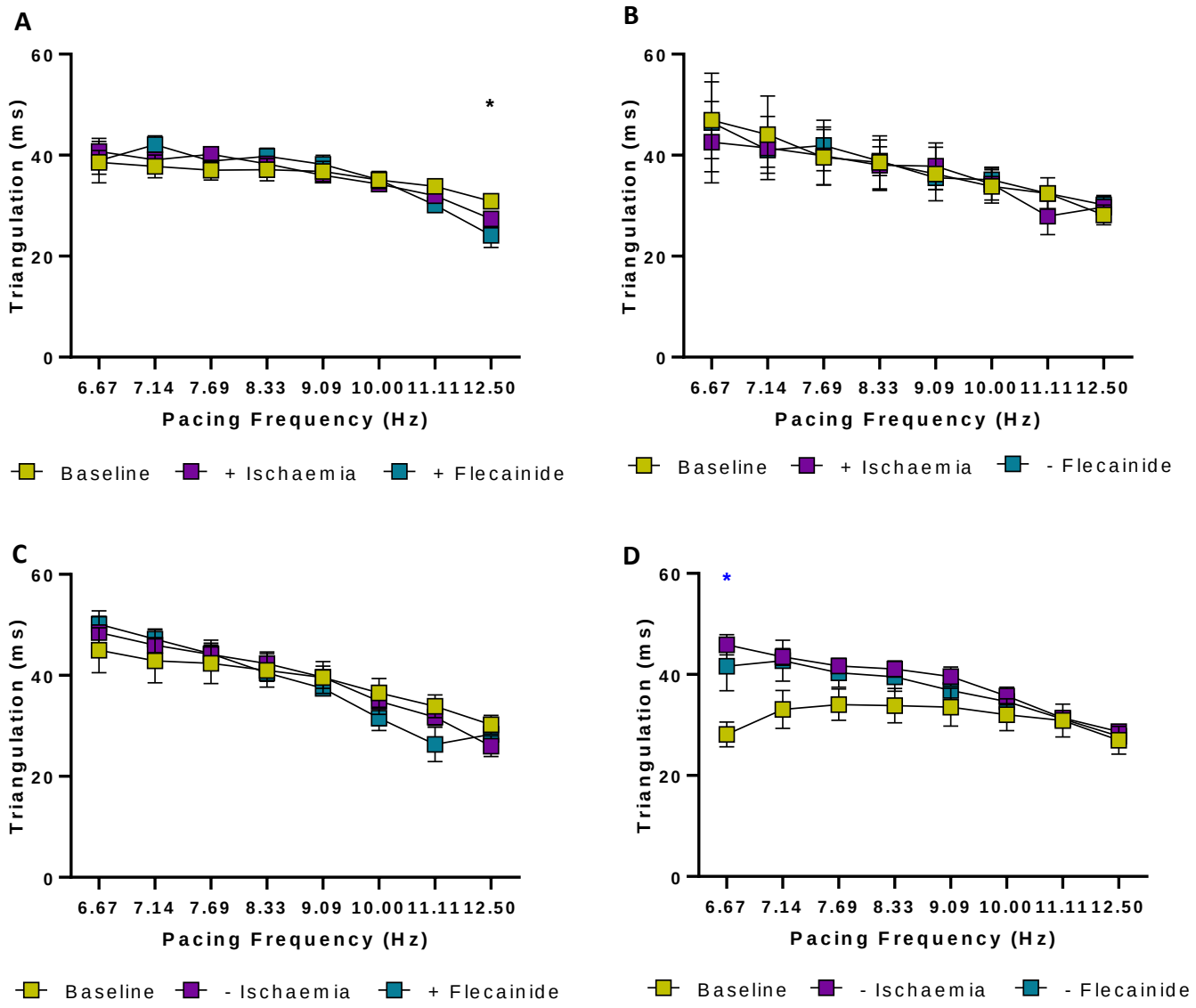

Figure 6.12A-D. APD triangulation in remote region of mouse hearts in presence and absence of ischaemia and flecainide. APD triangulation taken from remote region of ventricles at different pacing frequencies. A. Group +ischaemia and +flecainide. Significant difference between baseline and +flecainide at 12.5 Hz. B. Group +ischaemia and –flecainide. No significant difference observed between +ischaemia and –flecainide. C. Group –ischaemia and +flecainide. No significant difference observed between –ischaemia and +flecainide. D. Group –ischaemia and –flecainide. Significant difference observed between baseline and –ischaemia at 6.67 Hz; . Statistical significance determined by two-way ANOVA, significance quantified as $P<0.05$. * denotes $P<0.05$, ** denotes $P<0.01$, *** denotes $P<0.001$, **** denotes $P<0.0001$. * indicates significant difference between baseline and ± ischaemia, * indicates significant difference between baseline and ± flecainide, * indicates significant difference between ± ischaemia and ± flecainide.

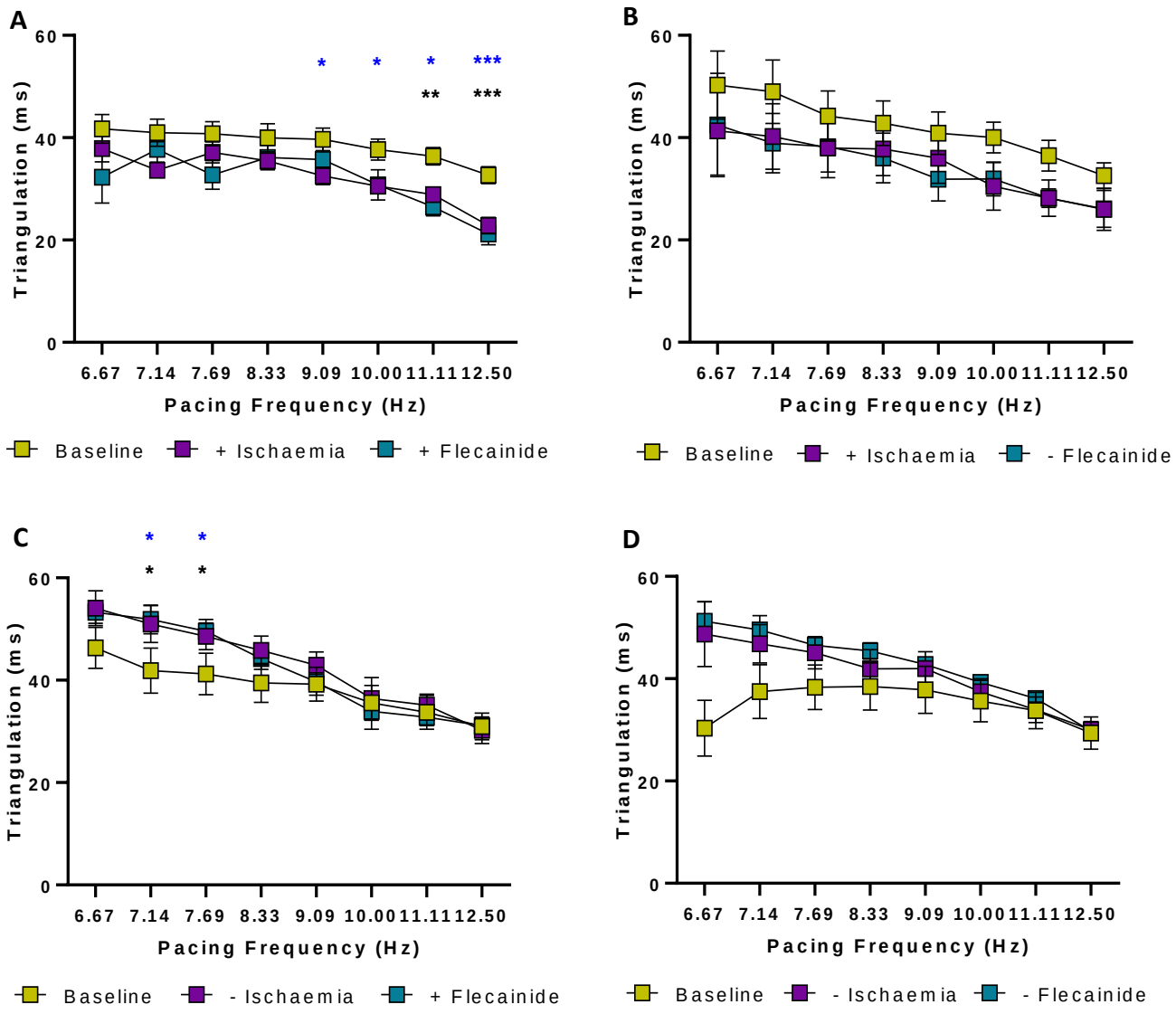

Figure 6.13A-D. APD triangulation in ischaemic region of mouse hearts in presence and absence of ischaemia and flecainide. APD triangulation taken from ischaemic region of ventricles at different pacing frequencies. A. Group +ischaemia and +flecainide. Significant difference observed at faster pacing frequencies. B. Group +ischaemia and –flecainide. No significant difference observed between groups. C. Group –ischaemia and +flecainide. Significant difference observed at 7.14 Hz and 7.69 Hz. D. Group –ischaemia and –flecainide. No significant difference observed. Statistical significance determined by two-way ANOVA, significance quantified as $P<0.05$. * denotes $P<0.05$, ** denotes $P<0.01$, *** denotes $P<0.001$, **** denotes $P<0.0001$. * indicates significant difference between baseline and ± ischaemia, * indicates significant difference between baseline and ± flecainide, * indicates significant difference between ± ischaemia and ± flecainide.

6.2.2. Effect of regional ischaemia and flecainide on conduction velocity

Following on from the APD measurements, we continued with analysing the conduction velocity from the whole ventricles, remote region and iscahemic region. Although ischaemia and flecainide showed little effect on the APD, the CV was affected to a much larger degree.

Ischaemia caused a slowing of the CV at all pacing frequencies. In the ischaemic region of ventricles, ischaemia significantly slowed the CV when compared to baseline. The degree to which the ischaemia slowed the CV was larger in the ischaemic area compared to the remote region. In the ischaemic region, CV was significantly slowed at most pacing frequencies, whereas in the remote region CV was significantly slowed at fewer frequencies, Figures 6.15A and 6.16A. However, the slowing of CV isn't significant at most frequencies in Figure 6. 16B. When ischaemia wasn't present, the CV did not show significant slowing, suggesting that the CV slowing we observe is the true effect of ischaemia.

When flecainide was added in hearts without ischaemia, flecainide caused a significant slowing of the CV at most pacing frequencies in the remote and ischaemic region, Figures 6.15C and 6.16C. In hearts where flecainide wasn't added, the CV does not change when compared to baseline or ischaemia, Figures 6.15B and D, and Figures 6.16B and D. Figure 6.14 shows the overall CV in the ventricles reflecting the effects of ischaemia and flecainide in the remote and ischaemic region.

In the ischaemic region, CV at baseline was 82.8 ± 23.3 cm/s. In the presence of ischaemia, flecainide reduced the CV to 33.3 ± 8.6 cm/s, a 59.8% decrease in CV. In the

absence of ischaemia, flecainide reduced the CV from 59.5 ± 10.8 cm/s at baseline to 39.8 ± 9.0 cm/s, a 33.1% decrease in CV. The increased slowing of CV when ischaemia is present, may be considered proarrhythmic. A slow CV makes it possible for multiple excitation waves to co-exist, causing re-entry [118].

A representative activation map from the ischaemic region, from a heart at baseline, with ischaemia, and with flecainide shows a progressive slowing of the activation time from 5.3 ms, to 6.5 ms and then to 8.6 ms, Figure 6.17. In the remote region, activation time went from 5.6 ms at baseline to 6.3 ms after ischaemia and 5.5 ms after flecainide perfusion, Figure 6.19. Representative activation curves and action potentials are shown from different regions at different timepoints in Figures 6.18 and 6.20.

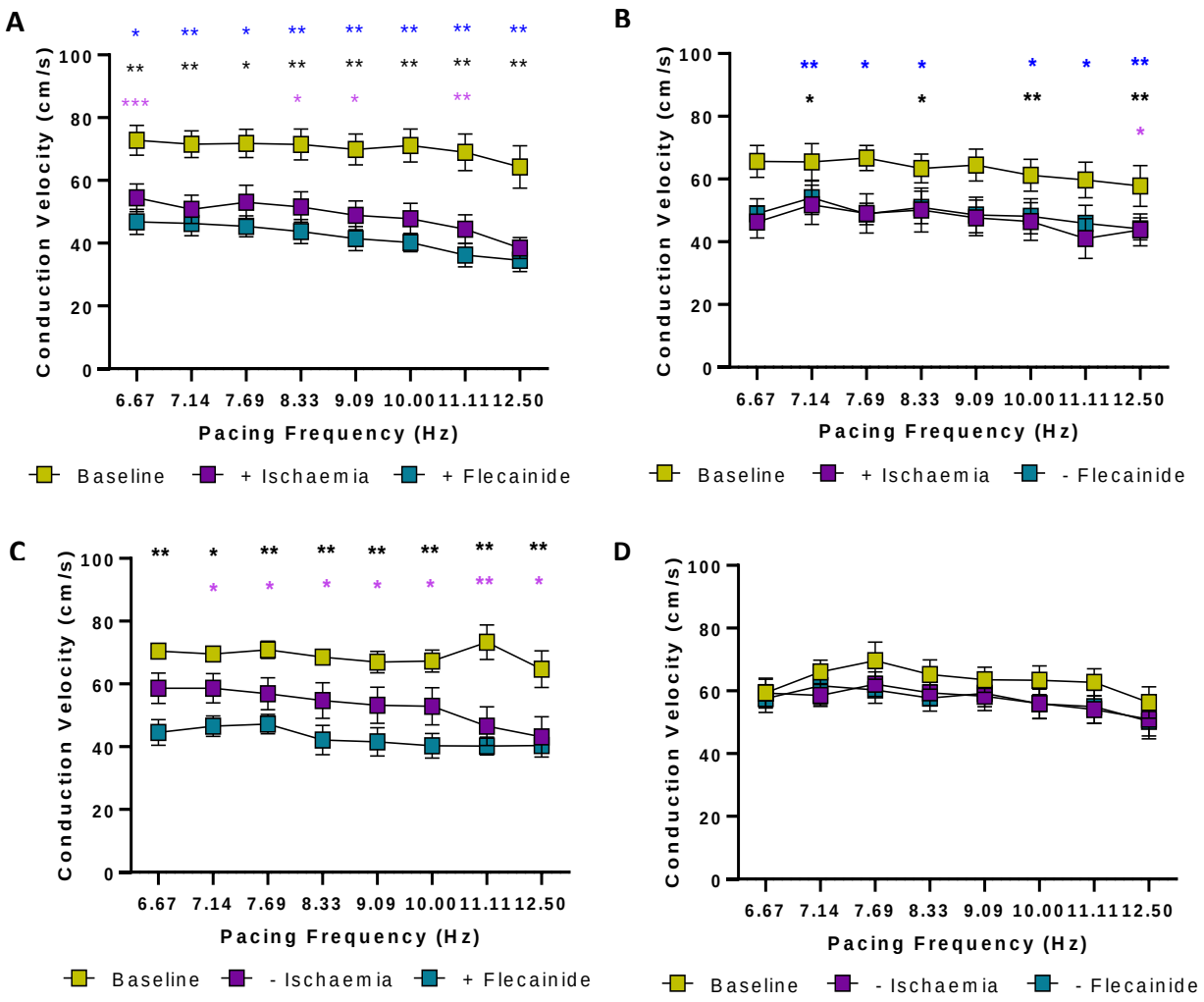

Figure 6.14A-D. Overall conduction velocity in mouse hearts in presence and absence of ischaemia and flecainide. CV taken from whole region of ventricles at different pacing frequencies. A. Group +ischaemia and +flecainide. Significant difference observed between baseline and +ischaemia, baseline and +flecainide, and +ischaemia and +flecainide at all pacing frequencies. B. Group +ischaemia and –flecainide. Significant difference between baseline and +ischaemia, and baseline vs. -flecainide (ischaemia) at most pacing frequencies. C. Group –ischaemia and +flecainide. Significant difference between baseline and +flecainide, and –ischaemia and +flecainide at all pacing frequencies. D. Group –ischaemia and –flecainide. No significant difference between –ischaemia and –flecainide. Statistical significance determined by two-way ANOVA, significance quantified as P<0.05. * denotes P<0.05, ** denotes P<0.01, *** denotes P<0.001, **** denotes P<0.0001. * indicates significant difference between baseline and ± ischaemia, * indicates significant difference between baseline and ± flecainide, * indicates significant difference between ± ischaemia and ± flecainide.

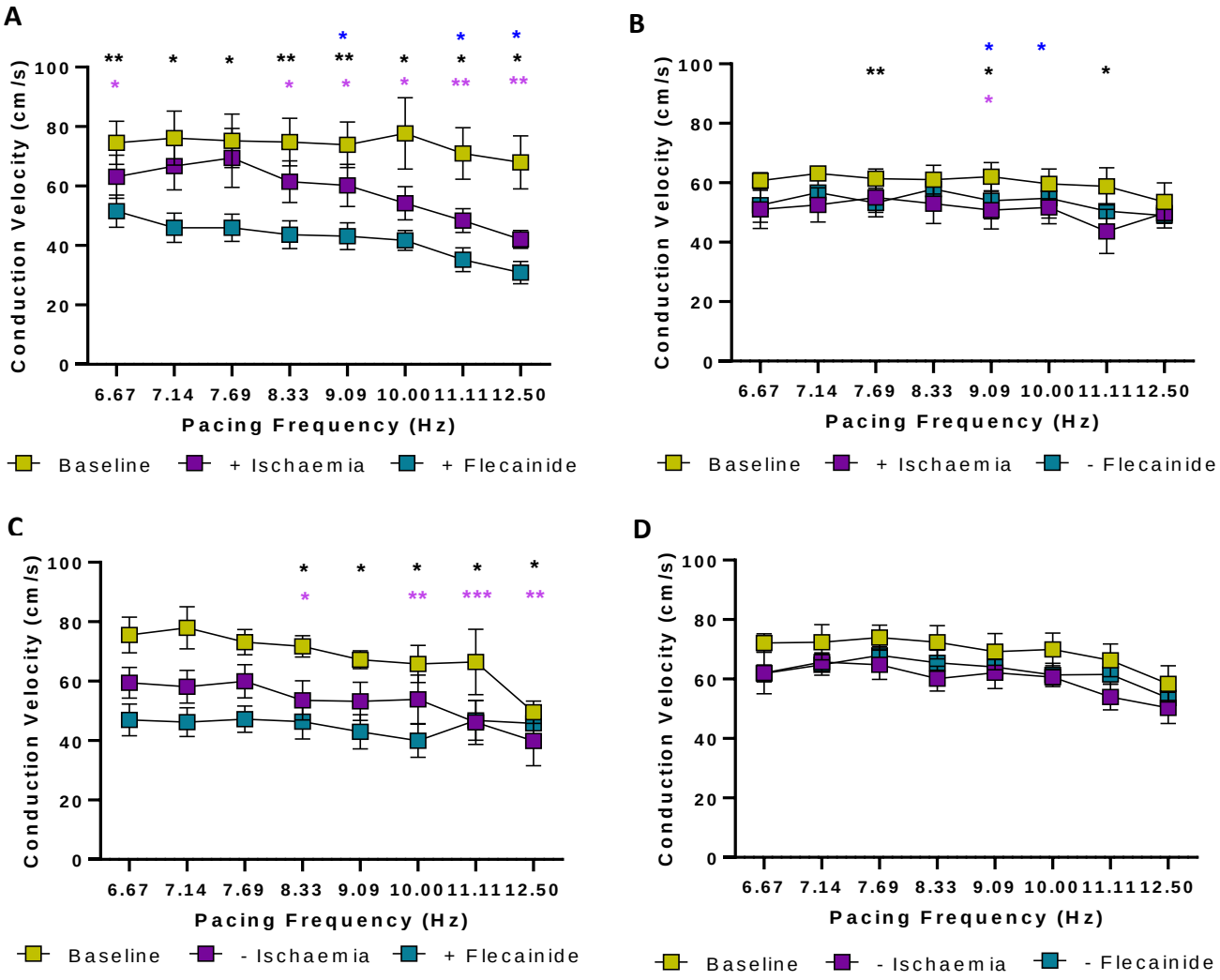

Figure 6.15A-D. Conduction velocity in remote region of mouse hearts in presence and absence of ischaemia and flecainide. CV taken from remote region of ventricles at different pacing frequencies. A. Group +ischaemia and +flecainide. Significant difference between baseline vs. +ischaemia and +ischaemia vs. +flecainide at faster pacing frequencies. Significant differences observed between baseline and +flecainide at all pacing frequencies. B. Group +ischaemia – flecainide. C. Group –ischaemia and +flecainide. Significant difference between baseline vs. +flecainide and -ischaemia vs. +flecainide at faster pacing frequency. D. Group –ischaemia and –flecainide. No significant difference observed. Statistical significance determined by two-way ANOVA, significance quantified as P<0.05. * denotes P<0.05, ** denotes P<0.01, *** denotes P<0.001, **** denotes P<0.0001. * indicates significant difference between baseline and ± ischaemia, * indicates significant difference between baseline and ± flecainide, * indicates significant difference between ± ischaemia and ± flecainide. N=5-8.

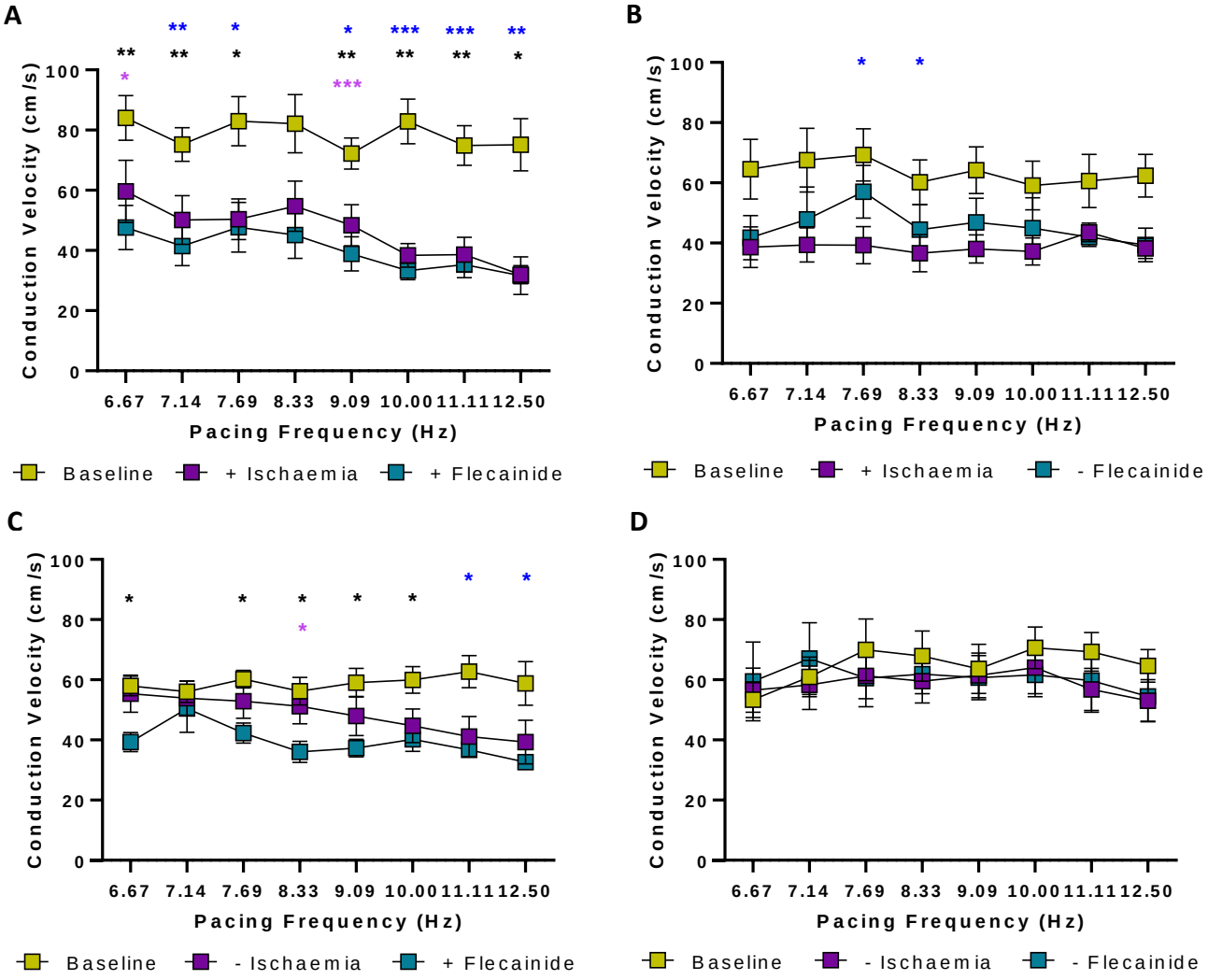

Figure 6.16A-D. Conduction velocity in ischaemic region of mouse hearts in presence and absence of ischaemia and flecainide. CV taken from ischaemic region of ventricles at different pacing frequencies. A. Group +ischaemia and +flecainide. Significant difference between baseline and +ischaemia, and baseline and flecainide at most pacing frequencies. B. Group +ischaemia and –flecainide. Significant difference observed between baseline and +ischaemia at 7.69 Hz and 8.33 Hz. C. Group –ischaemia and +flecainide. Significant difference between baseline and –ischaemia at 11.11 Hz and 12.5 Hz. Significant difference between baseline and +flecainide at most pacing frequencies. Significant difference between –ischaemia and +flecainide at 8.33 Hz. D. Group –ischaemia and –flecainide. No significant differences observed between groups. Statistical significance determined by two-way ANOVA, significance quantified as P<0.05. * denotes P<0.05, ** denotes P<0.01, *** denotes P<0.001, **** denotes P<0.0001. * indicates significant difference between baseline and ± ischaemia, * indicates significant difference between baseline and ± flecainide, * indicates significant difference between ± ischaemia and ± flecainide. N=5-8.

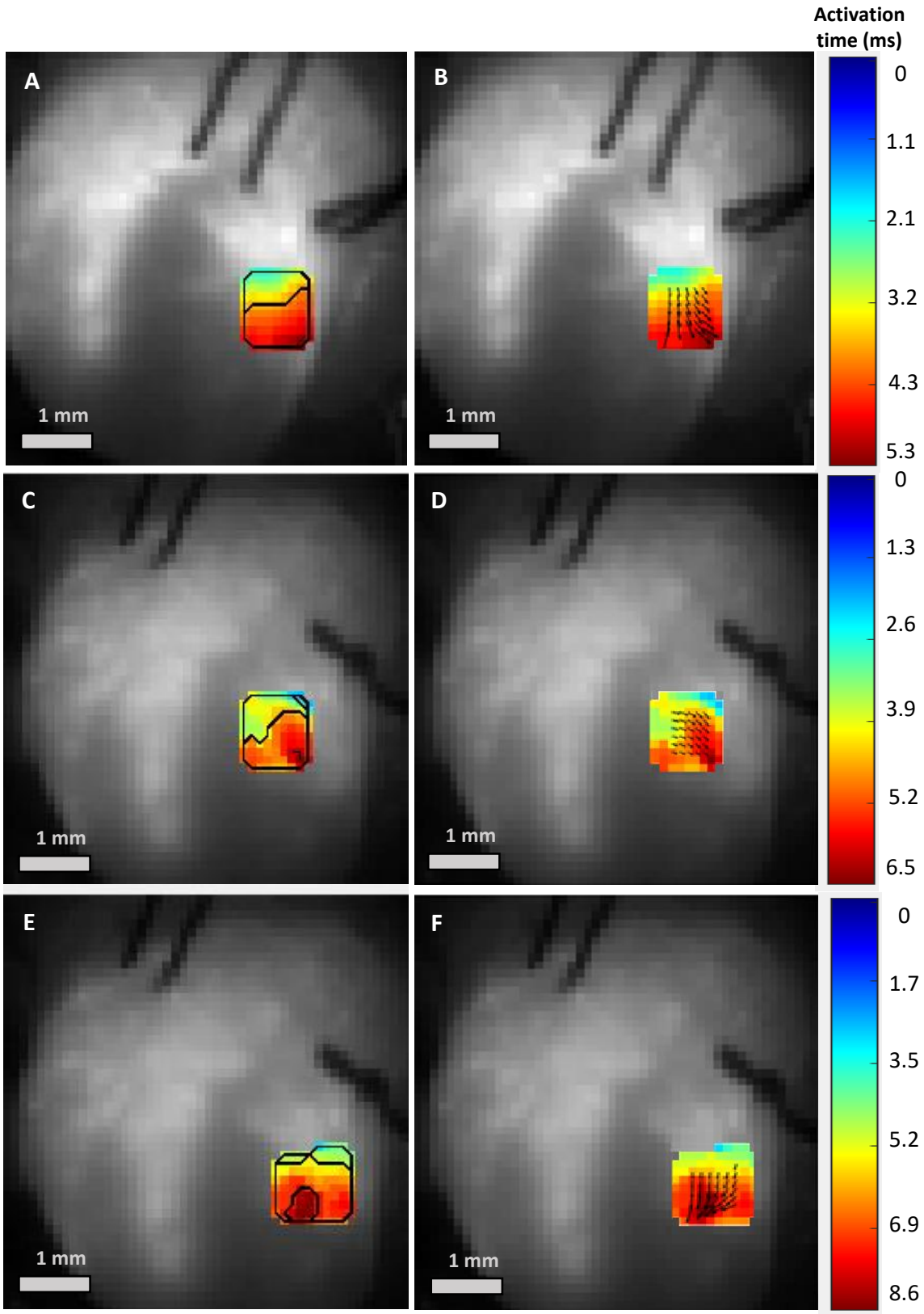

Figure 6.17A-F. Activation maps in ventricles in ischaemic region, at 10 Hz. A. Representative activation map in the LV at baseline at 10 Hz. Contour lines are spaced by 2 ms. B. Representative isomap with vectors in the LV at baseline at 10 Hz. C. Representative activation map in the LV after ischaemia, at 10 Hz. Contour lines are spaced at 2 ms. D. Representative isomap with vectors in the LV after ischaemia, at 10 Hz. E. Representative activation map in LV with ischaemia and 1 µM flecainide, at 10Hz. F. Representative isomap with vectors in LV with ischaemia and flecainide, at 10 Hz.

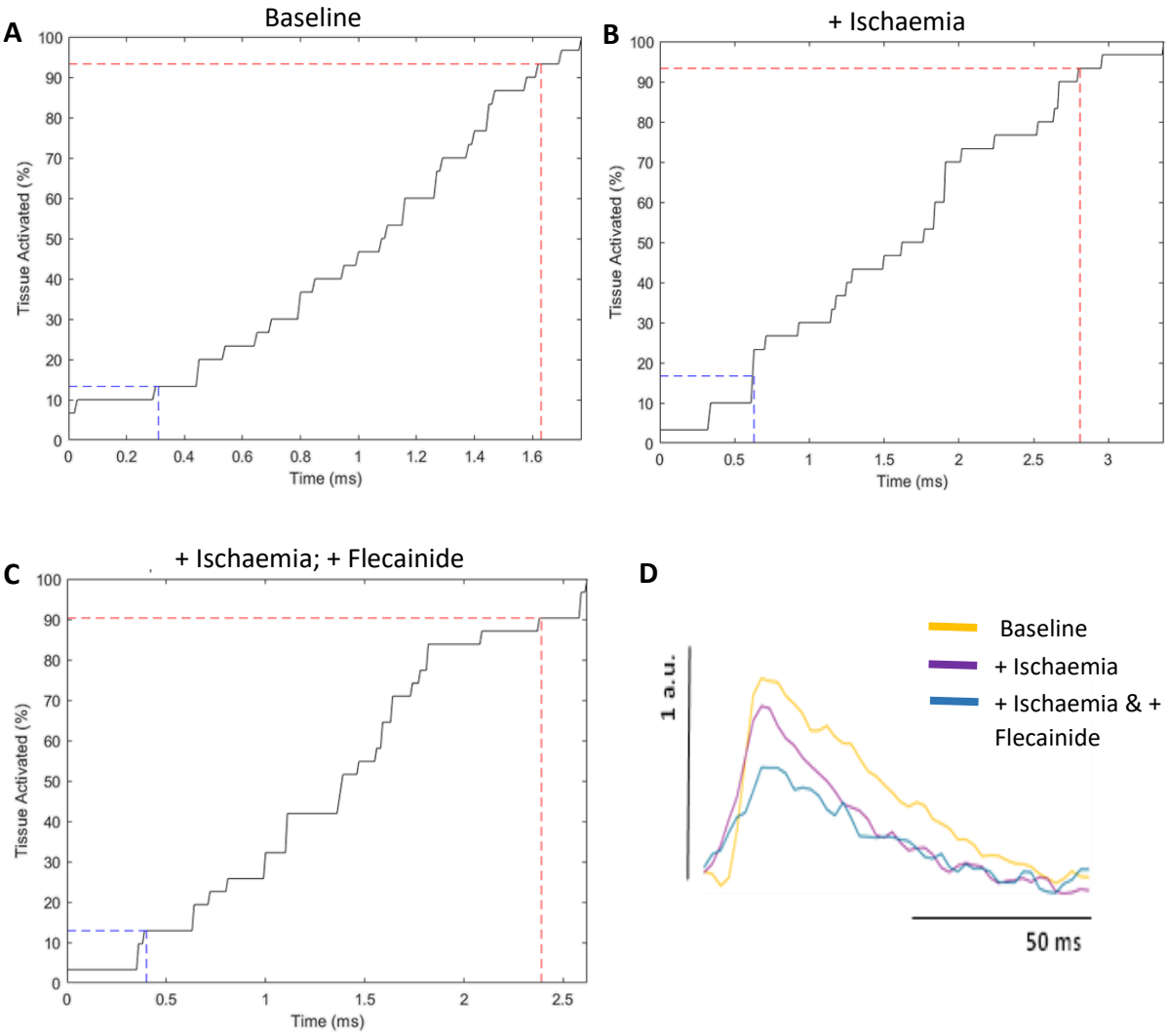

Figure 6.18A-D. Activation curves from ischaemic region in ventricles with different treatments, at 10 Hz. A. Representative activation curve from baseline at 10 Hz. B. Representative activation curve after ischaemia. C. Representative activation curve after ischaemia and flecainide. Blue dashed line indicates time it takes for 10% of tissue to be activated. Red dashed lines indicate time it takes for 90% of tissue to be activated. D. Representative action potential at baseline (yellow line), after ischaemia (purple line), and with ischaemia and flecainide (blue line).

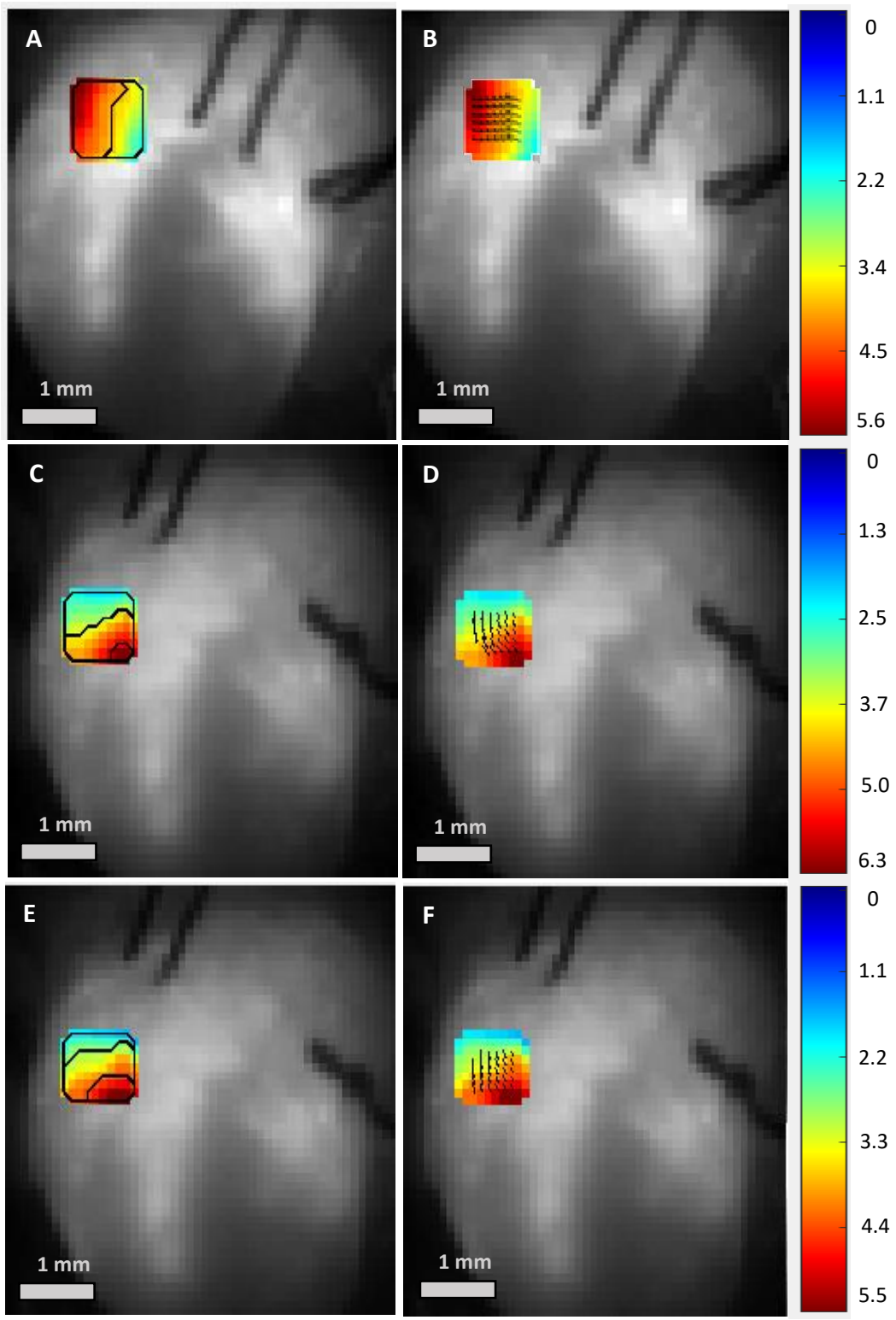

Figure 6.19A-F. Activation maps in ventricles in remote region, at 10 Hz. A. Representative activation map in the LV at baseline at 10 Hz. Contour lines are spaced by 2 ms. B. Representative isomap with vectors in the LV at baseline at 10 Hz. C. Representative activation map in the LV after ischaemia, at 10 Hz. Contour lines are spaced at 2 ms. D. Representative isomap with vectors in the LV after ischaemia, at 10 Hz. E. Representative activation map in LV with ischaemia and 1 µM flecainide, at 10Hz. F. Representative isomap with vectors in LV with ischaemia and flecainide, at 10 Hz.

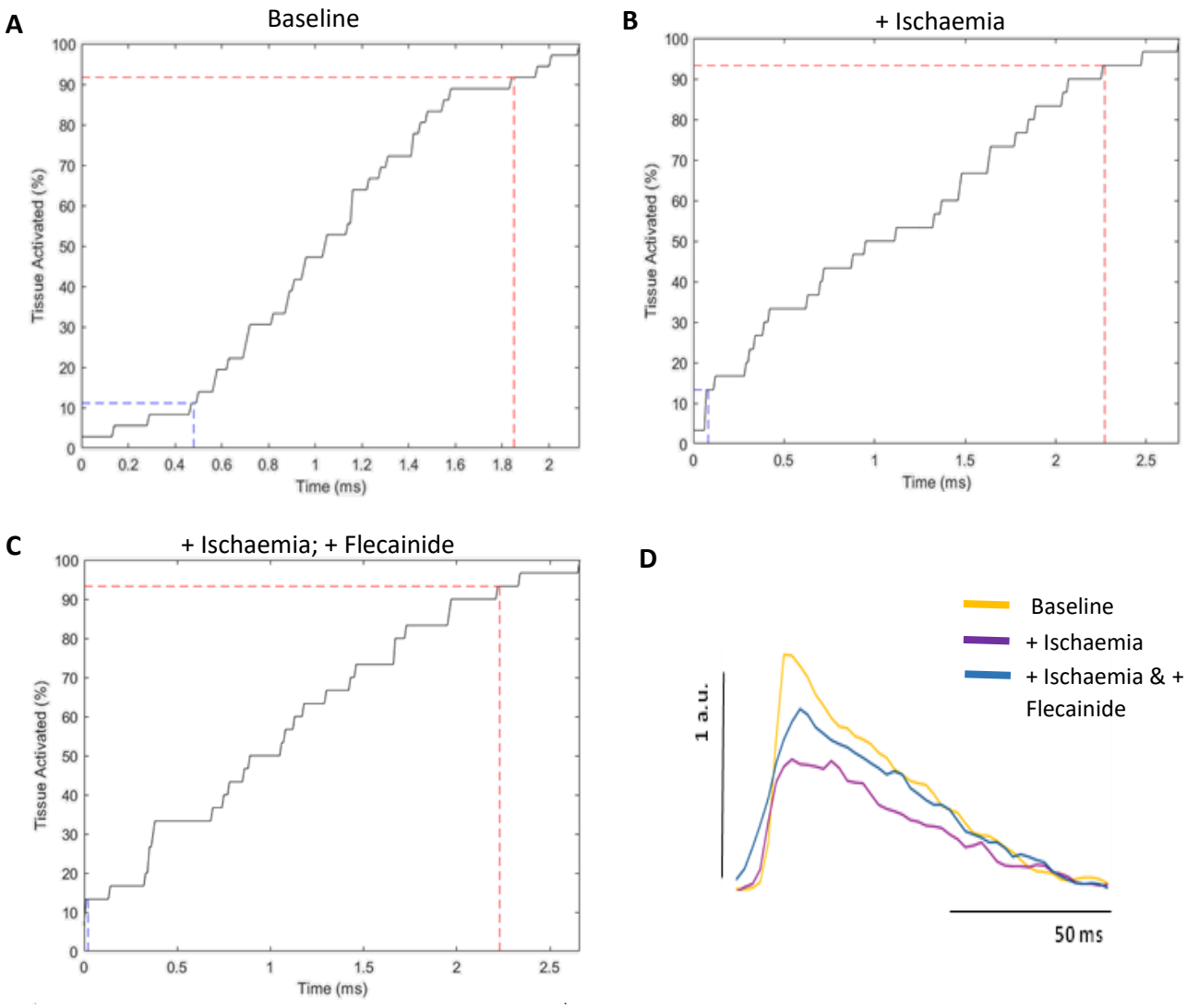

Figure 6.20A-D. Activation curves from remote region in ventricles with different treatments, at 10 Hz. A. Representative activation curve from baseline at 10 Hz. B. Representative activation curve after ischaemia. C. Representative activation curve after ischaemia and flecainide. Blue dashed line indicates time it takes for 10% of tissue to be activated. Red dashed lines indicate time it takes for 90% of tissue to be activated. D. Representative action potential at baseline (yellow line), after ischaemia (purple line), and with ischaemia and flecainide (blue line).

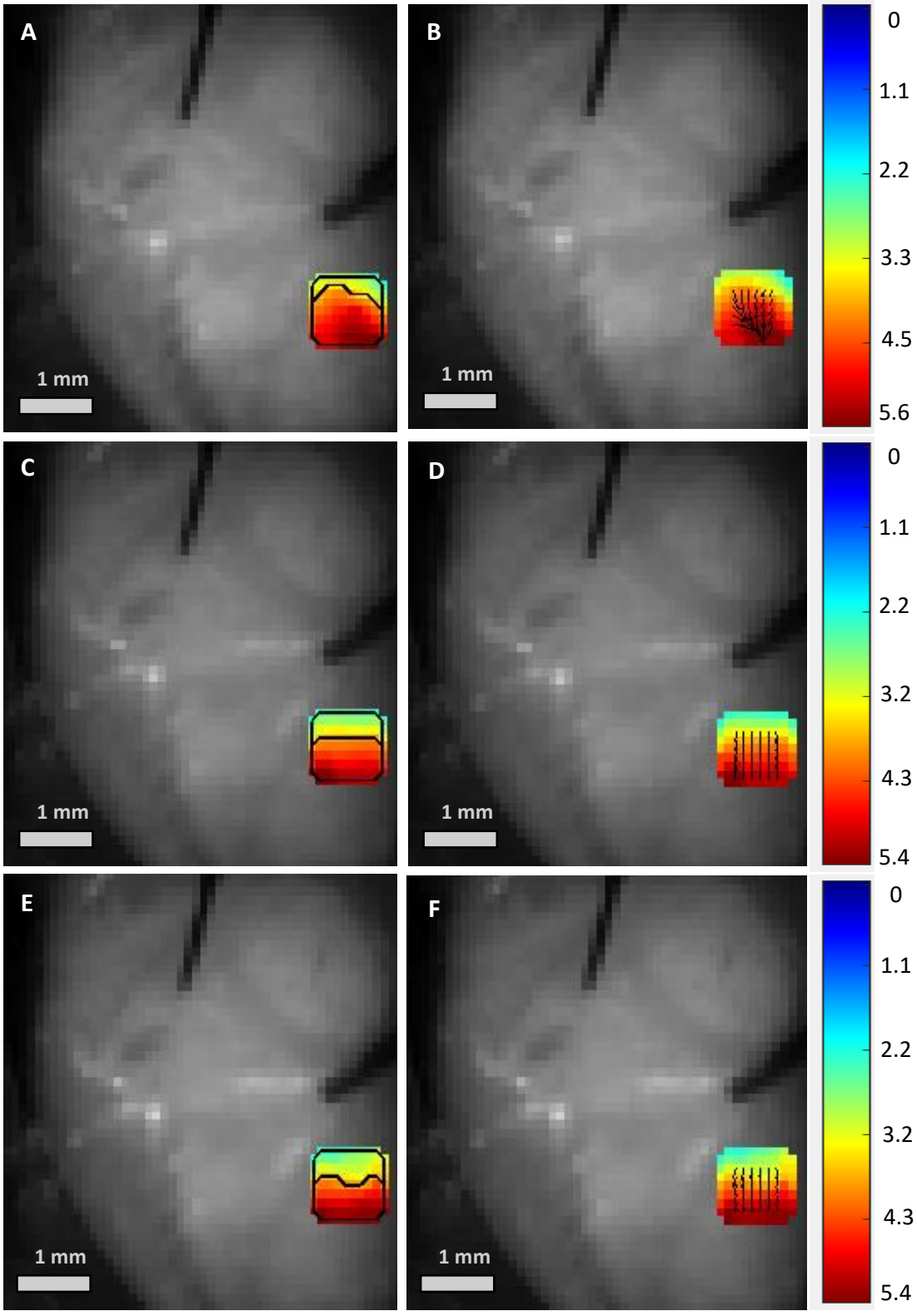

Figure 6.21A-F. Activation maps in ventricles without ischaemia and flecainide, at 10 Hz. A. Representative activation map in the LV at baseline at 10 Hz. Contour lines are spaced by 2 ms. B. Representative isomap with vectors in the LV at baseline at 10 Hz. C. Representative activation map in the LV after ischaemia control, at 10 Hz. Contour lines are spaced at 2 ms. D. Representative isomap with vectors in the LV after ischaemia control, at 10 Hz. E. Representative activation map in LV with ischaemia control and flecainide control, at 10Hz. F. Representative isomap with vectors in LV with ischaemia control and flecainide control, at 10 Hz.

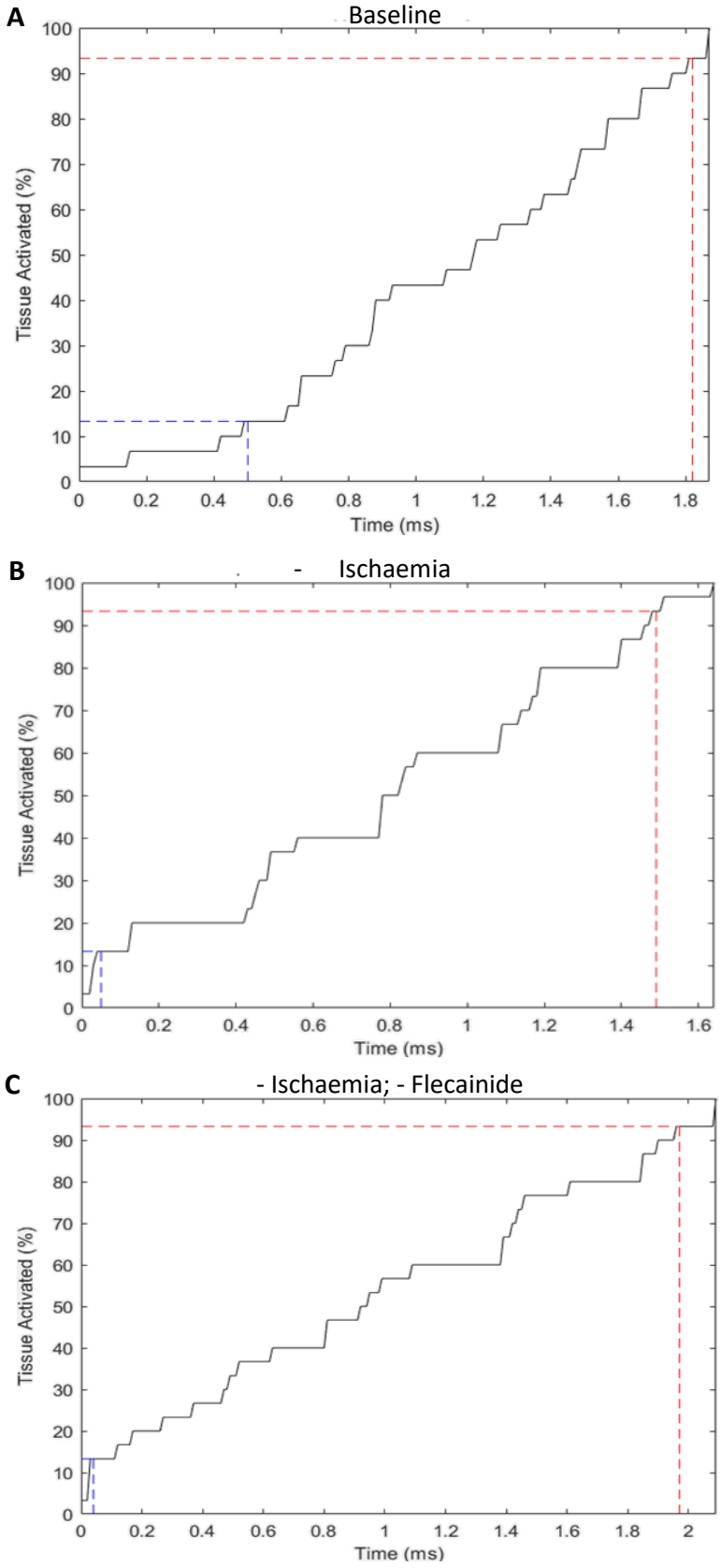

Figure 6.22A-D. Activation curves in ventricles without ischaemia and flecainide, at 10 Hz. A. Representative activation curves at different timepoints 10 Hz. Blue dashed line indicates time it takes for 10% of tissue to be activated. Red dashed lines indicate time it takes for 90% of tissue to be activated.

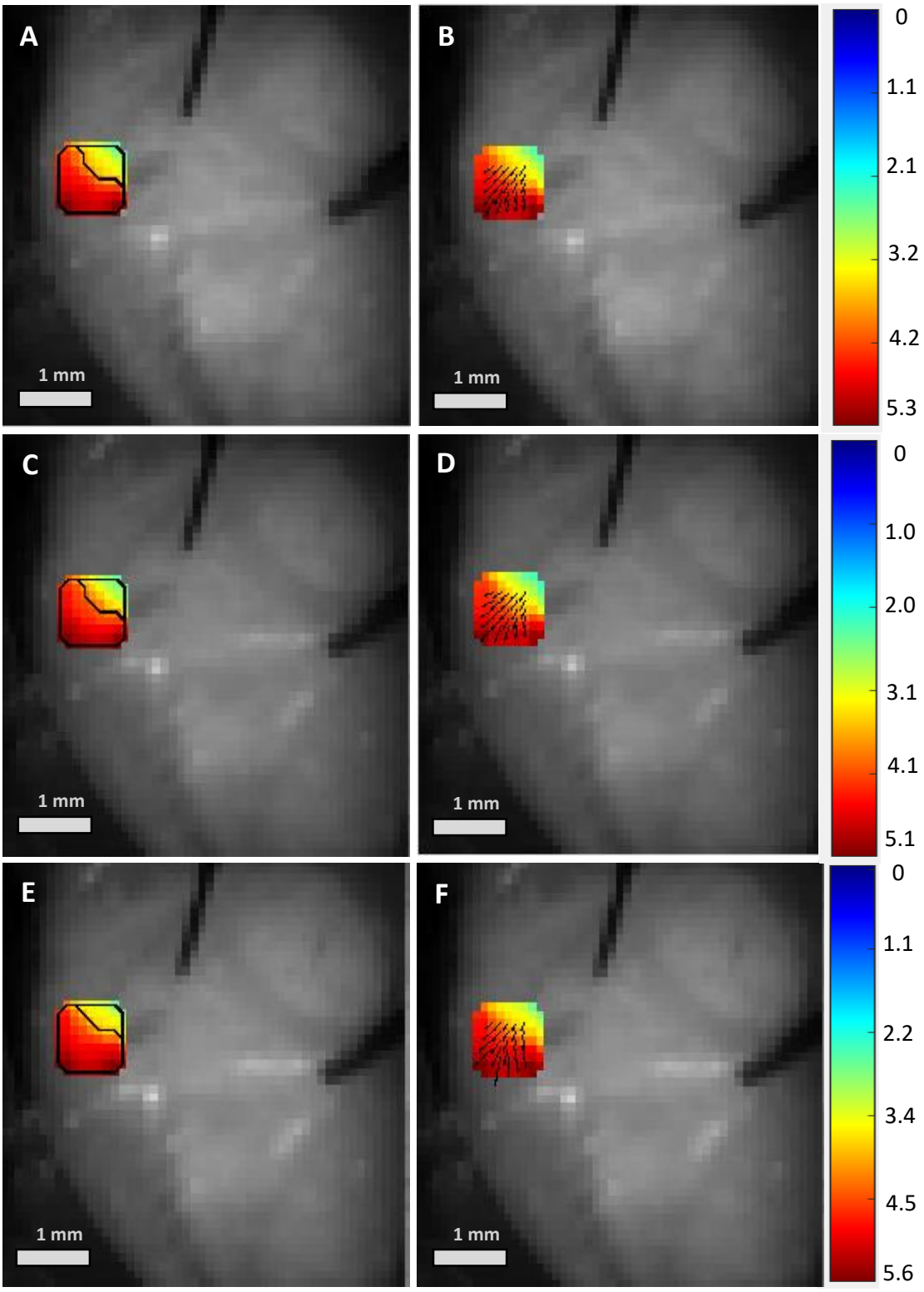

Figure 6.23A-F. Activation maps from remote region without ischaemia and flecainide, at 10 Hz. A. Representative activation map in the LV at baseline at 10 Hz. Contour lines are spaced by 2 ms. B. Representative isomap with vectors in the LV at baseline at 10 Hz. C. Representative activation map in the LV after ischaemia control, at 10 Hz. Contour lines are spaced at 2 ms. D. Representative isomap with vectors in the LV after ischaemia control, at 10 Hz. E. Representative activation map in LV with ischaemia control and flecainide control, at 10Hz. F. Representative isomap with vectors in LV with ischaemia control and flecainide control, at 10 Hz.

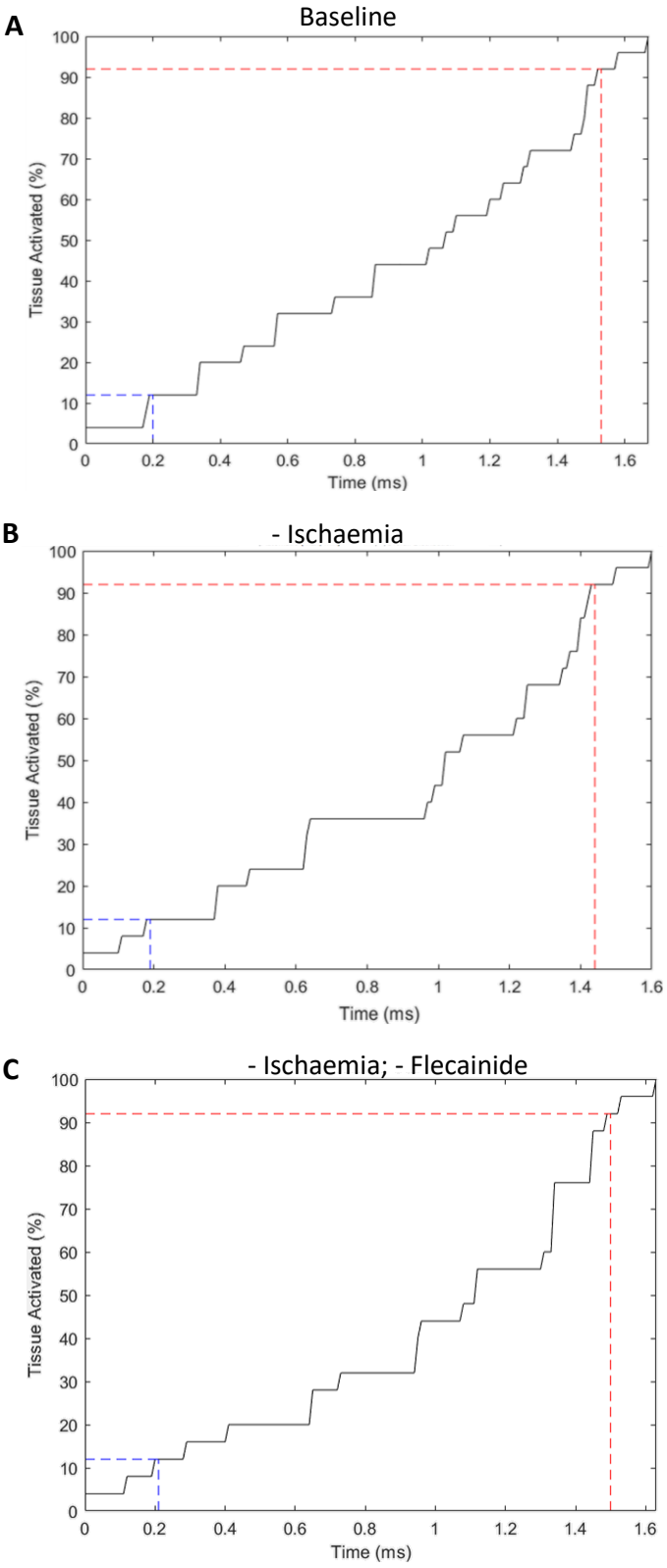

Figure 6.24A-D. Activation curves in ventricles without ischaemia and flecainide, from remote region, at 10 Hz. A. Representative activation curves at different timepoints 10 Hz. Blue dashed line indicates time it takes for 10% of tissue to be activated. Red dashed lines indicate time it takes for 90% of tissue to be activated.

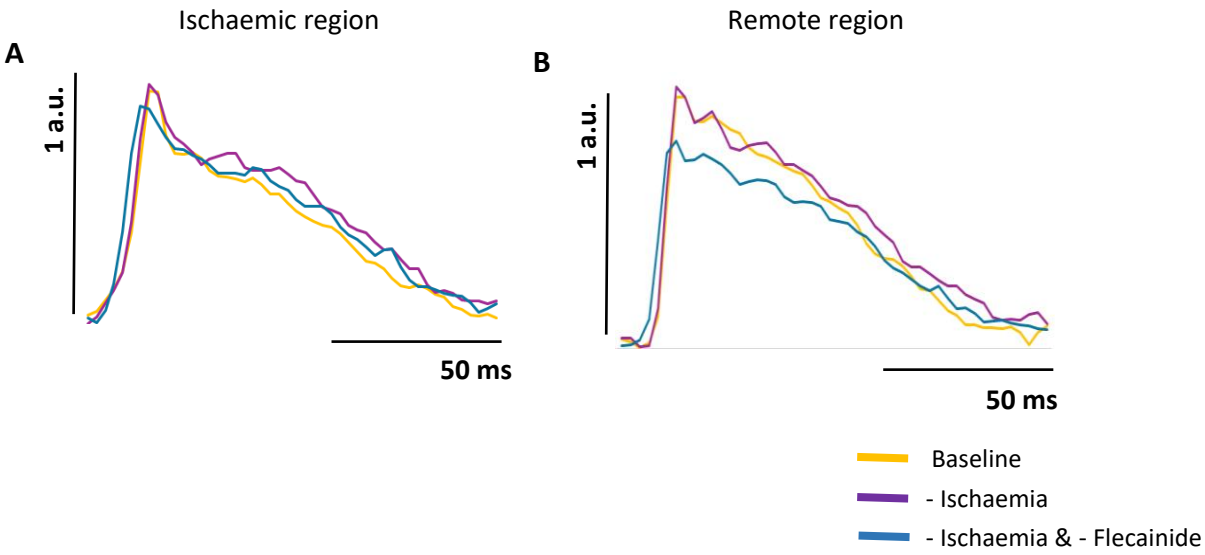

Figure 6.25A-B. Representative action potentials from ischaemic and remote region in control experiments, at 10 Hz. A. Representative action potentials at different timepoints from ischaemic region at 10 Hz. B. Representative action potentials at different timepoints from remote region at 10 Hz. Yellow line represents baseline, purple line represents – ischaemia and blue line represents – ischaemia & -flecainide.

6.2.3. Effect of regional ischaemia and flecainide on calcium transients

Calcium transients were recorded simultaneously with action potentials, using a calcium indicator, Rhod-2 AM. Like with the APD measurements, calcium transient duration (CaTD) and time to peak was measured from the remote and ligated region of the ventricles and an average overall value was taken from the whole ventricles. Overall, there was little change in CatD80 caused by ischaemia or flecainide. Ischaemia caused a significant shortening of CaTD80 from the baseline at 12.5 Hz in Figure 6.15A but did not cause a difference at any pacing frequency in Figure 6.15B. Significant difference was observed between baseline and -ischaemia at 7.69 Hz and 8.33 Hz, and between baseline and flecainide at 7.69 Hz. No significant differences were observed in control group.

In the remote region of ventricles, there is no overall significant difference between ischaemia and flecainide. At 7.69 Hz, there is a significant difference between baseline and –flecainide control, and at 10 Hz, between baseline and –ischaemia timepoint. We observe the decrease of CaTD80 with faster pacing frequencies in all groups.

In the ischaemic region of the ventricles, Figure 6.17, we observe a significant difference between baseline and ischaemia and baseline and flecainide at faster pacing frequencies only. At 8.33 Hz there was a significant difference between ischaemia and –flecainide timepoint, or, prolonged ischaemia. We also observed a significant difference between baseline and –ischaemia timepoint at several pacing frequencies, and between baseline and flecainide at slower pacing frequencies. No significant differences were observed in the control group, in the absence of ischaemia and flecainide.

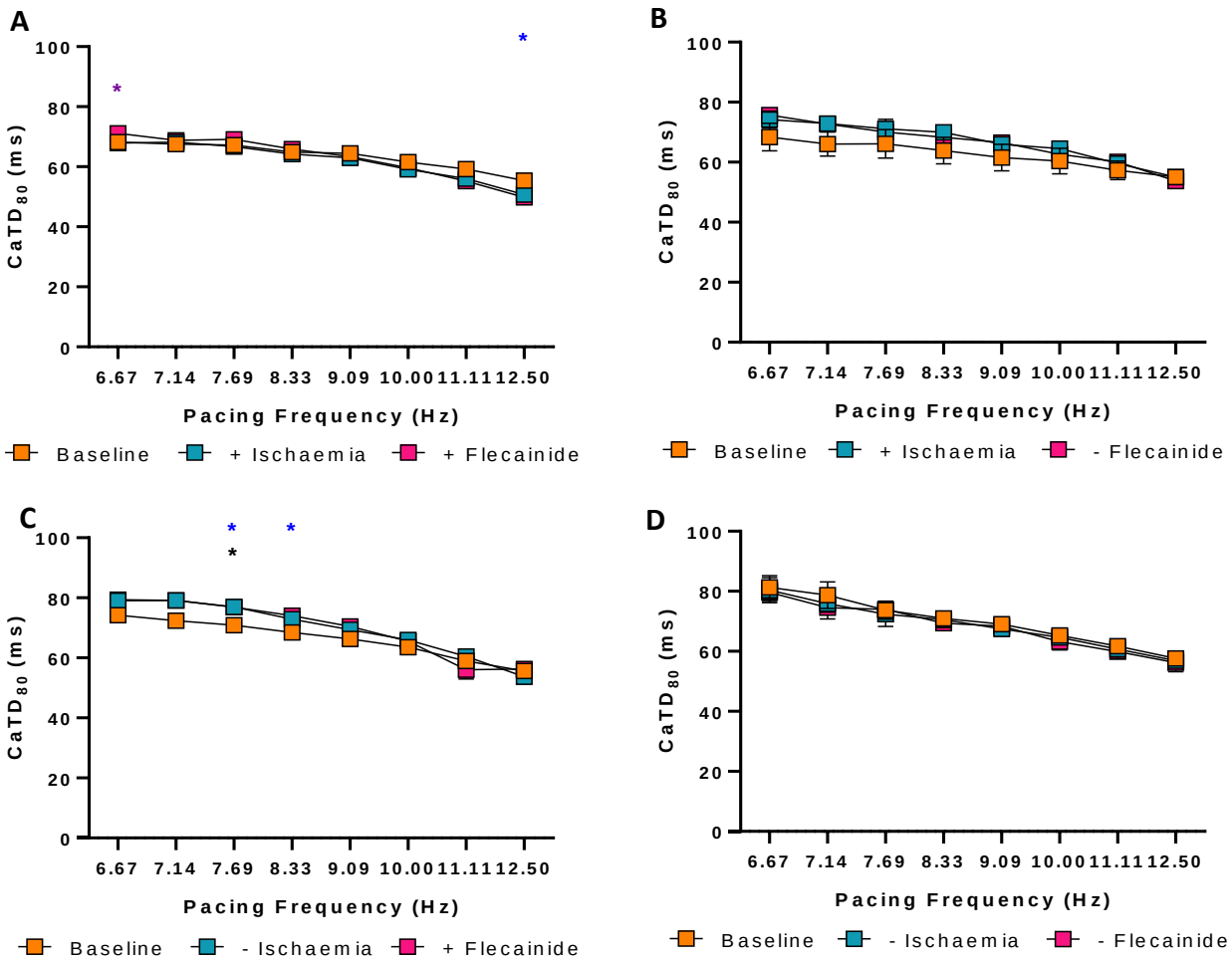

Figure 6.26A-D. Overall calcium transient duration mouse hearts in presence and absence of ischaemia and flecainide. CaTD taken from whole region of ventricles at different pacing frequencies. Each panel represents 4 treatment groups. A. Group +ischaemia and +flecainide. B. Group +ischaemia and –flecainide. C. Group –ischaemia and +flecainide. D. Group –ischaemia and –flecainide. Statistical significance determined by two-way ANOVA, significance quantified as P<0.05. * denotes P<0.05, ** denotes P<0.01, *** denotes P<0.001, **** denotes P<0.0001. * indicates significant difference between baseline and ± ischaemia, * indicates significant difference between baseline and ± flecainide, * indicates significant difference between ± ischaemia and ± flecainide.

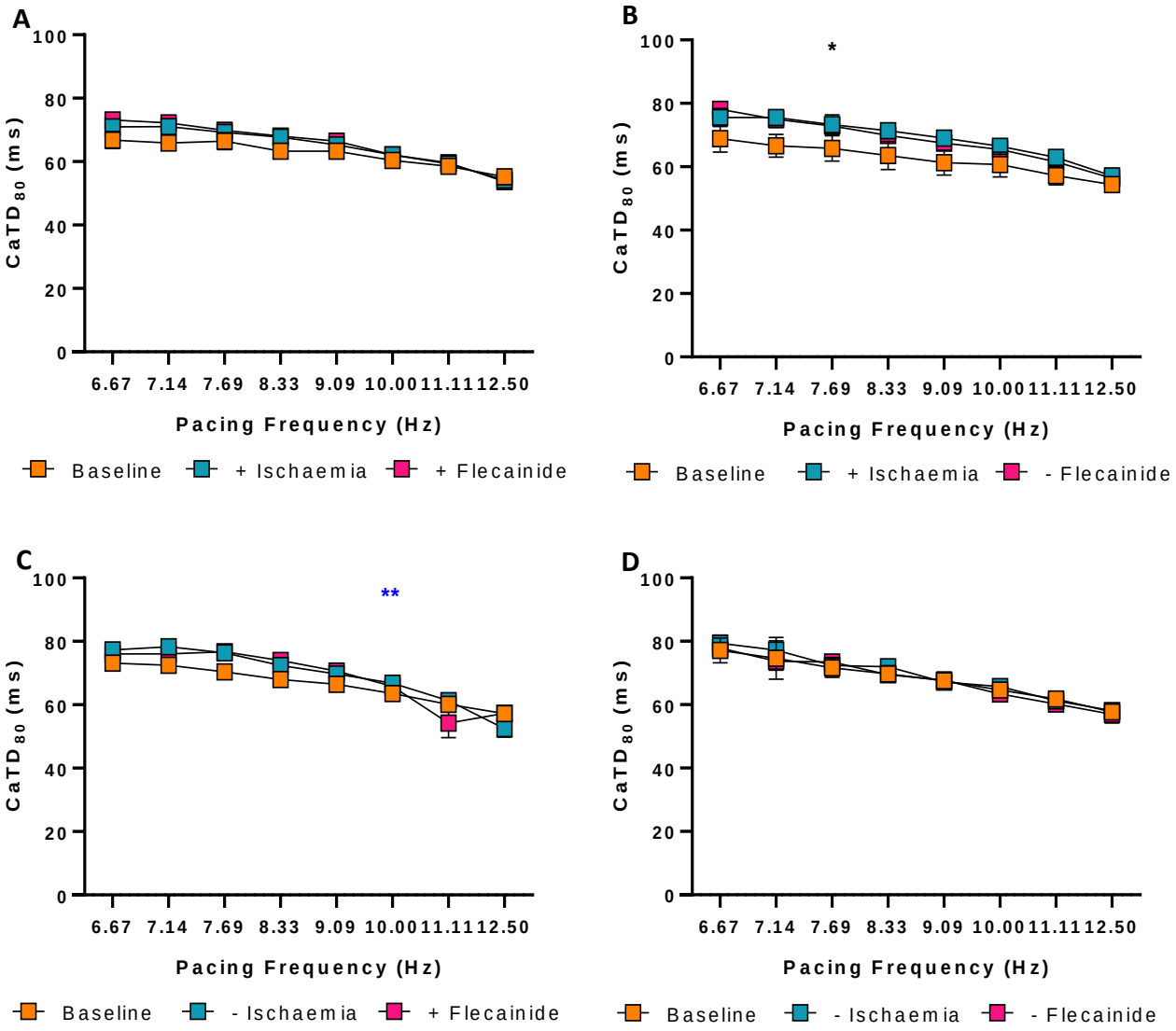

Figure 6.27A-D. Calcium transient duration from remote region of mouse hearts in presence and absence of ischaemia and flecainide. CaTD taken from remote region of ventricles at different pacing frequencies. Each panel represents 4 treatment groups. A. Group +ischaemia and +flecainide. B. Group +ischaemia and –flecainide. C. Group –ischaemia and +flecainide. D. Group –ischaemia and –flecainide. Statistical significance determined by two-way ANOVA, significance quantified as P<0.05. * denotes P<0.05, ** denotes P<0.01, *** denotes P<0.001, **** denotes P<0.0001. * indicates significant difference between baseline and ± ischaemia, * indicates significant difference between baseline and ± flecainide, * indicates significant difference between ± ischaemia and ± flecainide.

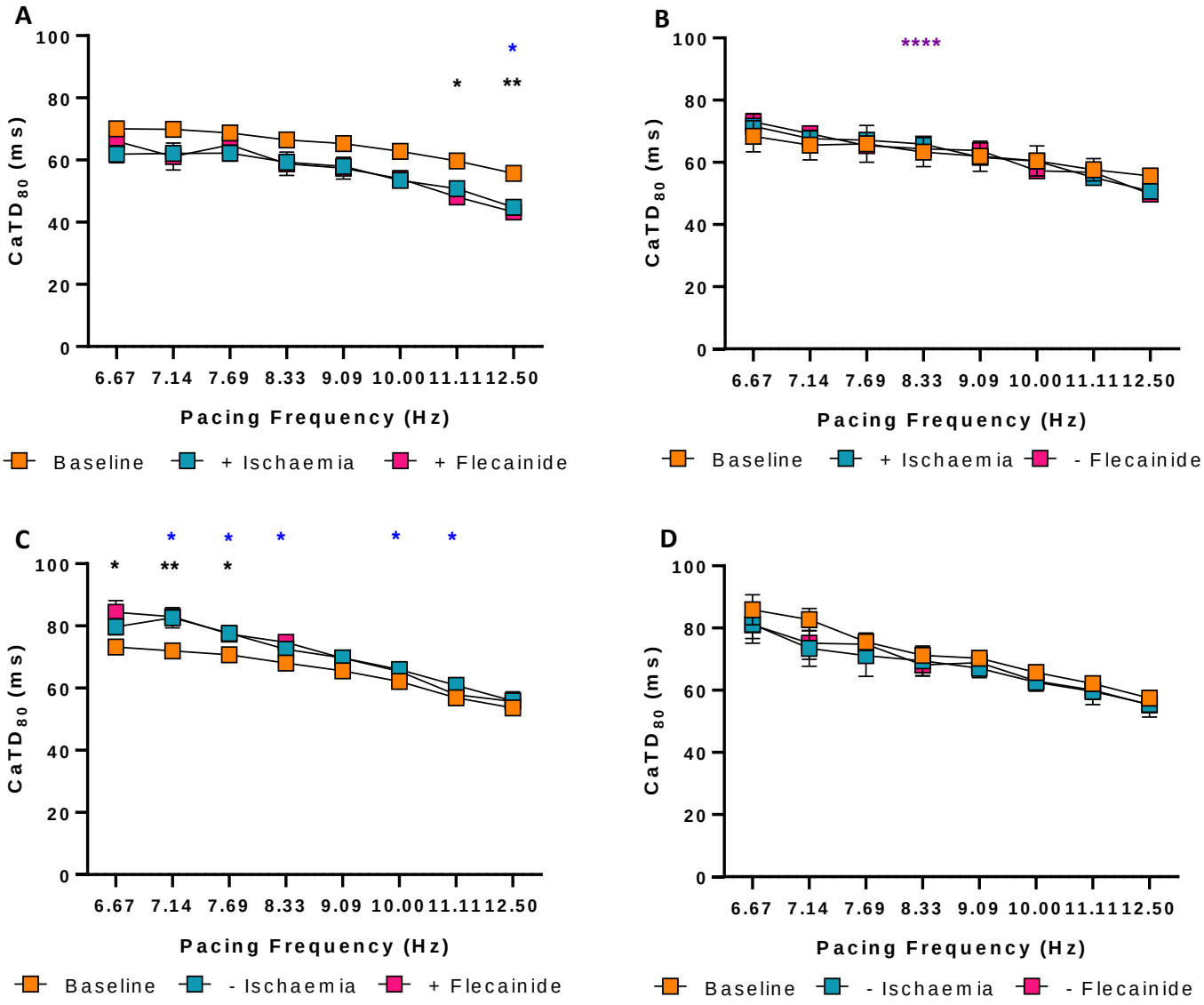

Figure 6.28A-D. Calcium transients from ischaemic region of mouse hearts in presence and absence of ischaemia and flecainide. CaTD taken from ischaemic region of ventricles at different pacing frequencies. Each panel represents 4 treatment groups. A. Group +ischaemia and +flecainide. B. Group +ischaemia and –flecainide. C. Group –ischaemia and +flecainide. D. Group –ischaemia and –flecainide. Statistical significance determined by two-way ANOVA, significance quantified as P<0.05. * denotes P<0.05, ** denotes P<0.01, *** denotes P<0.001, **** denotes P<0.0001. * indicates significant difference between baseline and ± ischaemia, * indicates significant difference between baseline and ± flecainide, * indicates significant difference between ± ischaemia and ± flecainide.

Along with the CaTD80, we also measured time to peak, i.e. the time it takes for intracellular calcium ions to reach the maximum level, following a stimulus. In the overall time to peak, ischaemia caused a slowing of time to peak at most pacing frequencies in Figure 6.18A, however did not show a significant effect in Figure 6.18B. Addition of flecainide did not affect the time to peak, Figure 6.18B to 6.18D.

In the remote region of the ventricles, away from the ligated area, the effect of ischaemia is only observed in one group at 9.09 Hz only, Figure 6.19A. Flecainide showed a significant slowing in time to peak only at 11.1 Hz in Figure 6.19A and at 6.67 Hz in Figure 6.19C.

In the ischaemic region, we see a more exaggerated effect of ischaemia and flecainide compared to the remote region. In Figure 6.20, ischaemia and flecainide significantly slowed time to peak at most pacing frequencies. We see a difference in –ischaemia timepoint and flecainide at 7.69 Hz only, Figure 6.20C.

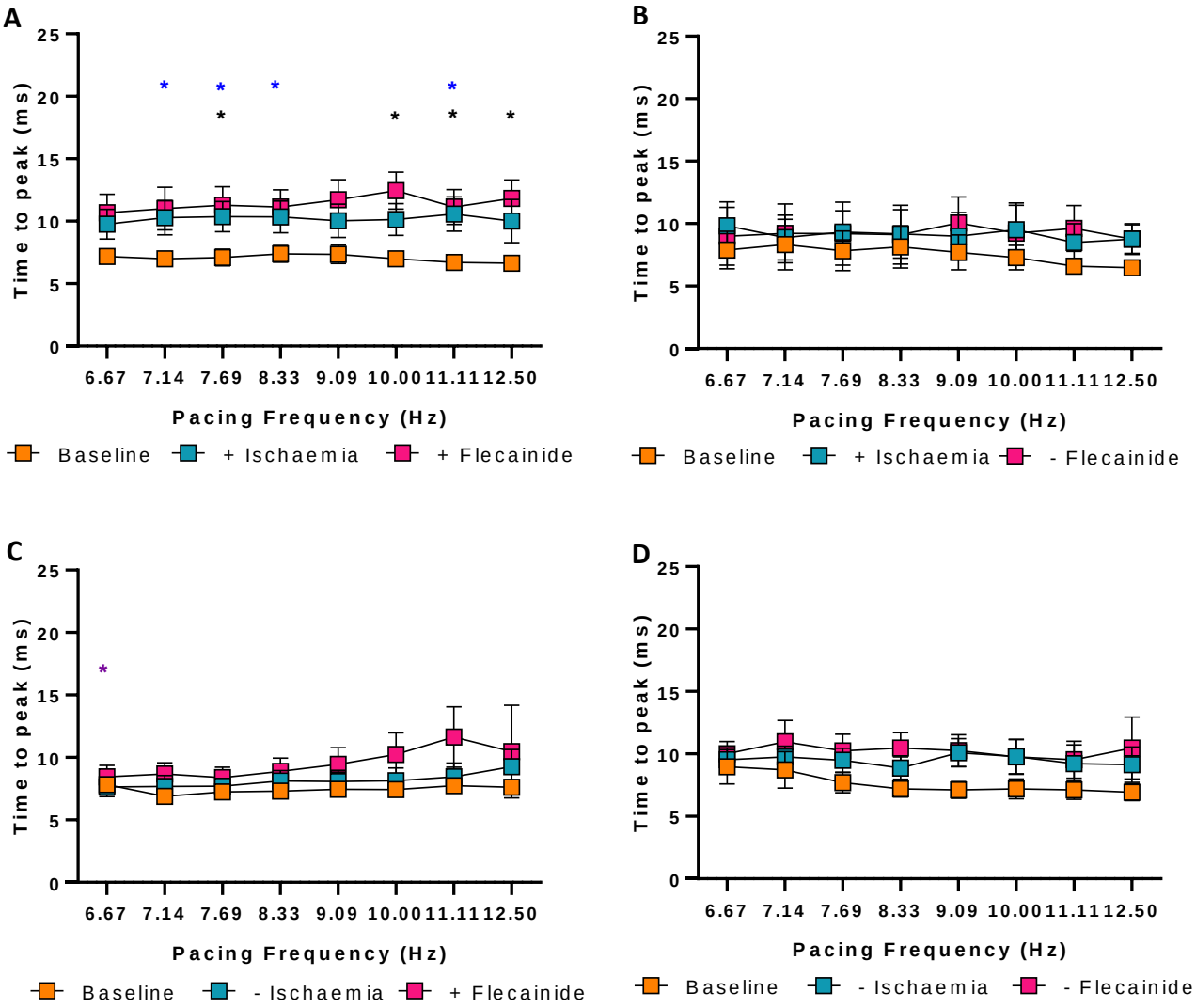

Figure 6.29A-D. Overall time to peak of calcium transients of mouse hearts in presence and absence of ischaemia and flecainide. CaT time to peak taken from whole region of ventricles at different pacing frequencies. Each panel represents 4 treatment groups. A. Group +ischaemia and +flecainide. B. Group +ischaemia and –flecainide. C. Group –ischaemia and +flecainide. D. Group –ischaemia and –flecainide. Statistical significance determined by two-way ANOVA, significance quantified as P<0.05. * denotes P<0.05, ** denotes P<0.01, *** denotes P<0.001, **** denotes P<0.0001. * indicates significant difference between baseline and ± ischaemia, * indicates significant difference between baseline and ± flecainide, * indicates significant difference between ± ischaemia and ± flecainide.

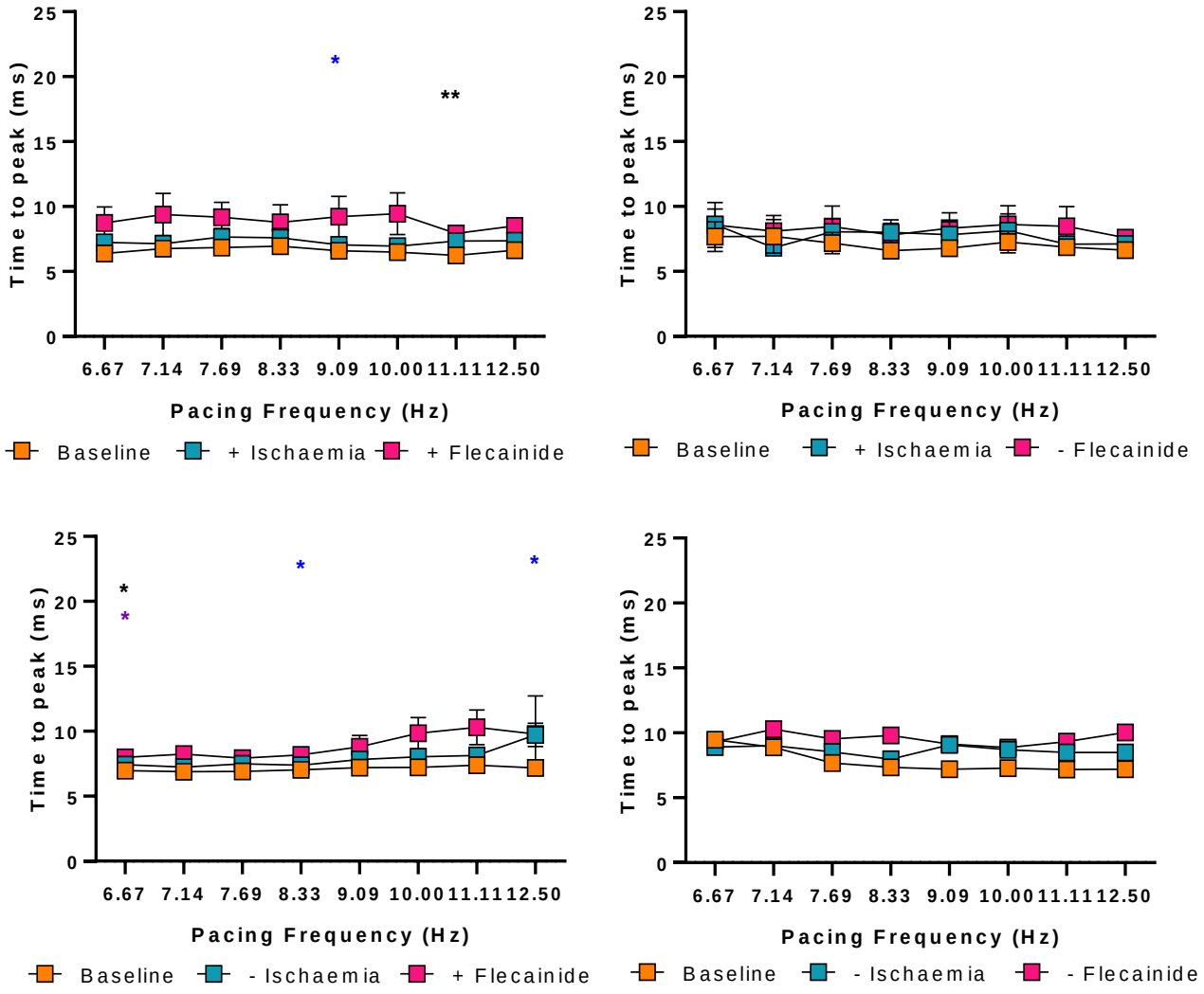

Figure 6.30A-D. Time to peak of calcium transients from remote region of mouse hearts in presence and absence of ischaemia and flecainide. CaT time to peak taken from remote region of ventricles at different pacing frequencies. Each panel represents 4 treatment groups. A. Group +ischaemia and +flecainide. B. Group +ischaemia and –flecainide. C. Group –ischaemia and +flecainide. D. Group –ischaemia and –flecainide. Statistical significance determined by two-way ANOVA, significance quantified as P<0.05. * denotes P<0.05, ** denotes P<0.01, *** denotes P<0.001, **** denotes P<0.0001. * indicates significant difference between baseline and ± ischaemia, * indicates significant difference between baseline and ± flecainide, * indicates significant difference between ± ischaemia and ± flecainide.

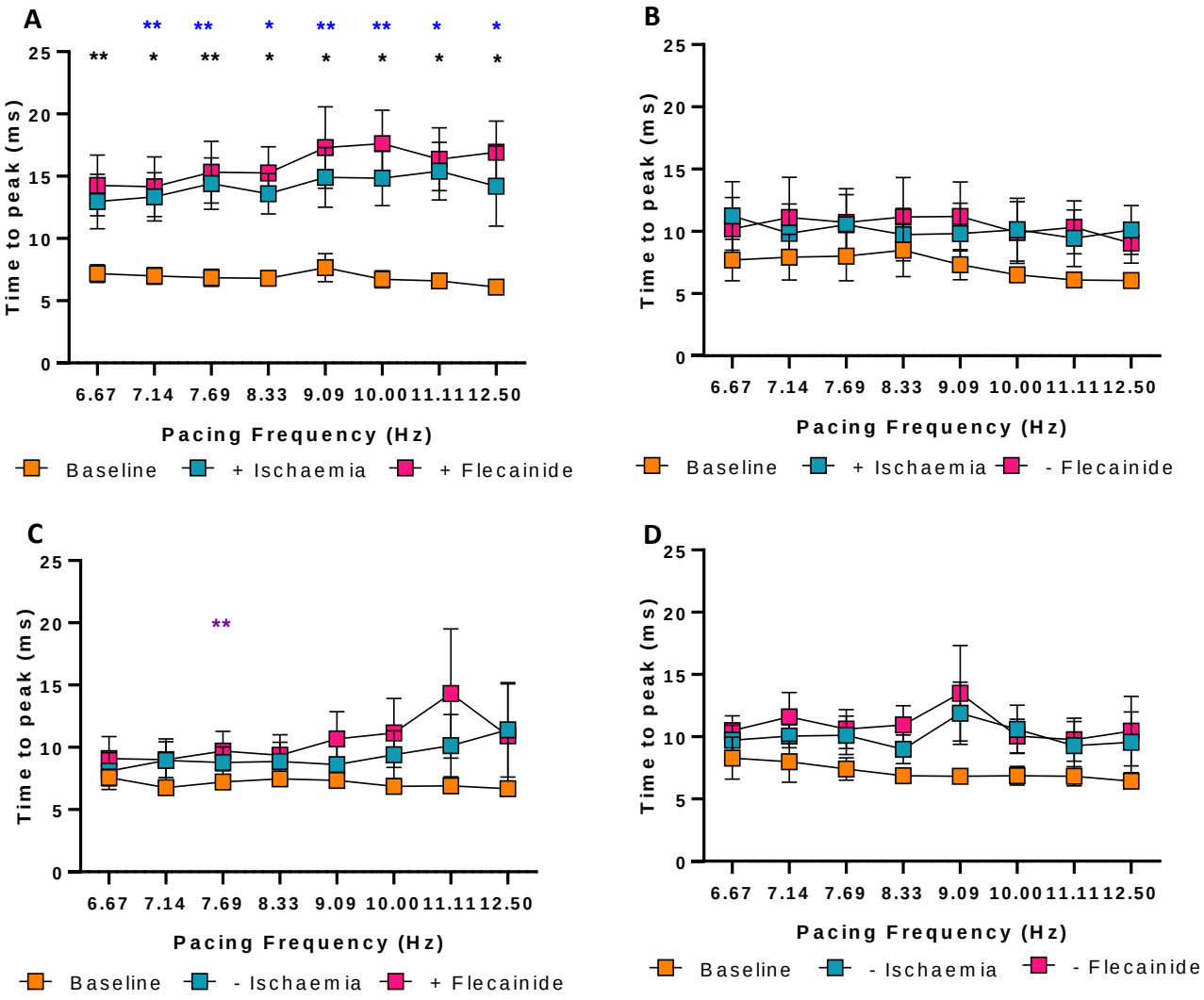

Figure 6.31A-D. Time to peak of calcium transients from ischaemic region of mouse hearts in presence and absence of ischaemia and flecainide. CaT time to peak taken from ischaemic region of ventricles at different pacing frequencies. Each panel represents 4 treatment groups. A. Group +ischaemia and +flecainide. B. Group +ischaemia and –flecainide. C. Group –ischaemia and +flecainide. D. Group –ischaemia and –flecainide. Statistical significance determined by two-way ANOVA, significance quantified as P<0.05. * denotes P<0.05, ** denotes P<0.01, *** denotes P<0.001, **** denotes P<0.0001. * indicates significant difference between baseline and ± ischaemia, * indicates significant difference between baseline and ± flecainide, * indicates significant difference between ± ischaemia and ± flecainide.

6.2.4. Arrhythmia analyses

ECGs were recorded through the duration of each experiment, enabling quantification of arrhythmic events. Arrhythmias were grouped and the incidence reported in each treatment group in Table 6.1. Four types of arrhythmias were identified, premature ventricular contractions (PVCs), couplets and triplets, atrioventricular block (AVB), and ventricular fibrillation (VF). AVB was consistently observed in all groups, especially at baseline and ischaemia timepoint, although the number of AVBs were observed in fewer non-ligated hearts. VF was observed in 1 heart at baseline, in group +ischaemia and +flecainide. At ischaemia timepoint, VF was observed in 1 heart in group +ischaemia and +flecainide, and in 2 hearts in group +ischaemia and -flecainide. However, VF developed in group -ischaemia and -flecainide, in 4 hearts, and in +ischaemia and +/- flecainide after flecainide timepoint. We also observe more PVCs after flecainide timepoint, with 4 hearts exhibiting PVC. At baseline, 2 hearts exhibited PVCs, and after ischaemia timepoint, 1 heart exhibited PVC. More couplets were observed after flecainide timepoint compared to at baseline and ischaemia timepoint. The number of mice with no arrhythmias observed were highest at flecainide timepoint. At flecainide timepoint, 7 hearts exhibited no arrhythmias, compared to 1 heart at ischaemia timepoint and 1 heart at baseline. The length of VF was also measured, and the VF was usually sustained between 5 ms and 50 ms. Further analyses distinguished between VF that was sustained for less than 10 ms, and more than 10 ms, Table 6.2. In groups with ischaemia, there were more incidences of VF sustained more than 10 ms.

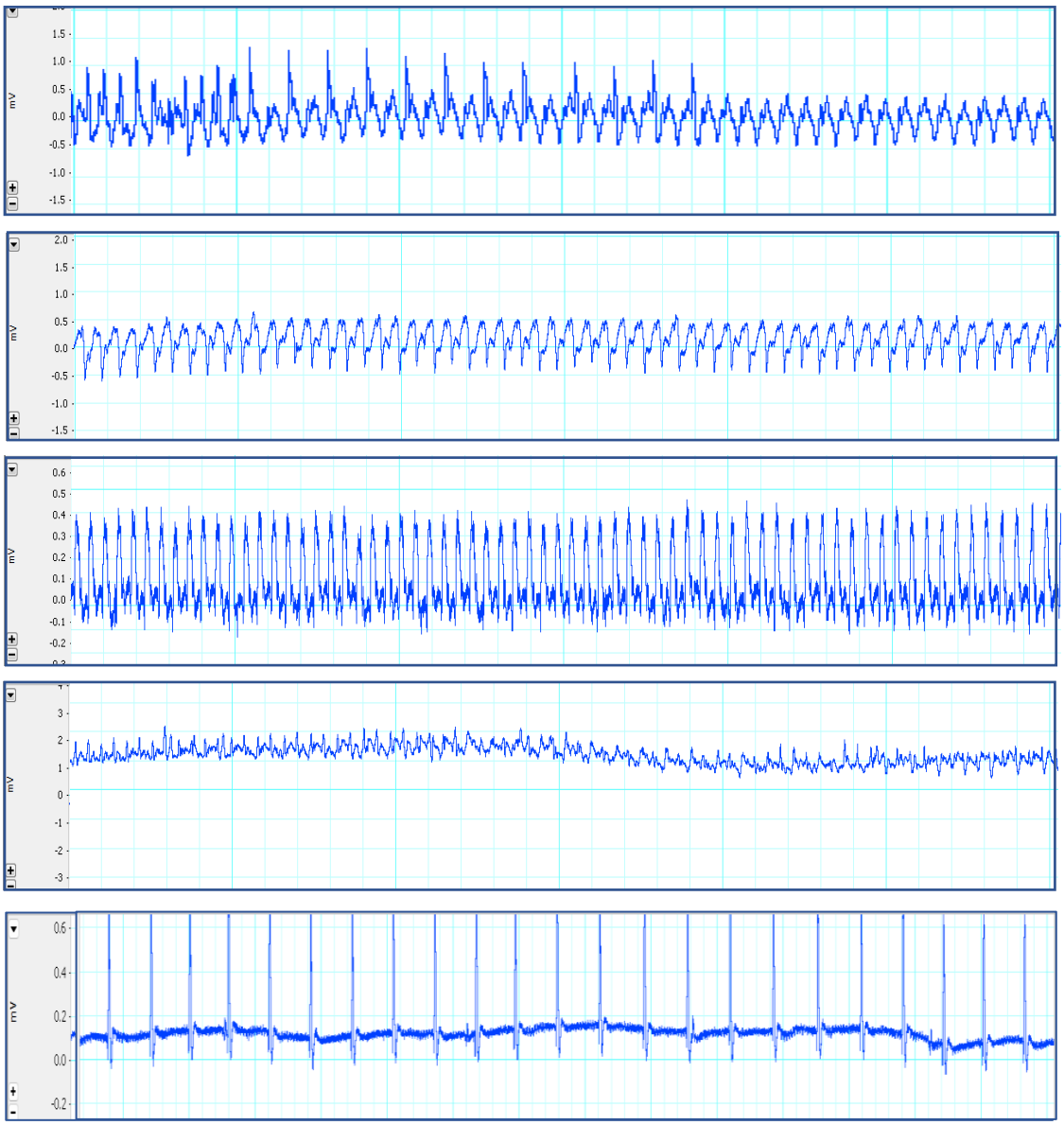

Figure 6.32. ECG observed in hearts. Recordings taken from ECG from 5 different hearts showing VF in the first four panels and 1 heart showing a normal sinus rhythm, in the fifth panel.

Baseline						
Group	Irregular HR	PVC	Couplets/ Triplets	AVB	VF	No arrhythmia
+ ischaemia/+ flecainide		I	I	III	I	
+ ischaemia/- flecainide	I			IIII		
- ischaemia/+ flecainide				III		II
- ischaemia/- flecainide		I	I	II		I
+/- Ischaemia						
Group	Irregular HR	PVC	Couplets/ Triplets	AVB	VF	No arrhythmia
+ ischaemia/+ flecainide				IIIIIIII	I	
+ ischaemia/- flecainide		I	I	IIIIIII	II	
- ischaemia/+ flecainide				IIIII		II
- ischaemia/- flecainide	I			II		I
+/- Flecainide						
Group	Irregular HR	PVC	Couplets/ Triplets	AVB	VF	No arrhythmia
+ ischaemia/+ flecainide		II	II	IIII	IIII	II
+ ischaemia/- flecainide			II	I	IIIII	I
- ischaemia/+ flecainide	I	II		I		III
- ischaemia/- flecainide			II	I	IIII	III

Table 6.1. Arrhythmias according to treatment group at different timepoints. Irregular heart rate, PVCs, couplets and triplets, AVBs, VFs and no arrhythmias reported in hearts at baseline, ischaemia timepoint and flecainide timepoint within all treatment groups, +ischaemia/+flecainide, +ischaemia/-flecainide, -ischaemia/+flecainide, and -ischaemia/-flecainide.

	Baseline		Ischaemia		Flecainide	
Group	<10 ms	>10 ms	<10 ms	>10 ms	<10 ms	>10 ms
+ischaemia/+flecainide		1		3		4
+ischaemia/-flecainide				2	3	1
-ischaemia/+flecainide						
-ischaemia/-flecainide				1	1	1

Table 6.2. Incidence of VF according to treatment groups at different timepoints. VF was separated into 2 groups, VF which lasted less than 10 ms, and VF which lasted more than 10 ms.

6.2.5. Confirmation of LAD block via ligation

At the end of each experiment, Evans blue, an azo dye, was perfused into the heart via a cannula, directly into the aorta. This was to determine that the LAD ligation had been successful. The lack of Evans blue in the ischaemic tissue mainly localised in the left ventricle demonstrates the infarcted region, Figure 6.21A to E. In control hearts, where a needle was inserted but LAD was not ligated, we see the Evans blue flow through the whole heart, Figure 6.21F.

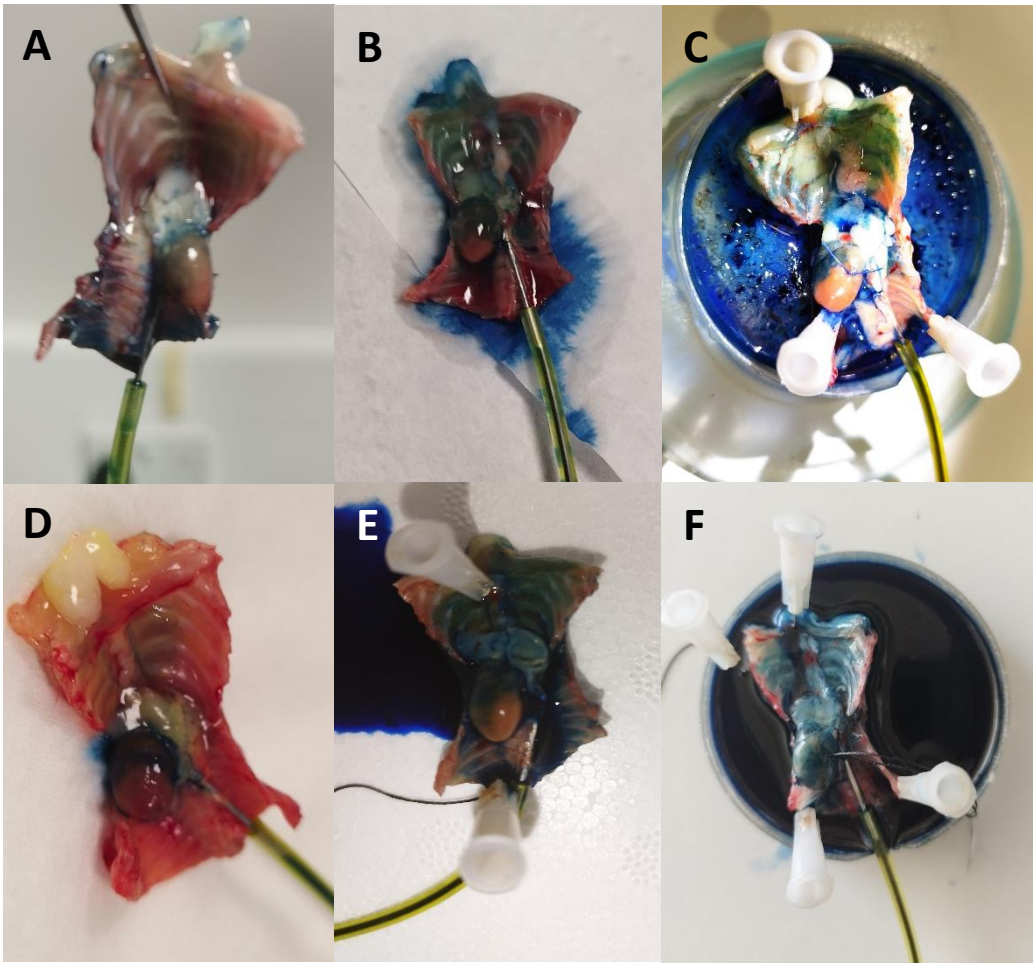

Figure 6.33. Evans blue perfusion. The Evans blue reveals infarcted region and non-infarcted region in the heart. A-E. Evans blue is unable to perfuse through the ligation to the infarcted area. E. Evans blue perfuses through whole hearts with no ligation.

6.3. Chapter Discussion

6.3.1. Overview of main findings

The main findings from this chapter are summarised as follows:

- Ischaemia caused a slowing of conduction velocity which was more pronounced in the ischaemic region compared to remote region.
- Ischaemia did not have a significant impact on action potential duration.
- Flecainide caused a slowing of conduction velocity, with or without ischaemia, in both ischaemic and remote regions.
- Presence of both ischaemia and flecainide caused a further slowing of conduction velocity compared to ischaemia alone.

6.3.2. Ischaemia causes little to no effect on APD

Interaction of ischaemia and flecainide was assessed by measuring its effects on conduction velocity (CV) and action potential durations (APD), in the presence and absence of one another. We previously looked at interaction of ischaemia and flecainide in a global ischaemia model, (Chapter 5), achieving global ischaemia via low perfusion pressure. Here, we performed a LAD ligation in WT mouse hearts to achieve local ischaemia. The control hearts functioned as sham controls: the needle with suture was inserted around the left anterior descending artery but the suture was not ligated. In the ischaemia groups, LAD was ligated.

APD measurements were taken at 30, 50 and 80% repolarisation. Analysis of APDs generally did not reveal effects of ischaemia and flecainide. The comparison of APD changes due to ischaemia did not correlate with data in literature. As shown in Figures 6.2, 6.3, 6.5, 6.6. 6.8 and 6.9, ischaemia either caused no change in APD or prolonged APD. The effect of ischaemia was more visible in the ischaemic region compared to the remote region, especially at earlier repolarisation stages. More significant differences were observed between baseline and ischaemia across different pacing frequencies in the ischaemic region compared to remote region. Shaw and Rudy demonstrated a shortening of APD caused by ischaemia, opposed to a prolongation which was observed in our studies. The ischaemia shortening of APD occurs through a combination of increased outward K^+ currents and decreased inward Ca^{2+} currents during repolarisation. Shaw and Rudy measured electrophysiologic effects of acute ischaemia which was reproduced by elevated $[K]_o$, acidic changes of fast Na^+ and L-type calcium currents, acidic reduction of [K]i, anoxia induced activation of a time independent outward current (IK(ATP)), and anoxic reduction of ICa(L), the major components of acute ischaemia. They conclude that $I_{K(ATP)}$ was the main cause of ischaemic APD shortening. It is generally thought that the cardiac ATP-sensitive K^+ current ($I_{K(ATP)}$) is the major contributor to action potential shortening during acute ischaemia, however, many studies have shown APD shortening during acute ischaemia occurs without involvement of IK(ATP) [198].

As demonstrated in literature, there is strong evidence for APD shortening during ischaemia. However, we observe the same phenomenon of APD prolongation with global ischaemia as well as local ischaemia. Bernikova *et al* aimed to investigate prolonged repolarisation in the early phase of ischaemia. Using a porcine model, they observed

transient repolarisation prolongation and subsequent shortening in the initial stages of ischaemia, lasting a few minutes. They were able to reproduce this effect in isolated cardiomyocytes through the activation of IK(ATP) current. We discussed previously the prolongation of APD during ischaemia lasting several minutes before shortening observed by Bernikiva *et al* 2023 [199]. The prolongation of APD we observed lasted more than several minutes and was observed even 40 minutes after ischaemia had been induced. A recent study published in 2021 investigated the role of unfolded protein response (UPR) in arrhythmia risk following myocardial infarction. They conclude that activation of UPR leads to a downregulation of cardiac ion currents including I_{to}, I_{K1} and I_{Ks} resulting in APD prolongation [200].

It is possible the puncturing of the heart with a suture needle could be damaging the surrounding tissue and affecting the APD, however, this effect is not always observed in all groups with ischaemia, therefore unlikely to be the cause of APD prolongation. In experiments where ischaemia was not present, APD did increase slightly, suggesting that the ligation is making the heart more prone to time dependent alterations. Our previous work has shown time dependent changes are minimal and remain insignificant [108].

APD triangulation is defined as the repolarisation time from APD30 to APD80 or APD90 [201]. Triangulation of APD refers to prolongation of action potential repolarization, specifically phase 2 or phase 3, or both, and is considered a risk factor for ventricular arrhythmias [202]. APD triangulation can be affected by dysfunction of ion channels involved in repolarisation and anti-arrhythmic drugs (AADs). Prolongation of APD is usually considered anti-arrhythmic and is the primary mechanism for Class II AADs. However, when

APD prolongation is associated with APD triangulation, it is often followed by proarrhythmia [201]. APD prolongation occurs through lengthening of phase 2, phase 3 or both phases. The current contributing towards phase 2 and phase 3 of the action potential are considerably different. During phase 2, inward currents flow through the slow inactivating Na^+ and L-type Ca^{2+} channels and outward currents flow through K^+ channels. During phase 3, the open inward channels and I_{Ks} close and I_{Kr} and I_{K1} channels open. Action potential triangulation is important in predicting proarrhythmia [201].

We measured AP triangulation in remote region and ligated region of the heart. With increased pacing frequency, triangulation became shorter, i.e. the APD80/APD30 ratio became smaller. This is to be expected since APD80 shortens when paced at faster frequencies to accommodate enough time for diastole. This shortening of APD 80 decreases the APD80 to APD30 ratio, hence shortening of the AP triangulation. In our study, ischaemia did not alter the AP triangulation in the remote region. In the ligated region, ischaemia caused a significantly less pronounced AP triangulation, at faster frequencies.

In order to distinguish significant effects of flecainide, we measured effects of flecainide in presence and absence of ischaemia. We did not consistently observe a significant difference of flecainide in the presence of ischaemia. Previous studies have shown 10 μM flecainide significantly prolongs APD50 in isolated neural cells [203]. Ikeda *et al* 1985 demonstrated APD50 was prolonged in isolated canine and rabbit myocardial fibres after flecainide treatment. With increasing flecainide concentration, APD50 became more prolonged [157]. Our previous study showed that flecainide did not affect the APD in the ventricles, however it did prolong the APD in the atria [108]. We concluded from that study that flecainide

affected the atria to a larger degree compared to the ventricles and this is further discussed in Chapter 2. In group 1, with both ischaemia and flecainide present, we see a bigger difference in APD30 compared to APD50 and APD80. Differences between baseline and ischaemia, baseline and flecainide, ischaemia and flecainide are more apparent at APD30. It is important to note that we see a further prolongation of APD30 and APD50 between ischaemia and flecainide, but we do not see an effect of flecainide on its own without ischaemia present. It is possible that the ischaemic condition of the heart is making it more prone to the effects of flecainide, i.e. APD prolongation. It is also important to note that we are seeing bigger differences in the earlier repolarisation stage as opposed to later repolarisation stage. It will be useful to measure beat to beat instability, as instability of APD along with triangulation can be an indicator of proarrhythmia whereas APD prolongation in the absence of APD instability and triangulation can be anti-arrhythmic [201]. This will give a better understanding on whether the action of flecainide with ischaemia present it either pro-arrhythmic or anti-arrhythmic.

6.3.3. Flecainide effects on conduction velocity in ischaemic conditions

Similarly to the global ischaemia data, we observe a stronger effect of ischaemia and flecainide reflected in CV measurements, compared to APD measurements. In both, remote and ligated regions, we observe an effect of CV slowing in the presence of ischaemia. In the ligated region, ischaemia significantly slows the CV at most pacing frequencies, whereas in the remote region, it slows CV at faster pacing frequencies only. In the ligated region, ischaemia caused a further slowing of CV compared to remote region. As expected, the

difference between ischaemia and flecainide is more pronounced in the remote region compared to ligated region. In the remote region, CV was significantly slower after flecainide treatment in the presence of ischaemia at most pacing frequencies but in the ligated region, it was only significant at 6.67 Hz and 9.09 Hz. In the presence of ischaemia, flecainide further slowed the CV significantly after the initial CV slowing caused by ischaemia. In the absence of ischaemia, flecainide still slowed the CV significantly, but to a lesser extent. The average percentage difference between baseline and flecainide in the presence of ischaemia was 53%. The average percentage difference between baseline and flecainide in the absence of ischaemia was 51%, indicating that ischaemia did not affect flecainide activity on the conduction. We know that flecainide is more effective at more positive resting membrane potential, and we also know that ischaemia causes the resting membrane potential to become more positive. It will be useful to investigate if the flecainide is more effective in ischaemic ventricles due to the RMP. To be able to study this further, ischaemic conditions can be duplicated for cardiomyocytes and test whether ischaemic ventricular cells exhibit similar traits to healthy atrial cells that allow flecainide preference.

6.3.4. Calcium transient duration decreases with ischaemia

Calcium transients were measured simultaneously to membrane voltage measurements. Hearts were loaded with Rhod-2 AM, a high affinity calcium indicator which fluoresces in the presence of calcium. Ischaemia causes an increase in intracellular calcium in cardiomyocytes, known as calcium overload. This can lead to significant changes in calcium

transients in cells. An increase in intracellular calcium is usually observed within minutes of ischaemia. Clusin 2008 found after rabbit hearts were rendered with ischaemia, calcium transient alternans occurred, where taller calcium transient with longer calcium transient duration (CaTD) is preceded by a shorter one and accompanied by a longer APD [204].

From our studies, we observe more differences in CaTD in the ischaemic region compared to remote region. Since ischaemia is marked by increased intracellular calcium, and remains elevated for an extended period, this prolongs the CaTD. We see that ischaemia prolongs CaTD only in remote region, Figure 6.16B. Figure 6.17A shows the opposite of what we expect and observe a shortening of CaTD in ischaemia.

Although flecainide is primarily a sodium channel blocker, it can have some effects on calcium transients. Flecainide has been shown to block RyR2, reducing calcium release from the sarcoplasmic reticulum [177]. Flecainide also affects intracellular calcium indirectly by inhibiting Na^+ channels which causes reducing of intracellular calcium [156]. In the remote region, we observe a significant difference between baseline and flecainide, Figure 6.16A, but not between ischaemia and flecainide, indicating the difference is down to ischaemia, and not flecainide.

The time to peak refers to the rise of intracellular calcium. The increase in intracellular calcium once ischaemia is established would lead to a faster time to peak. Demeter—Haludka 2019 showed in adult dogs the slowing of time to peak calcium transients after ischaemia compared to non ischaemia at baseline [205]. This contradicts our data, whereby the time to peak is significantly longer after ischaemia.

It is thought that impaired calcium regulation is the cause of ventricular fibrillation (VF) which is often observed in ischaemia. It is possible that the reason we do not observe a significant increase in VF is because the calcium transient is not significantly affected by ischaemia. However, although calcium transients were measured in all hearts, a lot of the data was omitted and the final n numbers totalled to 3 for each group.

6.3.5. Arrhythmia analysis

From our study, we identify four types of arrhythmias, premature ventricular contractions (PVC), couplets and triplets, atrioventricular block (AVB), and ventricular fibrillation (VF). Majority of the hearts exhibited AVBs which were triggered during baseline and remained during ischaemic timepoint. This suggests that AVB may be a manifestation of damage to the tissue caused by needle insertion. It may be that with that level of trauma, heart requires a longer period of time to recover than the standard 10 minutes we have used throughout the study. Gao *et al* 2010, developed a model of coronary artery ligation in mice and observed no difference in the frequency of AVB between sham controls and treated groups, in the first 30 minutes after surgery [206]. This correlates with our data, where we observe more AVBs in the first 30 minutes. Having a fifth group which served as a no treatment control group would have helped understand the trigger for AVBs. It may have been useful to collect tissues from the damaged area to measure for ischaemic or inflammatory markers. Comparing the levels of a common inflammatory marker such as interleukin-6 (IL-6) from no treatment

control, sham control tissue and tissue from ligated heart would have given us an indication of the level of ischaemia in the sham controls.

The observations of more PVCs and couplets after flecainide treatment may indicate flecainide's potential proarrhythmic effects. This is interesting because flecainide is thought to reduce PVCs. Studies have shown in patients with chronic ventricular arrhythmias, flecainide was able to reduce PVCs by more than 85% after a one-year period [207].

The number of hearts exhibiting VFs was highest at the ± flecainide time point, towards the end of the protocol. However, the number of hearts without arrhythmias was also the highest at the ± flecainide time point. This could be an effect of time. At this point, the hearts would be in ischaemia the longest. These results also indicate that VF sustained for more than 10 ms was more common in groups with ischaemia. Given that longer durations of VF are generally more life-threatening, this observation adds another layer of risk when considering flecainide therapy in the presence of ischaemia.

Overall, to do a thorough arrhythmia analysis and investigate the proarrhythmic effects of flecainide in the presence of ischaemia, more n numbers are required. Our n numbers varied between 5 and 8. Many arrhythmia studies have used an n number ranging between 29 and 70 [208] [209]. Increasing our n numbers would provide a more robust set of data.

7. Discussion

7.1. Overall findings of this thesis

The overall aim of this thesis was to characterise and unravel the electrophysiological differences between atria and ventricles and their response to flecainide in health and disease. Optical mapping was used to assess differences in action potential waveform and conduction in both the atria and ventricles and assess ischaemia and flecainide interaction in the ventricles. Additionally, this technique also enabled us to assess electrophysiological heterogeneity in ventricles and the chamber specific effects of the anti-arrhythmic drug, flecainide.

The main outcomes of this thesis are summarised below:

- **Conduction velocity is slower in the mouse LA than in mouse LV.** This is driven by alterations in sodium channel biophysical properties. Although the number of $Na_v1.5$ channels are greater in the atria compared to ventricles, atria display a greater negative shift in the voltage dependence of sodium channel inactivation [108]. The differential expression of $Na_v\beta2$ and $Na_v\beta4$ in atria and ventricles can cause differences in modulation of gating kinetics of I_{Na}.

- **Atria responded to flecainide to a larger degree than ventricles.** Flecainide demonstrated significant action potential duration (APD) prolongation and conduction velocity (CV) slowing compared to ventricles. This is due to

differences in channel gating kinetics and differences in resting membrane potential (RMP) between atria and ventricles. Atria have been shown to have a more positive RMP compared to ventricles and our previous study has shown a shift in RMP modifies the efficacy of flecainide [148] [108].

- **In the presence of ischaemia, flecainide was able to slow the CV to a greater degree in ventricles.** Ischaemia alone also slowed the CV but the combination of ischaemia and flecainide being present shower a larger percentage decrease in CV highlighting potential proarrhythmic effects of flecainide.

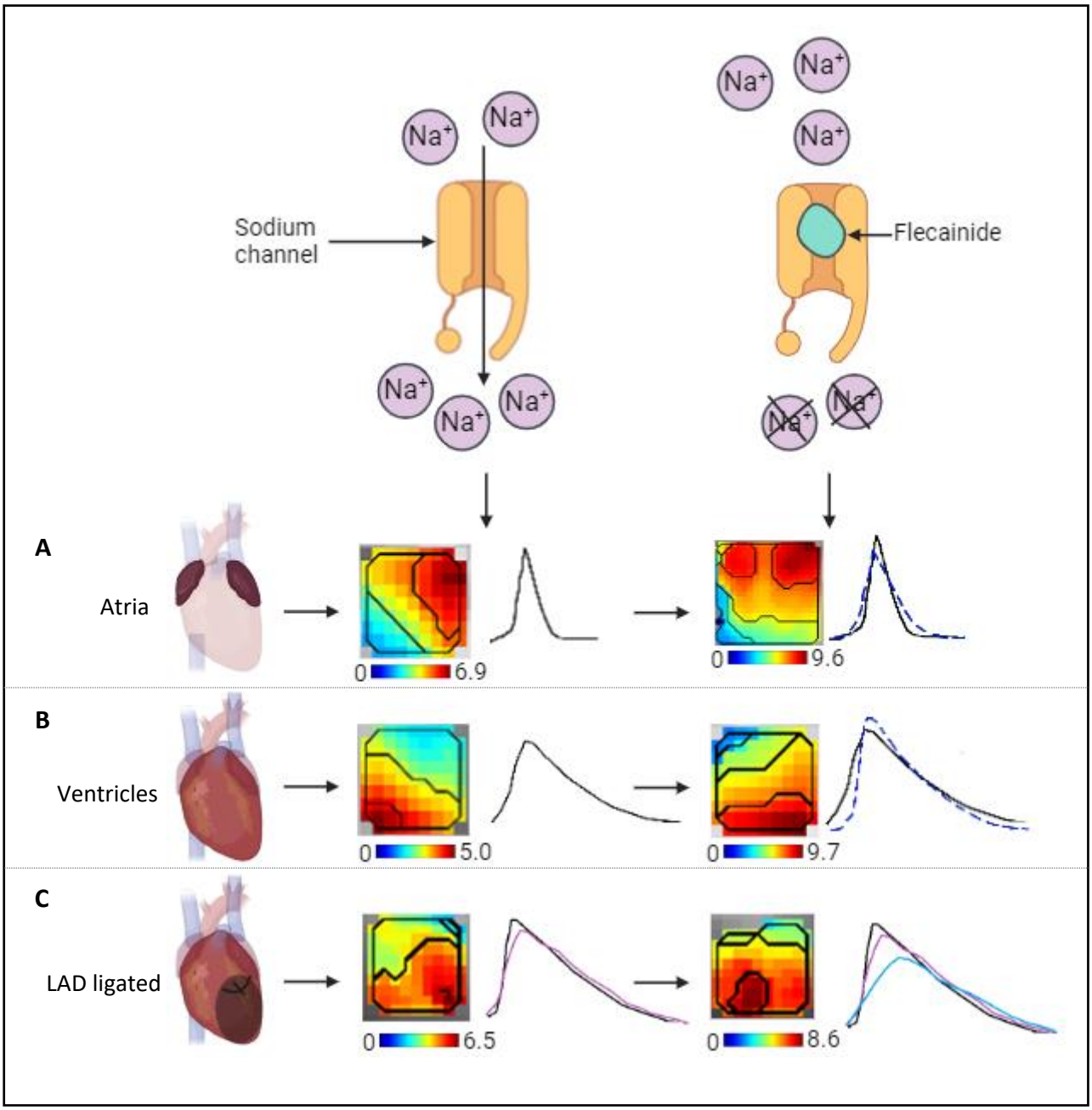

Figure 7.1 Summary of key findings from the study. A. Representative activation map and APD in atria (left) before and after flecainide at 10 Hz. B. Representative activation map and APD in ventricles before and after flecainide, at 10 Hz. C. Representative activation map and APD with ischaemia and after flecainide, at 10 Hz.

7.2. Distinct electrical properties of atria and ventricles

The first key finding of this thesis was the difference in conduction in the atria and ventricles. Based on previous findings, we hypothesised the conduction would be different in the left atria (LA) and the left ventricles (LV) due to differences in Na^+ channel protein expression and differences in Na^+ current density. Protein expression of $Na_v1.5$ was assessed in wildtype (WT) mouse atria and ventricles using western blot which showed that atria had greater $Na_v1.5$ protein expression compared to ventricles. $Na_v\beta2$ and $Na_v\beta4$ were also measured using western blotting. This data showed that both $Na_v\beta2$ and $Na_v\beta4$ were expressed at higher levels in the ventricles compared to the atria. The current density measured by patch clamp also revealed a smaller Na^+ current density in LA compared to LV at physiological resting membrane potential. The data was confirmed with conduction velocity (CV) measurements which showed CV was significantly slower in the LA compared to LV.

The conduction and ionic differences within the atria and ventricles lend itself as a potential target for atrial specific disorders such as atrial fibrillation (AF). Developing a drug that specifically targets the difference in atria and ventricles would minimise adverse effects. Our study provides further understanding of atrial and ventricular electrophysiological distinctions and may explain why atria are more prone to arrhythmias compared to ventricles. We already know the physical differences between atria and ventricles. Atria are thin walled, whereas the ventricles are much larger and are thick walled. Ion channel distribution is also different in atria and ventricles. I_{Kur}, I_{KACh} $K_{ir}3.1/K_{ir}3.4$ are predominantly found in the atria but not the ventricles. These

differences in ion channels are thought to be crucial in spiral wave re-entry and episodes of AF and ventricular fibrillation (VF) [22]. They are also the cause of differences in action potential waveform, with the atrial action potential displaying a shorter action potential compared to ventricular action potential. Atria are also more susceptible to fibrosis which can disrupt the normal electrical signals in the heart, leading to irregular impulses and arrhythmias [210]. As mentioned, the LA were shown to have slower CV compared to LV. Slower CV increases the likelihood of developing arrhythmia. When CV is slow, areas of tissue with conduction block or delay develops and creates re-entry circuits, perpetuating arrhythmia. Our previous study has also shown atria to present with a more positive resting membrane potential (RMP). A more positive RMP delays I_{Na} recovery, slows channel inactivation and decreases action potential upstroke velocity. These attributes also result in slowing of CV [148].

Along with slowed CV, we also observed a shorter action potential in atria compared to ventricle. A shortened action potential duration (APD) is often considered proarrhythmic. A shorter APD is usually closely associated with a shorter refractory period, meaning cells have a shorter time to recover after each action potential. This can increase the risk of re-entry circuits. As discussed in Chapter 3 discussion, the key difference causing action potential differences in atria and ventricles is attributed to potassium currents, specifically $I_{Kur,}$ I_{Kr} and I_{Ks} [154].

7.3. Importance of chamber specific anti-arrhythmic drugs

The differences observed between atria and ventricles highlight the need for chamber specific targets for anti-arrhythmic drugs. Distinguishing atrial and ventricular electrical properties is essential for effective treatment and deeper understanding of cardiac function and dysfunction. The I_{Kur} current has been known to be a strong potential target for anti-arrhythmic drugs (AAD). Vernakalant (RSD1235) is a new class III anti-arrhythmic drug developed to block I_{Kur} current. However, while IKur current block was observed in rat model and HEK293 cells, this has not been demonstrated in human atrial myocyctes [211]. Niferidil (RG-2) is also a new class III antiarrhythmic drug. Niferidil is also atrial specific and more than 85% effective at converting AF to normal sinus rhythm through I_{Kr} inhibition. However, some studies have shown off-target effects in the ventricles through inhibition of IKur and steady state current [212]. XEN-D0103 (S66913), is another novel, atrial specific inhibitor of I_{Kur}. Prolongation of action potential has been observed in atria only and no effect has been observed in ventricles. Clinical trials have shown that on its own, XEN-D0103 was ineffective at reducing AF burden and is effective in combination with other drugs. More research is required, and large sample sizes are needed to fully evaluate the effectiveness of these drugs.

Flecainide, a Na^+ channel blocker, is normally recommended as a first line therapy for AF patients without structural heart disease. Flecainide is not considered to be atrial specific as it does also affect ventricular action potential and QRS interval. The primary electrophysiological actions of flecainide are attributable to its greater effectiveness at inhibiting sodium channels in more depolarised cardiomyocyte, and use-dependent

block of voltage gated Na^+ channels [148]. Use dependence refers to increased flecainide effectiveness at faster heart/stimulation rates, making it effective at terminating atrial arrhythmias [91]. Flecainide has slow kinetics, meaning it is released slowly from its binding site, prolonging depolarisation and increasing refractoriness. We do not see a significant effect on ventricles under physiological conditions in our experiments. Flecainide did not significantly slow the CV in the ventricles and we saw no effects on APD. Consistent with these findings, the effect of flecainide was greater in LA compared to LV. Our previous data also showed atria had an increased sensitivity to flecainide compared to ventricles. LA and LV Na^+ currents measured using patch clamp with and without flecainide demonstrated a change in current-voltage curve morphology in both LA and LV. The addition of flecainide augmented the peak Na^+ current to a significantly greater degree in LA than in LV. This correlates with our data where CV is slowed in LA and LV after flecainide is introduced, but CV is slowed to a greater extent in the LA. It is apparent from these studies collectively, that although flecainide is not considered atrial specific, it has preferential affinity to atrial Na^+ channels. O'Brien *et al* 2021 further investigated the difference in biophysical properties of Na^+ channels in LA and LV which causes this preferential affinity of flecainide. The increased sensitivity of atrial Na^+ current density to flecainide is influenced by changes in the resting membrane potential (RMP) [148]. Atrial RMP has been found to have a more positive resting membrane potential than ventricular RMP. Atrial cardiomyocytes had an RMP of -70.8 mV, and ventricular cardiomyocytes had an RMP of -80 mV. The maximal upstroke velocity of the action potential was also higher in ventricular cells compared to atrial cells. These biophysical properties potentially affect the channels'

sensitivity to flecainide [108]. Our recent study investigated the anti-arrhythmic effects of several Na^+ channel blockers in atrial cells. The study found mice with reduced Pitx2c, a gene identified through genome wide association studies to be associated with increased AF burden [213] mRNA levels had a more depolarised resting membrane potential. The more positive resting membrane potential altered the effectiveness of Na^+ channel blockers, making it more effective at inhibiting Na^+ channels. Experiments in HEK cells also demonstrated that small changes in resting membrane potential altered Na^+ channel inhibition [214].

Consistent with our previous published findings, our shows a preferential effect of flecainide treatment on the atria compared to the ventricles.

7.4. Importance of understanding ischaemia and flecainide interaction

In clinical practice, ventricular pro-arrhythmia has been associated with Class Ic AADs such as flecainide. Clinical trials have reported proarrhythmic effects and increased mortality with the use of these drugs [215]. The Cardiac Arrhythmia Suppression Trial (CAST) was a clinical trial conducted in the late 1980s and was designed to assess whether suppressing ventricular arrhythmias with flecainide and encainide would reduce mortality. From the trial, it was concluded that flecainide and encainide caused a significantly higher mortality in patients after myocardial infarction, compared to patients who received placebo and patients receiving flecainide or encainide also had a higher incidence of ventricular arrhythmias compared to the placebo group. Due to the adverse outcomes of the antiarrhythmic drugs, the trial was terminated early and led to

a re-evaluation of the management of arrhythmias. Since the trial, flecainide and encainide are no longer recommended for patients with structural heart disease and is also avoided in patients with myocardial ischaemia or infarction or heart failure [91].

The Atrial Fibrillation Follow-up Investigation of Rhythm Management (AFFIRM) trial was conducted in 2002 and compared different treatment strategies for atrial fibrillation (AF). AFFIRM trial compared rate control and rhythm control strategies in patients with AF and high risk of stroke or death [216]. The aim was to determine whether a rhythm control strategy or a rate control strategy would be more effective in managing AF and reducing mortality rate in patients. Rate control strategy involved class II antiarrhythmic drugs such as beta-blockers, calcium channel blockers and digoxin. As the name suggests, the aim of rate control therapy is to control the heart rate and sustain it between 80 and 110 beats per minute. Rhythm control strategies include class Ia (quinidine, procainamide), class Ic (flecainide, propafenone) and class III agents (amiodarone, sotalol). The aim of rhythm control strategy is to maintain sinus rhythm in AF patients. The AFFIRM trial concluded there was no significance difference in mortality between rate control and rhythm control therapies. Both treatment approaches were equally effective in reducing mortality in patients with AF. The rate control strategy was associated with fewer adverse drug effects such as torsades de pointes, ventricular tachycardia and ischaemia stroke, compared to rhythm control strategy. Patients on rhythm control treatment strategy were significantly more likely to be hospitalised and experience adverse effects. Like in CAST, AADs were associated with increased mortality, indicating the beneficial effects of AADs are counteracted by their adverse effects.

The East-AFNET 4 trial demonstrated early rhythm control therapy, which included flecainide, amiodarone and dronedarone, led to fewer adverse effects in patients when compared to usual care, which included mainly rate control therapy. Patients diagnosed with AF within a year had significantly reduced morbidity when treated with early rhythm control. The trial ended early at the third interim analysis, due to efficacy [58].

Other clinical trials, such as Survival with Oral D-sotalol (SWORD) trial showed d-sotalol, a beta blocker, increased mortality after a myocardial infarction. Similarly, the Stroke Prevention in Atrial Fibrillation (SPAF) trial also showed increased mortality when patients with AF were prescribed with AADs [216].

The German Competence Network on Atrial Fibrillation, (AFNET), performed a randomised clinical trial investigating rhythm control therapy, rate control therapies and stroke prevention. They conclude anti arrhythmic drug treatment might be more beneficial in the early stages of AF, after cardioversion.

These trials reflect the need for further investigation into identifying new targets for anti-arrhythmic drugs with a good safety profile. Moreover, these studies evaluated the effects of AADs in patients with heart failure or AF with structural heart disease. Our study investigated the proarrhythmic effects of flecainide in ischaemic hearts without structural heart disease. Although the use of flecainide is moderately effective at suppressing AF and is considered safe and well tolerated in patients without structural heart disease, the decreased use of flecainide over time could be attributable to the CAST and its risk of ventricular proarrhythmia. It has been over 30 years since the results of CAST were published and the trial ended early due to increased risk of death and a

more up to date review is required. The East-AFNET 4 Trial is one of the more recent studies and has shown in contrast to the CAST, administering rhythm control therapy including flecainide did not cause pro-arrhythmia. Syeda *et al* 2016, showed that flecainide was able to abolish atrial arrhythmias in hearts with reduced Pitx2 expression. This was down to more depolarised resting membrane potential which increased the effectiveness of flecainide. Flecainide significantly eliminated atrial arrhythmias in hearts with reduced Pitx2 expression but was not able to eliminate arrhythmias in hearts with normal Pitx2 expression [214].

The goal of this study was to investigate the electrophysiological mechanism in which flecainide became pro-arrhythmic when ischaemia was present. Thus far, no study has provided a mechanism in which flecainide causes ventricular pro-arrhythmia. Brugada *et al* hypothesised that administering flecainide to patients post-myocardial infarction could alter the conduction, thereby promoting the onset of small reentrant circuits, leading to ventricular tachycardias and potentially sudden death [215]. From our results, we observed that CV was significantly affected by flecainide, especially in the presence of ischaemia. We observed that CV was slowed with ischaemia and flecainide caused a further slowing of the CV. This may indicate that flecainide exacerbates the effect of ischaemia in the ventricles. To understand the mechanism better, it may be useful to investigate whether flecainide has the same effect on the CV in the presence of ischaemia when the resting membrane potential is more depolarised. This would require performing experiments in isolated cells and recording electrophysiological parameters at different holding potentials within an ischaemic environment, such as a

hypoxic chamber. This would provide a better insight into how ischaemia and flecainide interact.

7.5. Study limitations

7.5.1. Optical mapping limitations

Cardiac optical mapping is a useful tool to characterise electrical activity and arrhythmias in mouse hearts. Optical mapping has many advantages to studying electrophysiology, but it comes with a few limitations. It requires the use of fluorescent dyes which helps users observe voltage membrane changes and calcium transients. Some fluorescent dyes have been shown to interact and alter electrical behaviour. There have been some studies highlighting the disadvantages to using fluorescent dyes. Di-4-ANEPPS has been shown to significantly alter basal heart rate and ventricular conduction in rabbit hearts [217]. The same study also showed ischaemic patterns to be less prominent and time delayed in hearts stained with Di-4-ANEPPS. In stained and non-stained hearts, ischaemia manifested as QRS prolongation, bradycardia and shortened QT interval. Prominent ischaemic hearts stained with Di-4-Anepps appeared 3 to 4 minutes after the non-stained hearts. In isolated guinea pig hearts, di-4-ANEPPS decreased both longitudinal and transverse CV in a dose dependent manner [218]. Other studies have also shown slowed CV and shortened APD. At higher concentrations, Di-4 ANEPPS internalises in the cells rapidly which can cause phototoxicity, hence it is often used in short term experiments [219].

Blebbistatin, a myosin inhibitor, is used to prevent motion artefacts whilst optically imaging hearts. Blebbistatin precipitates at 50 to 100 uM and the precipitated aggregates can attach to surfaces of microtubes and pipette tips thus slightly changing the intended concentration (Varkuti *et al* 2016). Another study showed blebbistatin has propensity to precipitate and accumulate in the vasculature [188]. Regardless, blebbistatin is still considered to be the electromechanical uncoupler of choice as it has minimal effects on cardiac electrophysiology compared to other excitation contraction uncouplers [220].

In an optical mapping system, electrodes are manually placed on the heart, allowing the user to pace the tissue. When pacing, the signal propagates across the epicardium through the tissue in an up or down manner. This does not represent physiological propagation of action potentials. In physiological conditions, signals are propagated in the myocardium and travels outwards, rather than up and down the tissue. It is likely that the measurement of CV in this manner shifts the CV values.

Finally, the interaction of tissue and light can alter signal morphology when recording signals optically in the heart tissue. Excited light will propagate into the tissue and excite fluorophores away from the epicardium. As a result, the recorded signals will be a total of optically recorded action potentials or calcium transients from the epicardium as well as cells from the myocardium [134].

7.5.2. Isolated heart method limitations

Performing experiments on isolated hearts usually come with some limitations. Surgical isolation of the heart is followed by a short period of asphyxia and ATP depletion, and it is important to ensure cardiac preparation is quick to minimise cardiac injury. Cardiac ATP levels decreases dramatically after 10 to 30 seconds of asphyxia [221]. Isolated contracting hearts usually have a higher demand for oxygen and metabolites and consequentially are at a higher risk of hypoxaemia. The use of blebbistatin lowers metabolic and oxygen demands and could result in ischaemia underestimation [220]. Isolated hearts are also retrograde perfused with Krebs-Henseleit buffer. In *in vivo*, blood is pumped out of the heart to the rest of the body via the aorta whereas in *ex vivo*, buffer is perfused into the heart in the opposite direction.

An alternative approach which removes these limitations listed above would be to apply mathematical and electromechanical modelling to simulate a cardiac system. Recent studies have been using this approach to study specific mechanisms, however this approach also comes with its own limitations.

7.5.3. Limitations of mouse models

Most studies using isolated heart models use mammalian hearts. Larger mammals are considered to be more physiologically similar to the human haemodynamic characteristics [222]. Larger hearts also enable better access and easier manipulation for surgeries. However larger animals are also expensive to breed and house. Moreover,

larger volumes of reagents and buffers are also required per experiment, thus making rodents a preferable alternative to larger mammals [221]. Rodents can be generated and bred with ease with a fast turnover and a variety of genetically modified strains are commercially available. There has been some controversy over the use of mice as animal models. Although there are genetic and physiological similarities between mice and humans, mouse models are not always able to mimic human disease phenotype. Mice do not develop AF naturally and usually require programmed electrical stimulation and genetic manipulation that can result in severe cardiac dysfunction and shortened lifespan [223]. There are also significant differences in size and electrophysiology of mouse hearts and human hearts. Resting heart rates and ion channel expressions differ massively between the two species and custom-made devices often need to be constructed specifically for mouse models [223]. There is generally a lack of suitable AF mouse model, possibly because of insufficient substrates for AF. It has been hypothesised that myocardial tissue is required to be of at least a certain size in order to sustain re-entrant arrhythmias. Re-entry has been demonstrated in mouse ventricles but has proved difficult to demonstrate in mouse atria. Mouse atrial tissue is thin and may not support transmural re-entry, a key driver in AF in humans (Fu *et al* 2022). This study investigated common mouse AF models and found that the models were unable to mimic AF phenotype seen in humans [224].

7.5. Future work

The nature of this study lends itself to multiple avenues for further investigation. In relation to atrial and ventricular differences, the CV differences we observe can be attributed to differences in Na^+ channel expression and density of gap junctions in atria and ventricles. It will be useful in quantifying gap junction density in atria and ventricles to provide full understanding of atrial and ventricular electrical differences. It would also be interesting to look at a diseased mouse model and measure whether ion channel expression and current density changes in atria and ventricles and as a result, how that affects electrical waveform and conduction. Changes in channel expression can be determined by Western blotting and changes in current density can be determined by patch clamp. The optical mapping system enables simultaneous mapping of hearts of voltage membrane potentials and calcium transients. While we have voltage membrane potential data from atria and ventricles, the data would be more complete with the addition of calcium transients.

Regarding the ischaemia and flecainide study, we attempted to measure calcium transients simultaneously to the membrane voltage data. However, the calcium transient experiments were not successful and n numbers were low. Future experiments can continue to investigate calcium transients in the presence of ischaemia. Flecainide has been commonly used with other drugs for the management of AF. In the case of ischaemia, it would be interesting to see the effects when flecainide is used in conjunction with a drug used in treating ischaemia, such as berberine. Although berberine is typically known for its use in herbal medicine, it has been found to alleviate

ischaemia-reperfusion injury induced inflammatory response. Jia *et al*'s 2022 study demonstrated attenuation of myocardial injury with berberine administration, through inhibition of downstream pro-ischaemia reperfusion injury effectors. This led to a suppression of inflammatory and oxidative stress which restored cardiac function and structure [225]. Berberine has also been found to prolong APD in ventricular myocytes without altering other variables of the action potential [226].

We were able to induce ischaemia using LAD ligation in *ex vivo*. In our ischaemia control group, hearts were pierced with a needle in the same way a non-ischaemic heart would be, and the suture was passed around the LAD but not ligated, hence a sham control. For a more complete dataset, having an additional control group where the heart was not ligated at all would prove useful. It can be argued that the actual insertion of needle is enough to cause damage to the heart, however studies show the opposite. Iyer *et al* 2016 evaluated the effect of sham surgery in a surgical model for coronary artery occlusion. They showed that sham surgery did not show signs of ischaemia, nor did it affect other physiology variables in the heart while hearts with myocardial infarction showed evidence of infarction [227]. It is important to note, however, the surgery was performed *in vivo* and used a minimally invasive approach therefore results shouldn't be directly compared to our study. Santer *et al* 2015 evaluated functional characterisation of left ventricular remodelling in *in vivo* and *ex vivo* model. They found significant differences between mice that underwent myocardial infarction surgery and mice that underwent sham surgery. After myocardial infarction, mice showed significantly reduced ejection fraction, reduced cardiac output and pump function, compared to sham [228].

From our studies, we see that ischaemia significantly affects the CV, CV becomes slower upon exposure to ischaemia, but the APD becomes prolonged after exposure to ischaemia, which is opposite to what we expect. We suggest the possibility of the ischaemia not being severe enough to cause a decrease in APD. Over time we see an insignificant increase in APD, and it is possible this phenomenon overrides the truncation of APD caused by ischaemia. Measuring protein expression for inflammatory markers such as interleukin 6 (IL-6) and other regulatory proteins such as troponin which is sensitive to cardiac injury may help to verify firstly the presence, and the severity of ischaemia. In the presence of ischaemia, these markers become elevated [229].

With more time and resources, performing LAD surgery in live mice would be insightful and would go a long way towards understanding ischaemia and flecainide interaction. Like with any technique, we must also be aware that performing LAD surgery in mice also comes with risk. With the classical LAD ligation surgery, mice require intubation. This can increase risk of death and also adds on time the mouse is under anaesthesia. However, there is development of the method without intubation, demonstrating a less damaging model of ischaemic injury and is more efficient [206]. *In vivo* experiments would provide a more physiological environment for studying ischaemia and would eliminate the effects of cardiac trauma through excision. This approach would also help with quantifying arrhythmias more accurately using ECG or ECHO.

Application of optical mapping to *in vivo* heart models is limited and the current applications are highly invasive and therefore limits its application in translational research. Moreover, uncouplers such as blebbistatin cannot be used *in vivo* studies.

There have been some studies that have aimed to develop and validate *in vivo* cardiac optical mapping in pig models [230]. The animals underwent open-chest surgery and used near-infrared voltage sensitive dyes to image APs and wave propagation. Ultimately, the ideal application would be of human hearts. We have seen some differences in CV among species and naturally gives rise to questions on how human CV will vary in atria and ventricles.

References

1. Boudoulas, K.D., Borer, J.S. and Boudoulas, H. (2015). Heart Rate, Life Expectancy and the Cardiovascular System: Therapeutic Considerations. Cardiology, [online] 132(4), pp.199–212. doi: https://doi.org/10.1159/000435947.

2. Janssen, P.M.L., Biesiadecki, B.J., Ziolo, M.T. and Davis, J.P. (2016). The Need for Speed. Circulation Research, 119(3), pp.418–421. doi: https://doi.org/10.1161/circresaha.116.309126.

3. Rehman, I. and Rehman, A. (2020). Anatomy, Thorax, Pericardium. [online] PubMed. Available at: https://www.ncbi.nlm.nih.gov/books/NBK482256/.

4. Tran, D.B. and Mahabadi, N. (2020). Anatomy, Thorax, Heart Muscles. [online] PubMed. Available at: https://www.ncbi.nlm.nih.gov/books/NBK545195/.

5. Hartsock, A. and Nelson, W.J. (2008). Adherens and tight junctions: Structure, function and connections to the actin cytoskeleton. Biochimica et Biophysica Acta (BBA) - Biomembranes, 1778(3), pp.660–669. doi: https://doi.org/10.1016/j.bbamem.2007.07.012.

6. Garrod, D. and Chidgey, M. (2008). Desmosome structure, composition and function. Biochimica et Biophysica Acta (BBA) - Biomembranes, 1778(3), pp.572–587. doi: https://doi.org/10.1016/j.bbamem.2007.07.014.

7. Goodenough, D.A. and Paul, D.L. (2009). Gap Junctions. Cold Spring Harbor Perspectives in Biology, [online] 1(1), pp.a002576–a002576. doi: https://doi.org/10.1101/cshperspect.a002576.

8. Harris, I.S. and Black, B.L. (2010). Development of the Endocardium. Pediatric Cardiology, [online] 31(3), pp.391–399. doi: https://doi.org/10.1007/s00246-010-9642-8.

9. Basit, H., Kashou, A.H., Kashou, H.E. and Chhabra, L. (2019). Physiology, Sinoatrial Node. [online] Nih.gov. Available at: https://www.ncbi.nlm.nih.gov/books/NBK459238/.

10. Alshak, M.N. and M Das, J. (2020). Neuroanatomy, Sympathetic Nervous System. [online] PubMed. Available at: https://pubmed.ncbi.nlm.nih.gov/31194352/.

11. Heaton, J. and Goyal, A. (2022). Atrioventricular Node. [online] PubMed. Available at: https://pubmed.ncbi.nlm.nih.gov/32491596/ [Accessed 30 Nov. 2022].

12. Fearnley, C.J., Roderick, H.L. and Bootman, M.D. (2011). Calcium Signaling in Cardiac Myocytes. Cold Spring Harbor Perspectives in Biology, 3(11), pp.a004242–a004242. doi: https://doi.org/10.1101/cshperspect.a004242.

13. Tandon, S. and Alzahrani, T. (2022). Physiology, AV Junction. [online] PubMed. Available at: https://www.ncbi.nlm.nih.gov/books/NBK546663/ [Accessed 11 May 2022].

14. Goyal, A., Basit, H. and Zeltser, R. (2020). Reentry Arrhythmia. [online] PubMed. Available at: https://www.ncbi.nlm.nih.gov/books/NBK537089/.

15. Sahu, K.N., Naidu, C.D., Satyam, M. and Sankar, K.J. (2015). Study of RF Signal Attenuation of Human Heart. Journal of Engineering, 2015, pp.1–8. doi: https://doi.org/10.1155/2015/484686.

16. Santana, L.F., Cheng, E.P. and Lederer, W.J. (2010). How does the shape of the cardiac action potential control calcium signaling and contraction in the heart? Journal of Molecular and Cellular Cardiology, 49(6), pp.901–903. doi: https://doi.org/10.1016/j.yjmcc.2010.09.005.

17. Wei, X., Yohannan, S. and Richards, J.R. (2022). Physiology, Cardiac Repolarization Dispersion and Reserve. [online] PubMed. Available at: https://www.ncbi.nlm.nih.gov/books/NBK537194/.

18. Pandit, S.V. (2018). 31 - Ionic Mechanisms of Atrial Action Potentials. [online] ScienceDirect. Available at: https://www.sciencedirect.com/science/article/abs/pii/B978032344733100031 6?via%3Dihub [Accessed 18 Sep. 2023].

19. Wahl-Schott, C., Fenske, S. and Biel, M. (2014). HCN channels: new roles in sinoatrial node function. Current Opinion in Pharmacology, 15, pp.83–90. doi: https://doi.org/10.1016/j.coph.2013.12.005.

20. Niwa, N. and Nerbonne, J.M. (2010). Molecular determinants of cardiac transient outward potassium current (Ito) expression and regulation. Journal of Molecular

and Cellular Cardiology, 48(1), pp.12–25. doi:https://doi.org/10.1016/j.yjmcc.2009.07.013.

21. Bartos, D.C., Grandi, E. and Ripplinger, C.M. (2015). Ion Channels in the Heart. Comprehensive Physiology, [online] 5(3), pp.1423–1464. doi:https://doi.org/10.1002/cphy.c140069.

22. Filgueiras-Rama, D. and Jalife, J. (2016). Structural and Functional Bases of Cardiac Fibrillation. JACC: Clinical Electrophysiology, 2(1), pp.1–13. doi:https://doi.org/10.1016/j.jacep.2015.12.011.

23. Grandi, E., Pandit, S.V., Voigt, N., Workman, A.J., Dobrev, D., Jalife, J. and Bers, D.M. (2011). Human Atrial Action Potential and Ca2+Model. Circulation Research, 109(9), pp.1055–1066. doi:https://doi.org/10.1161/circresaha.111.253955.

24. Jeevaratnam, K., Chadda, K.R., Huang, C.L.-H. . and Camm, A.J. (2017). Cardiac Potassium Channels: Physiological Insights for Targeted Therapy. Journal of Cardiovascular Pharmacology and Therapeutics, [online] 23(2), pp.119–129. doi:https://doi.org/10.1177/1074248417729880.

25. Jost N. (2007) 'Transmembrane ionic currents underlying cardiac action potential in mammalian hearts.' Advances in Cardiomyocyte Research, 37 (2), pp. 1-45.

26. Joukar, S. (2021). A comparative review on heart ion channels, action potentials and electrocardiogram in rodents and human: extrapolation of experimental insights to clinic. Laboratory Animal Research, 37(1). doi: https://doi.org/10.1186/s42826-021-00102-3.

27. Kaese, S. and Verheule, S. (2012). Cardiac electrophysiology in mice: a matter of size. Frontiers in Physiology, 3. doi: https://doi.org/10.3389/fphys.2012.00345.

28. Nerbonne, J.M., Nichols, C.G., Schwarz, T.L. and Escande, D. (2001). Genetic Manipulation of Cardiac K + Channel Function in Mice. Circulation Research, 89(11), pp.944–956. doi:https://doi.org/10.1161/hh2301.100349.

29. Eisner, D.A., Caldwell, J.L., Kistamás, K. and Trafford, A.W. (2017). Calcium and Excitation-Contraction Coupling in the Heart. Circulation research, [online] 121(2), pp.181–195. doi: https://doi.org/10.1161/CIRCRESAHA.117.310230.

30. Breitwieser, G.E. (2008). Extracellular calcium as an integrator of tissue function. The international journal of biochemistry & cell biology, [online] 40(8), pp.1467–1480. doi:https://doi.org/10.1016/j.biocel.2008.01.019.

31. Zacchia, M., Abategiovanni, M.L., Stratigis, S. and Capasso, G. (2016). Potassium: From Physiology to Clinical Implications. Kidney Diseases, [online] 2(2), pp.72–79. doi: https://doi.org/10.1159/000446268.

32. Bers, D.M. and Despa, S. (2009). Na+transport in cardiac myocytes; Implications for excitation-contraction coupling. IUBMB Life, [online] 61(3), pp.215–221. doi: https://doi.org/10.1002/iub.163.

33. Dong, C., Wang, Y., Ma, A. and Wang, T. (2020). Life Cycle of the Cardiac Voltage-Gated Sodium Channel NaV1.5. Frontiers in Physiology, 11. doi: https://doi.org/10.3389/fphys.2020.609733.

34. Salvage, S.C., Zhu, W., Habib, Z.F., Hwang, S.S., Joanne Frances Irons, Christopher L.-H. Huang, Silva, J.R. and Jackson, A.P. (2019). Gating control of the cardiac sodium channel Nav1.5 by its β3-subunit involves distinct roles for a transmembrane glutamic acid and the extracellular domain. Journal of Biological Chemistry, 294(51), pp.19752–19763. doi: https://doi.org/10.1074/jbc.ra119.010283.

35. Bouza, A.A. and Isom, L.L. (2018). Voltage-Gated Sodium Channel β Subunits and Their Related Diseases. Handbook of Experimental Pharmacology, [online] 246, pp.423–450. doi: https://doi.org/10.1007/164_2017_48.

36. Osadchii, O.E. (2017). Effects of Na+ channel blockers on the restitution of refractory period, conduction time, and excitation wavelength in perfused guinea-pig heart. PLOS ONE, 12(2), p.e0172683. doi:https://doi.org/10.1371/journal.pone.0172683.

37. Han, D., Tan, H., Sun, C. and Li, G. (2018). Dysfunctional Nav1.5 channels due to SCN5A mutations. Experimental Biology and Medicine, [online] 243(10), pp.852–863. doi: https://doi.org/10.1177/1535370218777972.

38. DeMarco, K.R. and Clancy, C.E. (2016). Cardiac Na Channels: Structure to Function. Current topics in membranes, [online] 78, pp.287–311. doi: https://doi.org/10.1016/bs.ctm.2016.05.001.

39. Yasaman Pirahanchi and Narothama Reddy Aeddula (2023). Physiology, Sodium Potassium Pump (Na+ K+ Pump). [online] Nih.gov. Available at: https://www.ncbi.nlm.nih.gov/books/NBK537088/.

40. Clausen MV, Hilbers F, Poulsen H. The Structure and Function of the Na,K-ATPase Isoforms in Health and Disease. Frontiers in Physiology. 2017 Jun 6;8.

41. Pavlovic et al 2013

42. Nicoll, D.A., Sawaya, M.R., Kwon, S., Cascio, D., Philipson, K.D. and Abramson, J. (2006). The Crystal Structure of the Primary Ca2+Sensor of the Na+/Ca2+Exchanger Reveals a Novel Ca2+Binding Motif. Journal of Biological Chemistry, 281(31), pp.21577–21581. doi: https://doi.org/10.1074/jbc.c600117200.

43. Giudicessi, J.R. and Ackerman, M.J. (2012). Potassium-channel mutations and cardiac arrhythmias—diagnosis and therapy. Nature Reviews Cardiology, 9(6), pp.319–332. doi: https://doi.org/10.1038/nrcardio.2012.3.

44. Rehman, R. and Hai, O. (2021). Digitalis Toxicity. [online] PubMed. Available at: https://pubmed.ncbi.nlm.nih.gov/29083729/ [Accessed 12 Nov. 2021].

45. Bers, D. (2003). Intracellular Na+ regulation in cardiac myocytes. Cardiovascular Research, 57(4), pp.897–912. doi:https://doi.org/10.1016/s0008-6363(02)00656-9.

46. Escudero, D.S., Néstor Gustavo Pérez and Romina Gisel Díaz (2021). Myocardial Impact of NHE1 Regulation by Sildenafil. Frontiers in Cardiovascular Medicine, 8. doi: https://doi.org/10.3389/fcvm.2021.617519.

47. Brazhe, A.R., Verisokin, A.Y., Verveyko, D.V. and Postnov, D.E. (2018). Sodium–Calcium Exchanger Can Account for Regenerative Ca2+ Entry in Thin Astrocyte Processes. Frontiers in Cellular Neuroscience, 12. doi: https://doi.org/10.3389/fncel.2018.00250.

48. Shigekawa, M. and Iwamoto, T. (2001). Cardiac Na + -Ca 2+ Exchange. Circulation Research, 88(9), pp.864–876. doi: https://doi.org/10.1161/hh0901.090298.

49. Armoundas, A.A., Hobai, I.A., Tomaselli, G.F., Winslow, R.L. and O'Rourke, B. (2003). Role of Sodium-Calcium Exchanger in Modulating the Action Potential of

Ventricular Myocytes From Normal and Failing Hearts. Circulation Research, 93(1), pp.46–53. doi: https://doi.org/10.1161/01.res.0000080932.98903.d8.

50. Tykocki, N.R., Jackson, W.F. and Watts, S.W. (2012). Reverse-mode Na+/Ca2+ exchange is an important mediator of venous contraction. Pharmacological Research, 66(6), pp.544–554. doi: https://doi.org/10.1016/j.phrs.2012.08.004.

51. Ren, X. and Philipson, K.D. (2013). The topology of the cardiac Na+/Ca2+ exchanger, NCX1. Journal of Molecular and Cellular Cardiology, 57, pp.68–71. doi: https://doi.org/10.1016/j.yjmcc.2013.01.010.

52. Shattock, M.J., Ottolia, M., Bers, D.M., Blaustein, M.P., Boguslavskyi, A., Bossuyt, J., Bridge, J.H.B., Chen-Izu, Y., Clancy, C.E., Edwards, A., Goldhaber, J., Kaplan, J., Lingrel, J.B., Pavlovic, D., Philipson, K., Sipido, K.R. and Xie, Z.-J. (2015). Na+/Ca2+exchange and Na+/K+-ATPase in the heart. The Journal of Physiology, 593(6), pp.1361–1382. doi:https://doi.org/10.1113/jphysiol.2014.282319.

53. Tse, G. (2016). Mechanisms of cardiac arrhythmias. Journal of Arrhythmia, [online] 32(2), pp.75–81. doi:https://doi.org/10.1016/j.joa.2015.11.003.
54. Pelat, M., Barbe, F., Daveu, C., Ly-Nguyen, L., Lartigue, T., Marque, S., Tavares, G., Ballet, V., Guillon, J.-M., Steinmeyer, K., Wirth, K., Gögelein, H., Arndt, P., Rackelmann, N., Weston, J., Bellevergue, P., McCort, G., Trellu, M., Lucats, L. and Beauverger, P. (2021). SAR340835, a Novel Selective Na+/Ca2+ Exchanger Inhibitor, Improves Cardiac Function and Restores Sympathovagal Balance in Heart Failure. Journal of Pharmacology and Experimental Therapeutics, [online] 377(2), pp.293–304. doi: https://doi.org/10.1124/jpet.120.000238.

55. Nollet, E.E., Manders, E.M., Goebel, M., Jansen, V., Brockmann, C., Osinga, J., Jolanda, Helmes, M. and Kuster, D. (2020). Large-Scale Contractility Measurements Reveal Large Atrioventricular and Subtle Interventricular Differences in Cultured Unloaded Rat Cardiomyocytes. Frontiers in physiology, 11. doi:https://doi.org/10.3389/fphys.2020.00815.

56. Blume, G.G., Mcleod, C.J., Barnes, M.E., Seward, J.B., Pellikka, P.A., Bastiansen, P.M. and Tsang, T.S.M. (2011). Left atrial function: physiology, assessment, and clinical implications. European Journal of Echocardiography, 12(6), pp.421–430. doi:https://doi.org/10.1093/ejechocard/jeq175.

57. Walklate, J., Ferrantini, C., Johnson, C.A., Tesi, C., Poggesi, C. and Geeves, M.A. (2021). Alpha and beta myosin isoforms and human atrial and ventricular

contraction. Cellular and Molecular Life Sciences, 78(23), pp.7309–7337. doi:https://doi.org/10.1007/s00018-021-03971-y.

58. Kirchhof, P., Camm, A.J., Goette, A., Brandes, A., Eckardt, L., Elvan, A., Fetsch, T., van Gelder, I.C., Haase, D., Haegeli, L.M., Hamann, F., Heidbüchel, H., Hindricks, G., Kautzner, J., Kuck, K.-H., Mont, L., Ng, G.A., Rekosz, J., Schoen, N. and Schotten, U. (2020). Early Rhythm-Control Therapy in Patients with Atrial Fibrillation. New England Journal of Medicine, 383(14). doi: https://doi.org/10.1056/nejmoa2019422.

59. Kornej, J., Börschel, C.S., Benjamin, E.J. and Schnabel, R.B. (2020). Epidemiology of Atrial Fibrillation in the 21st Century. Circulation Research, [online] 127(1), pp.4–20. doi: https://doi.org/10.1161/circresaha.120.316340.

60. Curtis, A. and Shukla (2013). Avoiding permanent atrial fibrillation: treatment approaches to prevent disease progression. Vascular Health and Risk Management, p.1. doi: https://doi.org/10.2147/vhrm.s49334.

61. Ludhwani, D. and Wieters, J.S. (2022). Paroxysmal Atrial Fibrillation. [online] PubMed. Available at: https://pubmed.ncbi.nlm.nih.gov/30571060/.

62. Lubitz, S.A., Benjamin, E.J. and Ellinor, P.T. (2010). Atrial Fibrillation in Congestive Heart Failure. Heart failure clinics, [online] 6(2), pp.187–200. doi: https://doi.org/10.1016/j.hfc.2009.11.001.

63. Khan, I.A. (2023). Atrial fibrillation: Interaction between trigger and substrate. www.bmj.com. [online] Available at: https://www.bmj.com/rapid-response/2011/10/28/atrial-fibrillation-interaction-between-trigger-and-substrate [Accessed 11 Sep. 2023].

64. Pellman, J. and Sheikh, F. (2015). Atrial Fibrillation: Mechanisms, Therapeutics, and Future Directions. Comprehensive Physiology, [online] 5(2), pp.649–665. doi:https://doi.org/10.1002/cphy.c140047.

65. Alonso, S., Weber, R. and Bär, M. (2016). Reentry and Ectopic Pacemakers Emerge in a Three-Dimensional Model for a Slab of Cardiac Tissue with Diffuse Microfibrosis near the Percolation Threshold. PloS one, [online] 11(11), pp.e0166972–e0166972. doi:https://doi.org/10.1371/journal.pone.0166972.

66. Waks, J.W. and Josephson, M.E. (2014). Mechanisms of Atrial Fibrillation – Reentry, Rotors and Reality. Arrhythmia & Electrophysiology Review, [online] 3(2), p.90. doi:https://doi.org/10.15420/aer.2014.3.2.90.

67. Rolfes, C. D., Howard, S. A., Goff, R. P. and Iaizzo, P. A. (2011). Cardiac remodeling as a consequence of atrial fibrillation: An anatomical study of perfusion-fixed human heart specimens. Journal of Geriatric Cardiology, 8(3), pp.141–146. doi: https://doi.org/10.3724/sp.j.1263.2011.00141.

68. Wijffels, M.C., Kirchhof, C.J., Dorland, R. and Allessie, M.A. (1995). Atrial fibrillation begets atrial fibrillation. A study in awake chronically instrumented goats. Circulation, [online] 92(7), pp.1954–1968. doi:https://doi.org/10.1161/01.cir.92.7.1954.

69. Hebbar, A.K. and Hueston, W.J. (2002). Management of common arrhythmias: Part I. Supraventricular arrhythmias. American Family Physician, [online] 65(12), pp.2479–2486. Available at: https://pubmed.ncbi.nlm.nih.gov/12086237/#:~:text=Patients%20with%20other%20supraventricular%20arrhythmias [Accessed 17 May 2024].

70. Willems, S., Borof, K., Brandes, A., Breithardt, G., Camm, A.J., Crijns, H.J.G.M., Eckardt, L., Gessler, N., Goette, A., Haegeli, L.M., Heidbuchel, H., Kautzner, J., Ng, G.A., Schnabel, R.B., Suling, A., Szumowski, L., Themistoclakis, S., Vardas, P., van Gelder, I.C. and Wegscheider, K. (2021). Systematic, early rhythm control strategy for atrial fibrillation in patients with or without symptoms: the EAST-AFNET 4 trial. European Heart Journal, 43(12), pp.1219–1230. doi:https://doi.org/10.1093/eurheartj/ehab593.

71. Houmsse, M., Amin, A., Houmsse, A., Ishola, A. and Tyler, J. (2016). The current approach of atrial fibrillation management. Avicenna Journal of Medicine, 6(1), p.8. doi:https://doi.org/10.4103/2231-0770.173580.

72. Salmasi, S., Loewen, P.S., Tandun, R., Andrade, J.G. and Vera, M.A.D. (2020). Adherence to oral anticoagulants among patients with atrial fibrillation: a systematic review and meta-analysis of observational studies. BMJ Open, [online] 10(4), p.e034778. doi:https://doi.org/10.1136/bmjopen-2019-034778.

73. Reading, S.R., Black, M.H., Singer, D.E., Go, A.S., Fang, M.C., Udaltsova, N., Harrison, T.N., Wei, R.X., Liu, I.-L.A. and Reynolds, K. (2019). Risk factors for medication non-adherence among atrial fibrillation patients. BMC

Cardiovascular Disorders, 19(1). doi:https://doi.org/10.1186/s12872-019-1019-1.

74. Reiter, M.J., Higgins, S.L., Payne, A.G. and Mann, D.E. (1986). Effects of quinidine versus procainamide on the QT interval. The American Journal of Cardiology, 58(6), pp.512–516. doi: https://doi.org/10.1016/0002-9149(86)90025-1.

75. Whittaker, D.G., Ni, H., Benson, A.P., Hancox, J.C. and Zhang, H. (2017). Computational Analysis of the Mode of Action of Disopyramide and Quinidine on hERG-Linked Short QT Syndrome in Human Ventricles. 8. doi: https://doi.org/10.3389/fphys.2017.00759.

76. An, Z., Yang, G., Liu, X., Zhang, Z. and Liu, G. (2018). New progress in understanding the cellular mechanisms of anti-arrhythmic drugs. Open Life Sciences, 13(1), pp.335–339. doi: https://doi.org/10.1515/biol-2018-0041.

77. King, G.S. and Hashmi, M.F. (2019). Antiarrhythmic Medications. [online] Nih.gov. Available at: https://www.ncbi.nlm.nih.gov/books/NBK482322/.

78. Martínez-Marcos, F.J., García-Garmendia, J.L., Ortega-Carpio, A., Fernández-Gómez, J.M., Santos, J.M. and Camacho, C. (2000). Comparison of intravenous flecainide, propafenone, and amiodarone for conversion of acute atrial fibrillation to sinus rhythm. The American Journal of Cardiology, [online] 86(9), pp.950–953. doi: https://doi.org/10.1016/s0002-9149(00)01128-0.

79. January, C.T., Wann, L.S., Alpert, J.S., Calkins, H., Cigarroa, J.E., Cleveland, J.C., Conti, J.B., Ellinor, P.T., Ezekowitz, M.D., Field, M.E., Murray, K.T., Sacco, R.L., Stevenson, W.G., Tchou, P.J., Tracy, C.M. and Yancy, C.W. (2014). 2014 AHA/ACC/HRS Guideline for the Management of Patients With Atrial Fibrillation. Circulation, [online] 130(23). doi: https://doi.org/10.1161/cir.0000000000000041.

80. Grandi, E. and Ripplinger, C.M. (2019). Antiarrhythmic mechanisms of beta blocker therapy. Pharmacological Research, 146, p.104274. doi:https://doi.org/10.1016/j.phrs.2019.104274.

81. Kalinowski, L., Dobrucki, L.W., Szczepanska-Konkel, M., Jankowski, M., Martyniec, L., Angielski, S. and Malinski, T. (2003). Third-Generation β-Blockers Stimulate Nitric Oxide Release From Endothelial Cells Through ATP Efflux.

Circulation, 107(21), pp.2747–2752. doi: https://doi.org/10.1161/01.cir.0000066912.58385.de.

82. Florek, J.B., Lucas, A. and Girzadas, D. (2023). Amiodarone. [online] PubMed. Available at: https://pubmed.ncbi.nlm.nih.gov/29489285/ [Accessed 18 Sep. 2023].

83. Quintana-Villamandos, B., Delgado-Martos, M.J. and Delgado-Baeza, E. (2019). Impact of a Multichannel Blocker in Attenuating Intramyocardial Artery Remodeling in Hypertensive Rats through Increased Nitric Oxide Bioavailability. BioMed Research International, [online] 2019, p.6374582. doi: https://doi.org/10.1155/2019/6374582.

84. Patel, C., Yan, G.-X. and Kowey, P.R. (2009). Dronedarone. Circulation, 120(7), pp.636–644. doi: https://doi.org/10.1161/circulationaha.109.858027.

85. Mubarik, A., Kerndt, C.C. and Cassagnol, M. (2020). Sotalol. [online] PubMed. Available at: https://www.ncbi.nlm.nih.gov/books/NBK534832/.

86. Aliot, E., Capucci, A., Crijns, H.J., Goette, A. and Tamargo, J. (2010). Twenty-five years in the making: flecainide is safe and effective for the management of atrial fibrillation. Europace, [online] 13(2), pp.161–173. doi: https://doi.org/10.1093/europace/euq382.

87. Salvage, S.C., K. Chandrasekharan, Kamalan Jeevaratnam, Dulhunty, A.F., Thompson, A., Jackson, A.P. and Christopher L.-H. Huang (2017). Multiple targets for flecainide action: implications for cardiac arrhythmogenesis. 175(8), pp.1260–1278. doi:https://doi.org/10.1111/bph.13807.

88. Ramos, E. and O'Leary, M.E. (2004). State-dependent trapping of flecainide in the cardiac sodium channel. The Journal of Physiology, 560(1), pp.37–49. doi: https://doi.org/10.1113/jphysiol.2004.065003.

89. Wang, Y., Mi, J., Lu, K., Lu, Y. and Wang, K. (2015). Comparison of Gating Properties and Use-Dependent Block of Nav1.5 and Nav1.7 Channels by Anti-Arrhythmics Mexiletine and Lidocaine. PLOS ONE, [online] 10(6), p.e0128653. doi: https://doi.org/10.1371/journal.pone.0128653.

90. Melgari, D., Zhang, Y., El Harchi, A., Dempsey, C.E. and Hancox, J.C. (2015). Molecular basis of hERG potassium channel blockade by the class Ic

antiarrhythmic flecainide. Journal of Molecular and Cellular Cardiology, 86, pp.42–53. doi: https://doi.org/10.1016/j.yjmcc.2015.06.021.

91. Echt, D. and Ruskin, J. (2020). Use of Flecainide for the Treatment of Atrial Fibrillation. The American Journal of Cardiology, [online] 125(7), pp.1123–1133. doi: https://doi.org/10.1016/j.amjcard.2019.12.041.

92. Kryshtal, D.O., Blackwell, D.J., Egly, C.L., Smith, A.N., Batiste, S.M., Johnston, J.N., Laver, D.R. and Knollmann, B.C. (2021). RYR2 Channel Inhibition Is the Principal Mechanism of Flecainide Action in CPVT. Circulation Research, [online] 128(3), pp.321–331. doi: https://doi.org/10.1161/CIRCRESAHA.120.316819.

93. Mehra, D., Imtiaz, M.S., van Helden, D.F., Knollmann, B.C. and Laver, D.R. (2014). Multiple Modes of Ryanodine Receptor 2 Inhibition by Flecainide. Molecular Pharmacology, [online] 86(6), pp.696–706. doi: https://doi.org/10.1124/mol.114.094623.

94. Salvage, S.C., Huang, C.L.-H. ., Fraser, J.A. and Dulhunty, A.F. (2022). How does flecainide impact RyR2 channel function? Journal of General Physiology, 154(9). doi: https://doi.org/10.1085/jgp.202213089.

95. Echt, D.S., Liebson, P.R., Mitchell, L.B., Peters, R.W., Obias-Manno, D., Barker, A.H., Arensberg, D., Baker, A., Friedman, L., Greene, H.L., Huther, M.L. and Richardson, D.W. (1991). Mortality and Morbidity in Patients Receiving Encainide, Flecainide, or Placebo. New England Journal of Medicine, 324(12), pp.781–788. doi: https://doi.org/10.1056/nejm199103213241201.

96. Klabunde, R.E. (2017). Cardiac electrophysiology: normal and ischemic ionic currents and the ECG. Advances in Physiology Education, [online] 41(1), pp.29–37. doi:https://doi.org/10.1152/advan.00105.2016.

97. Kalogeris, T., Baines, C.P., Krenz, M. and Korthuis, R.J. (2012). Cell Biology of Ischemia/Reperfusion Injury. International Review of Cell and Molecular Biology Volume 298, [online] 298(298), pp.229–317. doi:https://doi.org/10.1016/b978-0-12-394309-5.00006-7.

98. David, M.N.V. and Shetty, M. (2021). Digoxin. [online] PubMed. Available at: https://pubmed.ncbi.nlm.nih.gov/32310485/ [Accessed 21 Apr. 2021].

99. Kjeldsen, K. (2003). Myocardial Na,K-ATPase: Clinical aspects. Experimental & Clinical Cardiology, [online] 8(3), pp.131–133. Available at: https://www.ncbi.nlm.nih.gov/pmc/articles/PMC2716273/.

100. Ren, Y., Wu, S., Burdette, J.E., Cheng, X. and Kinghorn, A.D. (2021). Structural Insights into the Interactions of Digoxin and Na+/K+-ATPase and Other Targets for the Inhibition of Cancer Cell Proliferation. Molecules, 26(12), p.3672. doi: https://doi.org/10.3390/molecules26123672.

101. Kotecha, D., Bunting, K.V., Gill, S.K., Mehta, S., Stanbury, M., Jones, J.C., Haynes, S., Calvert, M.J., Deeks, J.J., Steeds, R.P., Strauss, V.Y., Rahimi, K., Camm, A.J., Griffith, M., Lip, G.Y.H., Townend, J.N. and Kirchhof, P. (2020). Effect of Digoxin vs Bisoprolol for Heart Rate Control in Atrial Fibrillation on Patient-Reported Quality of Life. JAMA, 324(24), p.2497. doi:https://doi.org/10.1001/jama.2020.23138.

102. Davies, J.R., Purawijaya, D.A., Bartlett, J.M. and Robinson, E.S.J. (2022). Impact of Refinements to Handling and Restraint Methods in Mice. Animals, 12(17), p.2173. doi:https://doi.org/10.3390/ani12172173.

103. Swift, F., Birkeland, K., N. Tovsrud, Enger, U.H., Aronsen, J.M., Louch, W.E., I. Sjaastad and Sejersted, O.M. (2008). Altered Na+/Ca2+-exchanger activity due to downregulation of Na+/K+-ATPase 2-isoform in heart failure. Cardiovascular research, [online] 78(1), pp.71–78. doi:https://doi.org/10.1093/cvr/cvn013.

104. Liao, R., Podesser, B.K. and Lim, C.C. (2012). The continuing evolution of the Langendorff and ejecting murine heart: new advances in cardiac phenotyping. American Journal of Physiology - Heart and Circulatory Physiology, [online] 303(2), pp.H156–H167. doi:https://doi.org/10.1152/ajpheart.00333.2012.

105. O'Shea, C., Holmes, A.P., Yu, T.Y., Winter, J., Wells, S.P., Correia, J., Boukens, B.J., De Groot, J.R., Chu, G.S., Li, X., Ng, G.A., Kirchhof, P., Fabritz, L., Rajpoot, K. and Pavlovic, D. (2019). ElectroMap: High-throughput open-source software for analysis and mapping of cardiac electrophysiology. Scientific reports, 9(1), p.1389. doi:https://doi.org/10.1038/s41598-018-38263-2.

106. Filgueiras-Rama, D. and Jalife, J. (2016). Structural and Functional Bases of Cardiac Fibrillation. JACC: Clinical Electrophysiology, 2(1), pp.1–13. doi: https://doi.org/10.1016/j.jacep.2015.12.011.

107. Varró, A., Tomek, J., Nagy, N., Virág, L., Passini, E., Rodriguez, B. and Baczkó, I. (2021). Cardiac transmembrane ion channels and action potentials: cellular physiology and arrhythmogenic behavior. Physiological Reviews, 101(3), pp.1083–1176. doi: https://doi.org/10.1152/physrev.00024.2019.

108. O' Brien, S., Holmes, A.P., Johnson, D.M., Kabir, S.N., O' Shea, C., O' Reilly, M., Avezzu, A., Reyat, J.S., Hall, A.W., Apicella, C., Ellinor, P.T., Niederer, S., Tucker, N.R., Fabritz, L., Kirchhof, P. and Pavlovic, D. (2022). Increased atrial effectiveness of flecainide conferred by altered biophysical properties of sodium channels. Journal of Molecular and Cellular Cardiology, 166, pp.23–35. doi: https://doi.org/10.1016/j.yjmcc.2022.01.009.

109. Temple, I.P., Inada, S., Dobrzynski, H. and Boyett, M.R. (2013). Connexins and the atrioventricular node. Heart Rhythm, [online] 10(2), pp.297–304. doi: https://doi.org/10.1016/j.hrthm.2012.10.020.

110. Kléber, A.G. and Rudy, Y. (2004). Basic mechanisms of cardiac impulse propagation and associated arrhythmias. Physiological Reviews, [online] 84(2), pp.431–488. doi: https://doi.org/10.1152/physrev.00025.2003.

111. Thomas, S.A., Schuessler, R.B., Berul, C.I., Beardslee, M.A., Beyer, E.C., Mendelsohn, M.E. and Saffitz, J.E. (1998). Disparate Effects of Deficient Expression of Connexin43 on Atrial and Ventricular Conduction. Circulation, 97(7), pp.686–691. doi: https://doi.org/10.1161/01.cir.97.7.686.

112. Draper, M.H. and M. Mya-Tu (1959). A COMPARISON OF THE CONDUCTION VELOCITY IN CARDIAC TISSUES OF VARIOUS MAMMALS. 44(1), pp.91–109. doi: https://doi.org/10.1113/expphysiol.1959.sp001379.

113. Kurtenbach, S., Kurtenbach, S. and Zoidl, G. (2014). Gap junction modulation and its implications for heart function. Frontiers in Physiology, 5. doi:https://doi.org/10.3389/fphys.2014.00082.

114. C. Vozzi, Dupont, E., Coppen, S.R., Yeh, H.-I. and Severs, N.J. (1999). Chamber-related Differences in Connexin Expression in the Human Heart. 31(5), pp.991–1003. doi:https://doi.org/10.1006/jmcc.1999.0937.

115. Burstein, B., Libby, E., Calderone, A. and Nattel, S. (2008). Differential Behaviors of Atrial Versus Ventricular Fibroblasts. Circulation, 117(13), pp.1630–1641. doi: https://doi.org/10.1161/circulationaha.107.748053.

116. JacquemetT, V., Virag, N. and Kappenberger, L. (2005). Wavelength and vulnerability to atrial fibrillation: Insights from a computer model of human atria. Europace, 7, pp.S83–S92. doi:https://doi.org/10.1016/j.eupc.2005.03.017.

117. Nattel, S. (2002). The 'Edge-To-Edge' Technique in Mitral Valve Repair. Heart Views, [online] 3(4), p.4. Available at: https://journals.lww.com/hrtv/fulltext/2002/03040/the__edge_to_edge__technique_in_mitral_valve.4.aspx [Accessed 17 May 2024].

118. Han, B., Trew, M.L. and Zgierski-Johnston, C.M. (2021). Cardiac Conduction Velocity, Remodeling and Arrhythmogenesis. Cells, 10(11), p.2923. doi:https://doi.org/10.3390/cells10112923.

119. Laerd Statistics (2018). SPSS Statistics Tutorials and Statistical Guides | Laerd Statistics. [online] Laerd.com. Available at: https://statistics.laerd.com/.

120. Sciencedirect.com. (2018). Heart Stroke Volume - an overview | ScienceDirect Topics. [online] Available at: https://www.sciencedirect.com/topics/nursing-and-health-professions/heart-stroke-volume.

121. Bayly, P.V., KenKnight, B.H., Rogers, J.M., Hillsley, R.E., Ideker, R.E. and Smith, W.M. (1998). Estimation of conduction velocity vector fields from epicardial mapping data. IEEE Transactions on Biomedical Engineering, 45(5), pp.563–571. doi:https://doi.org/10.1109/10.668746.

122. Knollmann, B.C., Schober, T., Petersen, A.O., Sirenko, S.G. and Franz, M.R. (2007). Action potential characterization in intact mouse heart: steady-state cycle length dependence and electrical restitution. American Journal of Physiology-Heart and Circulatory Physiology, 292(1), pp.H614–H621. doi: https://doi.org/10.1152/ajpheart.01085.2005.

123. De Clercq, D., Broux, B., Vera, L., Decloedt, A. and van Loon, G. (2018). Measurement variability of right atrial and ventricular monophasic action potential and refractory period measurements in the standing non-sedated

horse. BMC Veterinary Research, 14(1). doi:https://doi.org/10.1186/s12917-018-1399-y.

124. Haverinen, J. and Vornanen, M. (2006). Significance of Na+ current in the excitability of atrial and ventricular myocardium of the fish heart. The Journal of Experimental Biology, [online] 209(Pt 3), pp.549–557. doi: https://doi.org/10.1242/jeb.02044.

125. Franz, M.R., Jamal, S.M. and Narayan, S.M. (2012). The role of action potential alternans in the initiation of atrial fibrillation in humans: a review and future directions. Europace, [online] 14(Suppl 5), pp.v58–v64. doi: https://doi.org/10.1093/europace/eus273.

126. Workman, A.J., Marshall, G.E., Rankin, A.C., Smith, G.L. and Dempster, J. (2012). Transient outward K+current reduction prolongs action potentials and promotes afterdepolarisations: a dynamic-clamp study in human and rabbit cardiac atrial myocytes. The Journal of Physiology, 590(17), pp.4289–4305. doi: https://doi.org/10.1113/jphysiol.2012.235986.

127. Obergassel, J., O'Reilly, M., Laura Charlotte Sommerfeld, S. Nashitha Kabir, O'Shea, C., Syeda, F., Eckardt, L., Kirchhof, P. and Fabritz, L. (2021). Effects of genetic background, sex, and age on murine atrial electrophysiology. Europace, 23(6), pp.958–969. doi: https://doi.org/10.1093/europace/euaa369.

128. Shattock, M.J., Kyung Chan Park, Yang, H.-Y., Angela W.C. Lee, Niederer, S., MacLeod, K.T. and Winter, J. (2017). Restitution slope is principally determined by steady-state action potential duration. Cardiovascular Research, 113(7), pp.817–828. doi: https://doi.org/10.1093/cvr/cvx063.

129. Antzelevitch, C. and Burashnikov, A. (2011). Overview of Basic Mechanisms of Cardiac Arrhythmia. Cardiac Electrophysiology Clinics, [online] 3(1), pp.23–45. doi: https://doi.org/10.1016/j.ccep.2010.10.012.

130. George, S.A., Bonakdar, M., Zeitz, M., Davalos, R.V., Smyth, J.D. and Poelzing, S. (2016). Extracellular sodium dependence of the conduction velocity-calcium relationship: evidence of ephaptic self-attenuation. American Journal of Physiology-heart and Circulatory Physiology, 310(9), pp.H1129–H1139. doi: https://doi.org/10.1152/ajpheart.00857.2015.

131. Verheule, S., Batenburg, C.A.J.A.C., Coenjaerts, F.E.J., Kirchhofe, S., Willecke, K. and Jongsma, H.J. (1999). Cardiac Conduction Abnormalities in Mice Lacking the Gap Junction Protein Connexin40. Journal of Cardiovascular Electrophysiology, 10(10), pp.1380–1389. doi: https://doi.org/10.1111/j.1540-8167.1999.tb00194.x.

132. van Veen, T.A.B., van Rijen, H.V.M., van Kempen, M.J.A., Miquerol, L., Opthof, T., Gros, D., Vos, M.A., Jongsma, H.J. and de Bakker, J.M.T. (2005). Discontinuous Conduction in Mouse Bundle Branches Is Caused by Bundle-Branch Architecture. Circulation, 112(15), pp.2235–2244. doi: https://doi.org/10.1161/circulationaha.105.547893.

133. Sébastien Alcoléa, T. Jarry-Guichard, Jacques de Bakker, González, D., Lamers, W.H., Coppen, S.R., Barrio, L.C., Jongsma, H.J., Gros, D. and V.M, H. (2004). Replacement of Connexin40 by Connexin45 in the Mouse. Circulation Research, 94(1), pp.100–109. doi: https://doi.org/10.1161/01.res.0000108261.67979.2a.

134. O'Shea, C., Winter, J., Kabir, S.N., O'Reilly, M., Wells, S.P., Baines, O., Sommerfeld, L.C., Correia, J., Lei, M., Kirchhof, P., Holmes, A.P., Fabritz, L., Rajpoot, K. and Pavlovic, D. (2022). High resolution optical mapping of cardiac electrophysiology in pre-clinical models. Scientific Data, [online] 9(1), p.135. doi: https://doi.org/10.1038/s41597-022-01253-1.

135. Fu, F., Pietropaolo, M., Cui, L., Pandit, S., Li, W., Tarnavski, O., Shetty, S.S., Liu, J., Lussier, J.M., Murakami, Y., Grewal, P.K., Deyneko, G., Turner, G.M., Taggart, A.K.P., Waters, M.G., Coughlin, S. and Adachi, Y. (2022). Lack of authentic atrial fibrillation in commonly used murine atrial fibrillation models. PLOS ONE, 17(1), p.e0256512. doi: https://doi.org/10.1371/journal.pone.0256512.

136. Su, K., Ma, Y., Cacheux, M., Zeki Ilkan, Raad, N., Muller, G.K., Wu, X., Guerrera, N., Thorn, S., Sinusas, A.J., Foretz, M., Benoit Viollet, Akar, J.G., Akar, F.G. and Young, L.H. (2022). Atrial AMP-activated protein kinase is critical for prevention of dysregulation of electrical excitability and atrial fibrillation. JCI insight, 7(8). doi: https://doi.org/10.1172/jci.insight.141213.

137. Boukens, B.J., Hoogendijk, M.G., Verkerk, A.O., Linnenbank, A., van Dam, P., Remme, C.-A., Fiolet, J.W., Opthof, T., Christoffels, V.M. and Coronel, R. (2012). Early repolarization in mice causes overestimation of ventricular

activation time by the QRS duration. Cardiovascular Research, 97(1), pp.182–191. doi: https://doi.org/10.1093/cvr/cvs299.

138. Dusturia, N., Seung Wook Choi, Song, K.S. and Ki Moo Lim (2019). Effect of myocardial heterogeneity on ventricular electro-mechanical responses: a computational study. Biomedical Engineering Online, 18(1). doi: https://doi.org/10.1186/s12938-019-0640-7.

139. Lou, Q., Fedorov, V.V., Glukhov, A.V., Moazami, N., Fast, V.G. and Efimov, I.R. (2011). Transmural Heterogeneity and Remodeling of Ventricular Excitation-Contraction Coupling in Human Heart Failure. Circulation, 123(17), pp.1881–1890. doi: https://doi.org/10.1161/circulationaha.110.989707.

140. Antzelevitch, C., Sicouri, S., Litovsky, S.H., Lukas, A., Krishnan, S.C., Di Diego, J.M., Gintant, G.A. and Liu, D.W. (1991). Heterogeneity within the ventricular wall. Electrophysiology and pharmacology of epicardial, endocardial, and M cells. Circulation Research, 69(6), pp.1427–1449. doi: https://doi.org/10.1161/01.res.69.6.1427.

141. Franzone, P. C., Pavarino, L.F., Scacchi, S. and Taccardi, B. (2008). Modeling ventricular repolarization: Effects of transmural and apex-to-base heterogeneities in action potential durations. Mathematical Biosciences, 214(1-2), pp.140–152. doi:https://doi.org/10.1016/j.mbs.2008.06.006.

142. Seyika, S., Ichikawa, S., Tsutsumi, T. and Harumi, K. (1983). Nonuniform action potential durations at different sites in canine left ventricle. Japanese Heart Journal, [online] 24(6), pp.935–945. doi:https://doi.org/10.1536/ihj.24.935.

143. Kanai, A. and Salama, G. (1995). Optical Mapping Reveals That Repolarization Spreads Anisotropically and Is Guided by Fiber Orientation in Guinea Pig Hearts. Circulation Research, 77(4), pp.784–802. doi: https://doi.org/10.1161/01.res.77.4.784.

144. Waks, J.W. and Tereshchenko, L.G. (2016). Global Electrical Heterogeneity: A Review of the Spatial Ventricular Gradient. Journal of electrocardiology, [online] 49(6), pp.824–830. doi: https://doi.org/10.1016/j.jelectrocard.2016.07.025.

145. Sanguinetti, M.C. and Bennett, P.B. (2003). Antiarrhythmic Drug Target Choices and Screening. Circulation Research, 93(6), pp.491–499. doi:https://doi.org/10.1161/01.res.0000091829.63501.a8.

146. Lei, M., Wu, L., Terrar, D.A. and Huang, C.L.-H. . (2018). Modernized Classification of Cardiac Antiarrhythmic Drugs. Circulation, [online] 138(17), pp.1879–1896. doi:https://doi.org/10.1161/circulationaha.118.035455.

147. M Földi, Pesti, K., Zboray, K., Toth, A., Tamás Hegedűs, András Málnási-Csizmadia, Péter Lukács and Mike, Á. (2021). The mechanism of non-blocking inhibition of sodium channels revealed by conformation-selective photolabeling. British Journal of Pharmacology, 178(5), pp.1200–1217. doi:https://doi.org/10.1111/bph.15365.

148. Holmes, A.P., Saxena, P., Kabir, S.N., O'Shea, C., Kuhlmann, S.M., Gupta, S., Fobian, D., Apicella, C., O'Reilly, M., Syeda, F., Reyat, J.S., Smith, G.L., Workman, A.J., Pavlovic, D., Fabritz, L. and Kirchhof, P. (2021). Atrial resting membrane potential confers sodium current sensitivity to propafenone, flecainide and dronedarone. Heart Rhythm, 18(7), pp.1212–1220. doi:https://doi.org/10.1016/j.hrthm.2021.03.016.

149. Iwasaki, Y., Nishida, K., Kato, T. and Nattel, S. (2011). Atrial Fibrillation Pathophysiology. Circulation, 124(20), pp.2264–2274. doi: https://doi.org/10.1161/circulationaha.111.019893.

150. Desai, D.S. and Hajouli, S. (2020). Arrhythmias. [online] PubMed. Available at: https://www.ncbi.nlm.nih.gov/books/NBK558923/.

151. Haïssaguerre, M., Jaïs, P., Shah, D.C., Takahashi, A., Hocini, M., Quiniou, G., Garrigue, S., Le Mouroux, A., Le Métayer, P. and Clémenty, J. (1998). Spontaneous Initiation of Atrial Fibrillation by Ectopic Beats Originating in the Pulmonary Veins. New England Journal of Medicine, 339(10), pp.659–666. doi:https://doi.org/10.1056/nejm199809033391003.

152. T. Jared Bunch and Cutler, M.J. (2015). Is pulmonary vein isolation still the cornerstone in atrial fibrillation ablation? PubMed, [online] 7(2), pp.132–41. doi:https://doi.org/10.3978/j.issn.2072-1439.2014.12.46.

153. 1.Razavi M. Safe and effective pharmacologic management of arrhythmias. Texas Heart Institute Journal [Internet]. 2005 [cited 2023 Sep 29];32(2):209–11. Available from: https://pubmed.ncbi.nlm.nih.gov/16107117/

154. Schram, G., Pourrier, M., Melnyk, P. and Nattel, S. (2002). Differential Distribution of Cardiac Ion Channel Expression as a Basis for Regional Specialization in Electrical Function. Circulation Research, 90(9), pp.939–950. doi: https://doi.org/10.1161/01.res.0000018627.89528.6f.

155. Berecki, G., Wilders, R., de Jonge, B., van Ginneken, A.C.G. and Verkerk, A.O. (2010). Re-Evaluation of the Action Potential Upstroke Velocity as a Measure of the Na+ Current in Cardiac Myocytes at Physiological Conditions. PLoS ONE, 5(12), p.e15772. doi:https://doi.org/10.1371/journal.pone.0015772.

156. Andrikopoulos, G.K. (2015). Flecainide: Current status and perspectives in arrhythmia management. World Journal of Cardiology, [online] 7(2), p.76. doi:https://doi.org/10.4330/wjc.v7.i2.76.

157. Ikeda, N., Singh, B.N., Davis, L.S. and Hauswirth O (1985). Effects of flecainide on the electrophysiologic properties of isolated canine and rabbit myocardial fibers. Journal of the American College of Cardiology, 5(2), pp.303–310. doi:https://doi.org/10.1016/s0735-1097(85)80051-6.

158. Caballero, R., Dolz-Gaitón, P., Gómez, R., Amorós, I., Barana, A., González, M., Osuna, L., Duarte, J., López–Izquierdo, A., Moraleda, I., Gálvez, E., José Antonio Sánchez–Chapula, Tamargo, J. and Delpón, E. (2010). Flecainide increases Kir2.1 currents by interacting with cysteine 311, decreasing the polyamine-induced rectification. Proceedings of the National Academy of Sciences of the United States of America, 107(35), pp.15631–15636. doi:https://doi.org/10.1073/pnas.1004021107.

159. Proks, P., Puljung, M.C., Vedovato, N., Sachse, G., Mulvaney, R. and Ashcroft, F.M. (2016). Running out of time: the decline of channel activity and nucleotide activation in adenosine triphosphate-sensitive K-channels. Philosophical Transactions of the Royal Society B: Biological Sciences, 371(1700), p.20150426. doi:https://doi.org/10.1098/rstb.2015.0426.

160. Semenza, G.L. (2000). HIF-1: mediator of physiological and pathophysiological responses to hypoxia. Journal of Applied Physiology, 88(4), pp.1474–1480. doi:https://doi.org/10.1152/jappl.2000.88.4.1474.

161. Rodriquez, B., Trayanova, N. and Noble, D. (2006). Modeling Cardiac Ischemia. Annals of the New York Academy of Sciences, [online] 1080(1), pp.395–414. doi:https://doi.org/10.1196/annals.1380.029.

162. Jiang, W., Xiong, Y., Li, X. and Yang, Y. (2021). Cardiac Fibrosis: Cellular Effectors, Molecular Pathways, and Exosomal Roles. Frontiers in Cardiovascular Medicine, 8. doi: https://doi.org/10.3389/fcvm.2021.715258.

163. Ghuran, A.V. and Camm, A.J. (2001). Ischaemic heart disease presenting as arrhythmias. British Medical Bulletin, 59(1), pp.193–210. doi: https://doi.org/10.1093/bmb/59.1.193.

164. Santucci, A., Riccini, C. and Cavallini, C. (2020). Treatment of stable ischaemic heart disease: the old and the new. European Heart Journal Supplements, [online] 22(Supplement_E), pp.E54–E59. doi:https://doi.org/10.1093/eurheartj/suaa060.

165. Saini, V., Podrid, P.J., Slater, W. and Lown, B. (1989). Encainide and flecainide: Are they interchangeable? American Heart Journal, 117(6), pp.1253–1258. doi:https://doi.org/10.1016/0002-8703(89)90403-1.

166. Pratt, C.M. and MoyéL.A. (1995). The Cardiac Arrhythmia Suppression Trial. Circulation, 91(1), pp.245–247. doi:https://doi.org/10.1161/01.cir.91.1.245.

167. Kirchhof, P., Andresen, D., Bosch, R., Borggrefe, M., Meinertz, T., Parade, U., Ravens, U., Samol, A., Steinbeck, G., Treszl, A., Wegscheider, K. and Breithardt, G. (2012). Short-term versus long-term antiarrhythmic drug treatment after cardioversion of atrial fibrillation (Flec-SL): a prospective, randomised, open-label, blinded endpoint assessment trial. The Lancet, 380(9838), pp.238–246. doi:https://doi.org/10.1016/s0140-6736(12)60570-4.

168. Liao, R., Podesser, B.K. and Lim, C.C. (2012). The continuing evolution of the Langendorff and ejecting murine heart: new advances in cardiac phenotyping. American Journal of Physiology - Heart and Circulatory Physiology, [online] 303(2), pp.H156–H167. doi:https://doi.org/10.1152/ajpheart.00333.2012.

169. Assayag, P., Charlemagne, D., Marty, I., Joël de Leiris, Anne Marie Lompré, Boucher, F., Valere, P.E., S. Lortet, Swynghedauw, B. and Besse, S. (1998). Effects of sustained low-flow ischemia on myocardial function and calcium-regulating proteins in adult and senescent rat hearts. Cardiovascular Research, 38(1), pp.169–180. doi:https://doi.org/10.1016/s0008-6363(97)00283-6.

170. House, S.L., Bolte, C., Zhou, M., Doetschman, T., Klevitsky, R., Newman, G. and Schultz, J.E.J. (2003). Cardiac-specific overexpression of fibroblast growth factor-2 protects against myocardial dysfunction and infarction in a murine model of low-flow ischemia. Circulation, [online] 108(25), pp.3140–3148. doi:https://doi.org/10.1161/01.CIR.0000105723.91637.1C.

171. Ebel, D., P. Lipfert, J. FraÕßdorf, Benedikt Preckel, J. MuÕllenheim, V. ThaÕmer and Schlack, W. (2001). Lidocaine reduces ischaemic but not reperfusion injury in isolated rat heart. British Journal of Anaesthesia, 86(6), pp.846–852. doi:https://doi.org/10.1093/bja/86.6.846.

172. Bethell, H., Vandenberg, J.I., Smith, G. and Grace, A.A. (1998). Changes in ventricular repolarization during acidosis and low-flow ischemia. American Journal of Physiology-heart and Circulatory Physiology, 275(2), pp.H551–H561. doi:https://doi.org/10.1152/ajpheart.1998.275.2.h551.

173. Mačianskienė, R., Martišienė, I., Antanas Navalinskas, Rimantas Treinys, Andriulė, I. and Jurevičius, J. (2018). Mechanism of Action Potential Prolongation During Metabolic Inhibition in the Whole Rabbit Heart. Frontiers in Physiology, 9. doi:https://doi.org/10.3389/fphys.2018.01077.

174. Verkerk, A.O., Veldkamp, M.W., van Ginneken, A.C.G. and Bouman, L.N. (1996). Biphasic Response of Action Potential Duration to Metabolic Inhibition in Rabbit and Human Ventricular Myocytes: Role of Transient Outward Current and ATP-regulated Potassium Current. Journal of Molecular and Cellular Cardiology, 28(12), pp.2443–2456. doi:https://doi.org/10.1006/jmcc.1996.0237.

175. Wang, Z., Pelletier Lc, Talajic, M. and Nattel, S. (1990). Effects of flecainide and quinidine on human atrial action potentials. Role of rate-dependence and comparison with guinea pig, rabbit, and dog tissues. Circulation, 82(1), pp.274–283. doi:https://doi.org/10.1161/01.cir.82.1.274.

176. Lavalle, C., Magnocavallo, M., Straito, M., Santini, L., Forleo, G.B., Grimaldi, M., Badagliacca, R., Lanata, L. and Ricci, R.P. (2021). Flecainide How and When: A Practical Guide in Supraventricular Arrhythmias. Journal of Clinical Medicine, 10(7), p.1456. doi:https://doi.org/10.3390/jcm10071456.

177. Arunachalam, K. and Alzahrani, T. (2024). Flecainide. [online] PubMed. Available at:

https://www.ncbi.nlm.nih.gov/books/NBK542291/#:~:text=Mechanism%20of%20Action [Accessed 17 May 2024].

178. Stokoe, K.S., Balasubramaniam, R., Goddard, C.A., Colledge, W.H., Grace, A.A. and Christopher L.-H. Huang (2007). Effects of flecainide and quinidine on arrhythmogenic properties ofScn5a+/− murine hearts modelling the Brugada syndrome. The Journal of Physiology, 581(1), pp.255–275. doi:https://doi.org/10.1113/jphysiol.2007.128785.

179. Breindahl, T. (2000). Therapeutic drug monitoring of flecainide in serum using high-performance liquid chromatography and electrospray mass spectrometry. Journal of Chromatography B: Biomedical Sciences and Applications, 746(2), pp.249–254. doi:https://doi.org/10.1016/s0378-4347(00)00343-1.

180. Kléber, A.G., Janse, M.J., Wilms-Schopmann, F.J., Wilde, A.A. and Coronel, R. (1986). Changes in conduction velocity during acute ischemia in ventricular myocardium of the isolated porcine heart. Circulation, 73(1), pp.189–198. doi:https://doi.org/10.1161/01.cir.73.1.189.

181. Ferrero, Á., Chorro, F.J., Joaquín Cánoves, Mainar, L., Blasco, E. and Such, L. (2007). Effect of Flecainide on Longitudinal and Transverse Conduction Velocities in Ventricular Myocardium. An Experimental Study. Revista española de cardiología. doi:https://doi.org/10.1016/s1885-5857(07)60157-1.

182. Ihara, K., Sugiyama, K., Takahashi, K., Yamazoe, M., Sasano, T. and Furukawa, T. (2018). Electrophysiological Assessment of Murine Atria with High-Resolution Optical Mapping. Journal of Visualized Experiments, (132). doi:https://doi.org/10.3791/56478.

183. Hoeker, G.S., James, C.C., Tegge, A.N., Gourdie, R.G., Smyth, J.D. and Poelzing, S. (2020). Attenuating loss of cardiac conduction during no-flow ischemia through changes in perfusate sodium and calcium. American Journal of Physiology-heart and Circulatory Physiology, 319(2), pp.H396–H409. doi:https://doi.org/10.1152/ajpheart.00112.2020.

184. Kneller, J.P., Jérôme Kalifa, Zou, R., Zaitsev, A.V., Warren, M.E., Berenfeld, O., Vigmond, E.J., L. Joshua Leon, Nattel, S. and José Jalife (2005). Mechanisms of Atrial Fibrillation Termination by Pure Sodium Channel Blockade in an

Ionically-Realistic Mathematical Model. Circulation Research, 96(5). doi:https://doi.org/10.1161/01.res.0000160709.49633.2b.

185. Kondratyev, A.A., Julien, Munteanu, A., Rohr, S. and Kučera, J. (2007). Dynamic changes of cardiac conduction during rapid pacing. American Journal of Physiology-heart and Circulatory Physiology, 292(4), pp.H1796–H1811. doi:https://doi.org/10.1152/ajpheart.00784.2006.

186. Jeong, D.U. and Lim, K.M. (2018). The effect of myocardial action potential duration on cardiac pumping efficacy: a computational study. Biomedical engineering online, [online] 17(1), p.79. doi:https://doi.org/10.1186/s12938-018-0508-2.

187. Kazbanov, I.V., Clayton, R.H., Nash, M.P., Bradley, C.P., Paterson, D.J., Hayward, M.P., Taggart, P. and Panfilov, A.V. (2014). Effect of Global Cardiac Ischemia on Human Ventricular Fibrillation: Insights from a Multi-scale Mechanistic Model of the Human Heart. PLoS Computational Biology, [online] 10(11), p.e1003891. doi:https://doi.org/10.1371/journal.pcbi.1003891.

188. Swift, L.M., Asfour, H., Posnack, N.G., Arutunyan, A., Kay, M.W. and Sarvazyan, N. (2012). Properties of blebbistatin for cardiac optical mapping and other imaging applications. Pflügers Archiv - European Journal of Physiology, 464(5), pp.503–512. doi:https://doi.org/10.1007/s00424-012-1147-2.

189. Xiao, J. and Trayanova, N.A. (2010). Mechanisms for initiation of reentry in acute regional ischemia phase 1B. Heart Rhythm, 7(3), pp.379–386. doi:https://doi.org/10.1016/j.hrthm.2009.11.014.

190. Adnan, G., Singh, D.P. and Mahajan, K. (2020). Coronary Artery Thrombus. [online] PubMed. Available at: https://www.ncbi.nlm.nih.gov/books/NBK534808/.

191. Shahjehan, R.D. and Bhutta, B.S. (2023). Coronary Artery Disease. [online] PubMed. Available at: https://www.ncbi.nlm.nih.gov/books/NBK564304/.

192. Badran, H.M., Ibrahim, W.A., Alaksher, T. and Soltan, G. (2020). Impact of the left anterior descending artery wrapping around the left ventricular apex on cardiac mechanics in patients with normal coronary angiography. The Egyptian Heart Journal, 72(1). doi:https://doi.org/10.1186/s43044-020-00059-z.

193. Reichert, S., Schulz, S., Benten, A.-C., Lutze, A., Seifert, T., Schlitt, M., Werdan, K., Hofmann, B., Wienke, A., Schaller, H.-G. and Schlitt, A. (2016). Periodontal conditions and incidence of new cardiovascular events among patients with coronary vascular disease. Journal of Clinical Periodontology, 43(11), pp.918–925. doi:https://doi.org/10.1111/jcpe.12611.

194. Wang, X.-Y., Zhang, F., Zhang, C., Zheng, L.-R. and Yang, J. (2020). The Biomarkers for Acute Myocardial Infarction and Heart Failure. BioMed Research International, 2020, pp.1–14. doi:https://doi.org/10.1155/2020/2018035.

195. Kristián T. and Siesjö B.K. (1998). Calcium in Ischemic Cell Death. Stroke, 29(3), pp.705–718. doi:https://doi.org/10.1161/01.str.29.3.705.

196. Kirchhof, P., Breithardt, G., Camm, A.J., Crijns, H.J., Kuck, K.-H., Vardas, P. and Wegscheider, K. (2013). Improving outcomes in patients with atrial fibrillation: Rationale and design of the Early treatment of Atrial fibrillation for Stroke prevention Trial. American Heart Journal, [online] 166(3), pp.442–448. doi:https://doi.org/10.1016/j.ahj.2013.05.015.

197. Kristián T. and Siesjö B.K. (1998). Calcium in Ischemic Cell Death. Stroke, 29(3), pp.705–718. doi:https://doi.org/10.1161/01.str.29.3.705.

198. Yan, G.-X., Yamada, K.A., Kleber, A.G., J. Mchowat and Corr, P.B. (1993). Dissociation between cellular K+ loss, reduction in repolarization time, and tissue ATP levels during myocardial hypoxia and ischemia. Circulation Research, 72(3), pp.560–570. doi:https://doi.org/10.1161/01.res.72.3.560.

199. Bernikova, O.G., Tsvetkova, A.S., Gonotkov, M.A., Ovechkin, A.O., Demidova, M.M., Azarov, J.E. and Platonov, P.G. (2023). Prolonged repolarization in the early phase of ischemia is associated with ventricular fibrillation development in a porcine model. Frontiers in Physiology, [online] 14, p.1035032. doi:https://doi.org/10.3389/fphys.2023.1035032.

200. Liu, M., Liu, H., Parthiban, P., Kang, G.-J., Shi, G., Feng, F., Zhou, A., Gu, L., Karnopp, C., Tolkacheva, E.G. and Dudley, S.C. (2021). Inhibition of the unfolded protein response reduces arrhythmia risk after myocardial infarction. The Journal of Clinical Investigation, [online] 131(18). doi:https://doi.org/10.1172/JCI147836.

201. Hondeghem, L.M., Carlsson, L. and Duker, G. (2001). Instability and Triangulation of the Action Potential Predict Serious Proarrhythmia, but Action Potential Duration Prolongation Is Antiarrhythmic. Circulation, 103(15), pp.2004–2013. doi:https://doi.org/10.1161/01.cir.103.15.2004.

202. Ellermann, C., Coenen, A., Niehues, P., Leitz, P., Kochhäuser, S., Dechering, D.G., Fehr, M., Eckardt, L. and Frommeyer, G. (2019). Proarrhythmic Effect of Acetylcholine-Esterase Inhibitors Used in the Treatment of Alzheimer's Disease: Benefit of Rivastigmine in an Experimental Whole-Heart Model. Cardiovascular Toxicology, 20(2), pp.168–175. doi:https://doi.org/10.1007/s12012-019-09543-8.

203. Tsai, W.-C., Chen, P.-S. and Rubart-von, M. (2015). Abstract 15625: Flecainide Modulates Action Potential Properties of Cardiac Sympathetic Neurons. Circulation, 132(suppl_3). doi:https://doi.org/10.1161/circ.132.suppl_3.15625.

204. Clusin, W.T. (2008). Mechanisms of calcium transient and action potential alternans in cardiac cells and tissues. American Journal of Physiology-Heart and Circulatory Physiology, 294(1), pp.H1–H10. doi:https://doi.org/10.1152/ajpheart.00802.2007.

205. Demeter-Haludka, V., Kovács, M., Prorok, J., Nagy, N., Varró, A. and Végh, Á. (2019). Examination of the Changes in Calcium Homeostasis in the Delayed Antiarrhythmic Effect of Sodium Nitrite. International Journal of Molecular Sciences, [online] 20(22), p.5687. doi:https://doi.org/10.3390/ijms20225687.

206. Gao, E., Lei, Y.H., Shang, X., Huang, Z.M., Zuo, L., Boucher, M., Fan, Q., Chuprun, J.K., Ma, X.L. and Koch, W.J. (2010). A Novel and Efficient Model of Coronary Artery Ligation and Myocardial Infarction in the Mouse. Circulation Research, 107(12), pp.1445–1453. doi:https://doi.org/10.1161/circresaha.110.223925.

207. Vanhaleweyk, G., Balakumaran, K., Lubsen, J., ten Cate, F.J., Jovanovic, A., Hagemeijer, F., Withagen, A., Polak, B.C., Roelandt, J. and Hugenholtz, P.G. (1984). Flecainide: one-year efficacy in patients with chronic ventricular arrhythmias. European Heart Journal, [online] 5(10), pp.814–823. doi:https://doi.org/10.1093/oxfordjournals.eurheartj.a061570.

208. Merentie, M., Jukka Lipponen, Hedman, M., Hedman, A., Juha Hartikainen, Huusko, J., Line Lottonen-Raikaslehto, Viktor Parviainen, Laidinen, S., Karjalainen, P.P. and Seppo Ylä-Herttuala (2015). Mouse ECG findings in aging, with conduction system affecting drugs and in cardiac pathologies: Development and validation of ECG analysis algorithm in mice. Physiological Reports, 3(12), pp.e12639–e12639. doi:https://doi.org/10.14814/phy2.12639.

209. Aschar-Sobbi, R., Izaddoustdar, F., Korogyi, A.S., Wang, Q., Farman, G.P., Yang, F., Yang, W., Dorian, D., Simpson, J.A., Tuomi, J.M., Jones, D.L., Nanthakumar, K., Cox, B., Wehrens, X.H.T., Dorian, P. and Backx, P.H. (2015). Increased atrial arrhythmia susceptibility induced by intense endurance exercise in mice requires TNFα. Nature Communications, 6(1). doi:https://doi.org/10.1038/ncomms7018.

210. Everett, T.H. and Olgin, J.E. (2007). Atrial fibrosis and the mechanisms of atrial fibrillation. Heart Rhythm, 4(3), pp.S24–S27. doi:https://doi.org/10.1016/j.hrthm.2006.12.040.

211. Geng, M., Lin, A. and Nguyen, T.P. (2020). Revisiting Antiarrhythmic Drug Therapy for Atrial Fibrillation: Reviewing Lessons Learned and Redefining Therapeutic Paradigms. Frontiers in Pharmacology, [online] 11. doi:https://doi.org/10.3389/fphar.2020.581837.

212. Abramochkin, D.V., Alekseeva, E.I. and Vornanen, M. (2013). Inhibition of the cardiac inward rectifier potassium currents by KB-R7943. Comparative Biochemistry and Physiology Part C: Toxicology & Pharmacology, [online] 158(3), pp.181–186. doi:https://doi.org/10.1016/j.cbpc.2013.08.001.

213. Roselli, C., Chaffin, M.D., Weng, L.-C., Aeschbacher, S., Ahlberg, G., Albert, C.M., Almgren, P., Alonso, A., Anderson, C.D., Aragam, K.G., Arking, D.E., Barnard, J., Bartz, T.M., Benjamin, E.J., Bihlmeyer, N.A., Bis, J.C., Bloom, H.L., Boerwinkle, E., Bottinger, E.B. and Brody, J.A. (2018). Multi-ethnic genome-wide association study for atrial fibrillation. Nature Genetics, 50(9), pp.1225–1233. doi:https://doi.org/10.1038/s41588-018-0133-9.

214. Syeda, F., Holmes, A.B., Yu, T., Tull, S., Kuhlmann, S., Pavlovic, D., Betney, D., Riley, G., Kucera, J.P., Florian Jousset, Joris, Rohr, S., Brown, N.A., Fabritz, L. and Kirchhof, P. (2016). PITX2 Modulates Atrial Membrane Potential and the Antiarrhythmic Effects of Sodium-Channel Blockers. Journal of the American

College of Cardiology, 68(17), pp.1881–1894. doi:https://doi.org/10.1016/j.jacc.2016.07.766.

215. Brugada, J., Boersma, L., Kirchhof, C., Allessie, M. (1991). Proarrhythmic effects of flecainide. Experimental evidence for increased susceptibility to reentrant arrhythmias. Circulation, 84(4), pp.1808–1818. doi:https://doi.org/10.1161/01.cir.84.4.1808.

216. Wyse, D.G., Waldo, A.L., DiMarco, J.P., Domanski, M.J., Rosenberg, Y., Schron, E.B., Kellen, J.C., Greene, H.L., Mickel, M.C., Dalquist, J.E., Corley, S.D. and Atrial Fibrillation Follow-up Investigation of Rhythm Management (AFFIRM) Investigators (2002). A comparison of rate control and rhythm control in patients with atrial fibrillation. The New England journal of medicine, [online] 347(23), pp.1825–33. doi:https://doi.org/10.1056/NEJMoa021328.

217. Ronzhina, M., Tibor Stračina, Ľubica Lacinová, Katarína Ondáčová, Pavlovičová, M., Maršánová, L., Radovan Smíšek, Oto Janoušek, Kateřina Fialová, Kolářová, J., Novàkovâ, M. and Ivo Provazník (2021). Di-4-ANEPPS Modulates Electrical Activity and Progress of Myocardial Ischemia in Rabbit Isolated Heart. Frontiers in Physiology, 12. doi:https://doi.org/10.3389/fphys.2021.667065.

218. Larsen, A.P., Sciuto, K.J., Moreno, A.P. and Poelzing, S. (2012). The voltage-sensitive dye di-4-ANEPPS slows conduction velocity in isolated guinea pig hearts. Heart Rhythm, 9(9), pp.1493–1500. doi:https://doi.org/10.1016/j.hrthm.2012.04.034.

219. Kanaporis, G., Martišienė, I., Jurevičius, J., Rūta Vosyliūtė, Navalinskas, A., Treinys, R., Matiukas, A., and Pertsov, A.M. (2012). Optical mapping at increased illumination intensities. Journal of Biomedical Optics, [online] 17(9), pp.0960071–0960071. doi:https://doi.org/10.1117/1.jbo.17.9.096007.

220. Kappadan, V., Sohi, A., Parlitz, U., Luther, S., Uzelac, I., Fenton, F.H., Peters, N.S., Christoph, J. and Ng, F. S. (2023). Optical mapping of contracting hearts. 601(8), pp.1353–1370. doi:https://doi.org/10.1113/jp283683.

221. Olejnickova, V., Novakova, M. and Provaznik, I. (2015). Isolated heart models: cardiovascular system studies and technological advances. Medical & Biological Engineering & Computing, 53(7), pp.669–678. doi:https://doi.org/10.1007/s11517-015-1270-2.

222. Lelovas, P.P., Kostomitsopoulos, N.G. and Xanthos, T.T. (2014). A comparative anatomic and physiologic overview of the porcine heart. Journal of the American Association for Laboratory Animal Science : JAALAS, [online] 53(5), pp.432–8. Available at: https://www.ncbi.nlm.nih.gov/pmc/articles/PMC4181683/.

223. Schüttler, D., Bapat, A., Kääb, S., Lee, K., Tomsits, P., Clauss, S. and Hucker, W.J. (2020). Animal Models of Atrial Fibrillation. Circulation Research, 127(1), pp.91–110. doi:https://doi.org/10.1161/circresaha.120.316366.

224. Fu, F., Pietropaolo, M., Cui, L., Pandit, S., Li, W., Tarnavski, O., Shetty, S.S., Liu, J., Lussier, J.M., Murakami, Y., Grewal, P.K., Deyneko, G., Turner, G.M., Taggart, A.K.P., Waters, M.G., Coughlin, S. and Adachi, Y. (2022). Lack of authentic atrial fibrillation in commonly used murine atrial fibrillation models. PLOS ONE, 17(1), p.e0256512. doi:https://doi.org/10.1371/journal.pone.0256512.

225. Jia, X., Shao, W. and Tian, S. (2022). Berberine alleviates myocardial ischemia–reperfusion injury by inhibiting inflammatory response and oxidative stress: the key function of miR-26b-5p-mediated PTGS2/MAPK signal transduction. Pharmaceutical Biology, 60(1), pp.652–663. doi:https://doi.org/10.1080/13880209.2022.2048029.

226. Sánchez-Chapula, J. (1996). Increase in action potential duration and inhibition of the delayed rectifier outward current IK by berberine in cat ventricular myocytes. British Journal of Pharmacology, 117(7), pp.1427–1434. doi:https://doi.org/10.1111/j.1476-5381.1996.tb15302.x.

227. Iyer, R. P., Lisandra, Cannon, P.L., Ma, Y., DeLeon-Pennell, K.Y., Jung, M., Flynn, E.R., Henry, J.B., Bratton, D.R., White, J.A., Fulton, L.K., Grady, A.W. and Lindsey, M.L. (2016). Defining the sham environment for post-myocardial infarction studies in mice. American journal of physiology. Heart and circulatory physiology, [online] 311(3), pp.H822–H836. doi:https://doi.org/10.1152/ajpheart.00067.2016.

228. Santer, D., Nagel, F., Kreibich, M., Dzilic, E., Moser, P.T., Muschitz, G., Inci, M., Krssak, M., Plasenzotti, R., Bergmeister, H., Trescher, K. and Podesser, B.K. (2015). In vivoandex vivofunctional characterization of left ventricular remodelling after myocardial infarction in mice. ESC Heart Failure, 2(3), pp.171–177. doi:https://doi.org/10.1002/ehf2.12039.

229. Basit, H. and Huecker, M.R. (2021). Myocardial Infarction Serum Markers. [online] PubMed. Available at: https://www.ncbi.nlm.nih.gov/books/NBK532966/.

230. Lee, P., Quintanilla, J.G., Alfonso-Almazán, J.M., Galán-Arriola, C., Yan, P., Sánchez-González, J., Pérez-Castellano, N., Pérez-Villacastín, J., Ibañez, B., Loew, L.M. and Filgueiras-Rama, D. (2019). In vivo ratiometric optical mapping enables high-resolution cardiac electrophysiology in pig models. Cardiovascular Research, 115(11), pp.1659–1671. doi:https://doi.org/10.1093/cvr/cvz039.